TRAPPING ELUSIVE CP*CO(III) METALLACYCLES: IMPLICATIONS IN C-H FUNCTIONALIZATION PROCESSES

Jesus San Jose Orduna

UNIVERSITAT
ROVIRA i VIRGILI

Trapping Elusive Cp*Co[III] Metallacycles: Implications in C–H Functionalization Processes

Jesús San José Orduna
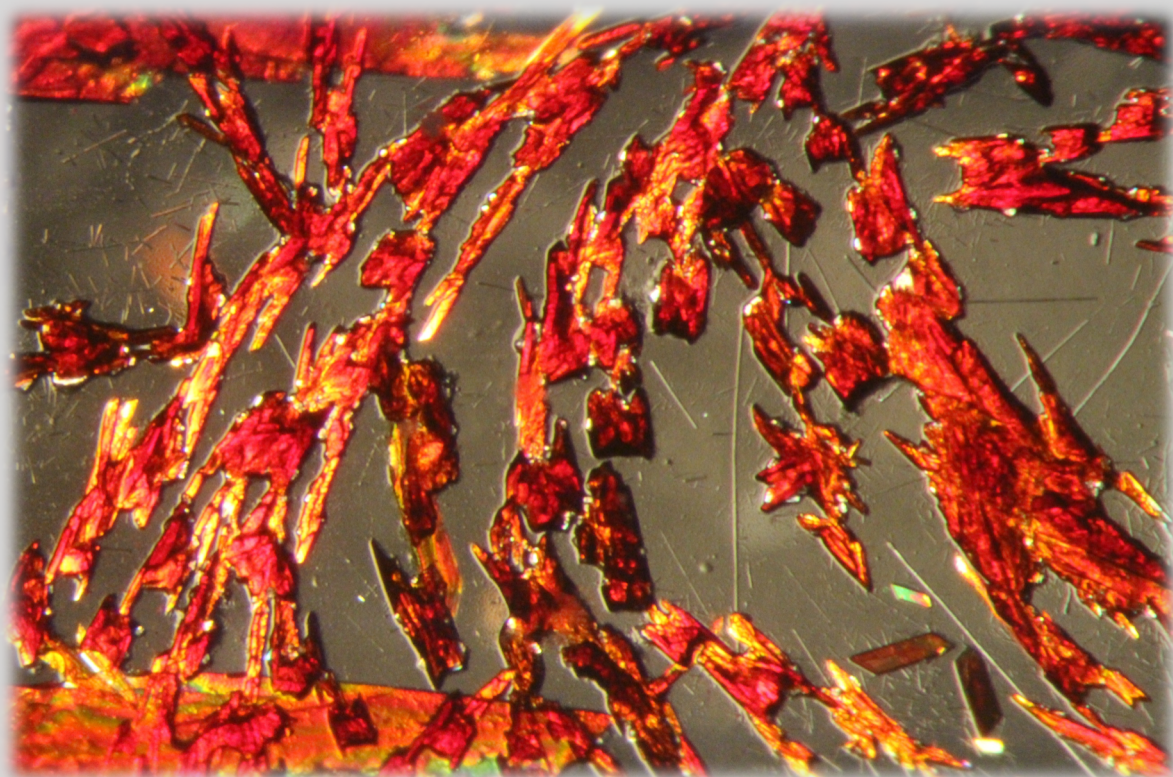
DOCTORAL THESIS
2020

Trapping Elusive Cp*Co^{III} Metallacycles: Implications in C−H Functionalization Processes

Doctoral Thesis by
Jesús San José Orduna

Developed under the supervision of
Dr. Mónica H. Pérez Temprano

Institut Català d'Investigació Química (ICIQ)

Universitat Rovira i Virgili (URV)

Departament de Química Analítica i Química Orgànica

UNIVERSITAT
ROVIRA i VIRGILI

ICIQ
Institut
Català
d'Investigació
Química

Tarragona
2020

Dr. Mónica H. Pérez Temprano, Group Leader at the Institute of Chemical Research of Catalonia (ICIQ).

I STATE that the present Doctoral Thesis, entitled "Trapping Elusive Cp*Co^{III} Metallacycles: Implications in C−H Functionalization Processes", presented by Jesús San José Orduna to receive the degree of Doctor, has been carried out under my supervision at the Institut Català d'Investigació Química (ICIQ).

Tarragona, November 2019

Doctoral Thesis Supervisor
Dr. Mónica H. Pérez Temprano

Financial Support

Curriculum Vitae

Jesús was born on April 19, 1991 and raised in Santa Coloma de Gramanet, near Barcelona (Spain). He studied chemistry at the University of Barcelona and obtained his BSc degree on September 2014. Then, he spent 6 months in the Prof. J. Vilarrasa and Prof. Anna M. Costa research group, trying to optimize Negishi cross-coupling reactions for its application in total synthesis. Stimulated by this visiting stay, he started his MSc degree in "Organic Chemistry" at the University of Barcelona, to perform his Master Thesis in the same research group. He obtained his MSc degree in September 2015.

Shortly afterwards, he joined the Pérez-Temprano group at the Institute of Chemical Research of Catalonia in Tarragona (Spain) as the first PhD student of the group, where he performed the research described in this thesis. He also spent three months as a visiting student in the group of Stuart A. Macgregor, in Edinburgh (Scotland). Under the invaluable tutelage of Prof. Macgregor, he learned the intricacies of computational chemistry, to help him in his doctoral studies.

During these 4 years of doctoral thesis he has published multiple first author publications in high-impact journals and obtained different international recognitions. He has contributed to multiple scientific meetings (16 in total), including 7 oral communications. From all his oral presentations, three were selected for the best talk award. In addition, he participated in a world-wide poster conference (>1900 contributors), organized by the Royal Society of Chemistry in Twitter, where his contribution won the 2018 best organic poster award. He has also co-organized the ICIQ II PhD Day, organized in Tarragona (Spain). Apart from this, he was invited to write a section in the Royal Society of Chemistry monthly magazine "Chemistry World" about his experience in a young and emerging research group (see **Annex III**). He also wrote another piece in the C&EN world-wide magazine section "Grad school, in students' own words". He has participated in a "Chemistry workshop for children" (sponsored by "La Caixa") and several online outreach activities. Among all of them, he has been selected as runner-up in the C&EN 2018 #Realtimechem Awards, the ACS Fall 2019 C&EN Chemistry in Pictures contest, and in the C&EN 2019 #RealTimeElements week. Last, but not least, in 2019 he was selected by the American Chemical Society, among a very competitive pool of >850 world-wide early-career researchers (PhDs and postdocs) to be a CAS Future Leader.

List of Publications

The work developed during this PhD thesis has resulted in the following publications:

[1] **Sanjosé-Orduna**, **J**.; Gallego, D.; Garcia-Roca, A.; Martin, E.; Benet-Buchholz, J.; Pérez-Temprano, M. H.*
"Capturing Elusive Cobaltacycle intermediates: A Real-Time Snapshot of the Cp*Co^{III}-catalyzed Oxidative Alkyne Annulation"
Angew. Chem. Int. Ed. **2017**, *56*, 12137−12141. ***Inside Cover*** *(vol. 56, 40)*

[2] **Sanjosé-Orduna**, **J**.;[‡] Sarria, J. M.;[‡] Pérez-Temprano, M. H.*
"HFIP-Assisted C−H Functionalization by Cp*Co^{III}: Accelerated Access to Key Reactive Intermediates and Implications in Catalysis"
Angew. Chem. Int. Ed. **2018**, *57,* 11369−11373. ([‡] equal contribution)

[3] **Sanjosé-Orduna**, **J**.; Benet-Buchholz, J.; Pérez-Temprano, M. H.*
"Molecular Aspects of Cobalt Reaction Intermediates and Their Implications in Reactivity"
Inorg. Chem. **2019**, *58*, 10569−10577. *Invited contribution to the ACS Inorganic Chemistry Forum titled: "Celebrating the Year of the Periodic Table: Emerging Investigators in Inorganic Chemistry"*

[4] **Sanjosé-Orduna**, **J**.;[‡] Mudarra, A. L.;[‡] Martínez de Salinas, S.;[‡] Pérez-Temprano, M. H.*
"Sustainable Knowledge-Based Strategies in Transition Metal-Catalyzed Transformations"
ChemSusChem **2019**, *12*, 2882−2897. *Invited contribution to the Special Issue − Sustainable Organic Synthesis.* ([‡] equal contribution)

[5] Yu, C.; **Sanjosé-Orduna**, **J**.; Patureau*, F. W.; Pérez-Temprano, M. H.*
"Emerging unconventional organic solvents for C−H bond and related functionalization reactions"
Chem. Soc. Rev. **2020**, DOI: 10.1039/c8cs00883c.

[6] **Sanjosé-Orduna**, **J**.; Pérez-Temprano, M. H.*
"Mechanistic landscape of the Cp*Co^{III} C−H functionalization reactions"
Angew. Chem. Int. Ed. **2020**. (Invited Review)

During the development of this doctoral thesis, other work not disclosed herein has been published. A brief summary of this project is shown in Annex I.

[7] Martínez de Salinas, S.; **Sanjosé-Orduna**, **J**.; Odena, C.; Barranco, S.; Benet-Buchholz, J.; Pérez-Temprano, M. H.*
"Weakly Coordinated Cobaltacycles: Trapping Catalytically Competent Intermediates in Cp*Co^{III} Catalysis"
Angew. Chem. Int. Ed. **2020**, DOI: 10.1002/anie.201916387.

Table of Contents

Preface

The work described in this dissertation has been performed during the period from February 2016 until October 2019 at the Institute of Chemical Research of Catalonia (ICIQ), under the supervision of Dr. Mónica H. Pérez-Temprano.

Due to the chemical and chronological coherence of all the publications developed during this PhD thesis, the dissertation will be presented as a compilation of articles. It will be divided into five sections: first, a brief overview of the state-of-the-art of the Cp*Co^{III}-catalyzed C−H functionalization reactions. Then, the objectives of this doctoral thesis will be presented. During all the research chapters, a more specific introduction related to the scientific results discussed will be given, followed by a copy of the published article with the corresponding supporting information. Finally, the general conclusions obtained from this work will be discussed. All the references and numbering of figures and schemes are independently organized by chapters.

Finally, three annexes will be found at the end of this doctoral thesis. The first annex will summarize, briefly, the work not described in the main text that also resulted in a publication. The second annex will assemble some of the most interesting unpublished results of this doctoral thesis. In the third annex it can be found a copy of the Royal Society of Chemistry monthly magazine section "Last Retort". In this section, the reader will be able to learn about the experience of starting in a research group from scratch, in a distended and light tone.

Summary

The sustainable synthesis of relevant scaffolds for their use in the pharmaceutical, agrochemical and material sectors constitutes one of the most urgent challenges that the chemistry community needs to overcome. In this context, over the past decades, noble transition metal-catalyzed C–H functionalization of petroleum-based derivatives has emerged as a powerful tool for the efficient generation of carbon–carbon and carbon–heteroatom bonds. Among these transformations, ligand-directed C–H activation have achieved remarkable progress, revolutionizing the synthesis of molecules and becoming a more sustainable alternative to traditional cross-coupling reactions. These strategies, involving metallacyclic intermediates, have the potential of allowing the control of site-selectivity of the chemical transformation by using substrates containing directing groups. During decades, these catalytic systems required noble transition metals such as ruthenium, rhodium or palladium, for the efficient construction of organic molecules. However, more cost-effective first-row metals, such as cobalt, have emerged as an attractive alternative to precious metals.

Over the past few years, the employment of Cp*Co^{III} complexes, analogous to active Cp*Rh^{III} catalysts for C–H activation, has represented a tremendous advance in cobalt catalysis. When compared to noble metals, cobalt catalysts offer obvious advantages, including being earth-abundant and cheaper. However, the most interesting feature of cobalt catalysts is the potential rich manifold of reactivity patterns that they can provide, not only mimicking precious metals but also exhibiting a unique and versatile reactivity. Despite the significant advances in this field, these cobalt systems are still at their infancy when compared to Rh- and Pd-based catalysts, especially due to the limited fundamental organometallic understanding of these systems. The investigation of the underlying reaction mechanisms of Cp*Co^{III}-catalyzed C–H functionalization reactions has been hampered by the difficulty of trapping high reactive transient cobalt intermediates due to the proposed reversible nature of the C–H metalation step, and the lack of stabilizing ligands.

The main goal of the PhD thesis was to gain mechanistic insight into the reaction mechanisms of Cp*Co^{III}-catalyzed C–H functionalization reactions. In this context, the first objective was the development of reliable synthetic routes for the synthesis, isolation and characterization of direct analogues of a long-sought cyclometallated Cp*Co^{III} intermediate. Taking into account the proposed reversible C–H bond cleavage by Cp*Co^{III} systems, an alternative synthetic route was explored, involving a ligand-assisted C(sp^2)–I oxidative addition to a Cp*Co^{I} metal center, followed by halide abstraction. The presence of a coordinating ligand, such as acetonitrile, turned out to be crucial for the stabilization of this otherwise unstable cobaltacycle

species. Mechanistic investigations demonstrated the intermediacy of this species in one of the most studied catalytic reaction: the oxidative alkyne annulation. This included the detection, under catalytic conditions, of a post-migratory insertion seven-membered ring cobalt metallacycle (see **Article 1**).

Next, a mechanistic investigation was performed to understand in more detail one of the fundamental steps in Cp*Co^{III}-catalyzed C−H functionalization reactions: the migratory insertion. The employment of different electrophiles revealed different insertion modes depending on the nature of the unsaturated coupling partner (see **Article 2**).

Finally, the challenges associated to the reversible nature of the C−H metalation step in Cp*Co^{III} systems were tackled. Taking advantage of the unique stabilizing properties of acetonitrile, a direct synthetic route by C−H cyclometalation for the isolation of cobaltacycles was described. In addition, it was revealed the beneficial effect of fluorinated alcohols not only in this cyclometalation but also in different benchmark catalytic transformations (see **Article 3**).

Abbreviations and Acronyms

During this doctoral thesis, several abbreviations and acronyms have been used, following the recommendations given by the American Chemical Society: [http://pubs.acs.org/paragonplus/submission/joceah/joceah_abbreviations.pdf].

For convenience, the most used abbreviations and acronyms in this doctoral thesis are referenced in the list below:

Å	angstrom(s)
Ac	acetyl
acac	acetylacetonate
AcOH	acetic acid
Ad	adamantyl
Alk	alkyl
AMLA	ambiphilic metal-ligand interaction
aq	aqueous
Ar	aryl
atm	atmosphere(s)
B	base
BIES	base-assisted internal electrophilic-type substitution
Bn	benzyl
Boc	*tert*-butyloxycarbonyl
br	broad (spectral)
^{i}Bu	iso-butyl
Bu, ^{n}Bu	normal (primary) butyl
^{t}Bu	*tert*-butyl
^{o}C	degrees Celsius
cat.	catalytic
CCA	chiral carboxylic acid
CIF	Crystallographic Information Framework
cm	centimeter(s)
CMD	concerted metalation-deprotonation
Cp	cyclopentadientyl
Cp*	pentamethylcyclopentadienyl
Cp^X	enantiopure cyclopentadientyl
Cy	cyclohexyl
δ	chemical shift (in part per million) downfield from tetramethylsilane
***o*DCB**	1,2-dichlorobenzene
DCE	1,2-dichloroethane
DCM	dichloromethane
DEPT	distortioneless enhancement by polarization transfer

DFT	density functional theory
DG	directing group
DMAD	dimethyl acetylenedicarboxylate
DMPU	1,3-dimethyl-3,4,5,6-tetrahydro-2(1*H*)-pyrimidinone
d.r.	diastereomer ratio
EDG	electron-donating group
equiv.	equivalent
e.r.	enantiomer ratio
ESI	electrospray ionization
Et	ethyl
Et$_2$O	diethyl ether
EWG	electron-withdrawing group
FG	functional group
g	gram(s); prefix to NMR abbreviation denoting gradient-selected
h	hour(s)
HFIP	1,1,1,3,3,3-hexafluoroisopropanol
HMBC	heteronuclear multiple bond correlation
HPLC	high-performance liquid chromatography
HRMS	high-resolution mass spectrometry
HSQC	heteronuclear single quantum correlation
Hz	hertz
IES	intramolecular electrophilic substitution
IR	infrared
IRC	intrinsic reaction coordinate
J	coupling constant (in NMR spectrometry)
K	kelvin(s) (absolute temperature)
L	liter(s)
L$_n$	undetermined ligand(s)
μ	micro
m	multiplet (spectral); meter(s); milli
M	molar (moles per liter)
M$^+$	parent molecular ion
MALDI	matrix-assisted laser desorption ionization
Me	methyl
MHz	megahertz
min	minute(s)
MO	molecular orbital
mol	mole(s)
mp	melting point
MS	mass spectrometry; molecular sieves
MW	molecular weight
m/z	mass-to-charge ratio

NBO	natural bond orbital
^{n}Hex	hexane
NMR	nuclear magnetic resonance
NOE	nuclear Overhauser effect
NOESY	nuclear Overhauser effect spectroscopy
Nu	nucleophile
OAc	acetate
OPiv	pivalate
Ph	phenyl
Piv	pivaloyl
PivOH	pivalic acid
ppb	part(s) per billion
ppm	part(s) per million
^{i}Pr	isopropyl
Py	pyridine
q	quartet (spectral)
ref.	reference
rt	room temperature
s	singlet (spectral); second(s)
SCF	self-consistent field
S_EAr	electrophilic aromatic substitution
SET	single electorn transfer
S_N1	unimolecular nucleophilic substitution
S_N2	bimolecular nucleophilic substitution
t	triplet (spectral); time
TEMPO	2,2,6,6,tetramethylpiperidin-1-oxyl
Tf	trifluoromethanesulfonyl (triflyl)
TFE	trifluoroethanol
THF	tetrahydrofuran
TLC	thin-layer chromatography
TM	transition metal
TMS	trimethylsilyl; tetramethylsilane
TOF	time-of-flight; turnover frequency
TON	turnover number
Ts	*para*-toluenesulfonyl (tosyl)
TS	transition state
UV	ultraviolet
Vis	visible
vol	volume
XRD	x-ray diffraction

Chapter 1

General Introduction

DG   *cat.* [Cp*Co^{III}]   DG

*reversible
C–H bond
cleavage*

DG
[Co^{III}]
A$^+$

Insertion
Dissociation

*elusive intermediate
via C–H activation*
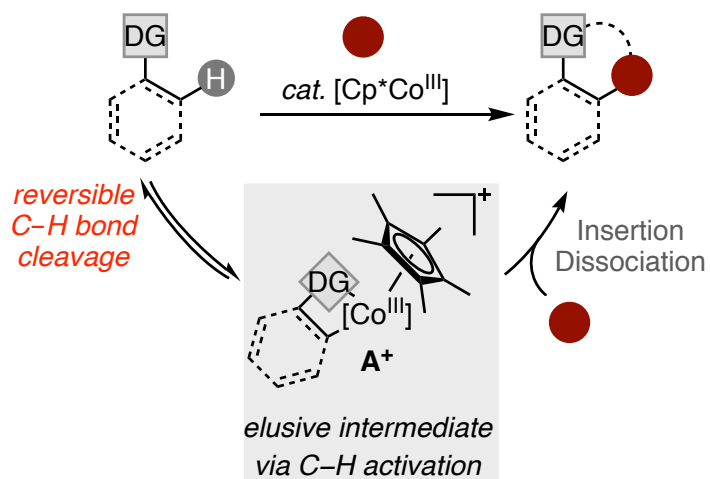
1.1 Transition-Metal-Catalyzed C−H Functionalization Reactions

1.1.1 From Cross-Coupling to C−H Functionalization

"*Organic chemistry has developed into an art form where scientists produce marvelous chemical creations in their test tubes. Mankind benefits from this in form of medicines, ever-more precise electronics and advanced technological materials.*" The Royal Swedish Academy of Sciences published this piece in 2010,[1] the year that Richard F. Heck, Ei-ichi Negishi and Akira Suzuki were awarded the Nobel Prize in Chemistry, for the palladium-catalyzed cross-coupling reaction. The discovery of this methodology supposed an extraordinary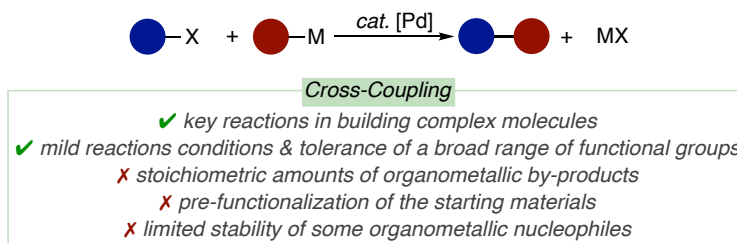 breakthrough in synthetic organic chemistry, opening the doors to a whole new chemical space. By bringing together an organic electrophile and different types of coupling partners (ranging from organometallic nucleophiles to alkenes), new C−C bonds could be created in a simple and modular way. However, it still presents some limitations, such as the formation of undesired waste due to the use of stoichiometric amounts of the organometallic nucleophiles, the requirement of pre-functionalized starting materials or the instability/toxicity of some of the coupling partners. These are, still now, unresolved challenges.

Cross-Coupling

✔ key reactions in building complex molecules
✔ mild reactions conditions & tolerance of a broad range of functional groups
✗ stoichiometric amounts of organometallic by-products
✗ pre-functionalization of the starting materials
✗ limited stability of some organometallic nucleophiles

Scheme 1.1. Pd-catalyzed cross-coupling reactions.

Because of that, the chemical community has devoted their efforts to develop alternatives that can improve the sustainability and/or the atom-economy of this transformation. In this context, C−H functionalization reactions, considered one of the holy grails of chemistry,[2] represents an ideal approach for constructing C−C and C−heteroatom bonds. During the past few decades, the strategies for the cleavage of "unreactive" C−H bonds have evolved from classical electrophilic or radical routes to transition-metal-mediated approaches (Scheme 1.2). In particular, the latter ones have become one of the cornerstones in modern synthetic organic

---

chemistry, since these strategies can promote regioselective functionalizations under milder reaction conditions.

Scheme 1.2. Strategies for the cleavage of unreactive C−H bonds.

The mechanisms of these transition-metal-catalyzed transformations can be divided in three main steps (Scheme 1.3): (i) a C−H activation that affords an alkyl/aryl−TM intermediate; (ii) reaction of the putative reactive species with the corresponding coupling partners; (iii) formation of the desired product and the regeneration of the active TM catalyst. In some cases, an extra re-oxidation step is required for regenerating the active catalyst and closing the catalytic cycle.
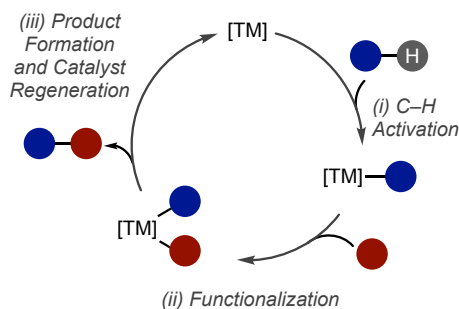
Scheme 1.3. General mechanism for the metal-assisted C−H functionalization.

1.1.2 Mechanistic Scenarios of C−H Metalation Assisted by Transition Metals

One of the common bottlenecks in TM-catalyzed C−H functionalization reactions is the cleavage of the C−H bond. Therefore, the chemistry community has devoted tremendous efforts on understanding how a C−H bond is activated by a transition metal.[3] Depending on the physical properties of the metallic center (e.g. oxidation state, coordination sphere environment) and the reaction conditions (e.g. solvent, additives), different modes of organometallic C−H activation can be identified, as depicted in Scheme 1.4:

(i) **Oxidative Addition**.[4] This mechanism starts with a reversible coordination of the metal center to the C−H bond. Then, a three-centered σ complex is formed. Due to a π-backdonation of the metal center to this specific bond, the cleavage of the C−H bond takes place. As a result, two new bonds in the TM are formed, modifying the coordination sphere around the metal center and increasing the oxidation state of the metal in two units. This mechanism is prevalent for electron-rich late transition metal complexes with d^8 and d^{10} configurations.

(ii) **σ-Bond Metathesis**.[5] This mechanism is a redox neutral concerted exchange, that involves the formation and cleavage of σ bonds via a [2+2] cycloaddition. It is dominant for early transition metals and lanthanides with d^0 and d^0f^n configurations, respectively.

(iii) **1,2-Addition**.[3b] This mode of activation share similarities with the σ-bond metathesis, but the insertion of the coupling partner takes place at a TM=X double bond (X = CR_2, CR, NR_2, NR, OR). It is also observed with early transition metals.

(iv) **Electrophilic Aromatic Substitution** (S_EAr).[6] The π-electronic cloud of an aromatic system interacts with an electron-deficient metal, forming a de-aromatized species, known as *Wheland* intermediate.[7] This metal-carbon interaction enhances the acidity of the proton, which now is prone to be abstracted by an external base to recover the initial aromaticity of the arene. This mechanism is predominant for electron-poor late-transition metals and electron-rich arene derivatives.

[3] (a) Ackermann, L. "Carboxylate-Assisted Transition-Metal-Catalyzed C−H Bond Functionalizations: Mechanism and Scope" *Chem. Rev.* **2011**, *111*, 1315−1345. (b) Balcells, D.; Clot, E.; Eisenstein, O. "C−H Bond Activation in Transition Metal Species from a Computational Perspective" *Chem. Rev.* **2011**, *110*, 749−823. (c) Labinger, J. A.; Bercaw, J. E. "Understanding and exploiting C−H bond activation" *Nature* **2002**, *417*, 504−514.

[4] Labinger, J. A. "Tutorial on Oxidative Addition" *Organometallics* **2015**, *34*, 4784−4795.

[5] Waterman, R. "σ-Bond Metathesis: A 30-Year Retrospective" *Organometallics* **2013**, *32*, 7249−7263.

[6] Galabov, B.; Nalbantova, D.; Schleyer, P. von R.; Schaefer, H. F. "Electrophilic Aromatic Substitution: New Insights into an Old Class of Reactions" *Acc. Chem. Res.* **2016**, *49*, 1191−1199.

[7] Wheland, G. W. "A Quantum Mechanical Investigation of the Orientation of Substituents in Aromatic Molecules" *J. Am. Chem. Soc.* **1942**, *64*, 900−908.

(v)   **Base-assisted C−H Metalation**.[3a] This mode of activation can undergo through multiple transition states. All of them display, in the coordination sphere of the metal, a ligand that can act as a Lewis base (B). It occurs, preferentially when using second- and third-row late transition metals, in the presence of additives that can act as bases.
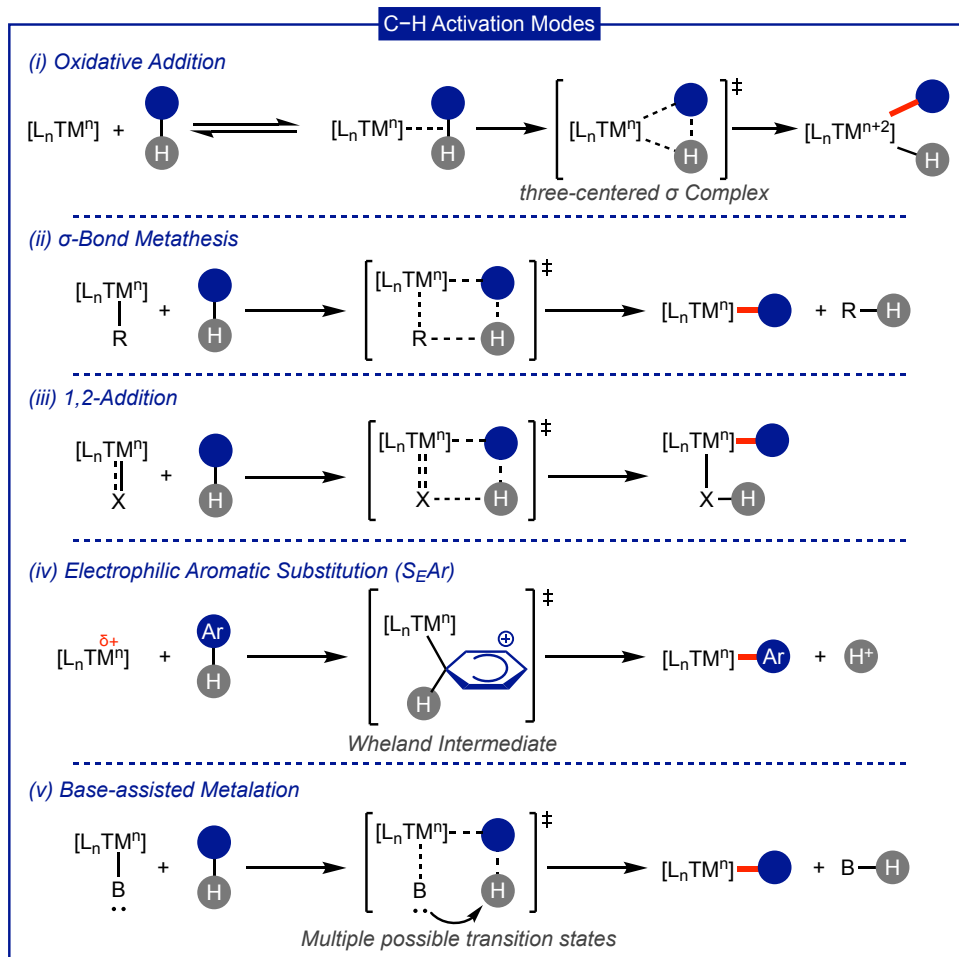
Scheme 1.4. Overview of modes of activation for TM-mediated C−H bond-cleavage.

Among the different strategies for the activation of a C−H bond, the base-assisted metalation mechanism has attracted the attention of the scientific community in the last years. Due to its popularity, this approach has been the aim of multiple investigations. As a result, several types of cyclic transition states have been proposed, depending on the nature of the base, its interaction with the metal center, and the reaction conditions (Scheme 1.5):

(v.i)   **Intramolecular electrophilic substitution** (IES)[8] is invoked when alkoxide bases are used and involves highly strained four-membered transition states.

(v.ii)   **Concerted metalation-deprotonation** (CMD)[9] involves the simultaneous formation of a TM−C bond and the cleavage of a C−H bond by intramolecular base assistance. This mechanism is proposed when using carboxylate bases and occurs via six-membered transition states.

(v.iii) **Ambiphilic metal-ligand interaction** (AMLA)[10] is a variation of the CMD mechanism and describes a simultaneous interaction of the C−H bond with the TM center and the carboxylate ligand. This mechanism is proposed for the activation of electron-deficient substrates.

(v.iv)   **Base-assisted internal electrophilic-type0 substitution** (BIES)[11] combines features of S_EAr and CMD and it is proposed to explain the activation of electron-rich substrates with the assistance of carboxylate bases.
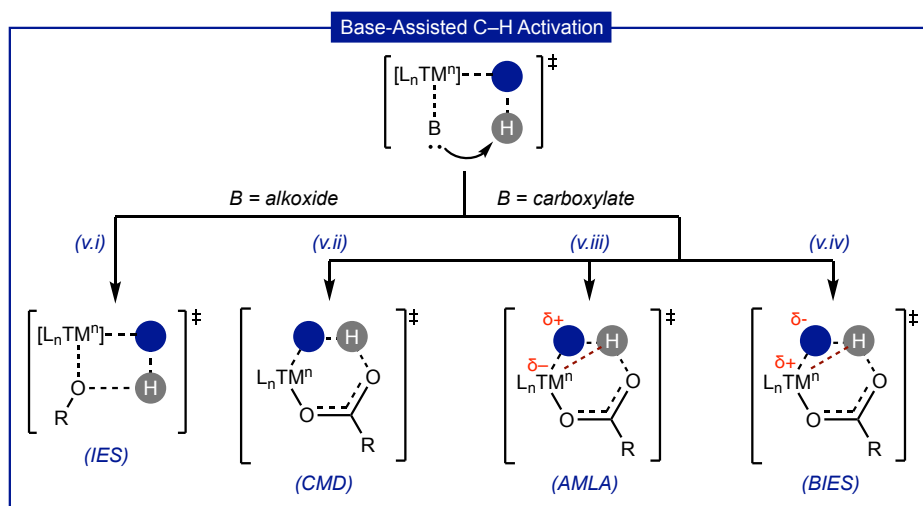
Scheme 1.5. Summary of the different base-assisted C−H metalation transition states.

[8] Oxgaard, J.; Tenn, W. J.; Nielsen, R. J.; Periana, R. A.; Goddard, W. A. "Mechanistic Analysis of Iridium Heteroatom C−H Activation: Evidence for an Internal Electrophilic Substitution Mechanism" *Organometallics* **2007**, *26*, 1565−1567.

[9] Lapointe, D.; Fagnour, K. "Overview of the Mechanistic Work on the Concerted Metallation-Deprotonation Pathway" *Chem. Lett.* **2010**, *39*, 1118−1126.

[10] Boutadla, Y.; Davies, D. L.; Macgregor, S. A.; Poblador-Bahamonde, A. I. "Mechanisms of C−H bond activation: rich synergy between computation and experiment" *Dalton Trans*. **2009**, *30*, 5820−5831.

[11] Ma, W.; Mei, R.; Tenti, G.; Ackermann, L. "Ruthenium(II)-Catalyzed Oxidative C−H Alkenylations of Sulfonic Acids, Sulfonyl Chlorides and Sulfonamides" *Chem. Eur. J.* **2014**, *20*, 15248−15251.

1.1.3 Site-Selective Control in TM-Catalyzed C−H Functionalization Reactions

One of the major challenges associated to the functionalization of C−H bonds relies on controlling the site-selectivity of the bond-cleavage. Because these bonds are usually ubiquitous moieties in most molecules, it is necessary to find a way to discriminate between multiple C−H bonds. Three major solutions have been described to overcome this problem (Scheme 1.6). First, the use of molecules that present bulky substituents, shielding some C−H bonds and preventing undesired side-reactions. Second, the use of electronically activated substrates, where the acidity of one of the C−H bonds is higher than the others. However, it can be anticipated that these two solutions present a very limited applicability, due to the intrinsic requirements of the substrate molecular scaffold. In sharp contrast, probably the most successful strategy for overcoming this inherit limitation has been the use of directing groups (DGs). This chelating moieties are usually Lewis-basic groups present in the molecule, that bind to the metal center, and brings it closer in space to a specific position, facilitating the reactivity with a proximal C−H bond.
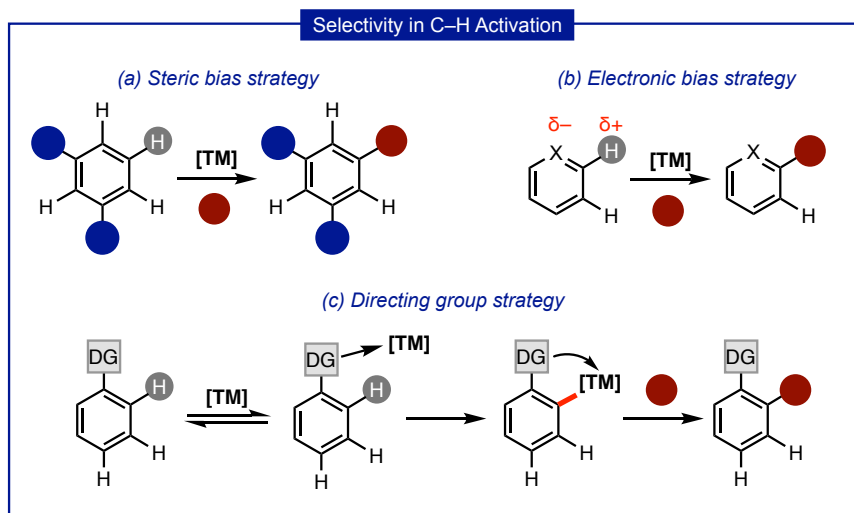
Scheme 1.6. Summary of strategies for the selective TM-catalyzed C−H functionalization.

The most significant breakthrough in this area was reported by Murai and Chatani in 1993.[12] The authors described the Ru-catalyzed hydroarylation of alkenes with aromatic ketones using a carbonyl functional group as chelating ligand. Since then, ligand-directed TM-catalyzed C−H functionalization reactions have become

---

[12] Murai, S.; Kakiuchi, F.; Sekine, S.; Tanaka, Y.; Kamatani, A.; Sonoda, M.; Chatani, N. "Efficient catalytic addition of aromatic carbon-hydrogen bonds to olefins" *Nature* **1993**, *366*, 529−531.

one of the most active fields in synthetic organic chemistry, proving to be very useful for the activation of C−H bonds. These protocols offer a wide variety of solutions for the *ortho*-functionalization of aromatic rings using monodentate (e.g. pyridines, pyrimidines, imines, amides or carbonyl moieties) or bidentate (e.g. 8-aminoquinoline or picolinamide) directing groups. Regarding *meta*- and *para*-functionalization (also known as remote), different T-, D- and U-shape templates have been developed by Yu and Maiti, among others, bringing the TM close to the desired distal position (Scheme 1.7).[13]
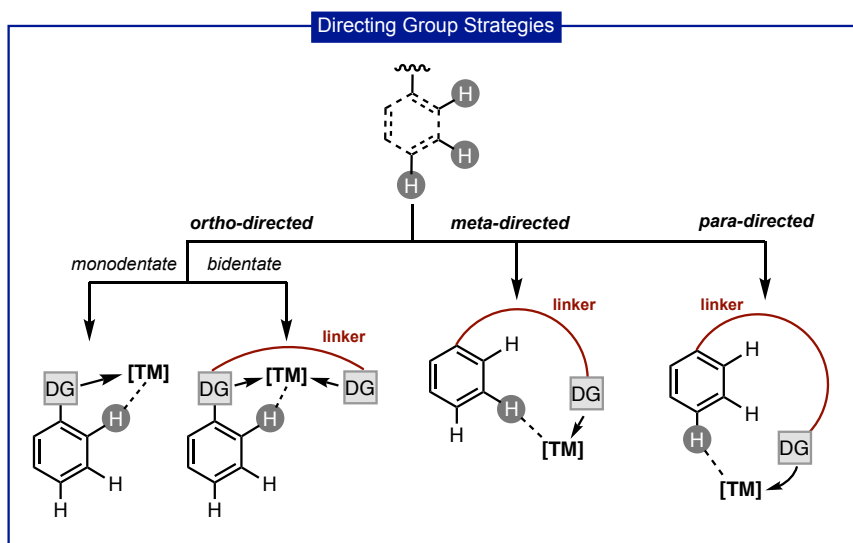
Scheme 1.7. Strategies for the selective TM-catalyzed C−H functionalization reactions.

During decades, these catalytic systems required noble transition metals such as ruthenium, rhodium or palladium[14] for the efficient construction of organic molecules. However, in the past few years, more cost-effective first-row metals, such as cobalt, have emerged as an attractive alternative to precious metals.

[13] (a) Leow, D.; Li, G.; Mei, T.-S.; Yu, J.-Q. "Activation of remote *meta*-C−H bond assisted by an end-on template" *Nature* **2012**, *486*, 518−522. (b) Tang, R.; Li, G.; Yu, J.-Q. "Conformation-induced remote *meta*-C−H activation of amines" *Nature* **2014**, *507*, 215−220. (c) Dey, A.; Sinha, S. K.; Achar, T. K.; Maiti, D. "Accessing Remote *meta*- and *para*-C(sp^2)-H Bonds with Covalently Attached Directing Groups" *Angew. Chem. Int. Ed*. **2019**, *58*, 10820−10843.
[14] (a) Ritleng, V.; Sirlin, C.; Pfeffer, M. "Ru-, Rh-, and Pd-Catalyzed C−C Bond Formation Involving C−H Activation and Addition on Unsaturated Substrates: Reactions and Mechanistic Aspects" *Chem. Rev*. **2002**, *102*, 1731−1769. (b) Wencel-Delord, J.; Glorius, F. "C−H Bond Activation Enables the Rapid Construction and Late-State Diversification of Functional Molecules" *Nat. Chem.* **2013**, *5*, 369−375. (c) Yamaguchi, J.; Yamaguchi, A. D.; Itami, K. "C−H Bond Functionalization: Emerging Synthetic Tools for Natural Products and Pharmaceuticals" *Angew. Chem. Int. Ed.* **2012**, *51*, 8960−9009.
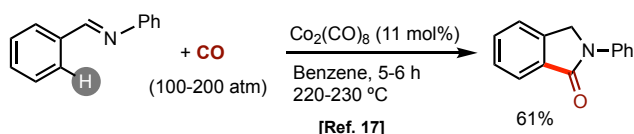
1.2 Cobalt-Catalyzed C−H Functionalization Reactions

Cobalt, the element 27 of the periodic table, was discovered in 1735. However, it has been used (inadvertently) since ancient times to impart a blue color to different decorations, like ceramics, jewelry and paintings.[15] It is found in the Earth's crust only in the form of cobalt compounds and has to be separated from different minerals in order to obtain it as pure metal. It is one of the more abundant transition metals in the Earth's crust (ca. 25 ppm), in concentrations several orders of magnitude higher than noble metals, such as rhodium and iridium (ca.1 ppb each) or palladium (ca. 15 ppb).[16]

In the context of TM-catalyzed transformations, cobalt catalysts offer several advantages when compared to noble metals, like the aforementioned abundance in Earth. However, without a doubt, the most interesting feature of cobalt catalysts is the potential rich manifold of reactivity patterns that they can provide. Apart from mimicking precious metals, they also exhibit a unique and versatile reactivity. This can be explained due to its small radius, low electronegativity and facile access to multiple oxidation states through 1 or 2 electron processes. In the following sections, we will cover from the early examples on cobalt-catalyzed C−H functionalization processes, using low valent cobalt complexes, to its renaissance by the employment of high-valent systems.

1.2.1 Early Catalytic Examples: Low-Valent Cobalt Catalysts

The first example of a transition-metal-catalyzed C−H functionalization reaction assisted by a directing group was described in 1955 by Murahashi.[17] This seminal work described the synthesis of 2-phenylphthalimidine using a cobalt precatalyst (Scheme 1.8).

**Scheme 1.8.** First cobalt-catalyzed C−H functionalization.

Surprisingly, it was not until more than 50 years later that cobalt-catalyzed directed C−H functionalization reactions arose as a promising tool in organic synthesis. Initially, this field was dominated by the use of low-valent cobalt salts. The first

---

[15] Encyclopædia Britannica. Cobalt. https://www.britannica.com/science/cobalt-chemical-element (accessed 18 Dec, 2019).

[16] Lide, D. R. CRC Handbook of Chemistry and Physics; CRC Press: Boca Raton, 2005; Section 14, Geophysics, Astronomy, and Acoustics; Abundance of Elements in the Earth's Crust and in the Sea.

[17] Murahashi, S. "Synthesis of Phthalimidines from Schiff Bases and Carbon Monoxide" *J. Am. Chem. Soc.* **1955**, *77*, 6403−6404.

example of a synthetic methodology highlighting the potential of Co[I] salts for C−H activation was reported by Kisch and co-workers.[18] They described the *ortho*-alkenylation of azo-compounds with sub-stoichiometric amounts of [CoH(N$_2$)(PPh$_3$)$_3$] (Scheme 1.9). However, the utilization of an unstable cobalt complex hampered the long-term applicability of this protocol.
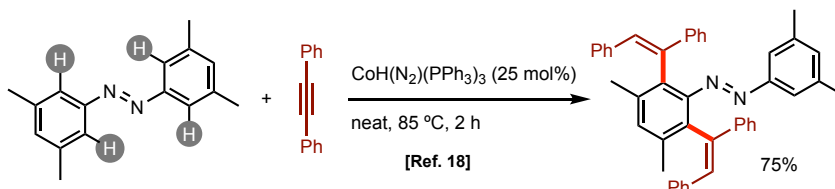
Scheme 1.9. First low-valent cobalt catalyzed C−H transformation.

In order to solve this problem, Yoshikai devised an alternative for the cobalt-catalyzed alkyne hydroarylation.[19] This time, a simple ternary catalytic system was described using a phosphine ligand, a simple and stable CoBr$_2$ and a Grignard reagent (Scheme 1.10a). Using this method, the active low-valent cobalt species is formed *in situ* by reduction with the Grignard reagent. Not long after that, Nakamura described an analogous methodology for the alkylation of benzamides with alkyl chlorides (Scheme 1.10b).[20]

(a) Cobalt-catalyzed hydroarylation of alkynes

(b) Cobalt-catalyzed alkylation of benzamides
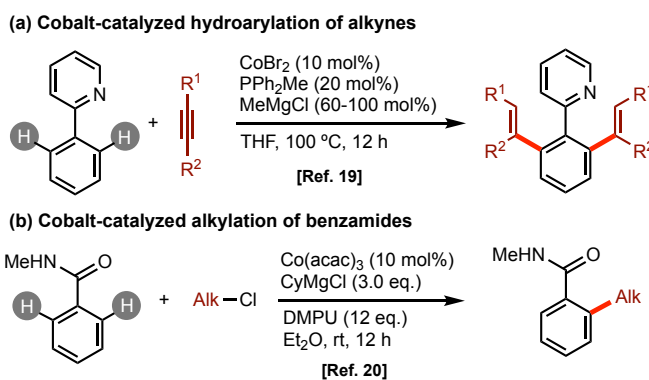
**Scheme 1.10.** Pioneering examples on low-valent cobalt-catalyzed C−H functionalization.

[18] Halbritter, G.; Knoch, F.; Wolski, A.; Kisch, H. "Functionalization of Aromatic Azo Compounds by the Cobalt-Catalyzed Regioselective Double Addition of Tolane: 2,6-Distilbenzylazobenzenes and 2,3-Dihydrocinnolines" *Angew. Chem. Int. Ed.* **1994**, *33*, 1603−1605.
[19] Gao, K.; Lee, P.-S.; Fujita, T.; Yoshikai, N. "Cobalt-catalyzed Hydroarylation of Alkynes through Chelation-Assisted C−H Bond Activation" *J. Am. Chem. Soc.* **2010**, *132*, 12249−12251.
[20] Chen, Q.; Illies, L.; Nakamura, E. "Cobalt-Catalyzed *ortho*-Alkylation of Secondary Benzamide with Alkyl Chloride through Directed C−H Bond Activation" *J. Am. Chem. Soc.* **2011**, *133*, 428−429.

Along all the examples described in the literature,[21] there are two main mechanisms operating (Scheme 1.11). First, in the reactions concerning the use of alkynes or alkenes to obtain new alkenylation products, the Co[II] precatalyst has to be activated. It is hypothesized that, in presence of an excess of a Grignard reagent, the metal species is reduced to Co[0] (however, it is not possible to rule out the possibility of having also Co[I] species in the media). After the reversible alkyne/alkene coordination, the C−H bond-cleavage occurs through an oxidative addition event, to form a metallacycle. Then, after the migratory insertion of the unsaturated molecule into the Co−C bond, the desired product is formed via a reductive elimination, regenerating the active Co[0] specie. The second typical scenario is considered to operate when using alkyl halides as coupling partners. This time, the reduction of the initial Co[II] is proposed to furnish Co[I] as the active species. Next, the cyclometalation with the substrate is thought to happen through a CMD mechanism. Then, the activation of the alkyl halide is suggested to proceed via a single electron transfer to form a cyclometalated Co[II] specie, which can suffer a radical recombination to form Co[III] species. The desired product is then obtained by reductive elimination.

The term "low-valent" is referred to the oxidation state of the initial, catalytically-active metallic specie. It is hypothesized to be Co[0] or Co[I], and can be accessed, usually, by reduction of Co[II] or Co[III] precatalysts.
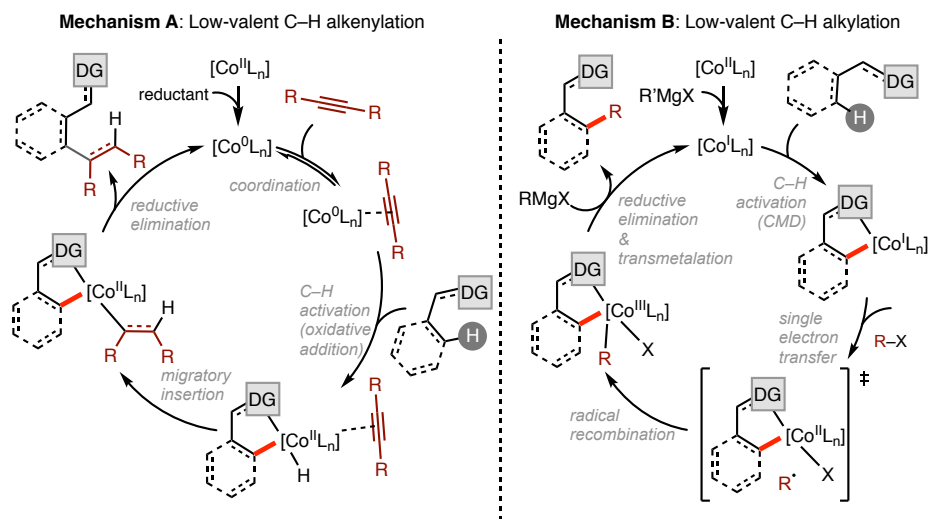

Scheme 1.11. Mechanistic summary of low-valent cobalt catalysis.

[21] (a) Gao, K.; Yoshikai, N. "Low-Valent Cobalt Catalysis: New Opportunities for C−H Functionalization" *Acc. Chem. Res.* **2014**, *47*, 1208−1219. (b) Moselage, M.; Li, J.; Ackermann, L. "Cobalt-Catalyzed C−H Activation" *ACS. Catal.* **2016**, *6*, 498−525.

1.2.2 High-Valent Cobalt-Catalyzed C−H Functionalization Reactions

The term "high-valent catalysis" is used for the transformations that are proposed to start the catalytic cycle with Co[III] species. In this context, there are two different high-valent cobalt-based systems reported in the literature, which offer great complementarity in terms of substrate scope and reactivity patterns.

In 2014, inspired by previous examples on palladium catalysis, Daugulis and co-workers reported the first example of oxidative C−H functionalization of substrates containing bidentate DGs using cobalt(II) salts in combination with an external oxidant (Scheme 1.12).[22a] In this seminal work, the authors described the generation of isoquinolones by the coupling of alkynes and 8-aminoquinolines, by a consecutive C−H/N−H activation.
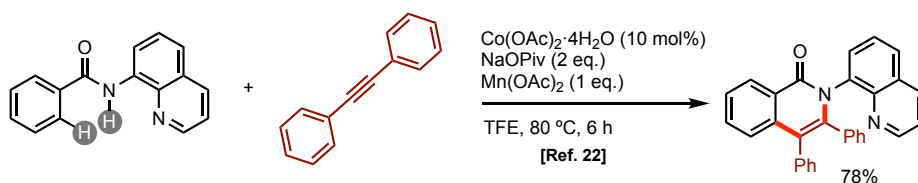
Scheme 1.12. First Co(OAc)$_2$-mediated C−H functionalization reaction.

Since this pioneering work, Maiti, Ackermann, Song, and Zhang among others, have also demonstrated the efficiency of these cobalt salts as precatalysts to promote C−C and C−heteroatom bond formation, not only with organic electrophiles, but also with nucleophiles.[22] Despite all this extraordinary progress, this methodology still presents some limitations. For instance, the use of stoichiometric oxidants is not always compatible with some functional groups. Moreover, the need for bidentate DGs precludes the versatility and applicability of these methods.

If cobalt has become one of the most promising 3d metals for promoting directed C−H functionalization reactions is due to the employment of Cp*Co[III]-based systems. The initial breakthrough was reported by Kanai and Matsunaga in 2013. They reported the coupling of monodentate 2-phenylpyridine derivatives with imines and α,β-unsaturated ketones using Cp*Co[III] complexes (Scheme 1.13).[23] Since then, the same group along with Ackermann, Glorius, Chang, and Ellman

[22] (a) Grigorjeva, L.; Daugulis, O. "Cobalt-Catalyzed, Aminoquinoline-Directed C(sp^2)−H Bond Alkenylation by Alkynes" *Angew. Chem. Int. Ed.* **2014**, *53*, 10209−10212. (b) Kommagalla, Y.; Chatani, N. "Cobalt(II)-catalyzed C−H functionalization using an *N,N'*-bidentate directing group" *Coord. Chem. Rev.* **2017**, *350*, 117−135.
[23] Yoshino, T.; Ikemoto, H.; Matsunaga, S.; Kanai, M. "A Cationic High-Valent Cp*Co[III] Complex for the Catalytic Generation of Nucleophilic Organometallic Species: Directed C−H Bond Activation" *Angew. Chem. Int. Ed.* **2013**, *52*, 2207−2211.

among others, have demonstrated the potential of Cp*Co^{III} complexes to catalyze C−H functionalization processes of substrates containing traditional monodentate directing groups (DGs) such as pyridines, pyrimidines or imines.[24] In the following section, it will be provided a brief outline of the most relevant reactivity patterns in the field of Cp*Co^{III}-catalyzed C−H functionalization reactions. Moreover, the limited fundamental knowledge available on these transformations will be discussed.
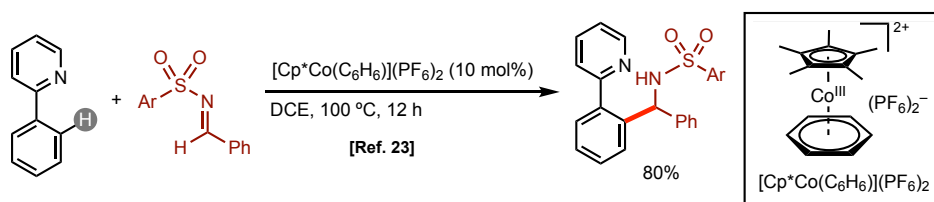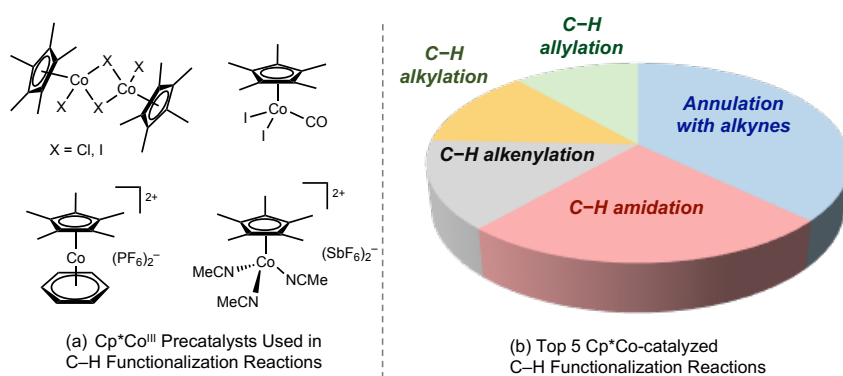

Scheme 1.13. First Cp*Co^{III}-catalyzed C−H functionalization reactions.

[24] (a) Wei, D.; Zhu, X.; Niu, J-L.; Song, M.-P. "High-valent-cobalt-catalyzed C−H functionalization based on concerted metalation-deprotonation and single-electron transfer mechanisms" *ChemCatChem* **2016**, *8*, 1242−1263. (b) Wang, S.; Chen, S-Y.; Yu, X-Q. "C-H functionalization by high-valent Cp*Co(III) catalysis" *Chem. Commun.* **2017**, *53*, 3165−3180. (c) Chirila, P. G.; Whiteoak, C. J. "Recent advances using [Cp*Co(CO)I₂] catalysts as a powerful tool for C−H functionalisation" *Dalton Trans.* **2017**, *46*, 9721−9739. (d) Yoshino, T.; Matsunaga, S. "(Pentamethylcyclopentadienyl)cobalt(III)-catalyzed C-H bond functionalization: from discovery to unique reactivity and selectivity" *Adv. Synth. Catal.* **2017**, *359*, 1245−1262. (e) Prakash, S.; Kuppusamy, R.; Cheng, C.-H. "Cobalt-catalyzed annulation reactions via C−H bond activation" *ChemCatChem* **2018**, *10*, 683−705. (f) Ghorai, J.; Anbarasan, P. "Developments in Cp*Co^{III}-Catalyzed C−H Bond Functionalizations" *Asian J. Org. Chem.* **2019**, *8*, 430−455. (g) Baccalini, A.; Vergura, S.; Dolui, P.; Zanoni, G.; Maiti, D. "Recent Advances in Cobalt-Catalysed C−H Functionalizations" *Org. Biomol. Chem.* **2019**, *17*, 10119−10141.

1.3 Cp*Co^{III}-Catalyzed Directed C−H Functionalization Reactions

Since the seminal work by Kanai and Matsunaga in 2013, Cp*Co^{III} systems have emerged as an attractive alternative to noble metals. The unique characteristics of the pentamethylcyclopentadienyl (Cp*) ligand, such as steric hindrance and high electron density, provide an excellent platform for the stabilization of active high-valent cobalt species. These precatalysts (Figure 1.1a) have the capability of promoting C−C and C−X bond-forming reactions via C−H activation using a wide variety of coupling partners. These cobalt complexes (specifically the neutral ones) usually require an external silver salt in order to form the active cationic species. Among the different reactivities that can be achieved with these precatalysts, the most studied is the annulation with alkynes (Figure 1.1b).

(a) Cp*Co^{III} Precatalysts Used in C−H Functionalization Reactions

(b) Top 5 Cp*Co-catalyzed C−H Functionalization Reactions

Figure 1.1. Overview of the Cp*Co^{III} precatalysts and the reactions more developed with these complexes.

As shown in Figure 1.2, the number of publications and citations in the field has increased tremendously in the last years.
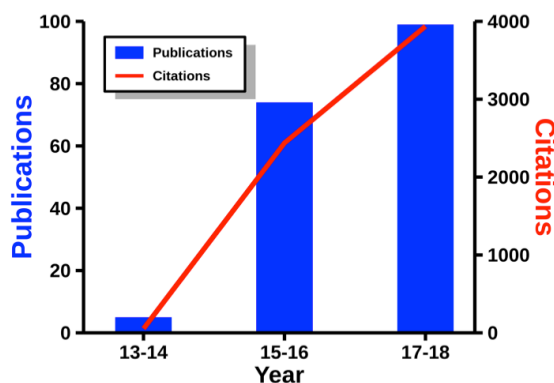

Figure 1.2. Summary of publications and citations about C−H functionalization reactions using Cp*Co^{III} catalysts until 2018.

The flourishing of this field is not only because Cp*Co^{III} catalysts can emulate the same reaction patterns of analogous Rh-based systems, but also because they can react with less electrophilic moieties in unique ways. This behavior can be explained by the higher polarization of the Cp*Co^{III}−C bond in the putative cobaltacycle formed after the C−H bond cleavage.

One of the first examples of the orthogonal reactivity between cobalt and rhodium was reported by Matsunaga and Kanai in 2014.[25] They were able to promote the C−C bond formation between indoles and alkynes. Whereas using a Cp*Rh^{III} catalyst they observed an alkenylation reaction, with cobalt an annulation reaction was predominating (Scheme 1.14).
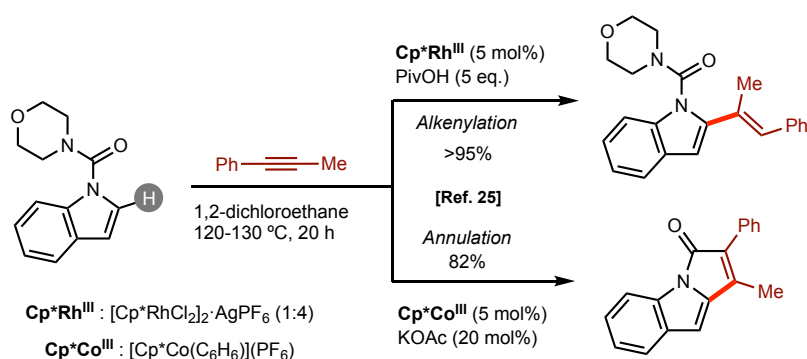
Scheme 1.14. First example of orthogonal reactivity with Cp*Co^{III} and Cp*Rh^{III} catalysts.

Since then, from a synthetic point of view, these Cp*Co^{III}-catalyzed transformations have enabled the activation of C(sp^2)−H and C(sp^3)−H bonds of substrates containing different monodentate DGs (strong or weakly chelating moieties).

1.3.1 Cp*Co^{III}-Catalyzed C(sp^2)−H Functionalization Reactions

1.3.1.1 C(sp^2)−C Bond-Forming Reactions

The formation of carbon−carbon bonds is one of the most fundamental and useful reactions in organic synthesis. In the context of Cp*Co^{III}-catalyzed C−H functionalization reactions, a vast array of coupling partners, including alkynes, alkenes, allenes, diazo compounds or cyanating agents, have been installed in organic scaffolds containing different DGs (i.e. pyridine, pyrimidine, imine, amides, or carbonyl moieties). Figure 1.3 contains some of the most relevant examples.

---

[25] Ikemoto, H.; Yoshino, T.; Sakata, K.; Matsunaga, S.; Kanai, M. "Pyrroloindolone Synthesis *via* a Cp*Co^{III}-Catalyzed Redox-Neutral Directed C−H Alkenylation/Annulation Sequence" *J. Am. Chem. Soc.* **2014**, *136*, 5424−5431.
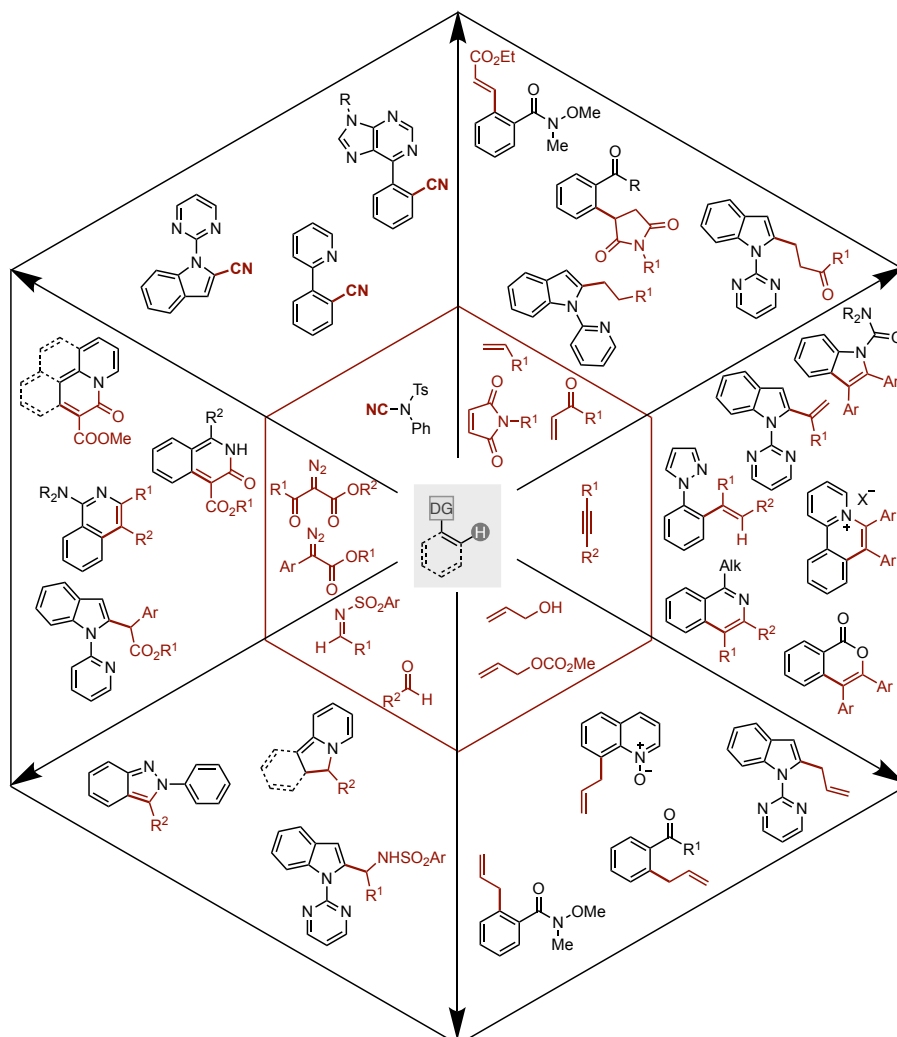
Figure 1.3. Selected Cp*Co^III-catalyzed C(sp^2)−C bond-forming reactions.

In addition to the examples depicted in Figure 1.3, there are other different reactivities that showcase the versatility of Cp*Co^III complexes for facilitating C−C bond-forming reactions. Among all of them, some of the most interesting literature precedents have been selected and will be discussed next.

Ellman and co-workers have described different Cp*Co^III-catalyzed three-component C−H bond addition cascades.[26] First, they described the highly

stereoselective reaction of aromatic C(sp^2)−H bonds with enones and aldehydes.[26a] In addition to this, they expanded the scope to *N*-substituted imines. In a subsequent work, they carried out, in a one-pot transformation, the coupling of dienes and aldehydes to benzamides.[26b] The methodology used amides as directing group and the final racemic product was obtained in exquisite regioselectivity (Scheme 1.15). More recently, they were able to expand the reaction scope to the insertion of substituted dienes to aldehydes and ketones.[26c]
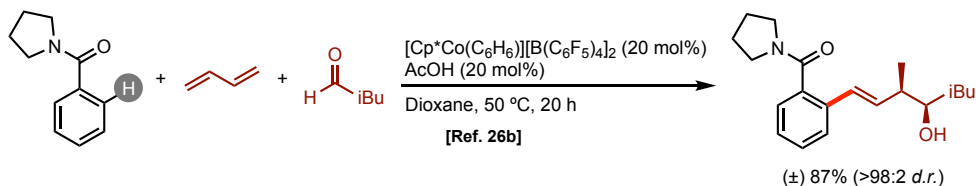
Scheme 1.15. Cp*Co^{III}-catalyzed three component C−H functionalization.

Ackermann *et al.* have been able to control the product formation during the hydroarylation of heterocycles,[27] by a rational choice of the additives (Scheme 1.16). After some mechanistic investigations, they realized that the switch in the mechanism was due to steric interactions during the product-determining transition states. Without any additives, the linear product was observed. On the other hand, when using bulky additives (i.e. 1-adamantylcarboxylic acid), the branched product was isolated selectively in excellent yields. Further discussion about this specific transformation mechanism will be found later in the introduction.
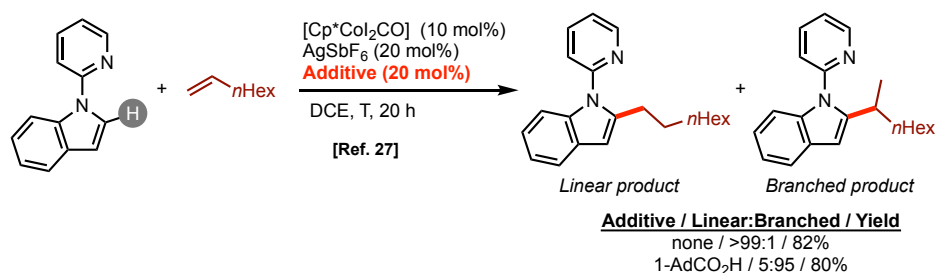

Scheme 1.16. Additive-controlled Cp*Co^{III}-mediated C−H alkylation of heterocycles.

[26] (a) Boerth, J. A.; Hummer, J. R.; Ellman, J. A. "Highly stereoselective cobalt(III)-catalyzed three component C−H bond addition cascade" *Angew. Chem. Int. Ed.* **2016**, *55*, 12650−12654. (b) Boerth, J. A.; Maity, S.; William, S. K.; Mercado, B. Q.; Ellman, J. A. "Selective and synergistic cobalt(III)-catalysed three-component C−H bond addition to dienes and aldehydes" *Nat. Catal.* **2018**, *1*, 673−679. (c) Dongbang, S.; Shen, Z.; Ellman, J. A. "Synthesis of Homoallylic Alcohols with Acyclic Quaternary Centers through Co^{III}-Catalyzed Three-Component C-H Bond Addition to Internally Substituted Dienes and Carbonyls" *Angew. Chem. Int. Ed.* **2019**, *58*, 12590−12594.
[27] Zell, D.; Bursch, M.; Müller, V.; Grimme, S.; Ackermann, L. "Full Selectivity Control in Cobalt(III)-Catalyzed C−H Alkylations by Switching of the C−H Activation Mechanism" *Angew. Chem. Int. Ed.* **2017**, *56*, 10378−10382.

In the context of chiral transformations, Ackermann and co-workers achieved the first enantioselective Cp*Co[III]-catalyzed C−H alkylation.[28] After some screening, they identified a chiral carboxylic acid (CCA) as crucial for an excellent enantioselectivity. This, in combination with an acidic additive, allow them to develop a methodology for the exclusive isolation of the (*R*)-enantiomer, Markovnikov product, in high yield (Scheme 1.17).
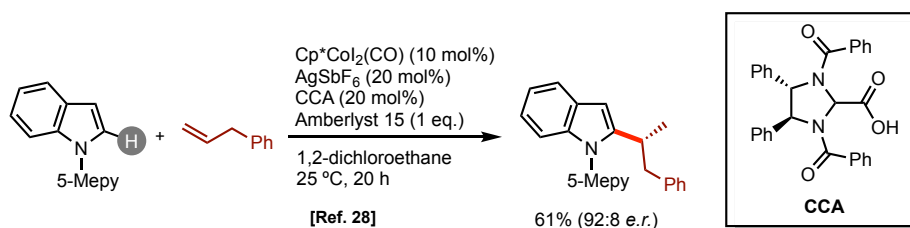
Scheme 1.17. First Cp*Co[III]-catalyzed asymmetric C−H activation using chiral carboxylic acids as additive.

Very recently, Cramer and co-workers devised an alternative strategy for asymmetric C−H functionalization reactions. They applied a family of enantiopure Cp ligands (Cp^X), already developed in the group,[29] to forge new stereocenters harnessing cobalt chemistry.[30] The group synthesized dihydroisoquinolones derivatives using *N*-chlorobenzamides and styrene as starting materials. Excellent yields and enantioselectivities were obtained for a range of different amides and alkenes (Scheme 1.18).
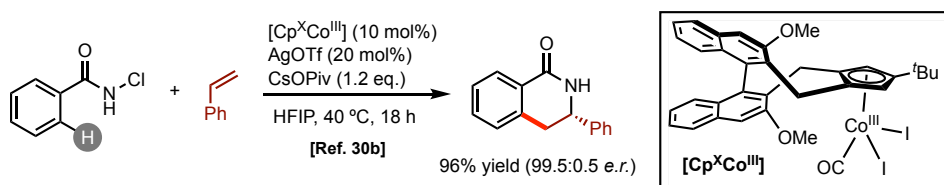

Scheme 1.18. Application of chiral Cp^X ligands in cobalt-catalyzed asymmetric synthesis.

[28] Pesciaioli, F.; Dhawa, U.; Oliveira, J. C. A.; Yin, R.; John, M.; Ackermann, L. "Enantioselective Cobalt(III)-Catalyzed C−H Activation Enabled by Chiral Carboxylic Acid Cooperation*" Angew. Chem. Int. Ed.* **2018**, *57*, 15425−15429.

[29] Ye, B.; Donets, P. A.; Cramer, N. "Chiral Cp-Rhodium(III)-Catalyzed Asymmetric Hydroarylations of 1,1-Disubstituted Alkenes" *Angew. Chem. Int. Ed.* **2014**, *53*, 507−511.

[30] (a) Smits, G.; Audic, B.; Wodrich, M. D.; Corminboeuf, C.; Cramer, N. "A β-Carbon elimination strategy for convenient in situ access to cyclopentadienyl metal complexes" *Chem. Sci.* **2017**, *8*, 7174−7179. (b) Ozols, K.; Jang, Y.-S.; Cramer, N. "Chiral Cyclopentadienyl Cobalt(III) Complexes Enable Highly Enantioselective 3d-Metal-Catalyzed C−H Functionalizations" *J. Am. Chem. Soc.* **2019**, *141*, 5675−5680.

Ackermann and co-workers have also applied Cp*Co[III] precatalysts to the late-stage functionalization of peptides (Scheme 1.19).[31] They reported an unprecedented cobalt(III)-catalyzed C−H allylation of a broad range of amino acids. This transformation has enormous potential for the bioorthogonal late-stage diversification of structurally complex peptides.
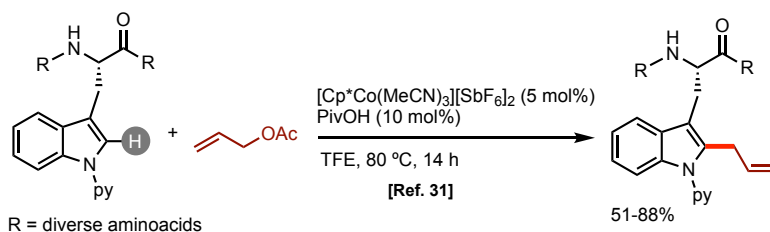

Scheme 1.19. Late-stage peptide functionalization with Cp*Co[III] catalyst.

1.3.1.2 C(*sp²*)−Heteroatom Bond-Forming Reactions

Although C−C bond forming reactions have received special attention in the context of Cp*Co[III]-catalyzed C−H functionalization reactions, multiple examples regarding C−heteroatom bond-forming reactions have been reported in the literature. Among them, the formation of C−N bonds, specially using dioxazolones as nitrogen sources, stands out. *N*-halide succinimides have been also employed as coupling partners for the introduction of halides in different organic scaffolds. In the context of C−chalcogen bonds, few methodologies have been recently reported for installing sulfur moieties such as thiolates or SCF$_3$. Figure 1.4 shows representative examples of these transformations. This includes the functionalization of organic scaffolds bearing as directing groups prevalent functional groups, such as ketones or amides. In this context, the employment of aldehydes remains practically unexplored.[32]

---

[31] Lorion, M. M.; Kaplaneris, N.; Son, J.; Kuniyil, R.; Ackermann, L. "Late-stage peptide diversification through cobalt-catalyzed C-H activation: Sequential multicatalysis for stapled peptides" *Angew. Chem. Int. Ed.* **2019**, *58*, 1684−1688.

[32] Tao. L.-M.; Li, C.-H.; Chen, J.; Liu, H. "Cobalt(III)-Catalyzed Oxidative Annulation of Benzaldehydes with Internal Alkynes via C−H Functionalization in Poly(ethylene glycol)" *J. Org. Chem*. **2019**, *84*, 6807−6812.
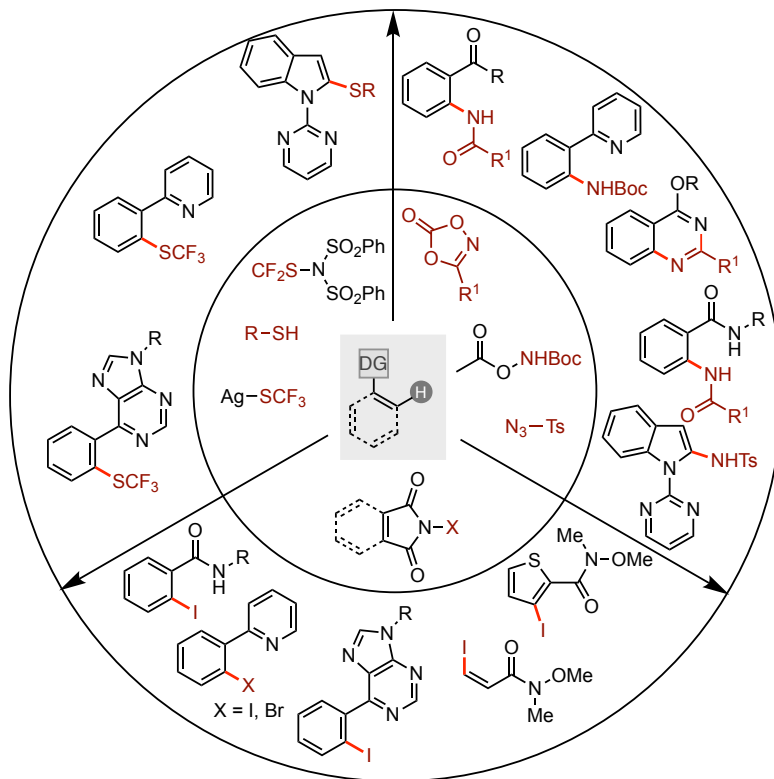
Figure 1.4. Selected Cp*Co^{III}-catalyzed C−heteroatom bond-forming reactions.

One of the few methodologies for the functionalization of aldehydes was presented by Li and co-workers.[33] They described the formation of a transient imine as DG by condensation of the aldehyde with an aniline derivative to overcome the challenges associated to the C−H metalation when using this functional group as auxiliary ligand. Using this approach, the authors were able to perform the C(sp^2)−H amidation with dioxazolone as nitrogen source. Subsequent hydrolysis of the imine with acid released the functionalized aldehyde (Scheme 1.20).
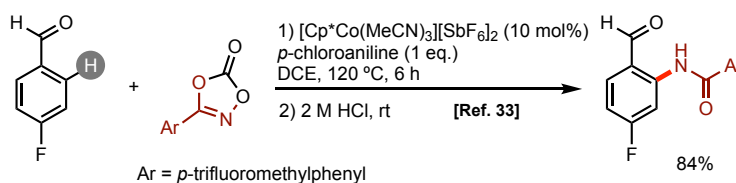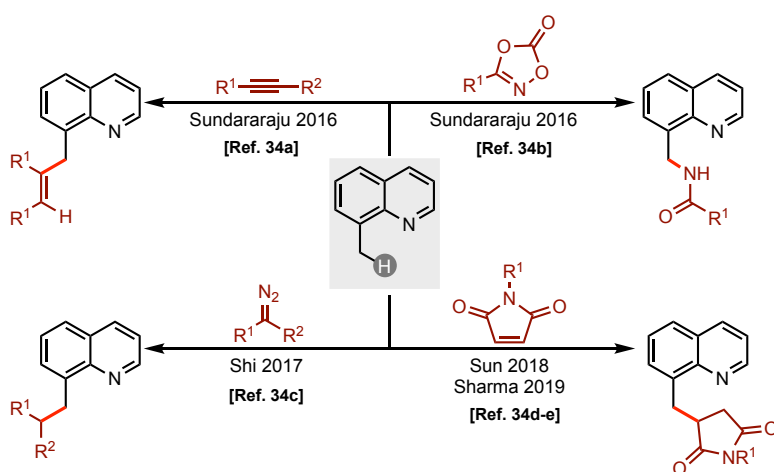

Scheme 1.20. C−H functionalization of aldehydes using transient directing groups.

[33] Huang, J.; Ding, J.; Ding, T.-M.; Zhang, S.; Wang, Y.; Sha, F.; Zhang, S.-Y.; Wu, X.-Y.; Li, Q. "Cobalt-Catalyzed Ortho-C(sp^2)-H Amidation of Benzaldehydes with Dioxazolones Using Transient Directing Groups" *Org. Lett.* **2019**, *21*, 7342−7345.

1.3.2 Cp*Co[III]-Catalyzed C(*sp³*)−H Functionalization Reactions

Compared to the Cp*Co[III]-catalyzed functionalization of aromatic C−H bonds, the conversion of C(*sp³*)−H into C(*sp³*)−C or C(*sp³*)−X is still very scarce.[34] The first example was reported by Sundararaju in 2016.[34a] The authors reported the alkenylation of 8-methylquinoline derivatives with alkynes. They observed very high regioselectivity and stereoselectivity, but the yield decreased considerably when using sterically hindered alkynes. Since then, different research groups have reported the functionalization of 8-methylquinoline-based substrates using diaxozolones, diazo-compounds and maleimides as coupling partners (Scheme 1.21).
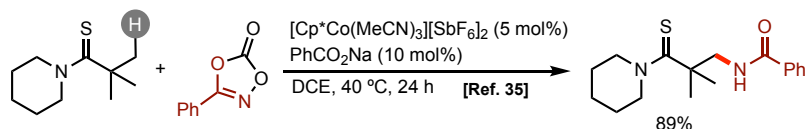

Scheme 1.21. Cp*Co[III]-catalyzed C(*sp³*)−H functionalization of 8-methylquinoline.

Interestingly, in 2017, Dixon and co-workers expanded the substrate scope to the C(*sp³*)−H functionalization of thioamides, using dioxazolones as nitrogen source (Scheme 1.22).[35]

[34] (a) Sen, M.; Emayavaramban, B.; Barsu, N.; Premkumar, J. R.; Sundararaju, B. "Cp*Co(III)-Catalyzed C(sp3)-H Bond Activation: A Highly Stereoselective and Regioselective Alkenylation of 8-Methylquinoline with Alkynes" *ACS Catal.* **2016**, *6*, 2792−2796. (b) Barsu, N.; Rahman, M. A.; Sen, M.; Sundararaju, B. "Cp*Co[III]-Catalyzed C(sp3)−H Bond Amidation of 8-methylquinoline" *Chem. Eur. J.* **2016**, *22*, 9135−9138. (c) Yan, S.-Y.; Ling, P.-X.; Shi, B.-F. "Cobalt(III)-Catalyzed Alkylation of Primary C(sp3)−H Bonds with Diazo Compounds" *Adv. Synth. Catal.* **2017**, *359*, 2912−2917. (d) Chen, X.-X.; Rn, J.-T.; Xu, J.-L.; Xie, H.; Sun, W.; Li, Y.-M.; Sun, M. "Cobalt(III)-Catalyzed 1,4-Addition of C(sp3)−H Bonds to Maleimides" *Synlett* **2018**, *29*, 1601−1606. (e) Kumar, R.; Kumar, R.; Chandra, D.; Sharma, U. "Cp*Co(III)-Catalyzed Alkylation of Primary and Secondary C(sp3)-H Bonds of 8-Alkylquinolines with Maleimides" *J. Org. Chem.* **2019**, *84*, 1542−11552.
[35] Tan, P. W.; Mak, A. M.; Sullivan, M. B.; Dixon, D. J.; Seayad, J. "Thioamide-Directed Cobalt(III)-Catalyzed Selective Amidation of C(sp3)−H Bonds" *Angew. Chem. Int. Ed*. **2017**, *56*, 16550−16554.

Scheme 1.22. Cp*Co[III]-catalyzed C(sp^3)−N bond formation.

In 2018, Matsunaga and Yoshino reported the enantioselective version of this reaction combining an achiral modified Cp*Co[III] precatalyst with a chiral carboxylic acid (CCA) as ligand.[36] Excellent enantiomeric ratios were obtained using *ortho*-dichlorobenzene (*o*DCB) as solvent, in the presence of a specific type of zeolites (MS13X) as additive (Scheme 1.23).
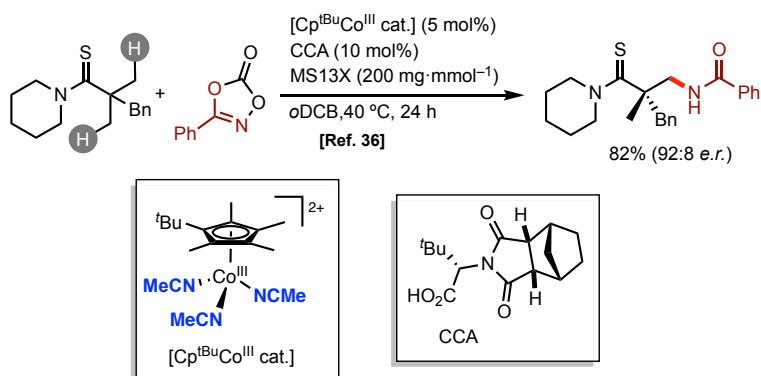
Scheme 1.23. Enantioselective version of the Cp*Co[III]-catalyzed C(sp^3)−N bond formation.

---

[36] Fukagawa, S.; Kato, Y.; Tanaka, R.; Kojima, M.; Yoshino, T.; Matsunaga, S. "Cobalt(III)/Chiral Carboxylic Acid-Catalyzed Enantioselective C(sp^3)−H Amidation of Thioamides" *Angew. Chem. Int. Ed*. **2019**, *58*, 1153−1157.

1.4 Mechanistic Picture of Cp*Co^{III}-Catalyzed C−H Functionalization Reactions

Along sections 1.2 and 1.3, Cp*Co^{III}-based precatalysts have been presented as a very appealing and attractive alternative to second and third-row transition metals for the functionalization of C−H bonds. However, when this doctoral thesis was started, there was a dramatic lack of fundamental knowledge of these transformations. This was associated to the hypothesized high reactivity of the transient cobalt species within the catalytic cycle, which prevented their isolation or even their detection in most cases. Therefore, these transformations were generally considered to proceed through mechanisms based on other noble transition metals, such as rhodium. As mentioned above, these catalytic cycles can be divided into three main stages (Figure 1.5): (i) a C−H activation step, where the targeted carbon-hydrogen bond is cleaved, and a new cobalt−carbon bond is formed through a cyclometalation reaction; (ii) a sequence of steps that involve the reaction of the putative cobaltacycle with the corresponding coupling partner; (iii) sometimes, regeneration of the catalyst into its active specie must occur, in order to close the catalytic cycle.
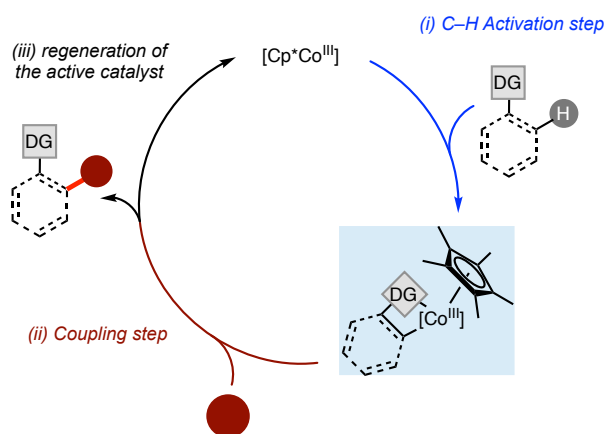

Figure 1.5. C−H functionalization reaction sequential steps.

In the next sections, we will discuss the mechanistic insights reported in the literature on these transformations, starting on the C−H metalation step.

1.4.1 C−H Activation Step

It is widely accepted that the first step of cobalt-catalyzed directed C−H functionalizations is a ligand-directed C−H bond activation at a Cp*Co^{III} center to afford a cyclometalated cobalt(III) intermediate. However, there is a crucial lack of understanding about this step. The mechanistic picture for the C−H metalation

relies almost exclusively on DFT calculations, supporting a CMD mechanisms in the presence of widely used carboxylate bases.[37]

In rhodium chemistry, after the C–H activation step, the resulting Cp*Rh[III] intermediates are really easily synthesized and characterized (Scheme 1.24a). Thanks to this, not only this elementary step has been investigated in detail, but also the resulting rhodacycles have been submitted to detailed kinetic investigations with different coupling partners.[38]

In stark contrast, the cobalt scenario was dramatically different at the beginning of this doctoral thesis. The proposed reversible nature of the C–H activation step and the lack of stabilizing ligands precluded the isolation of transient species proposed as the catalytically relevant (Scheme 1.24b). Therefore, the experimental mechanistic knowledge available on this step was limited to H/D exchange experiments, kinetic isotope effect (KIE) values and mass spectrometry (MS) analysis, which do not provide information at molecular level of the exact nature of the species involved. In addition, different computational studies have been carried out to partially alleviate the lack of understanding on this step.
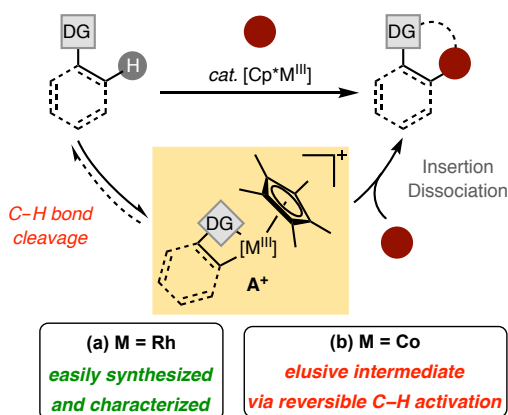

Scheme 1.24. Access to cyclometalated Cp*Rh[III] and Cp*Co[III] complexes by C–H activation.

[37] Davies, D. L.; Macgregor, S. A.; McMullin, C. L. "Computational Studies of Carboxylate-Assisted C–H Activation and Functionalization at Group 8-10 Transition Metal Centers" *Chem. Rev.* **2017**, *117*, 8649–8709.

[38] (a) Tauchert, M. E.; Incarvito, C. D.; Rheingold, A. L.; Bergman, R. G.; Ellman, J. A. "Mechanism of the Rhodium(III)-Catalyzed Arylation of Imines via C–H Bond Functionalization: Inhibition by Substrate" *J. Am. Chem. Soc*. **2012**, *134*, 1482–1485. (b) Brasse, M.; Cámpora, J.; Ellman, J. A.; Bergman, R. G. "Mechanistic Study of the Oxidative Coupling of Styrene with 2-Phenylpyridine Derivatives Catalyzed by Cationic Rhodium(III) via C–H Activation" *J. Am. Chem. Soc*. **2013**, *135*, 6427–6430. (c) Park, S. H.; Kwak, J.; Shin, K.; Ryu, J.; Park, Y.; Chang, S. "Mechanistic Studies of the Rhodium Catalyzed Direct C–H Amination Reaction Using Azides as the Nitrogen Source" *J. Am. Chem. Soc*. **2014**, *136*, 2492–2502. (d) Park, Y.; Park, K. T.; Kim, J. G.; Chang, S. "Mechanistic Studies on the Rh(III)-Mediated Amido Transfer Process Leading to Robust C–H Amination with a New Type of Amidating Reagent" *J. Am. Chem. Soc*. **2015**, *137*, 4534–4542.

The first mechanistic insight in a Cp*Co^{III}-catalyzed C−H functionalization was published by Kanai and co-workers in 2014.[25] They were the first ones to demonstrate the reversibility of the C−H cleavage in these transformations, by carrying out H/D scrambling experiments. Under the optimized catalytic reaction conditions, the authors monitored the deuterium insertion when using CD$_3$OD. They observed scrambling at the C2-position of the indole, demonstrating both the reversibility of the C−H activation and also an exquisite selectivity towards this position (Scheme 1.25).
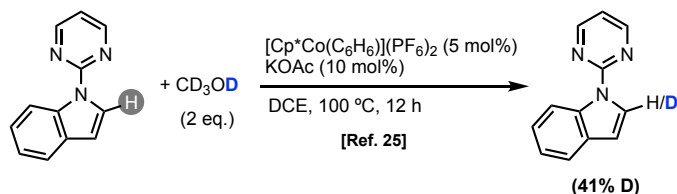
Scheme 1.25. Cp*Co^{III}-mediated indole H/D scrambling.

Another extremely useful technique for analyzing the C−H cleavage in the overall transformation is the kinetic isotope effect (KIE).[39] By comparison of the reaction rates when the C−H bond (K_H) is replaced by its isotope C−D (K_D), information can be withdrawn about the C−H bond-cleavage step. A primary KIE ($K_H/K_D > 2$) may be found when the substituted bond is being broken (or formed) during the rate-determining process. A secondary KIE (K_H/K_D between 1 and 1.4) can be observed when that bond is not broken (or formed), but the isotopically-labeled substrate is involved in the rate-determining process. When $K_H/K_D = 1$, it means that no KIE is observed in the transformation, and therefore, the cleavage or formation of that bond is irrelevant in the overall kinetics. Sometimes, an inverse KIE ($K_H/K_D < 1$) can be observed but it is usually limited to a few examples, like the reductive elimination of alkyl hydrides.

There are different ways of measuring a kinetic isotope effect. First, the reactions with unlabeled (C−H) and labelled (C−D) substrates are conducted independently. Another type of experiment involves an *inter*molecular competition between two different substrates in the same reaction flask. Finally, an *intra*molecular competition between a C−H bond and a C−D in the same substrate can be also performed. Among these scenarios, the only one that generally provides conclusive information about the C−H bond activation step is the first one.

---

[39] Simmons, E. M.; Hartwig, J. F. "On the Interpretation of Deuterium Kinetic Isotope Effect in C−H Bond Functionalizations by Transition-Metal Complexes" *Angew. Chem. Int. Ed.* **2012**, *51*, 3066−3072.

Ackermann and co-workers measured the kinetic isotope effect of the cyanation of 2-phenylpyridine and obtained a KIE of 1, when comparing independent reactions.[40] This value is in agreement with a kinetically irrelevant C−H metalation (Scheme 1.26a). On the other hand, the C−H amidation of oxazoline, following an analogue methodology, gave rise a KIE of 2.3, when comparing independent reactions.[41] Therefore, under these circumstances, C−H cleavage seemed to be rate-determining in the overall kinetics (Scheme 1.26b).

(a) C−H/D cyanation of 2-phenylpyridine

Cp*CoI$_2$(CO) (2.5 mol%)
AgSbF$_6$ (5 mol%)
KOAc (5 mol%)
DCE, 120 °C
[Ref. 40]

KIE = 1.0

(b) C−H/D amidation of oxazoline

Cp*CoI$_2$(CO) (5 mol%)
AgSbF$_6$ (20 mol%)
NaOAc (20 mol%)
DCE, 100 °C
[Ref. 41]

KIE = 2.3
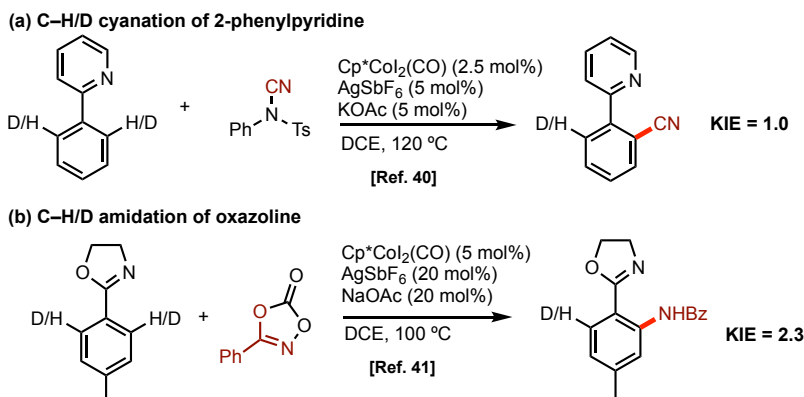
Scheme 1.26. Comparison of two methodologies with different KIE values.

In the absence of a kinetic isotope effect, like in Scheme 1.26a, it is not possible to get extract further information about the C−H bond cleavage, because of its lack of weight in the overall kinetics. On the other hand, in the scenarios with a KIE > 2, like in the example depicted in Scheme 1.26b, further experiments were performed to shine some light into the real nature of the C−H bond cleavage step (Scheme 1.27a).

The observation of H/D scrambling in the *ortho* position of the oxazoline, but only in absence of the coupling partner, suggested that the C−H cleavage step becomes irreversible when the whole catalytic cycle takes place. The addition of radical scavengers did not decrease the reaction yield, therefore a radical C−H activation was discarded. Moreover, in the intermolecular experiments between electronically diverse coupling partners, it turned out to be more reactive the substrates with electron-donating groups. All these results together suggested a **BIES** mechanism for the C−H bond cleavage step (Scheme 1.27b).

[40] Li, J.; Ackermann, L. "Cobalt-Catalyzed C−H Cyanation of Arenes and Heteroarenes" *Angew. Chem. Int. Ed.* **2015**, *54*, 3635−3638.
[41] Mei, R.; Loup, J.; Ackermann, L. "Oxazolinyl-Assisted C−H Amidation by Cobalt(III) Catalysis" *ACS Catal*. **2016**, *7*, 793−797.
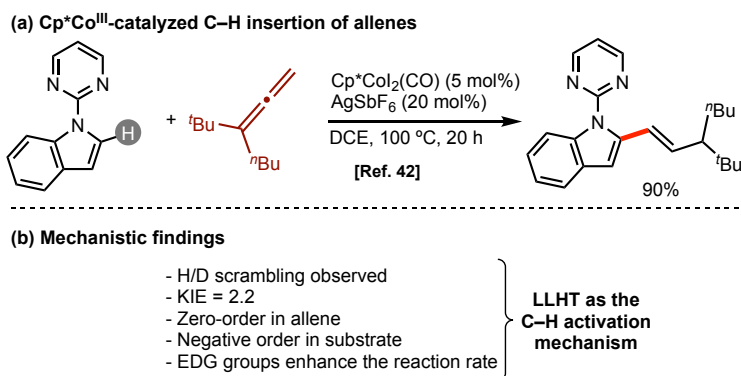
(a) Cp*Co^{III}-catalyzed C−N bond formation with dioxazolones

Reagents: Cp*CoI$_2$(CO) (5 mol%), AgSbF$_6$ (20 mol%), NaOAc (20 mol%), DCE, 100 ºC, 16 h **[Ref. 41]**

(b) Mechanistic findings

- H/D scrambling
- KIE = 2.3
- No radicals involved
- EDG groups enhance the reaction rate
- Presence of carboxylates

BIES as the C−H activation mechanism
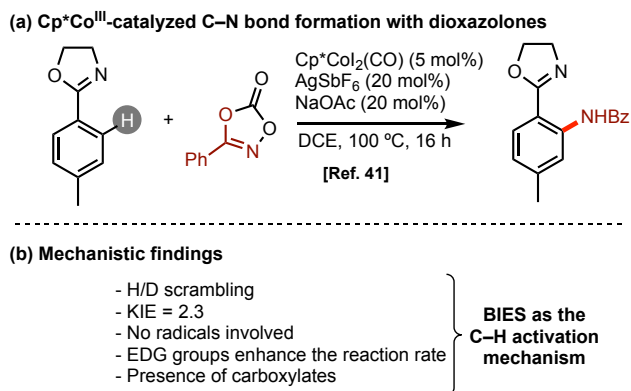
Scheme 1.27. Overview of the C−H bond cleavage of oxazolines with amidating reagents as coupling partners.

The Ackermann group also studied the mechanistic intricacies of the hydroarylation of arenes using allenes as coupling partners (Scheme 1.28).[42] Interestingly, this time the development of the methodology did not required the addition of external carboxylates. It was proposed that the substrate could also act as a surrogate base, promoting the C−H activation. After some mechanistic investigations, such as a KIE = 2.2 and a zero-order in allene, they suggested that the cyclometalation was the rate-determining step of the reaction. Unexpectedly, the kinetic order of the substrate was negative. This implies that a reversible dissociation of a second molecule of substrate in the coordination sphere of the metal is necessary, prior to the C−H bond cleavage. Next, the reaction of several substrates with different electronic properties was performed. They observed a faster reaction with more electron-deficient arenes. Given all this information, the authors proposed the C−H activation to be a ligand-to-ligand hydrogen transfer (**LLHT**), in analogy to literature precedents using nickel complexes.[43]

[42] Nakanowatari, S.; Mei, R.; Feldt, M.; Ackermann, L. "Cobalt(III)-Catalyzed Hydroarylation of Allenes via C−H Activation" *ACS Catal.* **2017**, *7*, 2511−2515.

[43] Guihaumé, J.; Halbert, S.; Eisenstein, O.; Perutz, R. N. "Hydrofluoroarylation of Alkynes with Ni Catalysts. C−H Activation via Ligand-to-Ligand Hydrogen Transfer, an Alternative to Oxidative Addition" *Organometallics* **2012**, *31*, 1300−1314.

(a) Cp*Co^{III}-catalyzed C−H insertion of allenes

(b) Mechanistic findings

- H/D scrambling observed
- KIE = 2.2
- Zero-order in allene
- Negative order in substrate
- EDG groups enhance the reaction rate

LLHT as the C−H activation mechanism

Scheme 1.28. Overview of the C−H hydroarylation of arenes with allenes.

In 2016, Glorius *et al.* investigated the effect of different additives in the C−H metalation step, changing the typically used silver salt by a Lewis acid (Scheme 1.29).[44] Using B(C$_6$F$_5$)$_3$ instead of AgSbF$_6$ they observed a higher H/D scrambling of a model imine. They proposed that the borane additive played two roles at the same time: the generation of the active Cp*Co^{III} species (by removal of the iodide ligands) and also acceleration of the C−H cleavage step.

(a) Cp*Co^{III}-catalyzed synthesis of isoquinolines

(b) Mechanistic findings

- H/D scrambling observed with B(C$_6$F$_5$)$_3$
- Extrusion of N$_2$ faster with B(C$_6$F$_5$)$_3$
- KIE = 1.1
- B(C$_6$F$_5$)$_3$ abstracts the iodide from the Cp*Co^{III} precatalyst

B(C$_6$F$_5$)$_3$ accelerates the formation of active cationic Co^{III} species
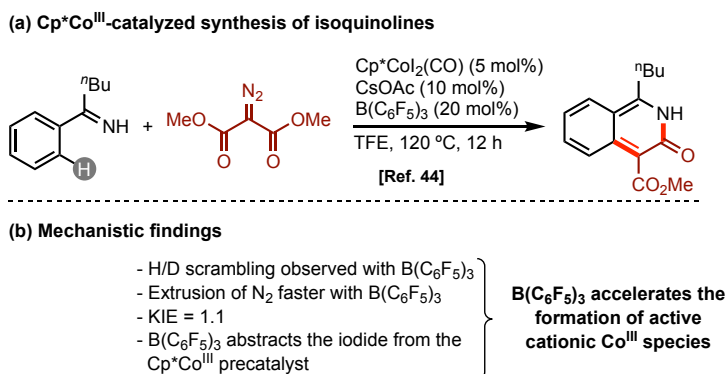
Scheme 1.29. Overview of the Cp*Co^{III}-mediated isoquinolines synthesis.

After this seminal work by Glorius, Chen and co-workers decided to study more in detail the role of this Lewis acid in the Cp*Co^{III}-catalyzed C−H/N−H activation.[45] Using DFT studies, they calculated the free energy associated to the formation of a wide variety of potential Cp*Co^{III} active species, in the context of this multicomponent catalytic system. Their results uncovered as the active catalyst a

---

[44] Kim, J. H.; Greßies, S.; Glorius, F. "Cooperative Lewis Acid/Cp*Co^{III} Catalyzed C−H Bond Activation for the Synthesis of Isoquinolin-3-ones" *Angew. Chem. Int. Ed.* **2016**, *55*, 5577−5581.

[45] Wang, Q.; Huang, F.; Jiang, L.; Zhang, C.; Sun, C.; Liu, J.; Chen, D. "Comprehensive Mechanistic Insight into Cooperative Lewis Acid/Cp*Co^{III}-Catalyzed C−H/N−H Activation for the Synthesis of Isoquinolin-3-ones" *Inorg. Chem.* **2018**, *57*, 2804−2814.

Cp*Co^{III} precatalyst bounded to two acetate ligands in a κ^2 and κ^1 fashion, with the latter one presenting a coordination to B(C$_6$F$_5$)$_3$ (highlighted in blue in Figure 1.6). However, their calculations discarded any acceleration effect of the studied borane in the C−H activation step *per se*. As observed in the Figure 1.6, the proposal of a sole Cp*Co^{III} active species is a very complex task, since several complexes can be depicted for the same chemical transformation. This is another obstacle in the way to understand any Cp*Co^{III}-catalyzed C−H functionalization reaction.
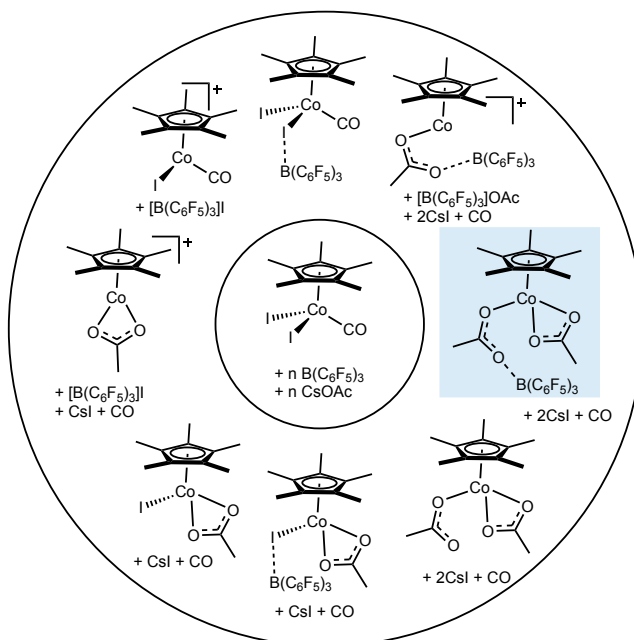
Figure 1.6. Computed Cp*Co^{III} active species by Chen and co-workers.

Apart from the characterization of possible active species, other computational simulations have also been done to further understand the C−H bond cleavage step. For example, Kanai and co-workers[25] simulated a carboxylate-assisted C−H bond activation using *N*-carbamoyl indoles as substrate. Different conformations and transition states (TS) were studied, taking into account both singlet and triplet-state structures, starting from a preformed Cp*Co^{III}(κ^2-acetate) complex with the substrate bonded through the oxygen atom of the carbamoyl moiety (Figure 1.7). It was found that the cleavage of one Co−O(acetate) bond, **TS(A-B)** (18.9 kcal/mol), and posterior rotation of the acetate, **TS(B-C)** (20.5 kcal/mol), were crucial in the overall pathway. The C−H activation was computed to happen through a concerted metalation-deprotonation, **TS(C-D)** (19.4 kcal/mol), in a six-membered transition state. Alternatively, a four-member transition state was calculated for this step, but it presented a higher free energy (36.5 kcal/mol). Triplet-state complexes were also simulated, and turned out to be very similar in energy, therefore, it was assumed

that the C−H activation could occur both by singlet- and triplet-state intermediates. The overall C−H activation process was found to be endergonic by 12.0 kcal/mol, which matches with an observable H/D scrambling experimentally and the lack of detection of Cp*Co^{III} cyclometalated species.
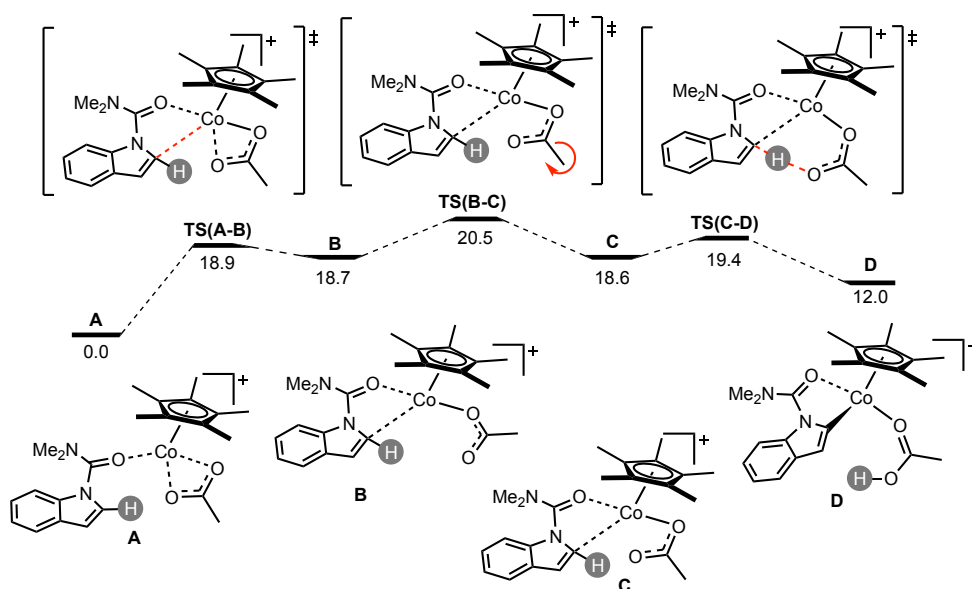
Figure 1.7. Full profile on the Cp*Co^{III}-mediated C−H bond activation by DFT calculations. Relative Gibbs free-energy diagram at 298.15 K (kcal/mol).

In alignment with this literature precedent, the vast majority of other research groups have proposed analogous Cp*Co^{III}-mediated C−H activation mechanisms, always in the presence of carboxylate salts.[46] However, we can find some exceptions to this common CMD mechanism.

As an example, and contrary to the traditional proposed mechanisms, Sundararaju proposed that the C(sp^3)−H cleavage of 8-methylquinoline takes place through an outer-sphere carboxylate-assisted cyclometalation.[34a] Supported by DFT modelling, they discarded the CMD mechanism in favor of an external deprotonation (Figure 1.8). Later, Seayad, Dixon and co-workers modelled the cleavage of a C(sp^3)−H bond for the amidation of thioamides.[35] Again, they also

[46] (a) Zhou, X.; Luo, Y.; Kong, L.; Xu, Y.; Zheng, G.; Lan, Y.; Li, X. "Cp*Co^{III}-Catalyzed Branch-Selective Hydroarylation of Alkynes via C−H Activation: Efficient Access to α-gem-Vinylindoles" *ACS Catal*. **2017**, *7*, 7296−7304. (b) Qu, S.; Cramer, C. J. "Mechanistic Study of Cp*Co^{III}/Rh^{III}-Catalyzed Directed C−H Functionalization with Diazo Compounds" *J. Org. Chem*. **2017**, *82*, 1195−1204. (c) Xing, Y.-Y.; Liu, J.-B.; Sun, C.-Z.; Huang, F.; Chen, D.-Z. "Mechanistic Exploration of Cp*Co^{III}/Rh^{III}-Catalyzed Carboamination/Olefination of N-Phenoxyacetamides with Alkenes" *Inorg. Chem*. **2018**, *57*, 10726−10735.

observed that an external carboxylate-assisted deprotonation was more likely in terms of free energy than the traditional CMD mechanism, being this 8.7 kcal/mol higher in energy.
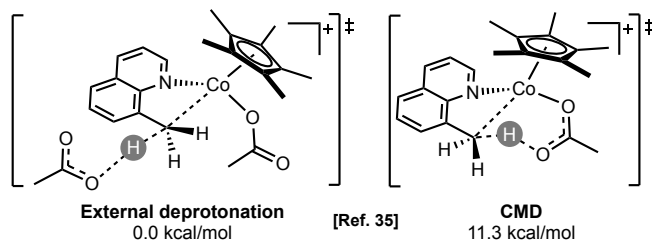
Figure 1.8. Comparison of C−H bond cleavage mechanisms by DFT by Sundararaju and co-workers.

1.4.2 Subsequent C−H Functionalization Steps

Prior to this doctoral thesis, there were very few literature precedents that provided chemical information on the whole Cp*Co^{III} C−H functionalization reaction mechanism. This is in alignment with section 1.4.1, because without information about the first step, the C−H activation reaction, it is even more challenging to understand the subsequent steps (i.e. coupling and regeneration steps) of the overall catalytic process.

In the absence of a reliable synthetic route via C−H metalation for accessing these cobalt intermediates, Kanai and co-workers envisioned an alternative route. They proposed a transmetalation of an organozinc compound with a well-known Cp*Co^{III} precursor, to obtain the cobalt metallacycle **2ppy-Co-Cl** (Scheme 1.30).[25] Unfortunately, this reaction presented several by-products and the cobaltacycle was obtained in low yield. Nevertheless, the Kanai group was able to isolate the desired cobalt complex in a scale that allowed them to characterize this cobaltacycle compound by X-ray crystallography. This neutral compound, **2ppy-Co-Cl**, is a surrogate of the putative reactive intermediate, since it can be formed by addition of a silver salt.
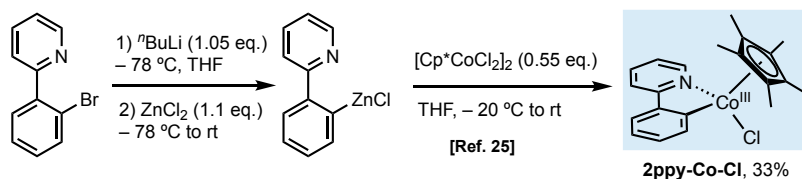
Scheme 1.30. Kanai group alternative route for the isolation of the first Cp*Co[III] metallacycle, **2ppy-Co-Cl**.

The same group applied, for the first time, computational chemistry to the understanding of Cp*Co[III] C−H functionalization reactions. First, they sought to understand the source of chemodivergence between rhodium and cobalt systems. Natural population analysis of analogue rhodium and cobalt cyclometalated species exhibited a key difference between the two metals. In the cobalt metallacycle, the aryl−cobalt bond turned out to be much more polarized in comparison with rhodium. The higher nucleophilicity of the carbon linked to cobalt is thought to be the source of divergence in reactivity in some of the Cp*Co[III]− catalyzed C−H functionalization reactions (Figure 1.9).

[Ref. 25]

Co–C bond more polarized than Rh–C
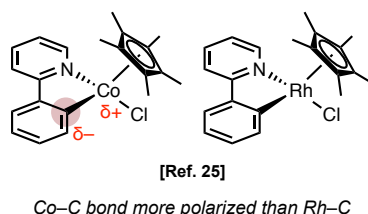
Figure 1.9. Polarization of the M−C bond for cobalt and rhodium metallacycles.

Inspired by this literature precedent, Chang and co-workers used **2ppy-Co-Cl** to interrogate its competence as precatalyst in C−H amidation reactions using phenyl dioxazolones as nitrogen source (Scheme 1.31a).[47] The formation of the desired product in excellent yield suggested that this type of species are involved in the catalytic cycle as cationic species. Moreover, they decided to study the reactivity of this compound with the amidating agent used in catalysis. Interestingly, they were able to detect, by MS analysis, a post C−H activation species, presumably formed after the dioxazolone insertion (Scheme 1.31b).

---

[47] Park, J.; Chang, S. "Comparative Catalytic Activity of Group 9 [Cp*M[III]] Complexes: Cobalt-Catalyzed C− H Amidation of Arenes with Dioxazolones as Amidating Reagents" *Angew. Chem. Int. Ed.* **2015**, *54*, 14103−14107.

(a) Involvement of cobalt metallacyclic species in catalysis
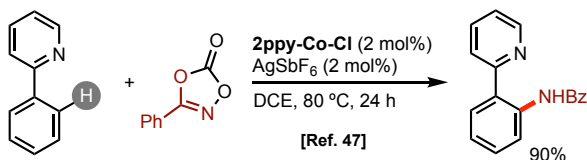
(b) Detection of amido-inserted species

Detected by MS
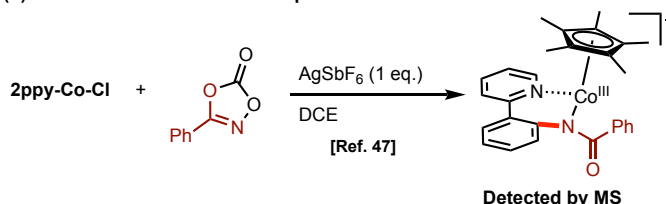
Scheme 1.31. Application of **2ppy-Co-Cl** in the mechanistic investigations of Cp*Co[III]-mediated C−N bond forming reactions.

Another unprecedented post C−H metalation species was found by Sundararaju and co-workers, in the allenylation reaction shown in Scheme 1.32.[48] They were able to synthesize and fully characterize a post-migratory insertion organometallic complex. Unfortunately, this compound turned out to be catalytically inactive under the optimized reaction conditions.

Detected by NMR/XRD/MS
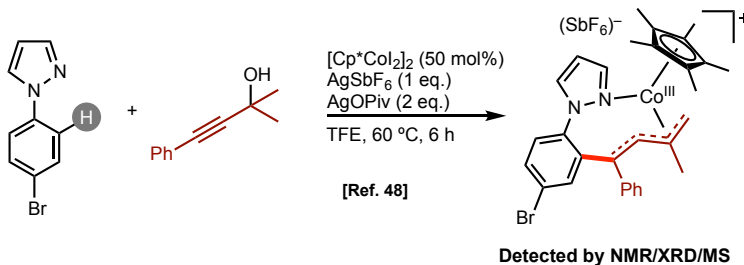
Scheme 1.32. Catalytically inactive post C−H activation Cp*Co[III] intermediate.

During the investigation of Cp*Co[III]-mediated alkenylation of indoles, Li and co-workers proposed by ESI-TOF a hypothetic cyclometalated cobalt species, formed right after the C−H activation reaction. They also proposed that this cyclometalation had to happen through a concerted metalation-deprotonation, using pivalate as base (Scheme 1.33).[49]

[48] Sen, M.; Dahiya, P.; Premkumar, J. R.; Sundararaju, B. "Dehydrative Cp*Co(III)-Catalyzed C−H Bond Allenylation" *Org. Lett.* **2017**, *19*, 3699−3702.
[49] Zhou, X.; Luo, Y.; Kong, L.; Xu, Y.; Zheng, G.; Lan, Y.; Li, X. "Cp*Co[III]-Catalyzed Branch-Selective Hydroarylation of Alkynes via C−H Activation: Efficient Access to α-gem-Vinylindoles" *ACS Catal.* **2017**, *7*, 7296−7304.
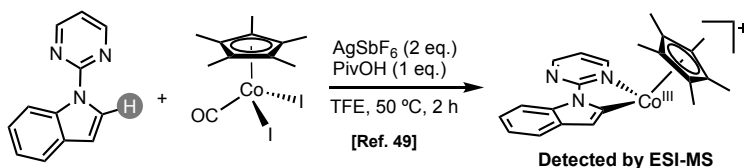
Scheme 1.33. Cobaltacycle detection by mass spectrometry.

In 2017, Ackermann and co-workers reported one of the few mechanistic and computational studies in the context of Cp*Co catalysis. (Scheme 1.34).[27] They described the regioselective C−H alkylation of aromatic rings, using alkenes as coupling partners. Understanding the C−H cleavage step allowed them to design the proper reaction conditions for the obtention of the linear or branched product. They performed several kinetic analyses to get further information of these two transformations. First, they obtained the kinetic orders of substrate and catalyst in both reactions. In the linear-selective insertion, there was a first-order dependence on substrate and catalyst. Interestingly, in the branched-selective insertion, the substrate featured a zero-order dependence. Moreover, doing temperature-dependent kinetic analyses, they were able to obtain experimental activation barriers.

(a) Additive-controlled regioselective C−H alkylation of indoles
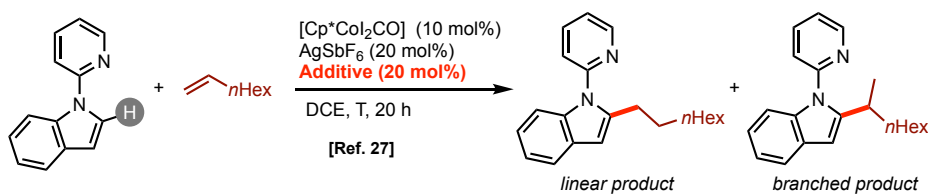
(b) Mechanistic findings

Linear product (no additive)
-H/D scrambling observed
-KIE = 1.2
-First-order dependence on substrate

Branched product (+ additive)
-H/D scrambling observed
-KIE = 1.7
-Zero-order dependence on substrate
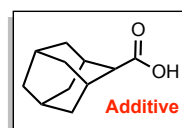
Additive

Scheme 1.34. Mechanistic investigations on the additive-controlled regioselective C−H alkylation of indoles.

In addition to these experimental mechanistic investigations, DFT studies were performed that provided two different mechanistic scenarios. For the linear product formation, without additive, the selectivity determining step turned out to be a concerted proto-demetallation/cyclometalation mediated by another molecule of substrate (Scheme 1.35). This mechanism was coined as a ligand-to-ligand hydrogen transfer, or **LLHT**.
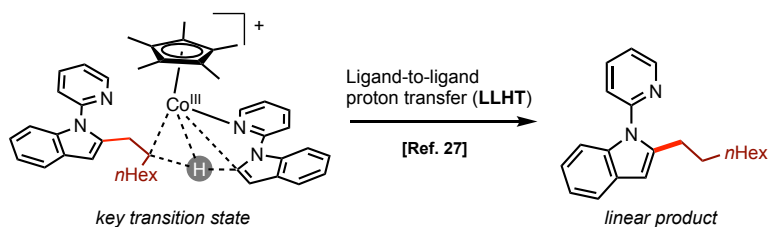
Scheme 1.35. Key transition state for the linear-selective Cp*Co[III]-catalyzed C−H alkylation.

In stark contrast, in the branch-selective transformation, the rate-determining step was proposed to be the proto-demetallation facilitated by a bulky carboxylic acid as additive (Scheme 1.36). Competitive experiments in this last scenario demonstrated a positive trend towards electron-rich arenes, providing support for a **BIES** mechanism in the C−H activation step. The understanding of these two possible C−H activation mechanisms turned out to be decisive in the development of a selective methodology to obtain a linear or branched alkylation.
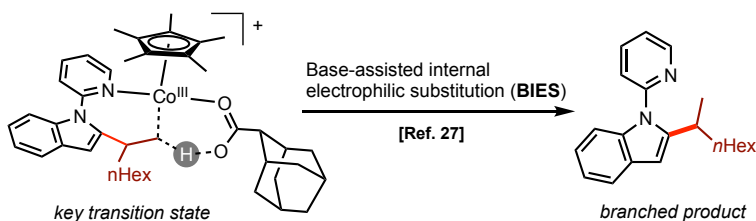
Scheme 1.36. Key transition state for the branched-selective Cp*Co[III]-catalyzed C−H alkylation.

In summary, as discussed in this section, the mechanistic intricacies of Cp*Co[III]-catalyzed C−H functionalization reactions have been seen as a "black box" since its beginning in 2013. Due to the limited understanding of these reactions at the molecular level, the vast majority of mechanistic proposals have been built upon comparison with other noble metals, such as rhodium or palladium. Although this limitation has been partially tackled by DFT calculations, the lack of proper strategies for the isolation or detection of metallacyclic intermediates still remains unsolved.

Motivated by the lack of information in both C−H activation and coupling reactions, we started to study the reliable access to key intermediates. The dearth of mechanistic information is of critical relevance for the future of the field, since it could condemn Cp*Co[III] catalysis to solely rely on extensive screenings and serendipitous discoveries.

1.5 References

[1] The Nobel Prize in Chemistry 2010. Press Release. 6 October 2010. https://www.nobelprize.org/prizes/chemistry/2010/press-release/ (accessed Dec 16, 2019).

[2] Arndtsen, B. A.; Bergman, R. G.; Mobley, T. A.; Peterson, T. H. "Selective Intermolecular Carbon-Hydrogen Activation by Synthetic Metal Complexes in Homogeneous Solution" *Acc. Chem. Res*. **1995**, *28*, 154−162.

[3] (a) Ackermann, L. "Carboxylate-Assisted Transition-Metal-Catalyzed C−H Bond Functionalizations: Mechanism and Scope" *Chem. Rev*. **2011**, *111*, 1315−1345. (b) Balcells, D.; Clot, E.; Eisenstein, O. "C−H Bond Activation in Transition Metal Species from a Computational Perspective" *Chem. Rev*. **2011**, *110*, 749−823. (c) Labinger, J. A.; Bercaw, J. E. "Understanding and exploiting C−H bond activation" *Nature* **2002**, *417*, 504−514.

[4] Labinger, J. A. "Tutorial on Oxidative Addition" *Organometallics* **2015**, *34*, 4784−4795.

[5] Waterman, R. "σ-bond metathesis: A 30-year retrospective" *Organometallics* **2013**, *32*, 7249−7263.

[6] Galabov, B.; Nalbantova, D.; Schleyer, P. von R.; Schaefer, H. F. "Electrophilic Aromatic Substitution: New Insights into an Old Class of Reactions" *Acc. Chem. Res.* **2016**, *49*, 1191−1199.

[7] Wheland, G. W. "A Quantum Mechanical Investigation of the Orientation of Substituents in Aromatic Molecules" *J. Am. Chem. Soc*. **1942**, *64*, 900−908.

[8] Oxgaard, J.; Tenn, W. J.; Nielsen, R. J.; Periana, R. A.; Goddard, W. A. "Mechanistic Analysis of Iridium Heteroatom C−H Activation: Evidence for an Internal Electrophilic Substitution Mechanism" *Organometallics* **2007**, *26*, 1565−1567.

[9] Lapointe, D.; Fagnour, K. "Overview of the Mechanistic Work on the Concerted Metallation-Deprotonation Pathway" *Chem. Lett*. **2010**, *39*, 1118−1126.

[10] Boutadla, Y.; Davies, D. L.; Macgregor, S. A.; Poblador-Bahamonde, A. I. "Mechanisms of C−H bond activation: rich synergy between computation and experiment" *Dalton Trans*. **2009**, *30*, 5820−5831.

[11] Ma, W.; Mei, R.; Tenti, G.; Ackermann, L. "Ruthenium(II)-Catalyzed Oxidative C−H Alkenylations of Sulfonic Acids, Sulfonyl Chlorides and Sulfonamides" *Chem. Eur. J*. **2014**, *20*, 15248−15251.

[12] Murai, S.; Kakiuchi, F.; Sekine, S.; Tanaka, Y.; Kamatani, A.; Sonoda, M.; Chatani, N. "Efficient catalytic addition of aromatic carbon-hydrogen bonds to olefins" *Nature* **1993**, *366*, 529−531.

[13] (a) Leow, D.; Li, G.; Mei, T.-S.; Yu, J.-Q. "Activation of remote *meta*-C−H bond assisted by an end-on template" *Nature* **2012**, *486*, 518−522. (b) Tang, R.; Li, G.; Yu, J.-Q. "Conformation-induced remote *meta*-C−H activation of amines" *Nature* **2014**, *507*, 215−220. (c) Dey, A.; Sinha, S. K.; Achar, T. K.; Maiti, D. "Accessing Remote *meta*- and *para*-C(sp^2)-H Bonds with Covalently Attached Directing Groups" *Angew. Chem. Int. Ed*. **2019**, *58*, 10820−10843.

[14] (a) Ritleng, V.; Sirlin, C.; Pfeffer, M. "Ru-, Rh-, and Pd-Catalyzed C−C Bond Formation Involving C−H Activation and Addition on Unsaturated Substrates: Reactions and Mechanistic Aspects" *Chem. Rev*. **2002**, *102*, 1731−1769. (b) Wencel-Delord, J.; Glorius, F. "C−H Bond Activation Enables the Rapid Construction and Late-State Diversification of Functional Molecules" *Nat. Chem*. **2013**, *5*, 369−375. (c) Yamaguchi, J.; Yamaguchi, A. D.; Itami, K. "C−H Bond Functionalization: Emerging Synthetic Tools for Natural Products and Pharmaceuticals" *Angew. Chem. Int. Ed.* **2012**, *51*, 8960−9009.

[15] Encyclopædia Britannica. Cobalt. https://www.britannica.com/science/cobalt-chemical-element (accessed 18 Dec, 2019).

[16] Lide, D. R. CRC Handbook of Chemistry and Physics; CRC Press: Boca Raton, 2005; Section 14, Geophysics, Astronomy, and Acoustics; Abundance of Elements in the Earth's Crust and in the Sea.

[17] Murahashi, S. "Synthesis of Phthalimidines from Schiff Bases and Carbon Monoxide" *J. Am. Chem. Soc*. **1955**, *77*, 6403−6404.

[18] Halbritter, G.; Knoch, F.; Wolski, A.; Kisch, H. "Functionalization of Aromatic Azo Compounds by the Cobalt-Catalyzed Regioselective Double Addition of Tolane: 2,6-Distilbenzylazobenzenes and 2,3-Dihydrocinnolines" *Angew. Chem. Int. Ed.* **1994**, *33*, 1603−1605.

[19] Gao, K.; Lee, P.-S.; Fujita, T.; Yoshikai, N. "Cobalt-catalyzed Hydroarylation of Alkynes through Chelation-Assisted C−H Bond Activation" *J. Am. Chem. Soc.* **2010**, *132*, 12249−12251.

[20] Chen, Q.; Illies, L.; Nakamura, E. "Cobalt-Catalyzed *ortho*-Alkylation of Secondary Benzamide with Alkyl Chloride through Directed C−H Bond Activation" *J. Am. Chem. Soc.* **2011**, *133*, 428−429.

[21] (a) Gao, K.; Yoshikai, N. "Low-Valent Cobalt Catalysis: New Opportunities for C−H Functionalization" *Acc. Chem. Res.* **2014**, *47*, 1208−1219. (b) Moselage, M.; Li, J.; Ackermann, L. "Cobalt-Catalyzed C−H Activation" *ACS. Catal.* **2016**, *6*, 498−525.

[22] (a) Grigorjeva, L.; Daugulis, O. "Cobalt-Catalyzed, Aminoquinoline-Directed C(sp^2)−H Bond Alkenylation by Alkynes" *Angew. Chem. Int. Ed.* **2014**, *53*, 10209−10212. (b) Kommagalla, Y.; Chatani, N. "Cobalt(II)-catalyzed C−H functionalization using an *N,N'*-bidentate directing group" *Coord. Chem. Rev.* **2017**, *350*, 117−135.

[23] Yoshino, T.; Ikemoto, H.; Matsunaga, S.; Kanai, M. "A Cationic High-Valent Cp*Co^{III} Complex for the Catalytic Generation of Nucleophilic Organometallic Species: Directed C−H Bond Activation" *Angew. Chem. Int. Ed.* **2013**, *52*, 2207−2211.

[24] (a) Wei, D.; Zhu, X.; Niu, J-L.; Song, M.-P. "High-valent-cobalt-catalyzed C−H functionalization based on concerted metalation-deprotonation and single-electron transfer mechanisms" *ChemCatChem* **2016**, *8*, 1242−1263. (b) Wang, S.; Chen, S-Y.; Yu, X-Q. "C-H functionalization by high-valent Cp*Co(iii) catalysis" *Chem. Commun.* **2017**, *53*, 3165−3180. (c) Chirila, P. G.; Whiteoak, C. J. "Recent advances using [Cp*Co(CO)I$_2$] catalysts as a powerful tool for C−H functionalisation" *Dalton Trans.* **2017**, *46*, 9721−9739. (d) Yoshino, T.; Matsunaga, S. "(Pentamethylcyclopentadienyl)cobalt(III)-catalyzed C-H bond functionalization: from discovery to unique reactivity and selectivity" *Adv. Synth. Catal.* **2017**, *359*, 1245−1262. (e) Prakash, S.; Kuppusamy, R.; Cheng, C.-H. "Cobalt-catalyzed annulation reactions via C−H bond activation" *ChemCatChem* **2018**, *10*, 683−705. (f) Ghorai, J.; Anbarasan, P. "Developments in Cp*Co^{III}-Catalyzed C−H Bond Functionalizations" *Asian J. Org. Chem.* **2019**, *8*, 430−455. (g) Baccalini, A.; Vergura, S.; Dolui, P.; Zanoni, G.; Maiti, D. "Recent Advances in Cobalt-Catalysed C−H Functionalizations" *Org. Biomol. Chem.* **2019**, *17*, 10119−10141.

[25] Ikemoto, H.; Yoshino, T.; Sakata, K.; Matsunaga, S.; Kanai, M. "Pyrroloindolone Synthesis via a Cp*Co^{III}-Catalyzed Redox-Neutral Directed C−H Alkenylation/Annulation Sequence" *J. Am. Chem. Soc.* **2014**, *136*, 5424−5431.

[26] (a) Boerth, J. A.; Hummer, J. R.; Ellman, J. A. "Highly stereoselective cobalt(III)-catalyzed three component C−H bond addition cascade" *Angew. Chem. Int. Ed.* **2016**, *55*, 12650−12654. (b) Boerth, J. A.; Maity, S.; William, S. K.; Mercado, B. Q.; Ellman, J. A. "Selective and synergistic cobalt(III)-catalysed three-component C−H bond addition to dienes and aldehydes" *Nat. Catal.* **2018**, *1*, 673−679. (b) Dongbang, S.; Shen, Z.; Ellman, J. A. "Synthesis of Homoallylic Alcohols with Acyclic Quaternary Centers through Co^{III}-Catalyzed Three-Component C−H Bond Addition to Internally Substituted Dienes and Carbonyls" *Angew. Chem. Int. Ed.* **2019**, *58*, 12590−12594.

[27] Zell, D.; Bursch, M.; Müller, V.; Grimme, S.; Ackermann, L. "Full Selectivity Control in Cobalt(III)-Catalyzed C−H Alkylations by Switching of the C−H Activation Mechanism" *Angew. Chem. Int. Ed.* **2017**, *56*, 10378−10382.

[28] Pesciaioli, F.; Dhawa, U.; Oliveira, J. C. A.; Yin, R.; John, M.; Ackermann, L. "Enantioselective Cobalt(III)-Catalyzed C−H Activation Enabled by Chiral Carboxylic Acid Cooperation" *Angew. Chem. Int. Ed.* **2018**, *57*, 15425−15429.

[29] Ye, B.; Donets, P. A.; Cramer, N. "Chiral Cp-Rhodium(III)-Catalyzed Asymmetric Hydroarylations of 1,1-Disubstituted Alkenes" *Angew. Chem. Int. Ed.* **2014**, *53*, 507−511.

[30] (a) Smits, G.; Audic, B.; Wodrich, M. D.; Corminboeuf, C.; Cramer, N. "A β-Carbon elimination strategy for convenient in situ access to cyclopentadienyl metal complexes" *Chem. Sci.* **2017**, *8*, 7174–7179. (b) Ozols, K.; Jang, Y.-S.; Cramer, N. "Chiral Cyclopentadienyl Cobalt(III) Complexes Enable Highly Enantioselective 3d-Metal-Catalyzed C−H Functionalizations" *J. Am. Chem. Soc*. **2019**, *141*, 5675−5680.

[31] Lorion, M. M.; Kaplaneris, N.; Son, J.; Kuniyil, R.; Ackermann, L. "Late-stage peptide diversification through cobalt-catalyzed C-H activation: Sequential multicatalysis for stapled peptides" *Angew. Chem. Int. Ed.* **2019**, *58*, 1684−1688.

[32] Tao. L.-M.; Li, C.-H.; Chen, J.; Liu, H. "Cobalt(III)-Catalyzed Oxidative Annulation of Benzaldehydes with Internal Alkynes via C−H Functionalization in Poly(ethylene glycol)" *J. Org. Chem*. **2019**, *84*, 6807−6812.

[33] Huang, J.; Ding, J.; Ding, T.-M.; Zhang, S.; Wang, Y.; Sha, F.; Zhang, S.-Y.; Wu, X.-Y.; Li, Q. "Cobalt-Catalyzed Ortho-C(sp^2)-H Amidation of Benzaldehydes with Dioxazolones Using Transient Directing Groups" *Org. Lett*. **2019**, *21*, 7342−7345.

[34] (a) Sen, M.; Emayavaramban, B.; Barsu, N.; Premkumar, J. R.; Sundararaju, B. "Cp*Co(III)-Catalyzed C(sp^3)-H Bond Activation: A Highly Stereoselective and Regioselective Alkenylation of 8-Methylquinoline with Alkynes" *ACS Catal*. **2016**, *6*, 2792−2796. (b) Barsu, N.; Rahman, M. A.; Sen, M.; Sundararaju, B. "Cp*Co^{III}-Catalyzed C(sp^3)−H Bond Amidation of 8-methylquinoline" *Chem. Eur. J*. **2016**, *22*, 9135−9138. (c) Yan, S.-Y.; Ling, P.-X.; Shi, B.-F. "Cobalt(III)-Catalyzed Alkylation of Primary C(sp^3)−H Bonds with Diazo Compounds" *Adv. Synth. Catal*. **2017**, *359*, 2912−2917. (d) Chen, X.-X.; Rn, J.-T.; Xu, J.-L.; Xie, H.; Sun, W.; Li, Y.-M.; Sun, M. "Cobalt(III)-Catalyzed 1,4-Addition of C(sp^3)−H Bonds to Maleimides" *Synlett* **2018**, *29*, 1601−1606. (e) Kumar, R.; Kumar, R.; Chandra, D.; Sharma, U. "Cp*Co(III)-Catalyzed Alkylation of Primary and Secondary C(sp^3)-H Bonds of 8-Alkylquinolines with Maleimides" *J. Org. Chem*. **2019**, *84*, 1542−11552.

[35] Tan, P. W.; Mak, A. M.; Sullivan, M. B.; Dixon, D. J.; Seayad, J. "Thioamide-Directed Cobalt(III)-Catalyzed Selective Amidation of C(sp^3)−H Bonds" *Angew. Chem. Int. Ed*. **2017**, *56*, 16550−16554.

[36] Fukagawa, S.; Kato, Y.; Tanaka, R.; Kojima, M.; Yoshino, T.; Matsunaga, S. "Cobalt(III)/Chiral Carboxylic Acid-Catalyzed Enantioselective C(sp^3)−H Amidation of Thioamides" *Angew. Chem. Int. Ed*. **2019**, *58*, 1153−1157.

[37] Davies, D. L.; Macgregor, S. A.; McMullin, C. L. "Computational Studies of Carboxylate-Assisted C−H Activation and Functionalization at Group 8-10 Transition Metal Centers" *Chem. Rev*. **2017**, *117*, 8649−8709.

[38] (a) Tauchert, M. E.; Incarvito, C. D.; Rheingold, A. L.; Bergman, R. G.; Ellman, J. A. "Mechanism of the Rhodium(III)-Catalyzed Arylation of Imines via C−H Bond Functionalization: Inhibition by Substrate" *J. Am. Chem. Soc*. **2012**, *134*, 1482−1485. (b) Brasse, M.; Cámpora, J.; Ellman, J. A.; Bergman, R. G. "Mechanistic Study of the Oxidative Coupling of Styrene with 2-Phenylpyridine Derivatives Catalyzed by Cationic Rhodium(III) via C−H Activation" *J. Am. Chem. Soc*. **2013**, *135*, 6427−6430. (c) Park, S. H.; Kwak, J.; Shin, K.; Ryu, J.; Park, Y.; Chang, S. "Mechanistic Studies of the Rhodium Catalyzed Direct C−H Amination Reaction Using Azides as the Nitrogen Source" *J. Am. Chem. Soc*. **2014**, *136*, 2492−2502. (d) Park, Y.; Park, K. T.; Kim, J. G.; Chang, S. "Mechanistic Studies on the Rh(III)-Mediated Amido Transfer Process Leading to Robust C−H Amination with a New Type of Amidating Reagent*" J. Am. Chem. Soc*. **2015**, *137*, 4534−4542.

[39] Simmons, E. M.; Hartwig, J. F. "On the Interpretation of Deuterium Kinetic Isotope Effect in C−H Bond Functionalizations by Transition-Metal Complexes" *Angew. Chem. Int. Ed*. **2012**, *51*, 3066−3072.

[40] Li, J.; Ackermann, L. "Cobalt-Catalyzed C−H Cyanation of Arenes and Heteroarenes" *Angew. Chem. Int. Ed*. **2015**, *54*, 3635−3638.

[41] Mei, R.; Loup, J.; Ackermann, L. "Oxazolinyl-Assisted C−H Amidation by Cobalt(III) Catalysis" *ACS Catal*. **2016**, *7*, 793−797.

[42] Nakanowatari, S.; Mei, R.; Feldt, M.; Ackermann, L. "Cobalt(III)-Catalyzed Hydroarylation of Allenes via C−H Activation" *ACS Catal.* **2017**, *7*, 2511−2515.

[43] Guihaumé, J.; Halbert, S.; Eisenstein, O.; Perutz, R. N. "Hydrofluoroarylation of Alkynes with Ni Catalysts. C−H Activation via Ligand-to-Ligand Hydrogen Transfer, an Alternative to Oxidative Addition" *Organometallics* **2012**, *31*, 1300−1314.

[44] Kim, J. H.; Greßies, S.; Glorius, F. "Cooperative Lewis Acid/Cp*Co[III] Catalyzed C−H Bond Activation for the Synthesis of Isoquinolin-3-ones" *Angew. Chem. Int. Ed.* **2016**, *55*, 5577−5581.

[45] Wang, Q.; Huang, F.; Jiang, L.; Zhang, C.; Sun, C.; Liu, J.; Chen, D. "Comprehensive Mechanistic Insight into Cooperative Lewis Acid/Cp*Co[III]-Catalyzed C−H/N−H Activation for the Synthesis of Isoquinolin-3-ones" *Inorg. Chem.* **2018***, 57*, 2804−2814.

[46] (a) Zhou, X.; Luo, Y.; Kong, L.; Xu, Y.; Zheng, G.; Lan, Y.; Li, X. "Cp*Co[III]-Catalyzed Branch-Selective Hydroarylation of Alkynes via C−H Activation: Efficient Access to α-gem-Vinylindoles" *ACS Catal*. **2017**, *7*, 7296−7304. (b) Qu, S.; Cramer, C. J. "Mechanistic Study of Cp*Co[III]/Rh[III]-Catalyzed Directed C−H Functionalization with Diazo Compounds" *J. Org. Chem*. **2017**, *82*, 1195−1204. (c) Xing, Y.-Y.; Liu, J.-B.; Sun, C.-Z.; Huang, F.; Chen, D.-Z. "Mechanistic Exploration of Cp*Co[III]/Rh[III]-Catalyzed Carboamination/Olefination of N-Phenoxyacetamides with Alkenes" *Inorg. Chem*. **2018**, *57*, 10726−10735.

[47] Park, J.; Chang, S. "Comparative Catalytic Activity of Group 9 [Cp*M[III]] Complexes: Cobalt-Catalyzed C−H Amidation of Arenes with Dioxazolones as Amidating Reagents" *Angew. Chem. Int. Ed.* **2015**, *54*, 14103−14107.

[48] Sen, M.; Dahiya, P.; Premkumar, J. R.; Sundararaju, B. "Dehydrative Cp*Co(III)-Catalyzed C−H Bond Allenylation" *Org. Lett*. **2017**, *19*, 3699−3702.

[49] Zhou, X.; Luo, Y.; Kong, L.; Xu, Y.; Zheng, G.; Lan, Y.; Li, X. "Cp*Co[III]-Catalyzed Branch-Selective Hydroarylation of Alkynes via C−H Activation: Efficient Access to α-gem-Vinylindoles" *ACS Catal*. **2017**, *7*, 7296−7304.

Chapter 2

Objectives

The main goals of this Doctoral Thesis are:

1. Development of a novel synthetic approach for accessing direct analogues of widely invoked Cp*Co^{III} intermediates (**A$^+$**) and employment of different physical organic tools such as kinetic studies, to demonstrate their intermediacy in Cp*Co^{III}-catalyzed C−H functionalization reactions.

2. With a collection of cobaltacycles in hand, reveal previously inaccessible mechanistic intricacies on Cp*Co^{III}-catalyzed oxidative alkyne annulation reactions, including fundamental knowledge on the migratory insertion step (**B$^+$**) in the catalytic cycle and the nature of the active cobalt species at molecular level.

3. Overcome the proposed reversibility of the C−H cyclometalation with cobalt for accessing Cp*Co^{III} metallacycles and investigate the effect of 1,1,1,3,3,3-hexafluoroisopropanol (HFIP) not only in this elementary step but also in catalysis.
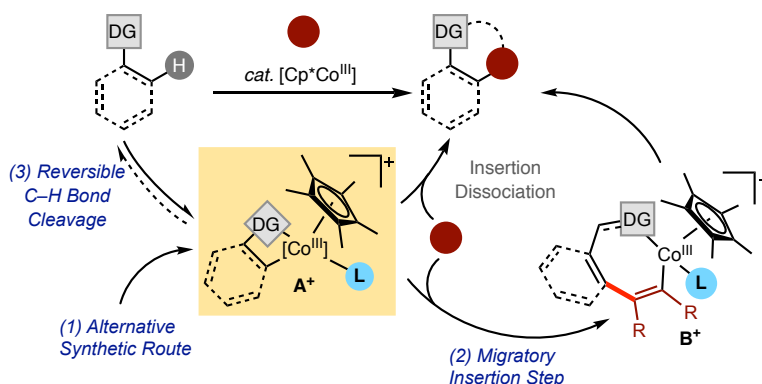
Chapter 3

Accessing Key Intermediates in Cp*Co^{III} C–H Functionalization Reactions and New Insights into the Insertion of Electrophiles

Aim

Reveal previously inaccessible mechanistic intricacies on Cp*Co^{III}-catalyzed oxidative alkyne annulation reactions, including fundamental knowledge on the elementary steps involved in the catalytic cycle and the nature of the active cobalt species at molecular level.

Strategy

Development of a novel synthetic approach for accessing direct analogues of widely invoked Cp*Co^{III} intermediates and employment of different physical organic tools such as kinetic studies.

The work presented in this chapter belongs to the following publications:

Sanjosé-Orduna, J.; Gallego, D.; Garcia-Roca, A.; Martin, E.; Benet-Buchholz, J.; Pérez-Temprano, M. H.*
"Capturing Elusive Cobaltacycle intermediates: A Real-Time Snapshot of the Cp*Co^{III}-catalyzed Oxidative Alkyne Annulation"
Angew. Chem. Int. Ed. **2017**, *56,* 12137−12141. (**Article 1**)

Sanjosé-Orduna, J.; Benet-Buchholz, J.; Pérez-Temprano, M. H.*
"Molecular Aspects of Cobalt Reaction Intermediates and Their Implications in Reactivity"
Inorg. Chem. **2019**, *58*, 10569−10577. (**Article 2**)

3.1 Introduction

As mentioned in the general overview, over the past few years, the employment of Cp*Co^{III} complexes, analogous to the widespread Cp*Rh^{III} catalysts for C−H activation and known since mid-70s, has represented a tremendous advance in cobalt catalysis. These high-valent cobalt catalysts overcome the limited functional group tolerance presented by low-valent cobalt systems due to the use of Grignard reagents. Kanai/Matsunaga, Ackermann, Glorius, Chang, and Ellman, among others, have demonstrated the potential of Cp*Co^{III} complexes to catalyze directed C−H functionalization processes using different types of coupling partners. Despite the significant growth of this field, these Co^{III} systems are at their infancy when compared to Rh− and Pd−based catalysts. Apart from some synthetic limitations, such as the minimal precedent for C(sp^3)−H functionalization or the paucity of reactivity based on remote C−H activation, the real gap to close is the lack of fundamental understanding of these transformations.

As described in **Chapter 1**, at the point our research group was started, the vast majority of the mechanistic proposal were a black box, even when using well-established electrophilic coupling partners such as alkynes or alkenes. This was associated to the high reactivity of the transient cobalt species within the catalytic cycle, which precluded their isolation or even their detection in most cases. Indeed, there are only sporadic examples of stable cobalt metallacycles synthesized via C−H bond-cleavage described in the literature, and only a few of them are relevant for catalysis. This aspect will be discussed in the following section, along with reported strategies for accessing different types of organometallic Cp*Co^{III} complexes that are relevant for the work described in this chapter. As part of our ongoing interest on gaining further insights into Cp*Co^{III}-catalyzed C−H functionalization reactions, in this chapter we will investigate the mechanistic details of its most exploited reactivity, the oxidative alkyne annulation. Therefore, in this introduction, we will also cover relevant mechanistic information on one of the elementary steps involved in these transformations, the insertion of electrophiles, such as alkynes or alkenes, into M−C bonds.

3.2 Strategies for Accessing Cobalt Cyclometalated Species

3.2.1 Preparation by Transmetalation Reaction

In 1967 Gourley and Cope described one of the first cobalt cyclometalated species (besides porphyrin-based complexes).[1] The transmetalation of cobalt(II) chloride with a formed *in situ* lithiated *N,N*-dimethylbenzylamine, gave rise a Co^{III} complex, stabilized by three ligands (Scheme 3.1).
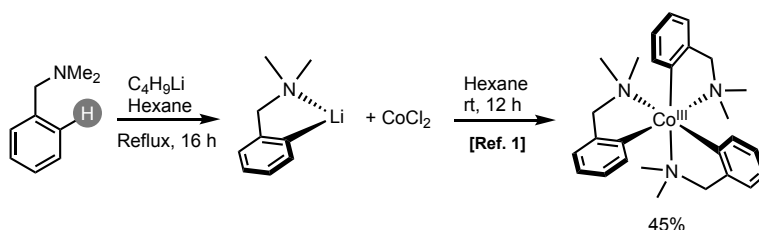
Scheme 3.1. First Co^{III} metallacycle by transmetalation with lithium.

Following an analogue procedure as Cope and co-workers, Pfeffer isolated a [CpCo^{III}(C^N)I] complex *via* transmetalation with an organolithium reagent (Scheme 3.2).[2]
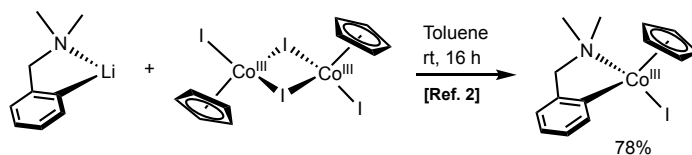
Scheme 3.2. First CpCo^{III} metallacycle obtained by lithium transmetalation.

3.2.2 Preparation by C−H Metalation

In the late 80s, Broderick and Legg described for the first time the synthesis of a cyclometalated cobalt(III) complex *via* C−H metalation.[3] They used a polyamine carboxylate-type ligand to stabilize the metal center (Scheme 3.3). Oxidation of the highly coordinated initial Co^{II} species, gave rise an isolable cobalt(III) agostic intermediate (only in the presence of strong field ligands). Then, addition of a base

[1] Cope, A. C.; Gourley, R. N. "A New σ-bonded Aryl Cobalt(III) Complex" *J. Organometal. Chem.* **1967**, *8*, 527−533.

[2] Meneghetti, M. R.; Grellier, M.; Pfeffer, M.; Dupont, J.; Fischer, J. "Synthesis of Configurationally Stable, Optically Active Organocobalt Compounds" *Organometallics* **1999**, *18*, 5560−5570.

[3] (a) Kanamori, K.; Broderick, W. E.; Jordan, R. F.; Willett, R. D.; Legg, J. I. "Intramolecular C−H Bond Activation in Aqueous Solution: Preparation of a Unique Cobalt(III)-Alkyl Complex by Deprotonation of an Agostic Intermediate. Crystal Structure of [Co^{III}(dacoda-C(2))(H₂O)]·2H₂O" *J. Am. Chem. Soc.* **1986**, *108*, 7122−7124. (b) Broderick, W. E.; Kanamori, K.; Willett, R. D.; Legg, J. I: "Intramolecular C-H Bond Activation: Preparation, Structure, and Properties of a Unique Cobalt(III) Complex, K[Co^{III}(dacoda)(SO₃)]·5H₂O, Containing a Weak Agostic Interaction in Aqueous Solution" *Inorg. Chem.* **1991**, *30*, 3875−3881.

yielded the final cobaltacycle. It was determined later that the C−H bond activation was preceded by an agostic interaction of the oxidized Co[III] metal center and the activated alkyl C−H bond.[2b]
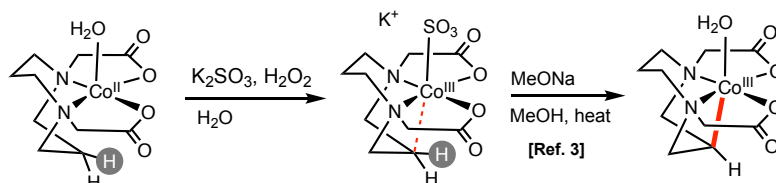
Scheme 3.3. First Co[III] metallacycle by C−H activation.

Later, Klein described the reaction between a [MeCo[I](PMe)$_4$] and azobenzene to isolate the cobalt(I) metallacycle shown in Scheme 3.4.[4] This reaction is proposed to occur *via* a ligand-assisted oxidative addition of the C−H bond to the Co[I] metal center. Then, the resulting aryl-Co[III]-hydride intermediate is proposed to undergo subsequent reductive elimination, releasing methane in the process (Scheme 3.3).
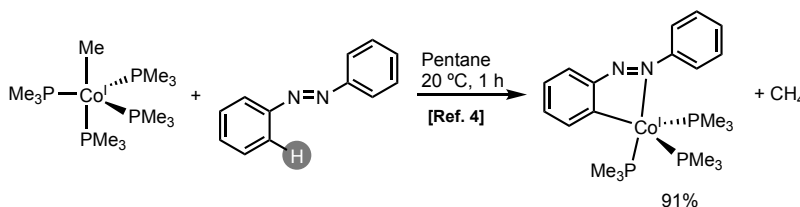
Scheme 3.4. First Co[I] metallacycle isolated.

Using again azobenzene as substrate, Avilés *et al*. demonstrated that half-sandwich Co[I] complexes can also participate in C−H metalation reactions under the proper reaction conditions.[5] Although the authors were able to synthesize and fully characterize the targeted cobaltacycle, they did not further explore its reactivity (Scheme 3.5).

[4] Klein, H.-F.; Helwig, M.; Koch, U.; Flörke, U.; Haupt, H.-J. "Coordination and Reactions of Diazenes in Trimethylphosphinecobalt(I) Complexes — Syntheses and Structures of Complexes Containing μ^2-(N,N')-Benzo[c]cinnoline and η^2-Azobenzene Ligands" *Z. Naturforsch B*. **1993**, *48*, 778−784.
[5] Avilés, T.; Dinis, A.; Calhorda, M. J.; Pinto, P.; Félix, V.; Drew, M. G. B. "Synthesis, X-ray structure, and theoretical studies of novel cationic mono-cyclopentadienyl complexes of Co(III): the orthometalation of trans-azobenzene" *J. Organomet. Chem.* **2001**, *625*, 186−194.
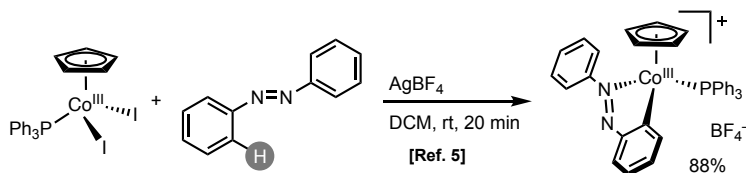
Scheme 3.5. First CpCo^{I} metallacycle isolated.

In the context of cobalt-catalyzed directed C−H functionalization reactions, Daugulis and Maiti have been able to synthesize and characterize organometallic Co^{III} metallacyclic intermediates through a C−H activation step by reaction of Co(OAc)$_2$ with aminoquinoline derivatives in the presence of oxidants (Scheme 3.6).[6]
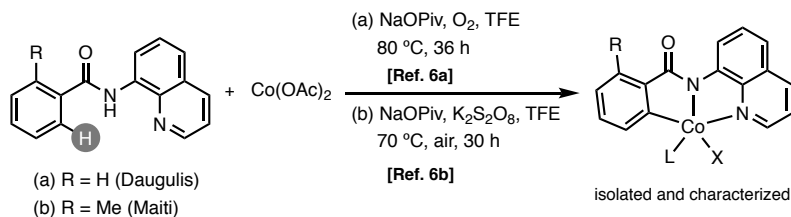
Scheme 3.6. Synthesis of stable aryl-Co^{III} complexes through C−H activation.

Following the same approach, Ribas and co-workers were able to cyclometalate a model substrate containing a tridentate directing group (Scheme 3.7).[7] The resulting cobalt(III) complex was used as platform for investigating its reactivity towards different coupling partners such as alkynes or diazo compounds. Furthermore, they investigated the reactivity of these cobalt(III) complexes and different coupling partners such as alkynes[7a] or diazo compounds.[7b]

[6] (a) Grigorjeva, L.; Daugulis, O. "Cobalt-Catalyzed, Aminoquinoline-Directed C(sp^2)−H Bond Alkenylation by Alkynes" *Angew. Chem. Int. Ed.* **2014**, *53*, 10209−10212. (b) Maity, S.; Kancherla, R.; Dhawa, U.; Hoque, E.; Pimparkar, S.; Maiti, D. "Switch to Allylic Selectivity in Cobalt-Catalyzed Dehydrogenative Heck Reactions with Unbiased Aliphatic Olefins" *ACS Catal.* **2016**, *6*, 5493−5499.
[7] (a) Planas, O.; Whiteoak, C. J.; Martin-Diaconescu, V.; Gamba, I.; Luis, J. M.; Parella, T.; Company, A.; Ribas, X. "Isolation of Key Organometallic Aryl-Co(III) Intermediates in Cobalt-Catalyzed C(sp^2)−H Functionalizations and New Insights into Alkyne Annulation Reaction Mechanisms" *J. Am. Chem. Soc.* **2016**, *138*, 14388−14397. (b) Planas, O.; Roldán-Gómez, S.; Martin-Diaconescu, V.; Gamba, I.; Luis, J. M.; Parella, T.; Company, A.; Ribas, X. "Carboxylate-Assisted Formation of Aryl-Co(III) Masked-Carbenes in Cobalt-Catalyzed C−H Functionalization with Diazo Esters" *J. Am. Chem. Soc.* **2017**, *139*, 14649−14655.

Scheme 3.7. Cyclometalation of aminoquinoline derivatives with Co(OAc)$_2$ through C−H activation.

3.2.3 Precedents on the Isolation of Cp*Co^{III} Metallacycles

Prior to this thesis, the only example in the literature to access pentamethylcyclopentadienyl-containing cobalt metallacycles was described by Kanai, as already presented in section 1.4.2. They designed an alternative route for the isolation of a Cp*Co^{III} metallacycle, by means of a transmetalation with an organozinc compound (Scheme 3.8).[8] However, the low yield and lack of reproducibility of this transformation encouraged us to search other more convenient approaches.
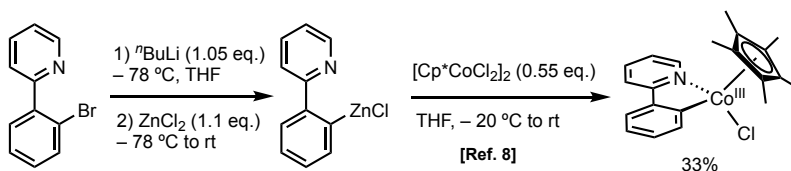
Scheme 3.8. Isolation of the first Cp*Co^{III} metallacycle by transmetalation.

In the **Article 1** of this doctoral thesis we reported our initial attempts for surmounting the proposed reversibility of the C−H activation by Cp*Co^{III} complexes and access well-defined and isolable cobaltacycles via oxidative addition.[9]

---

[8] Ikemoto, H.; Yoshino, T.; Sakata, K.; Matsunaga, S.; Kanai, M. "Pyrroloindolone Synthesis via a Cp*Co^{III}-Catalyzed Redox-Neutral Directed C−H Alkenylation/Annulation Sequence" *J. Am. Chem. Soc.* **2014**, *136*, 5424−5431.

[9] Albrecht, M. "Cyclometalation Using d-Block Transition Metals: Fundamental Aspects and Recent Trends" *Chem. Rev*. **2010**, *110*, 576−623.

3.3 Reactivity with Electrophiles

The insertion of electrophiles, such alkynes or alkenes, into M−C bonds is one of most relevant reactions in organometallic chemistry and plays a crucial role in different types of catalytic systems, ranging from polymerizations[10] to the Mizoroki-Heck reactions.[11] In the context of group 9 Cp*M^{III} complex-catalyzed C−H functionalization reactions, the migratory insertion step is involved in annulation and hydroarylation processes. From a fundamental point of view, different insertion modes have been reported, depending on the nature of the cyclometalated complex and/or the electrophilic coupling partners. In this section we will discuss some of the most relevant examples described in the literature.

3.3.1 Alkyne Insertion on Iridium and Rhodium Metallacycles

In 2008 Jones and co-workers studied the migratory insertion step of a highly electrophilic alkyne, dimethylacetylenedicarboxylate (DMAD), into M−C (M = Ir, Rh) bonds of neutral metallacycles.[12] The resulting seven-membered ring metallacycles where isolated in quantitative yields for both metals (Scheme 3.9).
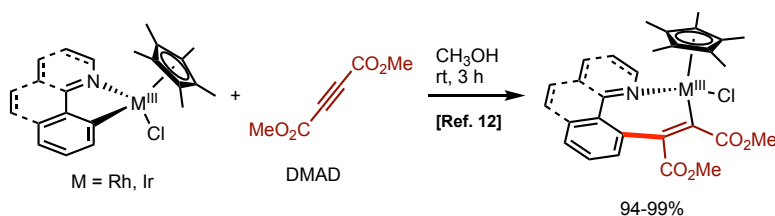
Scheme 3.9. DMAD insertion into Ir and Rh neutral metallacycles.

Not long after that, the same group expanded the scope of electrophiles.[13] First, they tested ethylene. Interestingly, differences were observed depending on the metal center. For iridium, a freely rotating coordinated ethylene was observed by ^{1}H NMR spectroscopy. The authors proposed a chlorine dissociation to give rise a 16-electron iridium complex, readily available to coordinate ethylene. On the other hand, for rhodium, a six-membered ring was obtained and characterized. In this

---

[10] (a) Ittel, S. D.; Johnson, L. K.; Brookhart, M. "Late-Metal Catalysts for Ethylene Homo- and Copolymerization" *Chem. Rev.* **2000**, *100*, 1169−1204. (b) Nakamura, A.; Ito, S.; Nozaki, K. "Coordination-Insertion Copolymerization of Fundamental Polar Monomers" *Chem. Rev.* **2009**, 109, 5215−5244.

[11] (a) Beletskaya, I. P.; Chepakrov, A. V. "The Heck Reaction as a Sharpening Stone of Palladium Catalysis" *Chem. Rev.* **2000**, *100*, 3009−3066. (b) Dounay, A. B.; Overman, L. E. "The Asymmetric Intramolecular Heck Reaction in Natural Product Total Synthesis" *Chem. Rev.* **2003**, *103*, 2945−2964.

[12] Li, L.; Brennessel, W. W.; Jones, W. D. "An Efficient Low-Temperature Route to Polycyclic Isoquinoline Salt Synthesis via C−H Activation with [Cp*MCl$_2$]$_2$ (M = Rh, Ir)" *J. Am. Chem. Soc.* **2008**, *130*, 12414−12419.

[13] Li, L.; Jiao, Y.; Brennessel, W. W.; Jones, W. D. "Reactivity and Regioselectivity of Insertion of Unsaturated Molecules into M−C (M = Ir, Rh) Bonds of Cyclometalated Complexes" *Organometallics* **2010**, *29*, 4593−4605.

case, a new chiral carbon center was generated after the insertion. This behavior was explained by a [1,1]-insertion instead of a [1,2]-insertion (Scheme 3.10).
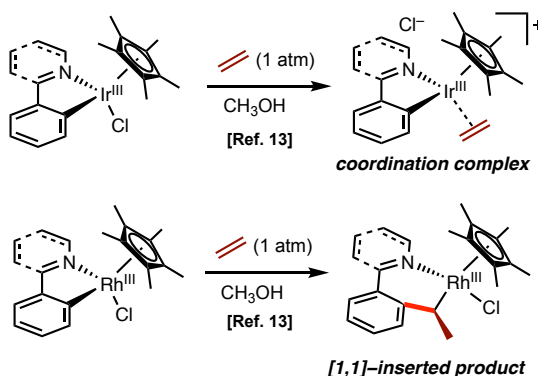
Scheme 3.10. Ethylene insertion into Ir and Rh neutral metallacycles.

In this work, Jones and co-workers also studied the insertion of alkynes. When using phenylacetylene, they observed that two equivalents were inserted into the metallacycle. After the insertion of one molecule of diphenylacetylene, the authors proposed that a second molecule could coordinate to the metal center, isomerize as a vinylidene, and insert to give the final double inserted product (Scheme 3.11).
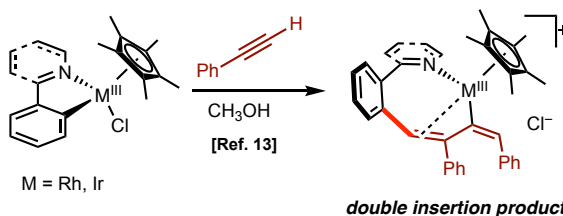
Scheme 3.11. Terminal alkyne insertion to Ir and Rh neutral metallacycles.

In addition, they tested a series of asymmetrical alkynes. For ethyl 2-butynoate only one single product was obtained. However, when trying a bulkier alkyne, i.e. ethyl phenylpropiolate, different regioisomers were obtained. After analyzing the reaction mixtures, the authors detected, as the major isomer, the product with the bulkier aryl group closer to the metal center. In addition to that, they also tested ethyl 4,4,4-trifluoro-2-butynoate (exchanging the aryl group for a CF_3) and again it gave a mixture of isomers. This time, the major isomer turned out to be the one with the more electron-withdrawing substituent close to the metal center, in an analogous fashion as ethyl phenylpropiolate (Scheme 3.12).
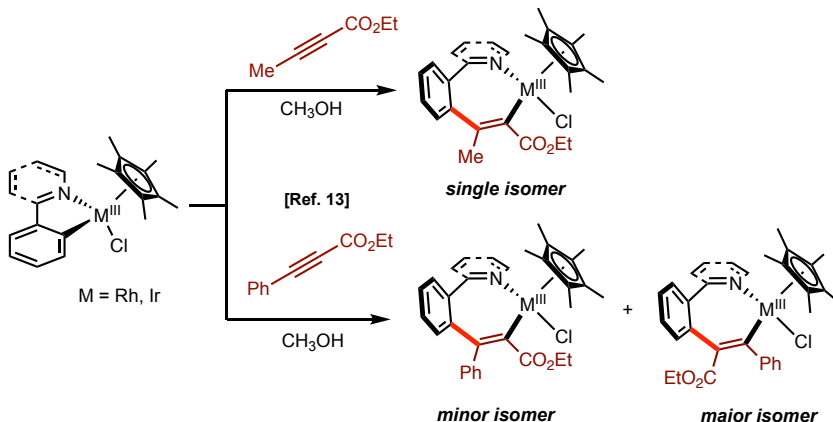
Scheme 3.12. Asymmetric alkyne insertion to Ir and Rh neutral metallacycles.

Not long after that, Davies and co-workers decided to investigate the reactivity of cationic iridium oxazoline-based metallacycles.[14] Starting from the neutral metallacycle, they dissociated the chlorine atom with KPF_6, to obtain a cationic iridacycle, stabilized by a labile acetonitrile of the solvent. With this compound in hand, they successfully accomplished the diphenylacetylene insertion (Scheme 3.13).
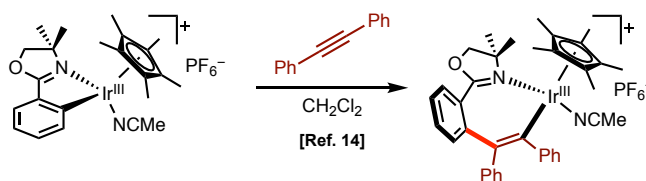
Scheme 3.13. Insertion of symmetric alkyne to an iridium cationic metallacycle.

In this work, the authors also investigated the regioselectivity of the alkyne insertion. When using ethyl phenylpropiolate as coupling partner, they only observed a single regioisomer which contains the ester group closer to the metal center, and the phenyl group next to the oxazoline moiety (Scheme 3.14). Interestingly, this alkyne insertion presents opposite regioselective as observed before with neutral metallacycles by Jones and co-workers. When the authors tried phenylacetylene, a single regioisomer was isolated, corresponding to the phenyl scaffold located itself close to the metal center. If the neutral oxazoline-derived metallacycle was used, complex mixtures were observed by mass spectrometry, in agreement with the multiple alkyne insertion to neutral metallacycles, as seen before.

---

[14] Davies, D. L.; Al-Duaij, O.; Fawcett, J.; Singh, K. "Reactions of Cyclometalated Oxazoline Half-Sandwich Complexes of Iridium and Ruthenium with Alkynes and CO" *Organometallics* **2010**, *29*, 1413−1420.
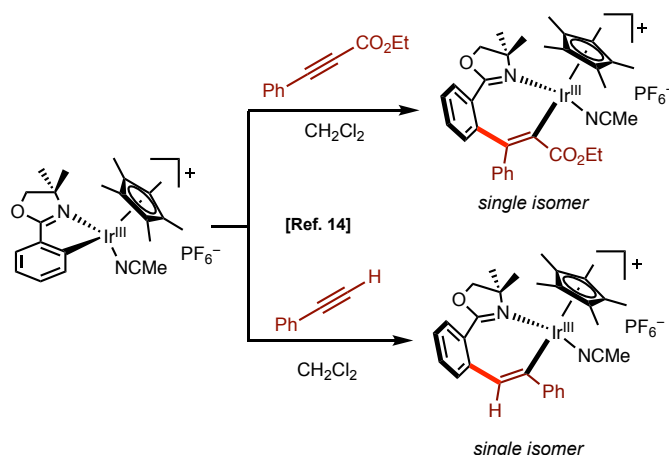
Scheme 3.14. Asymmetric alkyne insertion to an iridium cationic metallacycle.

These are just representative examples of the mechanistic studies performed with iridium and rhodium metallacycles during the last decades. However, regarding cobalt complexes, the literature precedents in the migratory insertion step are extremely scarce.

3.3.2 Alkyne Insertion on Cobaltacycles

The first example of an alkyne insertion to a cobalt metallacycle was described by Bruce and co-workers back in 1972.[15a] They reported the insertion of hexafluorobutyne into a Co[I] *N*-based ligand metallacycle A couple of years later, they were able to identify a seven-membered ring cobaltacycle resulting from the migratory insertion of the alkyne (Scheme 3.15).[15b] Although pioneer, this precedent turned out to be extremely limited in terms of scope.
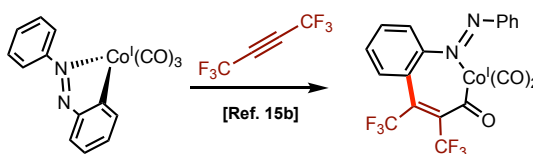
Scheme 3.15. First alkyne insertion into a cobalt metallacycle.

---

[15] (a) Bruce, M. I.; Goodall, B. L.; Redhouse, A. D.; Stone, F. G. A. "Reactions of Azobenzene-Cobalt Carbonyl Complexes with $C_2(CF_3)_2$: Structure of $PhN:NC_6H_4C(CF_3):C(CF_3)COCo(CO)_2$, and a New Quinolone Synthesis" *J. Chem. Soc. Chem. Commun.* **1972**, 1228–1229. (b) Bruce, M. I.; Goodall, B. L.; Stone, F. G. A. "Cyclometallation Reactions. Part 11. Reactions of Tricarbonyl[2-(pheny1azo)phenyl-C[1]*N*']cobalt and Related Complexes with Hexafluorobut-2-yne" *J. Chem. Soc. Dalton Trans*. **1975**, 1651–1655.

Later on, Fischer and Pfeffer envisioned the use of another cobalt system, this time using a CpCo^{III} metallacycle.[16] While no reaction was observed with internal alkynes, interesting reactivity was displayed when using terminal alkynes. The authors were able to identify two major products in comparable yields: an organic product as a result of a [2,1]-inserted transformation, along with a cobalt product. Close examination of the X-ray diffraction molecular structure of the organometallic species unraveled a [1,2]-inserted product, where the cyclopentadienyl ligand was activated by a migration of the alkenyl group (Scheme 3.16).

[2,1]–inserted product   **[1,2]–inserted product**
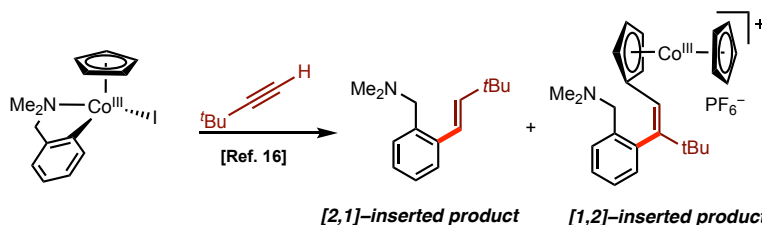
Scheme 3.16. Precedents on the cobalt-mediated migratory insertion step.

Despite all these precedents, there is not a single example in the literature about a mechanistic investigation of the migratory insertion step in Cp*Co^{III} systems. This is very surprising, because, as it was discussed in the section 1.3 of this thesis, the annulation of alkynes is the most used reaction in the field. Encouraged by that, and taking advantage of the isolated cobaltacycles described in **Article 1**, we decided to use them to study in more detail the migratory step with different electrophiles. The results will be found in **Article 2**.

---

[16] Meneghetti, M. R.; Grellier, M.; Pfeffer, M.; Fischer, J. "Reactivity of Cyclocobaltated Benzylamine Derivatives toward Terminal Alkynes" *Organometallics* **2000**, *19*, 1935–1939.

3.4 References

[1] Cope, A. C.; Gourley, R. N. "A New σ-bonded Aryl Cobalt(III) Complex" *J. Organometal. Chem.* **1967**, *8*, 527–533.

[2] Meneghetti, M. R.; Grellier, M.; Pfeffer, M.; Dupont, J.; Fischer, J. "Synthesis of Configurationally Stable, Optically Active Organocobalt Compounds" *Organometallics* **1999**, *18*, 5560–5570.

[3] (a) Kanamori, K.; Broderick, W. E.; Jordan, R. F.; Willett, R. D.; Legg, J. I. "Intramolecular C–H Bond Activation in Aqueous Solution: Preparation of a Unique Cobalt(III)-Alkyl Complex by Deprotonation of an Agostic Intermediate. Crystal Structure of [Co^{III}(dacoda-C(2))(H$_2$O)]·2H$_2$O" *J. Am. Chem. Soc.* **1986**, *108*, 7122–7124. (b) Broderick, W. E.; Kanamori, K.; Willett, R. D.; Legg, J. I: "Intramolecular C-H Bond Activation: Preparation, Structure, and Properties of a Unique Cobalt(III) Complex, K[Co^{III}(dacoda)(SO$_3$)]·5H$_2$O, Containing a Weak Agostic Interaction in Aqueous Solution" *Inorg. Chem.* **1991**, *30*, 3875–3881.

[4] Klein, H.-F.; Helwig, M.; Koch, U.; Flörke, U.; Haupt, H.-J. "Coordination and Reactions of Diazenes in Trimethylphosphinecobalt(I) Complexes − Syntheses and Structures of Complexes Containing μ^2-(N,N')-Benzo[c]cinnoline and η^2-Azobenzene Ligands" *Z. Naturforsch B*. **1993**, *48*, 778–784.

[5] Avilés, T.; Dinis, A.; Calhorda, M. J.; Pinto, P.; Félix, V.; Drew, M. G. B. "Synthesis, X-ray structure, and theoretical studies of novel cationic mono-cyclopentadienyl complexes of Co(III): the orthometalation of *trans*-azobenzene" *J. Organomet. Chem.* **2001**, *625*, 186–194.

[6] (a) Grigorjeva, L.; Daugulis, O. "Cobalt-Catalyzed, Aminoquinoline-Directed C(sp^2)−H Bond Alkenylation by Alkynes" *Angew. Chem. Int. Ed.* **2014**, *53*, 10209–10212. (b) Maity, S.; Kancherla, R.; Dhawa, U.; Hoque, E.; Pimparkar, S.; Maiti, D. "Switch to Allylic Selectivity in Cobalt-Catalyzed Dehydrogenative Heck Reactions with Unbiased Aliphatic Olefins" *ACS Catal.* **2016**, *6*, 5493–5499.

[7] (a) Planas, O.; Whiteoak, C. J.; Martin-Diaconescu, V.; Gamba, I.; Luis, J. M.; Parella, T.; Company, A.; Ribas, X. "Isolation of Key Organometallic Aryl-Co(III) Intermediates in Cobalt-Catalyzed C(sp2)−H Functionalizations and New Insights into Alkyne Annulation Reaction Mechanisms" *J. Am. Chem. Soc.* **2016**, *138*, 14388–14397. (b) Planas, O.; Roldán-Gómez, S.; Martin-Diaconescu, V.; Gamba, I.; Luis, J. M.; Parella, T.; Company, A.; Ribas, X. "Carboxylate-Assisted Formation of Aryl-Co(III) Masked-Carbenes in Cobalt-Catalyzed C−H Functionalization with Diazo Esters" *J. Am. Chem. Soc.* **2017**, *139*, 14649–14655.

[8] Ikemoto, H.; Yoshino, T.; Sakata, K.; Matsunaga, S.; Kanai, M. "Pyrroloindolone Synthesis via a Cp*Co^{III}-Catalyzed Redox-Neutral Directed C−H Alkenylation/Annulation Sequence" *J. Am. Chem. Soc.* **2014**, *136*, 5424–5431.

[9] Albrecht, M. "Cyclometalation Using d-Block Transition Metals: Fundamental Aspects and Recent Trends" *Chem. Rev*. **2010**, *110*, 576–623.

[10] (a) Ittel, S. D.; Johnson, L. K.; Brookhart, M. "Late-Metal Catalysts for Ethylene Homo- and Copolymerization" *Chem. Rev.* **2000**, *100*, 1169–1204. (b) Nakamura, A.; Ito, S.; Nozaki, K. "Coordination-Insertion Copolymerization of Fundamental Polar Monomers" *Chem. Rev*. **2009**, 109, 5215–5244.

[11] (a) Beletskaya, I. P.; Chepakrov, A. V. "The Heck Reaction as a Sharpening Stone of Palladium Catalysis" *Chem. Rev.* **2000**, *100*, 3009–3066. (b) Dounay, A. B.; Overman, L. E. "The Asymmetric Intramolecular Heck Reaction in Natural Product Total Synthesis" *Chem. Rev.* **2003**, *103*, 2945–2964.

[12] Li, L.; Brennessel, W. W.; Jones, W. D. "An Efficient Low-Temperature Route to Polycyclic Isoquinoline Salt Synthesis via C−H Activation with [Cp*MCl$_2$]$_2$ (M = Rh, Ir)" *J. Am. Chem. Soc*. **2008**, *130*, 12414–12419.

[13] Li, L.; Jiao, Y.; Brennessel, W. W.; Jones, W. D. "Reactivity and Regioselectivity of Insertion of Unsaturated Molecules into M−C (M = Ir, Rh) Bonds of Cyclometalated Complexes" *Organometallics* **2010**, *29*, 4593–4605.

[14] Davies, D. L.; Al-Duaij, O.; Fawcett, J.; Singh, K. "Reactions of Cyclometalated Oxazoline Half-Sandwich Complexes of Iridium and Ruthenium with Alkynes and CO" *Organometallics* **2010**, *29*, 1413−1420.

[15] (a) Bruce, M. I.; Goodall, B. L.; Redhouse, A. D.; Stone, F. G. A. "Reactions of Azobenzene-Cobalt Carbonyl Complexes with $C_2(CF_3)_2$: Structure of $PhN:NC_6H_4C(CF_3):C(CF_3)COCo(CO)_2$, and a New Quinolone Synthesis" *J. Chem. Soc. Chem. Commun.* **1972**, 1228−1229. (b) Bruce, M. I.; Goodall, B. L.; Stone, F. G. A. "Cyclometallation Reactions. Part 11. Reactions of Tricarbonyl[2-(pheny1azo)phenyl-C¹*N'*]cobalt and Related Complexes with Hexafluorobut-2-yne" *J. Chem. Soc. Dalton Trans*. **1975**, 1651−1655.

[16] Meneghetti, M. R.; Grellier, M.; Pfeffer, M.; Fischer, J. "Reactivity of Cyclocobaltated Benzylamine Derivatives toward Terminal Alkynes" *Organometallics* **2000**, *19*, 1935−1939.

Article *1*
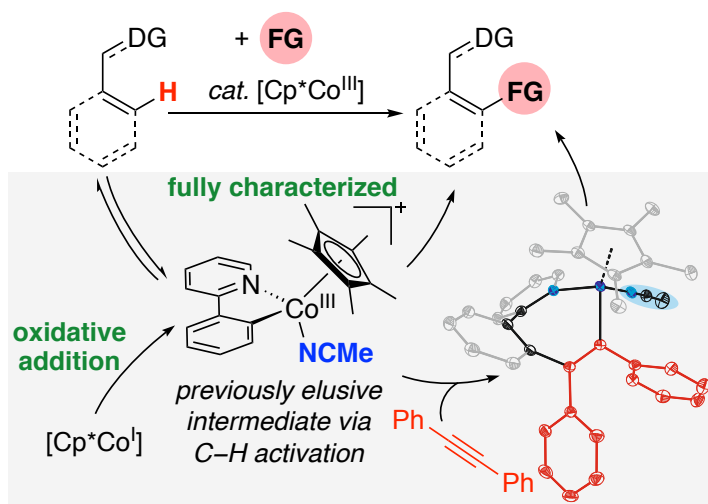
DG + **FG**

H *cat.* [Cp*Co^{III}]

DG

FG

fully characterized

oxidative addition

[Cp*Co^{I}]

N···Co^{III}

NCMe

previously elusive intermediate via C–H activation

Ph

Ph

Capturing Elusive Cobaltacycle Intermediates: A Real-Time Snapshot of the Cp*CoIII-Catalyzed Oxidative Alkyne Annulation

*Jesús Sanjosé-Orduna, Daniel Gallego, Alèria Garcia-Roca, Eddy Martin, Jordi Benet-Buchholz, and Mónica H. Pérez-Temprano**

***Abstract:** Despite Cp*CoIII catalysts having emerged as a very attractive alternative to noble transition metals for the construction of heterocyclic scaffolds through C−H activation, the structure of the reactive species remains uncertain. Herein, we report the identification and unambiguous characterization of two long-sought cyclometalated Cp*CoIII complexes that have been proposed as key intermediates in C−H functionalization reactions. The addition of MeCN as a stabilizing ligand plays a crucial role, allowing the access to otherwise highly reactive species. Mechanistic investigations demonstrate the intermediacy of these species in oxidative annulations with alkynes, including the direct observation, under catalytic conditions, of a previously elusive post-migratory insertion seven-membered cobaltacycle.*

Directed C−H functionalization has become one of the most powerful synthetic tools for the construction of organic scaffolds.[1] For decades, this field has been dominated by the use of noble metals, such as Pd or Rh.[1] Earth-abundant first-row transition-metal catalysts,[2] in particular Cp*CoIII complexes,[3] have recently shown their potential to construct C−C and C−X bonds,[4] not only representing a low-cost alternative to Cp*RhIII catalysts[1a,l,5] but also offering a unique catalytic reactivity.[3e] Despite the significant progress in this field, Cp*CoIII-catalyzed C−H functionalization is still at its infancy, in part, due to the limited fundamental organometallic understanding of these systems.

In contrast to Rh-based systems,[6] the nature of the putative cobalt reactive species within the catalytic cycle of directed C−H functionalization reactions still remains elusive. This is likely due to the proposed reversibility of the C−H cleavage en route to **A**,[4b−n, 7] along with the high reactivity of the targeted metallacyclic intermediates, which hampers their isolation and characterization (Scheme 1).[4j,8,9] Unravelling how Cp*Co-based catalysts promote C−H functionalization would be particularly relevant, not only for organometallic chemistry but also to set the basis for designing fundamental new reactivity within Co catalysis.

In particular, Cp*CoIII systems have demonstrated their great capability to catalyze oxidative annulations with alky-

[*] J. Sanjosé-Orduna, Dr. D. Gallego, A. Garcia-Roca, Dr. E. Martin, Dr. J. Benet-Buchholz, Dr. M. H. Pérez-Temprano
Institute of Chemical Research of Catalonia (ICIQ)
Avgda. Països Catalans 16, 43007 Tarragona (Spain)
E-mail: mperez@iciq.es

Supporting information and the ORCID identification number(s) for the author(s) of this article can be found under:
https://doi.org/10.1002/anie.201704744.
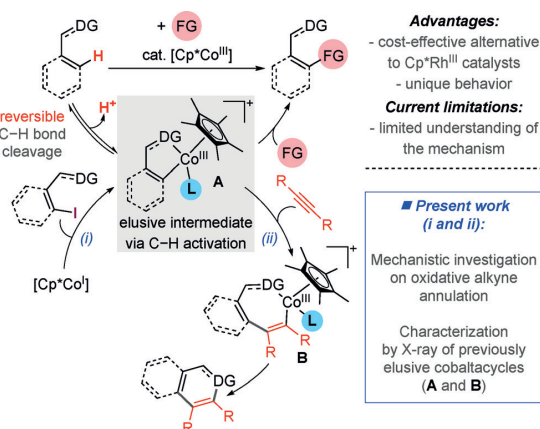
Scheme 1. Cp*CoIII-catalyzed C−H functionalization reactions.

nes.[4b,l,m,10] These coupling reactions provide a facile route for the construction of privileged heterocyclic frameworks of particular interest in medicinal chemistry and materials science.[4a,b,11] Challenged by the lack of mechanistic information, we wondered whether it would be possible to design a new approach to access some of the putative cobaltacycle intermediates aiming at a more comprehensive picture of Cp*CoIII-catalyzed C−H oxidative alkyne annulation. Herein, we reveal previously inaccessible mechanistic intricacies of these transformations, including: 1) The intermediacy of cyclometalated CoIII species (**A** and **B**) in the reaction mechanism (Scheme 1); 2) the higher catalytic activity of **A**-type complexes compared to the widely used [Cp*CoI2(CO)] catalyst; and 3) the first experimental evidence of the formation of a key seven-membered cobaltacycle intermediate, **B**, under catalytic conditions.

We initiated our study by targeting the synthesis of cationic 2-phenylpyridine-derived cyclometalated Cp*CoIII complexes. Such species, that is, **A** in Scheme 1, have been proposed as key transient intermediates in Cp*CoIII-catalyzed C−H functionalization reactions,[4a,f,h,j,7a,12] including annulation processes.[10d,f] Due to the proposed reversible C−H cobaltation using Cp*CoIII systems, we envisioned that an alternative strategy, involving a ligand-assisted Csp2-I oxidative addition to CoI followed by halide abstraction, would facilitate the access to a direct analogue of a C−H-activated CoIII metallacycle.[13,14] As shown in Scheme 2, the reaction of 2-(2-iodophenyl)pyridine (**1-I**) with **2-CO** in THF, at 60°C for 24 h, resulted in the formation of the cobaltacycle **3-I** in 81% isolated yield.[15,16] Interestingly, when a more labile ligand,
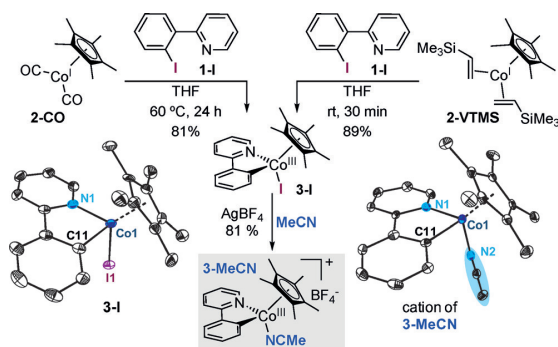
Scheme 2. Oxidative addition of **1-I** to [Cp*Co^{I}L$_2$] and formation of the cationic species **3-MeCN**. ORTEP structures for **3-I** and **3-MeCN** are shown with thermal ellipsoids set at 50% of probability (H atoms and counter anion BF$_4^-$ have been omitted for clarity).

such as vinyltrimethylsilane (VTMS), is bound to the Co^I metal center (**2-VTMS**), the oxidative addition proceeded smoothly at room temperature (89% isolated yield) in less than 30 min. Initial attempts at forming the desired cationic cobaltacycle led to rapid decomposition upon treatment of **3-I** with AgBF$_4$ in CH$_2$Cl$_2$. We solved this problem by performing the reaction of **3-I** with AgBF$_4$ in MeCN, which affords the desired cationic cobaltacycle stabilized by acetonitrile coordination (**3-MeCN**) (Scheme 2). In addition to ESI-MS,[17] the structure of **3-MeCN** was unequivocally confirmed by NMR spectroscopy and single-crystal X-ray diffraction.[18]

With a reliable route in hand to one of the most widely invoked intermediates in Cp*Co^{III}-catalyzed C–H functionalization reactions, we next investigated not only whether **3-MeCN** could be catalytically competent in oxidative C–H alkyne annulation reactions but also its efficiency compared to [Cp*CoI$_2$(CO)] (Table 1).[4c] To our delight, using diphenylacetylene (**4**) as a coupling partner,[19] **3-MeCN** efficiently catalyzes the formation of the annulation product **5** (89% isolated yield) in less than 2 h (entry 1). **5** was obtained in

comparable yields when using [Cp*CoI$_2$(CO)] as the catalyst (entry 2). Importantly, we do not observe a decrease in yield when the reaction is performed with only 1 mol% of **3-MeCN** (entry 3), the lowest catalyst loading reported to date for this type of reactions. This is in stark contrast with the significant decrease in yield obtained with [Cp*CoI$_2$(CO)] (entry 4). Notably, **3-MeCN** also showed a superior reactivity compared to [Cp*CoI$_2$(CO)] at even lower temperatures (35°C; entries 5,6).[20,21]

Encouraged by the mild conditions shown in entries 5 and 6, we questioned whether we could detect key reactive cobalt intermediates under catalytic conditions. Although no transient species was detected by ^{1}H NMR spectroscopy when [Cp*CoI$_2$(CO)] was used as the catalyst precursor, we were delighted to observe the in situ formation of a long-lived intermediate (**6**) using **3-MeCN** as pre-catalyst (Figure 1),[22] suggesting that MeCN plays a crucial role in facilitating the access/detection of otherwise elusive cobalt intermediates.
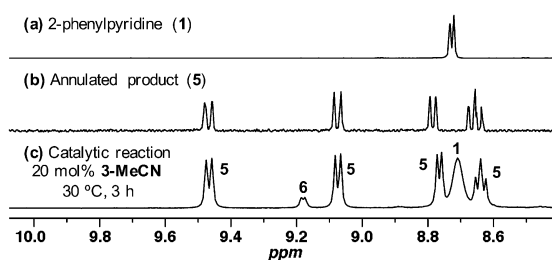
Figure 1. Detection of long-lived intermediate (**6**) under catalytic conditions in CD$_2$Cl$_2$ at 30°C.

To elucidate the molecular structure of this transient species and gain further insights into the mechanism of these processes, we performed a series of stoichiometric studies between **3-MeCN** and **4** (Figure 2). Gratifyingly, when we monitored the progress of the alkyne annulation reaction by ^{1}H NMR spectroscopy at 30°C in CD$_2$Cl$_2$, we observed the fast conversion of **3-MeCN** to the same cobalt complex (**6**) observed in the catalytic experiments. Consumption of **6** was accompanied by formation of the C–N-coupled product, **5** (Figure 2a). Moreover, the reductive elimination step was considerably slowed down by the addition of an excess of MeCN (20 equiv) allowing the clean observation of intermediate **6** (Figure 2b). Despite being highly reactive, **6** could be unambiguously characterized by X-ray crystallography (Figure 2).[23] X-ray analysis reveals a seven-membered cationic cobaltacycle structure generated by the migratory insertion of the alkyne **4** into the Co^{III}–C$_{sp2}$ bond. Whereas numerous reports have postulated the intermediacy of analogous cobaltacycles in annulation reactions, until now none of them provided structural evidences of their formation. The experimental kinetic data shown in Figure 2 also provide other very interesting mechanistic features of the annulation reaction such that the migratory insertion of **4** seems to be faster than the final C–N reductive elimination step. Furthermore, the strong inhibitory effect of MeCN on the reaction progress implies that **3-MeCN** and **6** are off-cycle

Table 1: Comparison between the catalytic activity of **3-MeCN** and [Cp*CoI$_2$(CO)] in oxidative alkyne annulation.[a]

entry	Catalyst	mol%	T [°C]	t [h]	Yield [%][b]
1	**3-MeCN**	10	100	2	89
2	[Cp*CoI$_2$(CO)]	10	100	2	84
3	**3-MeCN**	1	100	2	90
4	[Cp*CoI$_2$(CO)]	1	100	2	66
5	**3-MeCN**[c]	10	35	24	64
6	[Cp*CoI$_2$(CO)][c]	10	35	24	39

[a] Reaction conditions: **1** (0.1 mmol), **4** (0.3 mmol), [Cp*Co^{III}] (10 mol%, 0.01 mmol), AgBF$_4$ (0.01 mmol), Cu(OAc)$_2$ (0.1 mmol), DCE (1.0 mL) under Ar. [b] Reactions were run in duplicate and the yields are for the isolated product. [c] Reaction carried out in DCM.

Figure 2. Kinetic profile of the stoichiometric reactions of **3-MeCN** with 3 equiv of **4** in CD$_2$Cl$_2$ at 30 °C: a) in absence of MeCN, b) in the presence of 20 equiv of MeCN. ORTEP structure for **6** is shown with thermal ellipsoids set at 50% of probability (H atoms and counter anion BF$_4^-$ have been omitted for clarity).

species that coexist in equilibrium with highly reactive cationic cobaltacycles possessing a vacant coordination site.[17,23] This is consistent with **6** being the resting state in catalysis. The direct observation and full characterization of a cobalt resting state during Cp*Co-catalyzed C−H functionalization is unprecedented.

Efforts to isolate and characterize the remaining [Cp*Co^I] species after the formation of the annulated product were unsuccessful. However, the addition of **1-I** to the reaction mixture resulted in the clean formation of **3-I**, suggesting indirectly the presence of this [Cp*Co^I] species after the reductive elimination step (Scheme 3). Taken together, these results provide strong evidence for a catalytic cycle consisting of a Co^I/Co^{III} couple.
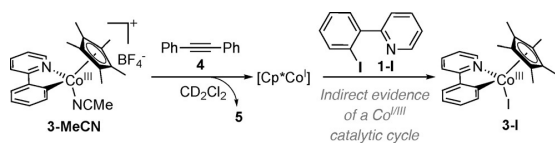
Scheme 3. Indirect detection of Cp*Co^I species after the C−N reductive elimination step.

On the basis of the above experimental data, a plausible catalytic cycle using **3-MeCN** as pre-catalyst is depicted in Scheme 4. First, the cationic cobaltacycle **7** is generated from **3-MeCN**. Then, alkyne coordination followed by a fast migratory insertion into the Co^{III}−C bond leads to the formation of **8**, which is stabilized by MeCN in an equilibrium forming **6**, a seven-membered cyclometalated compound that is the resting state of the catalytic cycle. Subsequent C−N
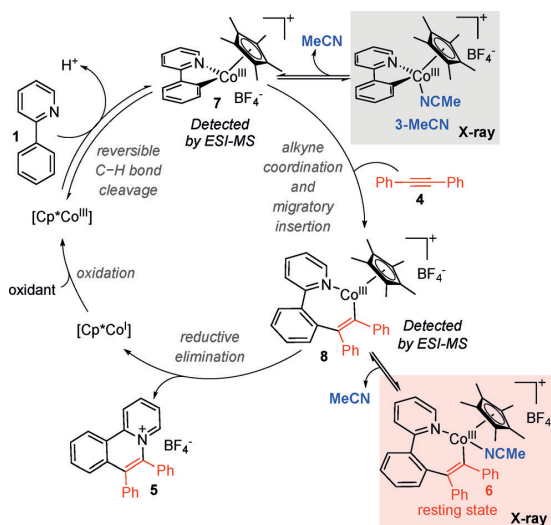
Scheme 4. Proposed mechanism.

reductive elimination from **8** affords the desired coupled product **5** and a [Cp*Co^I] species. The resultant Co^I species is re-oxidized to the active [Cp*Co^{III}] by copper or silver salts, that ultimately regenerates **7** upon reversible C−H activation.[24]

In conclusion, we have described a mechanistic study that unravels the role of cobaltacycle intermediates in C−H oxidative annulation reactions. Our work unambiguously demonstrates the intermediacy of cyclometalated Cp*Co^{III} species, due to the unique ability of MeCN to stabilize highly reactive cobalt intermediates. We anticipate that this work will set the basis for future developments in the area of cobalt catalysis. Work on these goals is currently ongoing in our laboratory.

Acknowledgements

Conflict of interest

The authors declare no conflict of interest.

[1] For selected recent reviews on transition-metal-catalyzed directed C−H functionalization, see: a) D. A. Colby, R. G. Bergman, J. A. Ellman, *Chem. Rev.* **2010**, *110*, 624; b) T. W. Lyons, M. S. Sanford, *Chem. Rev.* **2010**, *110*, 1147; c) C. S. Yeung, V. M. Dong, *Chem. Rev.* **2011**, *111*, 1215; d) K. M. Engle, T.-S. Mei, M. Wasa, J.-Q. Yu, *Acc. Chem. Res.* **2012**, *45*, 788; e) S. R. Neufeldt, M. S. Sanford, *Acc. Chem. Res.* **2012**, *45*, 936; f) J. Yamaguchi, A. D. Yamaguchi, K. Itami, *Angew. Chem. Int. Ed.* **2012**, *51*, 8960; *Angew. Chem.* **2012**, *124*, 9092; g) J. Wencel-Delord, F. Glorius, *Nat. Chem.* **2013**, *5*, 369; h) G. Rouquet, N. Chatani, *Angew. Chem. Int. Ed.* **2013**, *52*, 11726; *Angew. Chem.* **2013**, *125*, 11942; i) Z. Chen, B. Wang, J. Zhang, W. Yu, Z. Liu, Y. Zhang, *Org. Chem. Front.* **2015**, *2*, 1107; j) K. Shin, H. Kim, S. Chang, *Acc. Chem. Res.* **2015**, *48*, 1040; k) O. Daugulis, J. Roane, L. D. Tran, *Acc. Chem. Res.* **2015**, *48*, 1053; l) B. Ye, N. Cramer, *Acc. Chem. Res.* **2015**, *48*, 1308; m) R.-Y. Zhu, M. E. Farmer, Y.-Q. Chen, J.-Q. Yu, *Angew. Chem. Int. Ed.* **2016**, *55*, 10578; *Angew. Chem.* **2016**, *128*, 10734.

[2] For reviews on C−H functionalization catalyzed by first-row transition-metals, see: a) A. A. Kulkarni, O. Daugulis, *Synthesis* **2009**, 4087; b) E. Nakamura, N. Yoshikai, *J. Org. Chem.* **2010**, *75*, 6061; c) J. Yamaguchi, K. Muto, K. Itami, *Eur. J. Org. Chem.* **2013**, 19; d) K. Gao, N. Yoshikai, *Acc. Chem. Res.* **2014**, *47*, 1208; e) L. Ackermann, *J. Org. Chem.* **2014**, *79*, 8948; f) B. Su, S.-C. Cao, Z.-J. Shi, *Acc. Chem. Res.* **2015**, *48*, 886; g) J. Miao, H. Ge, *Eur. J. Org. Chem.* **2015**, 7859; h) W. Liu, L. Ackermann, *ACS Catal.* **2016**, *6*, 3743.

[3] For recent reviews on Cp*Co[III]-catalyzed C−H functionalization reactions, see: a) T. Hyster, *Catal. Lett.* **2015**, *145*, 458; b) M. Moselage, J. Li, L. Ackermann, *ACS Catal.* **2016**, *6*, 498; c) D. Wei, X. Zhu, J.-L. Niu, M.-P. Song, *ChemCatChem* **2016**, *8*, 1242; d) S. Wang, S.-Y. Chen, X.-Q. Yu, *Chem. Commun.* **2017**, *53*, 3165; e) T. Yoshino, S. Matsunaga, *Adv. Synth. Catal.* **2017**, *359*, 1245.

[4] For selected reports on Cp*Co[III]-catalyzed C−H functionalization reactions, see: a) T. Yoshino, H. Ikemoto, S. Matsunaga, M. Kanai, *Angew. Chem. Int. Ed.* **2013**, *52*, 2207; *Angew. Chem.* **2013**, *125*, 2263; b) H. Ikemoto, T. Yoshino, K. Sakata, S. Matsunaga, M. Kanai, *J. Am. Chem. Soc.* **2014**, *136*, 5424; c) B. Sun, T. Yoshino, S. Matsunaga, M. Kanai, *Adv. Synth. Catal.* **2014**, *356*, 1491; d) D.-G. Yu, T. Gensch, F. de Azambuja, S. Vasquez-Cespedes, F. Glorius, *J. Am. Chem. Soc.* **2014**, *136*, 17722; e) J. R. Hummel, J. A. Ellman, *J. Am. Chem. Soc.* **2015**, *137*, 490; f) A. B. Pawar, S. Chang, *Org. Lett.* **2015**, *17*, 660; g) J. Li, L. Ackermann, *Angew. Chem. Int. Ed.* **2015**, *54*, 3635; *Angew. Chem.* **2015**, *127*, 3706; h) D. Zhao, J. H. Kim, L. Stegemann, C. A. Strassert, F. Glorius, *Angew. Chem. Int. Ed.* **2015**, *54*, 4508; *Angew. Chem.* **2015**, *127*, 4591; i) J. Li, L. Ackermann, *Angew. Chem. Int. Ed.* **2015**, *54*, 8551; *Angew. Chem.* **2015**, *127*, 8671; j) J. Park, S. Chang, *Angew. Chem. Int. Ed.* **2015**, *54*, 14103; *Angew. Chem.* **2015**, *127*, 14309; k) M. Sen, D. Kalsi, B. Sundararaju, *Chem. Eur. J.* **2015**, *21*, 15529; l) A. Lerchen, S. Vásquez-Céspedes, F. Glorius, *Angew. Chem. Int. Ed.* **2016**, *55*, 3208; *Angew. Chem.* **2016**, *128*, 3261; m) Y. Liang, N. Jiao, *Angew. Chem. Int. Ed.* **2016**, *55*, 4035; *Angew. Chem.* **2016**, *128*, 4103; n) D. Zell, Q. Bu, M. Feldt, L. Ackermann, *Angew. Chem. Int. Ed.* **2016**, *55*, 7408; *Angew. Chem.* **2016**, *128*, 7534; o) J. A. Boerth, J. R. Hummer, J. A. Ellman, *Angew. Chem. Int. Ed.* **2016**, *55*, 12650; *Angew. Chem.* **2016**, *128*, 12840; p) A. Lerchen, T. Knecht, C. G. Daniliuc, F. Glorius, *Angew. Chem. Int. Ed.* **2016**, *55*, 15166; *Angew. Chem.* **2016**, *128*, 15391.

[5] For selected reviews on Cp*Rh[III]-catalyzed C−H functionalization reactions, see: a) T. Satoh, M. Miura, *Chem. Eur. J.* **2010**, *16*, 11212; b) G. Song, F. Wang, X. Li, *Chem. Soc. Rev.* **2012**, *41*, 3651; c) F. W. Patureau, J. Wencel-Delord, F. Glorius, *Aldrichimica Acta* **2012**, *45*, 31; d) G. Song, X. Li, *Acc. Chem. Res.* **2015**, *48*, 1007.

[6] For selected mechanistic investigations on Cp*Rh[III]-catalyzed C−H functionalization, see: a) M. E. Tauchert, C. D. Incarvito, A. L. Rheingold, R. G. Bergman, J. A. Ellman, *J. Am. Chem. Soc.* **2012**, *134*, 1482; b) M. Brasse, J. Campora, J. A. Ellman, R. G. Bergman, *J. Am. Chem. Soc.* **2013**, *135*, 6427; c) N. Wang, B. Li, H. Song, S. Xu, B. Wang, *Chem. Eur. J.* **2013**, *19*, 358; d) S. H. Park, J. Kwak, K. Shin, J. Ryu, Y. Park, S. Chang, *J. Am. Chem. Soc.* **2014**, *136*, 2492; e) Y. Park, K. T. Park, J. G. Kim, S. Chang, *J. Am. Chem. Soc.* **2015**, *137*, 4534; f) Y. Park, J. Heo, M.-H. Baik, S. Chang, *J. Am. Chem. Soc.* **2016**, *138*, 14020; g) R. Thenarukandiyil, S. K. Gupta, J. Choudhury, *ACS Catal.* **2016**, *6*, 5132.

[7] a) P. Patel, S. Chang, *ACS Catal.* **2015**, *5*, 853; b) Y. Liang, Y.-F. Liang, C. Tang, Y. Yuan, N. Jiao, *Chem. Eur. J.* **2015**, *21*, 16395; c) R. Mei, J. Loup, L. Ackermann, *ACS Catal.* **2016**, *6*, 793.

[8] For mass spectrometric detection of cyclometalated Cp*Co[III] compounds, see: a) T. Gensch, F. J. R. Klauck, F. Glorius, *Angew. Chem. Int. Ed.* **2016**, *55*, 11287; *Angew. Chem.* **2016**, *128*, 11457; b) W. Yu, W. Zhang, Z. Liu, Y. Zhang, *Chem. Commun.* **2016**, *52*, 6837.

[9] For a cationic cyclometalated (η^5-C$_5$H$_5$)Co[III] complex synthesized by an orthometalation reaction, see: T. Avilés, A. Dinis, M. J. Calhorda, P. Pinto, V. Félix, M. G. B. Drew, *J. Organomet. Chem.* **2001**, *625*, 186.

[10] For representative examples on Cp*Co[III]-catalyzed oxidative alkyne annulation, see: a) B. Sun, T. Yoshino, M. Kanai, S. Matsunaga, *Angew. Chem. Int. Ed.* **2015**, *54*, 12968; *Angew. Chem.* **2015**, *127*, 13160; b) Q. Lu, S. Vásquez-Céspedes, T. Gensch, F. Glorius, *ACS Catal.* **2016**, *6*, 2352; c) Z.-Z. Zhang, B. Liu, J. W. Xu, S.-Y. Yan, B.-F. Shi, *Org. Lett.* **2016**, *18*, 1776; d) S. Prakash, K. Muralirajan, C.-H. Cheng, *Angew. Chem. Int. Ed.* **2016**, *55*, 1844; *Angew. Chem.* **2016**, *128*, 1876; e) K. Muralirajan, R. Kuppusamy, S. Prakash, C.-H. Cheng, *Adv. Synth. Catal.* **2016**, *358*, 774; f) Y.-X. Lao, S.-S. Zhang, X.-G. Liu, C.-Y. Jiang, J.-Q. Wu, Q. Li, Z.-S. Huang, H. Wang, *Adv. Synth. Catal.* **2016**, *358*, 2186; g) G. Sivakumar, A. Vijeta, M. Jeganmohan, *Chem. Eur. J.* **2016**, *22*, 5899; h) X. Yu, K. Chen, F. Yang, S. Zha, J. Zhu, *Org. Lett.* **2016**, *18*, 5412; i) R. Mandal, B. Sundararaju, *Org. Lett.* **2017**, *19*, 2544.

[11] a) T. Eicher, S. Hauptmann, *The Chemistry of Heterocycles: Structure, Reactions, Syntheses and Applications*, 2nd ed., Wiley-VCH, Weinheim, **2003**; b) A. Mishra, C.-Q. Ma, P. Bäuerle, *Chem. Rev.* **2009**, *109*, 1141; c) J. Alvarez-Builla, J. J. Vaquero, J. Barluenga, *Modern Heterocyclic Chemistry*, Wiley-VCH, Weinheim, **2011**; d) M. Gulías, J. L. Mascareñas, *Angew. Chem. Int. Ed.* **2016**, *55*, 11000; *Angew. Chem.* **2016**, *128*, 11164.

[12] a) X. Chen, X. Hu, Y. Deng, H. Jiang, W. Zeng, *Org. Chem.* **2016**, *18*, 4742; b) X.-G. Liu, Q. Li, H. Wang, *Adv. Synth. Catal.* **2017**, *359*, 1942.

[13] For recent literature precedents on the synthesis of metallacycles through ligand-directed oxidative addition, see: a) M. Albrecht, *Chem. Rev.* **2010**, *110*, 576; b) J. Guenther, S. Mallet-Ladeira, L. Estevez, K. Miqueu, A. Amgoune, D. Bourissou, *J. Am. Chem. Soc.* **2014**, *136*, 1778; c) J. Serra, T. Parella, X. Ribas, *Chem. Sci.* **2017**, *8*, 946.

[14] For a seminal report on the synthesis of [Cp*Co[III]R$_F$I(CO)] through the oxidative addition of perfluoroalkyl iodides (R_f-I) to Cp*Co[I] complexes, see: R. B. King, M. B. Efraty, W. M. Douglas, *J. Organomet. Chem.* **1973**, *56*, 345.

[15] **3-I** is analogous to a cobaltacycle synthesized by Kanai, Matsunaga, and co-workers through a transmetalation reaction (33 % reported yield, see Ref. [4b]). See Supporting Information for full characterization.

[16] Chang and co-workers showed the catalytic activity of the **3-I** analogue synthetized by Kanai, Matsunaga, and co-workers in the cobalt-catalyzed C−H amidation with dioxazolones, see Ref. [4i].

[17] By using ESI-MS, we observed complex **3-MeCN** along with the cationic species without the acetonitrile coordinated (**7**).

[18] CCDC 1540811 (**3-I**) and 1540812 (**3-MeCN**) contain the supplementary crystallographic data for this paper. These data can be obtained free of charge from The Cambridge Crystallographic Data Centre.

[19] We selected analogous reaction conditions to those reported previously by Wang and co-workers (Ref. [9f]): **1** (1 equiv), **4** (3 equiv), [Cp*Co^{III}I$_2$(CO)] (10 mol%), AgBF$_4$ (1 equiv), Cu-(OAc)$_2$ (1 equiv), DCE, 100°C, 24 h.

[20] While **5** could be obtained in 78% at 35°C with **3-I**, the combination of **3-I** (10 mol%) with MeCN (10 mol%) afforded a comparable yield relative to **3-MeCN**. In sharp contrast, a significant erosion in yield is observed when using **3-I** at 100°C. At present, we believe these results showcase the inherent proclivity of cobaltacycles to decomposition. See Supporting Information for more details.

[21] The yield of **5** decreased dramatically when [Cp*Co(MeCN)$_3$]-(BF$_4$)$_2$ was used as precatalyst. Based on our stoichiometric results, we hypothesized that the presence of excess of MeCN inhibited the reaction. See Supporting Information for more details.

[22] See Supporting Information for more details.

[23] CCDC 1540813 (**6**) contains the supplementary crystallographic data for this paper. These data can be obtained free of charge from The Cambridge Crystallographic Data Centre. **6** was also fully characterized by NMR spectroscopy and ESI-MS. The cationic species (**8**) without the acetonitrile coordinated was also detected by ESI-MS. See Supporting Information for more details.

[24] As expected, we observed H/D scrambling at the *ortho* position of **1** under catalytic conditions at 30°C in CD$_2$Cl$_2$, in the absence of **4** and AgBF$_4$ and in the presence of D$_2$O using **3-MeCN** as catalyst.

3.6 Supporting Information for Article 1

Table of Contents

3.6.1 General Procedures

All experiments were conducted under an argon-filled glove box (mBraun Unilab 4420) with concentrations of O_2 and H_2O < 0.1 ppm or using Schlenk techniques under argon atmosphere.

All the glassware was oven-dried at 100 ºC overnight and cooled under vacuum prior use.

NMR spectrum were obtained on a Bruker 400 MHz or a 500 MHz cryoprobe spectrometers. ^1H, ^{13}C and ^{19}F NMR chemical shifts are reported in parts per million (ppm), relative to tetramethylsilane (TMS) for ^1H and ^{13}C with the residual solvent peak used as an internal reference, and relative to CCl_3F (Freon) for ^{19}F. Multiplicities are reported as follows: singlet (s), doublet (d), doublet of doublets (dd), triplet of doublets (td), triplet (t), broad signal (br) and multiplet (m).

High Resolution Mass Spectrometry (HRMS) data was recorded on a LCT-Premier (Waters) or a MicroTOF Focus (Bruker Daltonics) mass spectrometers using ESI ionization technique and acetonitrile as solvent.

The details for the X-ray structure determination can be found in page 80.

3.6.2 Materials and Methods

Commercially available reagents 2-phenylpyridine, N-Iodosuccinimide, $Pd(OAc)_2$, 1,2,3,4,5-pentamethylcyclopentadiene, 1,3-cyclohexadiene, ^nBuLi, $Co_2(CO)_8$, $CoCl_2$, Zn, vinyltrimethylsilane, AgBr, AgCl, $AgBF_4$, diphenylacetylene, $Cu(OAc)_2$, 1,2-dichloroethane, methanol, ethyl acetate and acetone were used without further purification directly as received from the commercial supplier, and stored under inert gas and/or low temperature when required.

If necessary, the solvents (^nhexane, Et_2O, THF, CH_2Cl_2, MeCN) were used from a solvent purification system *pure-solv* (SPS-400, Innovative Technology) and stored under argon with activated 4 Å molecular sieves.

Solvents were degassed (when necessary) by bubbling an argon stream at 0 ºC for at least 2 h.

Deuterated solvents ($CDCl_3$, CD_2Cl_2, CD_3CN) were stored under argon with activated 4 Å molecular sieves.

2-CO,[1a] [Cp*CoI$_2$(CO)][1a] and [Cp*Co(MeCN)$_3$][BF$_4$]$_2$[1b] were synthesized according to previous literature procedures.

---

[1] (a) Chan, N. H.; Roache, J. H.; Jones, W. D. *Inorganica Chimica Acta* **2015**, *437*, 36. (b) Yu, D.-G.; Gensch, T.; de Azambuja, F.; Vásquez-Céspedes, S.; Glorius, F. *J. Am. Chem. Soc.* **2014**, *136*, 17722.

3.6.3 Modified Procedures

3.6.3.1 Synthesis of 1-I

1 (1 equiv)   (1.2 equiv)   (5 mol%)   **1-I** 47%
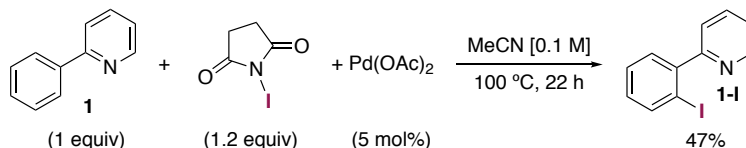
Synthetic procedure for the preparation of **1-I** was similar to the already reported procedure by Sanford and coworkers[2] adding an extra step in the purification.

In a J-Young Schlenk tube, **1** (2.1 mL, 14.7 mmol), N-Iodosuccinimide (3.9 g, 17.6 mmol) and Pd(OAc)$_2$ (160 mg, 0.7 mmol) were weighed successively and dissolved in 120 mL of anhydrous MeCN. The mixture was heated at 100 °C for 22 h. The solvent was removed *in vacuo*. The resulting crude was dissolved in CH$_2$Cl$_2$ and filtered through a pad of silica. The filtrate was concentrated to yield a yellow oil which was purified by column chromatography on silica gel using a gradient from *n*hexane (100%) to *n*hexane / AcOEt (8:2). The yellowish oil was washed with *n*hexane (3x5 mL) in order to precipitate the yellow impurities and extract the desired product **1-I** as 1.88 g (47%) of a colorless pure oil. Spectroscopic data was in agreement with the described in the literature.[2]

3.6.3.2 Synthesis of 2-VTMS

(1 equiv)   (1.1 equiv)   **2-VTMS** 65%
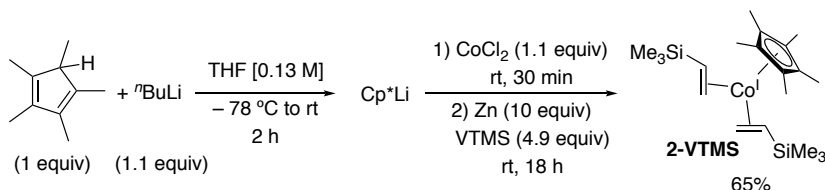
The synthesis was similar to the reported procedure by Brookhart and coworkers[3] using Zn powder as reducing agent instead of Na/Hg amalgam. A 1.6 M solution of *n*BuLi in *n*hexane (0.9 mL, 1.44 mmol) was added to a previously cooled (−78 °C) solution of 1,2,3,4,5-pentamethylcyclopentadiene (181 mg, 1.33 mmol) in 10 mL of anhydrous degassed THF. The reaction was left to warm up to room temperature during 2 h while stirring, forming a white cloudy suspension. In parallel in the glove box, CoCl$_2$ (189 mg, 1.46 mmol) was weighed in a previously dried Schlenk flask with a magnetic stirrer and suspended in 10 mL of anhydrous degassed THF. The

[2] Kalyani, D.; Dick, A. R.; Anani. W. Q.; Sanford, M. S. *Org. Lett*, **2006**, *8*, 2523.
[3] Lenges, C. P.; White, P. S.; Brookhart, M. *J. Am. Chem. Soc*. **1998**, *120*, 6965.

Cp*Li suspension was cannula transferred into the $CoCl_2$ suspension under vigorous stirring changing the color immediately to green and then to a dark blue solution. The reaction mixture was left stirring at room temperature for 30 min. In parallel, in another dried Schlenk flask with a magnetic stirrer, excess of Zn powder (866 mg, 13.24 mmol) was weighed in the glove box. Before adding the previous reaction mixture into the Zn powder, excess of vinyltrimethylsilane (1.0 mL, 6.51 mmol), changing the color to dark green, was added. Right after the addition of the silane, the reaction mixture was cannula transferred into the Zn powder while stirring vigorously. The reaction mixture was left stirring overnight (approx. 18 h) at room temperature changing the color to dark red. The solution was filtered via cannula to a dried Schlenk flask. All volatiles were removed under vacuum forming a dark brown paste. It was treated with 60 mL of dried ^{n}hexane and filtered via cannula to another dried Schlenk flask obtaining a dark red solution. All volatiles were removed under vacuum obtaining the product as a foamy dark red solid in high purity (338 mg, 65% yield). Spectroscopic data was identical to the described in the literature.[3]

3.6.4 Synthesis of 3-I through the Oxidative Addition of 1-I to 2-L

3.6.4.1 Using 2-CO
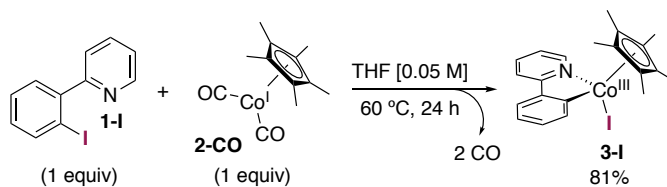
2-CO was weighed (20.2 mg, 80.7 μmol) in a Schlenk flask inside the glove box. Outside, in another Schlenk flask, a solution of **1-I** (22.5 mg, 80.0 μmol) in 1.6 mL of anhydrous degassed THF was prepared. The aryl iodide solution was cannula transferred into the cobalt(I) solution, giving a red mixture. After stirring at 60 °C for 24 h, the resulting dark brown solution was evaporated. The crude was dissolved in CH_2Cl_2, filtered with a cannula, evaporated *in vacuo* and washed with ^{n}hexane to yield 31.0 mg (81%) of the desired compound **3-I** as a brown solid.

3.6.4.2 Using 2-VTMS
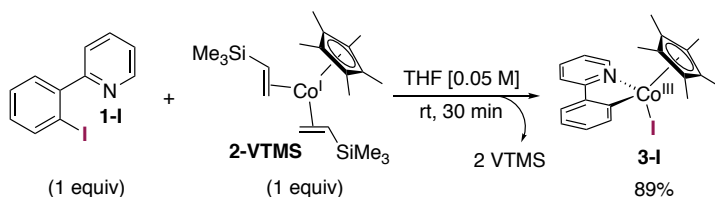
2-VTMS was weighed (39.2 mg, 99.3 µmol) in a Schlenk flask inside the glove box. Outside, in another Schlenk flask, a solution of **1-I** (28.0 mg, 99.6 µmol) in 2.0 mL of anhydrous degassed THF was prepared. The aryl iodide solution was cannula transferred into the cobalt(I) solution, giving a red mixture. After stirring at rt for 30 min the resulting dark brown solution was evaporated. The crude was dissolved in dichloromethane, filtered with a cannula, evaporated *in vacuo* and washed with ^{n}hexane to yield 42.2 mg (89%) of the desired compound **3-I** as a brown solid.

3.6.5 Isolation of 3-MeCN by Reaction of 3-I with AgBF$_4$
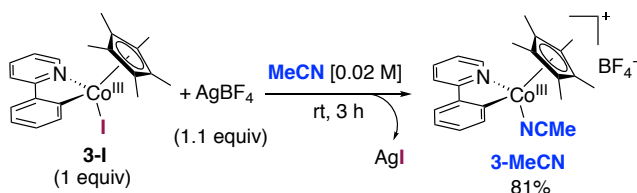
In the glove box, **3-I** (95.8 mg, 0.202 mmol) and AgBF$_4$ (44.2 mg, 0.227 mmol) were weighed in a previously dried 50 mL Schlenk flask containing a magnetic stirrer. Once the Schlenk flask was adapted to the Schlenk line under Ar atmosphere, 10 mL of anhydrous MeCN were added under vigorous stirring. The color changed immediately to orange while a voluminous white precipitate was formed. The reaction was left under stirring for 3 h at room temperature. The solution was cannula filtered to another vacuum dried Schlenk flask. All volatiles were removed under vacuum obtaining a sticky orange oily product. This product was treated with 30 mL of anhydrous Et$_2$O for 3 h at room temperature forming an orange-reddish solid, which was filtered off via cannula. The solid was recrystallized by slow liquid diffusion, re-dissolving it in 3.0 mL of anhydrous CH$_2$Cl$_2$ and adding 40 mL of anhydrous ^{n}hexane on the top of this solution. Orange crystals were obtained after standing in the fridge at 5 °C overnight. The crystals were filtered off via cannula and dried under vacuum to give rise to 78.0 mg (81%) of **3-MeCN**.

3.6.6 Characterization of 3-I, 3-MeCN and 6

Characterization of **3-I**
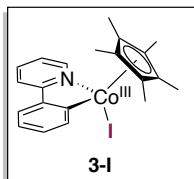
¹H NMR (500 MHz, CD$_2$Cl$_2$, 25 °C): δ 9.19 (d, 1H), 8.24 (dd, 1H), 7.69−7.65 (m, 2H), 7.59 (dd, 1H), 7.27 (td, 1H), 7.12−7.02 (m, 2H), 1.47 (s, 15H).

¹³C NMR (126 MHz, CD$_2$Cl$_2$, 25 °C): δ 182.0, 167.2, 155.3, 146.2, 142.8, 137.1, 129.2, 123.4, 122.81, 121.6, 118.8, 93.8, 10.4.

HRMS-ESI (m/z): [M+Na]⁺ calcd for C$_{21}$H$_{23}$CoINNa, 498.0105; Found, 498.0099; [M−I]⁺ calcd for C$_{21}$H$_{23}$CoN, 348.1162; Found, 348.1149.

Characterization of **3-MeCN**
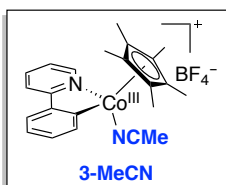
¹H NMR (400 MHz, CDCl$_3$, 25 °C): δ 9.35 (d, 1H), 8.07 (d, 1H); 7.82 (td, 1H), 7.72 (d, 1H), 7.61 (d, 1H), 7.42 (t, 1H), 7.36 (t, 1H), 7.22 (t, 1H), 2.27 (s, 3H), 1.37 (s, 15H).

¹³C NMR (100 MHz, CDCl$_3$, 25 °C): δ 176.0, 166.6, 154.6, 147.1, 139.1, 138.8, 130.3, 130.0, 124.8, 124.0, 123.6, 119.1, 96.5, 9.4, 4.4.

¹⁹F NMR (376 MHz, CDCl$_3$, 25 °C): δ −152.8 (s).

HRMS-ESI (m/z): [M]⁺ calcd for C$_{23}$H$_{26}$CoN$_2$ 389.1422; Found, 389.1423; [M−MeCN]⁺ calcd for C$_{21}$H$_{23}$CoN, 348.1162; Found, 348.1151.

Characterization of **6**
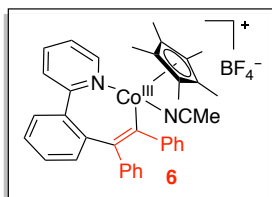
¹H NMR (400 MHz, CD$_2$Cl$_2$, −20 °C): δ 9.04 (d, 1H), 7.98 (t, 1H), 7.70 (d, 1H), 7.52 (m, 1H), 7.42−7.26 (m, 6H), 7.25−7.17 (m, 2H), 7.02−6.96 (m, 2H), 6.93 (d, 1H), 6.84 (t, 1H). 6.64 (br, 1H), 5.64 (br, 1H), 1.00 (s, 15H).

¹³C NMR data could not be obtained due to the instability of the complex over the timescale required for the experiment.

¹⁹F NMR (376 MHz, CD$_2$Cl$_2$, −20 °C): δ −151.7 (s).

HRMS-ESI (m/z): [M−MeCN]⁺ calcd for C$_{35}$H$_{33}$CoN 526.1945; Found, 526.1929.

3.6.7 Catalytic reactions

General modified procedure
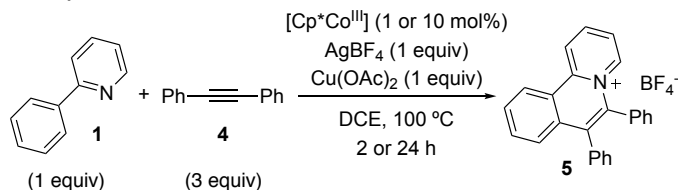
The reported procedure by Lao *et al.*[4], with minor changes in the purification step, was followed for the synthesis of the annulated product.

In the glove box, diphenylacetylene (53.4 mg, 0.3 mmol), Cu(OAc)$_2$ (18.2 mg, 0.1 mmol), the [Cp*Co^{III}] catalyst and AgBF$_4$ (19.5 mg, 0.1 mmol) were added into a 5 mL screw cap vial followed by the addition of a stock solution of 2-phenylpyridine (**1**) (15.5 mg, 0.1 mmol) in 1,2-dichloroethane (1.0 mL). The resulting reaction mixture was stirred outside the glove box at the temperature and time described in **Table S1**. After cooling down to room temperature, the reaction mixture was then purified by flash column chromatography on silica gel using CH$_2$Cl$_2$ / ^{n}hexane (1:3) to remove the excess of the alkyne, and then MeOH / CH$_2$Cl$_2$ (1:35) as the eluent.

---

[4] Lao, Y.-X.; Zhang, S.-S.; Liu, X.-G.; Jiang, C.-Y.; Wu, J.-Q.; Li, Q.; Huang, Z.-S.; Wang, H. *Adv. Synth. Catal.* **2016**, *358*, 2186.

The resulting solid was washed successively with acetone and Et$_2$O to give the pure cyclized product **5** as a white solid.

The catalysis conditions were optimized focused on the catalyst loading, temperature and time variables. The results are summarized in the following table.

Table S1. Optimization of the parameters for the catalytic obtention of **5** with [Cp*Co^{III}] catalysts.

Entry	Catalyst	mol%	T (ºC)	Time (h)	Yield (%)[a]
1	**3-MeCN**	10	100	2	89
2	**3-I**	10	100	2	66
3	[Cp*CoI$_2$(CO)]	10	100	2	84
4	**3-MeCN**	1	100	2	90
5	**3-I**	1	100	2	46
6	[Cp*CoI$_2$(CO)]	1	100	2	66
7	[Cp*Co(MeCN)$_3$][BF$_4$]$_2$	1	100	2	40
8	**3-MeCN**	10	35	24	64[b]
9	**3-I**	10	35	24	78[b]
10	**3-I**	10	35	24	62[b,c]
11	[Cp*CoI$_2$(CO)]	10	35	24	39[b]
12	[Cp*Co(MeCN)$_3$][BF$_4$]$_2$	10	35	24	37[b]

[a] Reactions were run in duplicate and the yields are for the isolated product
[b] In DCM. [c] 10 mol% MeCN added.

3.6.8. Intermediate Observation in Catalytic Conditions

3.6.8.1 Using Standard Conditions
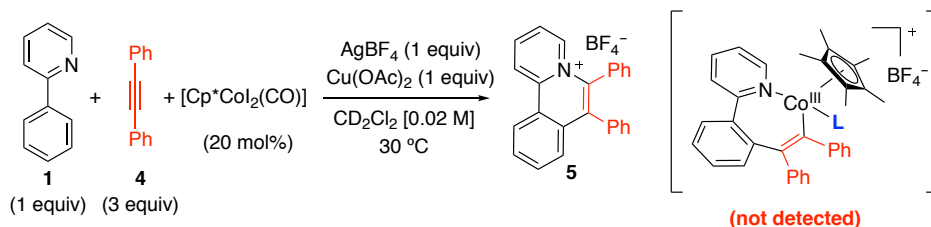
In an NMR tube inside the glove box were added [Cp*CoI$_2$(CO)] (2.1 mg, 4.4 μmol), Cu(OAc)$_2$ (3.7 mg, 20 μmol), diphenylacetylene (11 mg, 62 μmol) and AgBF$_4$ (3.9 mg, 20 μmol). Then, outside the glove box, 2-phenylpyridine (2.9 μL, 20 μmol) and CD$_2$Cl$_2$ (0.50 ml) were added successively under argon stream at −50 °C. The reaction mixture was heated to 30 °C and monitored by ^{1}H NMR.
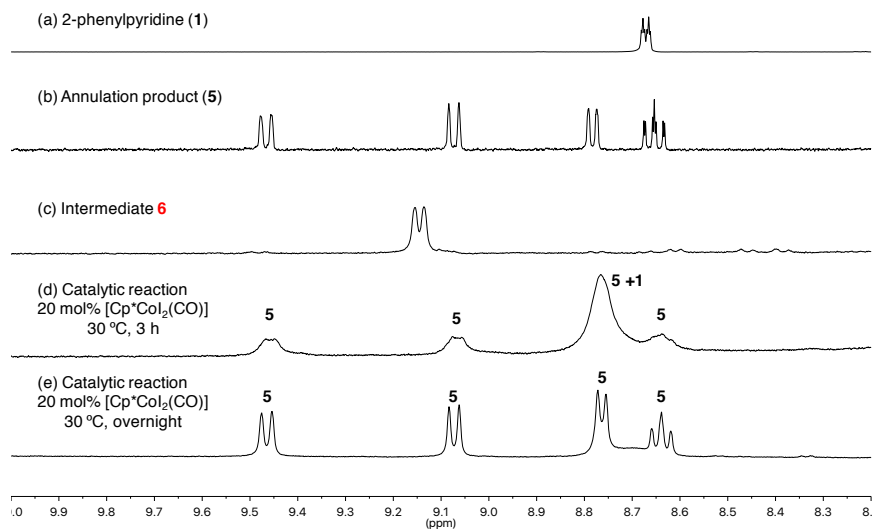
Figure S1. Standard catalytic reaction monitored by ^{1}H NMR.

3.6.8.1 Using 3-MeCN as the Catalyst
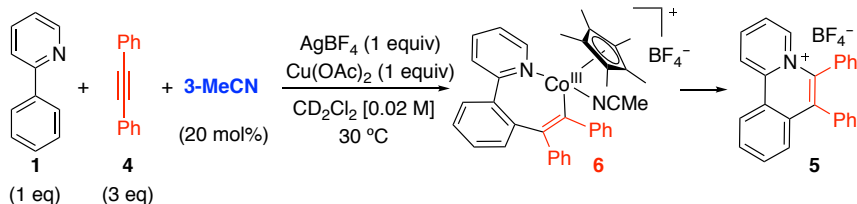
In an NMR tube inside the glove box were added **3-MeCN** (2.3 mg, 4.8 μmol), Cu(OAc)$_2$ (3.8 mg, 21 μmol), diphenylacetylene (11 mg, 62 μmol) and AgBF$_4$ (3.6 mg, 18 μmol). Then, outside the glove box, 2-phenylpyridine (2.9 μL, 20 mmol) and CD$_2$Cl$_2$ (0.50 ml) were added successively under argon stream at −50 °C. The reaction mixture was heated to 30 °C and monitored by ^{1}H NMR.
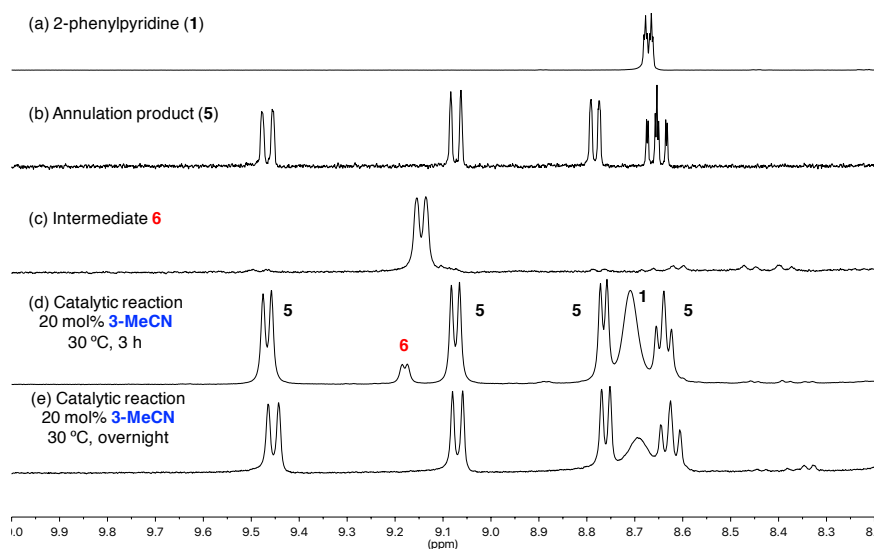
Figure S2. Catalytic reaction using **3-MeCN** as the catalyst monitored by ^{1}H NMR.

3.6.9. Stoichiometric Experiments

3.6.9.1 Reaction of 3-MeCN with Diphenylacetylene
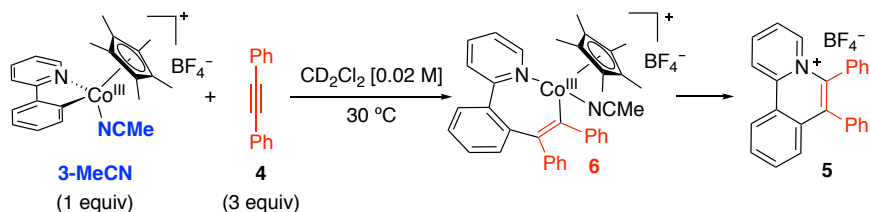
In an NMR tube inside the glove box were added **3-MeCN** (4.7 mg, 9.8 µmol) and diphenylacetylene (5.2 mg, 29.2 µmol). Then, outside the glove box, CD$_2$Cl$_2$ (0.50 ml) was added under argon stream at −50 °C. The reaction was monitored into a previously thermostated NMR spectrometer at 30 °C. Conversion data was acquired from the integration of the ^{1}H NMR signals of **3-MeCN**, **6** and **5**.
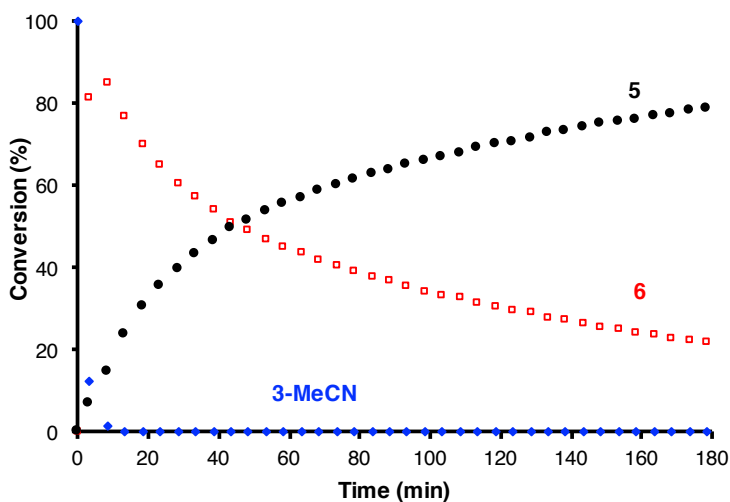
Figure S3. Kinetic profile for the stoichiometric reaction between **3-MeCN** and **4** at 30 °C in CD$_2$Cl$_2$.

3.6.9.2 Addition of Excess of MeCN
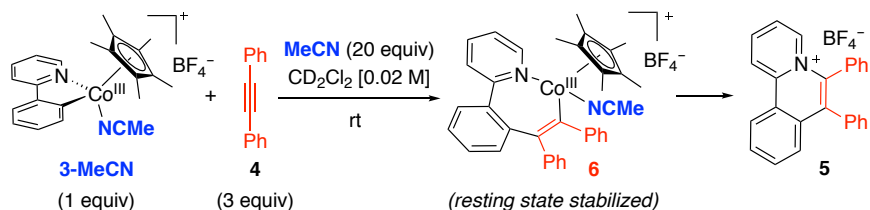
In an NMR tube inside the glove box were added **3-MeCN** (4.7 mg, 9.8 µmol) and diphenylacetylene (5.2 mg, 29.2 µmol). Then, outside the glove box, a 0.4 M stock solution of CD_3CN (10 µL, 19.2 µmol) in CD_2Cl_2 (0.50 ml) was added under argon stream. The reaction was monitored at room temperature. Conversion data was acquired from the integration of the ${}^1H$ NMR signals of **3-MeCN**, **6** and **5**.
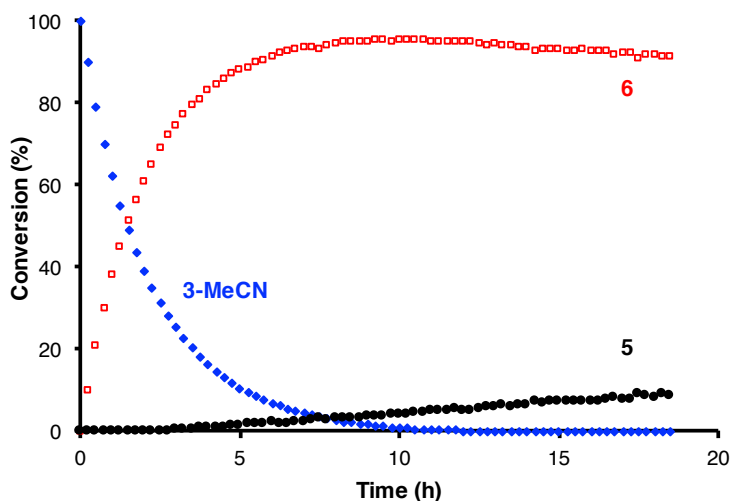
Figure S4. Kinetic profile for the addition of MeCN (20 equiv) to the stoichiometric reaction between **3-MeCN** and **4** at 30 ºC in CD_2Cl_2.

3.6.9.3 Indirect Detection of Cp*Co^I Species
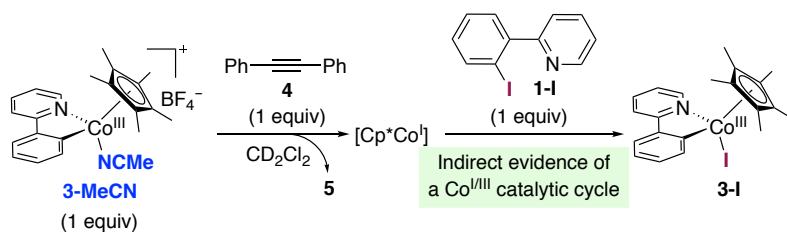
In an NMR tube inside the glove box were added **3-MeCN** (5.0 mg, 11 μmol) and diphenylacetylene (1.3 mg, 11.0 μmol). Then, outside the glove box, CD$_2$Cl$_2$ (0.50 ml) was added under argon stream. The reaction was monitored at room temperature. After 30 min, **1-I** was added (3.0 mg, 11 μmol) under argon stream. The reaction was monitored at room temperature.
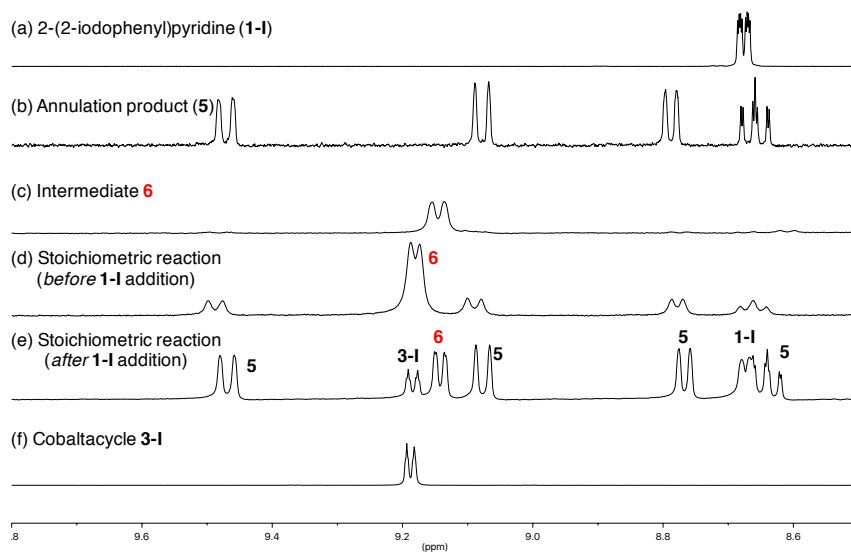
Figure S5. Reaction monitoring by ^{1}H NMR for the indirect observation of [Cp*Co^I] species.

3.6.10 Deuterium Insertion Reaction
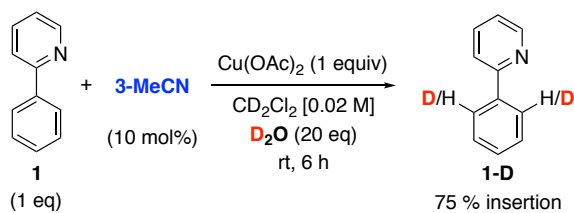
In an NMR tube inside the glove box were added **3-MeCN** (0.9 mg, 2 μmol) and Cu(OAc)$_2$ (3.6 mg, 20 μmol). Then, outside the glove box, CD$_2$Cl$_2$ (0.50 ml), 2-phenylpyridine (2.8 μL, 20 μmol) and D$_2$O (7.2 μL, 400 μmol) were added successively under argon stream. After 6 h at rt we observed by ^{1}H NMR a 75% insertion.

3.6.11 Single Crystal X-Ray Structure Determination of 3-I, 3-MeCN and 6
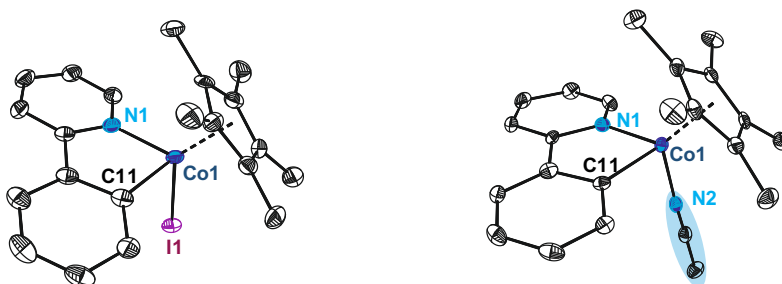
Figure S6. ORTEP drawings (thermal ellipsoids are rendered at 50% probability) of the structures of **3-I** (left) and **3-MeCN** (right). Hydrogen atoms and, in case of being present, solvent molecules or anions have been omitted for clarity.
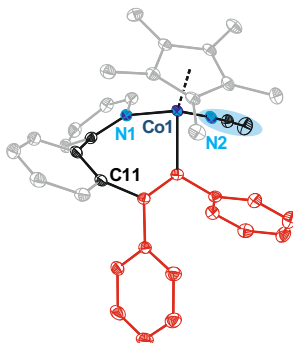
Figure S7. ORTEP drawing (thermal ellipsoids are rendered at 50% probability) of the structure **6**. Hydrogen atoms and, in case of being present, solvent molecules or anions have been omitted for clarity.

Crystal preparation: Crystals of **3-I, 3-MeCN** and **6** were grown by slow diffusion of ^{n}hexane into solutions of dichloromethane at −32 ºC. The measured crystals were prepared under inert conditions, immersed in perfluoropolyether as protecting oil on a glass slide before being mounted on a capton loop. In the case of **6**, the crystals decomposed quickly at temperatures above −32 ºC so the perfluoropolyether oil was previously cooled by adding $CO_{2(s)}$ under the glass slide. The crystals were handled quickly before being mounted.

Data collection: Crystal structure determinations of **3-MeCN** and **6** were carried out using a Apex DUO Kappa 4-axis goniometer equipped with an APPEX 2 4K CCD area detector, a Microfocus Source E025 IuS using MoK$_\alpha$ radiation (0.71073 Å), Quazar MX multilayer Optics as monochromator and an Oxford Cryosystems low

temperature device Cryostream 700 plus (*T* = −173 ˚C). Full-sphere data collection was used with ω and φ scans. *Programs used:* Data collection APEX-2,[5a] data reduction Bruker Saint[5b] V/.60A and absorption correction SADABS[5c] and TWINABS[5d] for **3-MeCN** and **6**.

Crystal structure determination for compound **3-I** was carried out using a Rigaku diffractometer equipped with a Pilatus 200K area detector, a Rigaku MicroMax-007HF microfocus rotating anode with MoK$_\alpha$ radiation, Confocal Max Flux optics and an Oxford Cryosystems low temperature device Cryostream 700 plus (*T* = −183 ˚C). Full-sphere data collection was used with ω and φ scans. *Programs used:* Data collection CrystalClear,[5e] data reduction with CrysAlisPro[5f] V/.60A and absorption correction with Scale3 Abspack scaling algorithm.[5g]

Structure Solution and Refinement: Crystal structure solution was achieved using the computer program SHELXT.[5h] Visualization was performed with the program SHELXle.[5i] Missing atoms were subsequently located from difference Fourier synthesis and added to the atom list. Least-squares refinement on F^2 using all measured intensities was carried out using the program SHELXL 2015.[5j] All non-hydrogen atoms were refined including anisotropic displacement parameters.

Comments to the structures: Compound **3-I** crystallized as a dichloromethane solvate in a ratio 1:1. The asymmetric unit for the structure of **3-MeCN** contains two molecules of the cationic cobalt metal complex attached to an acetonitrile molecule, two BF$_4$-anions and two dichloromethane molecules. One of the Cp*-ligands, one BF$_4$-anion and one dichloromethane molecule are disordered in two orientations (ratios: Cp* 50:50, BF$_4^-$ 60:40 and dichloromethane 70:30). The charge balance is 0. The measured sample is formed by a minimum of three crystals with a ratio of 64:23:13. The collected data for all three crystals were processed with TWINABS taking in account overlapping reflections. The asymmetric unit of the structure of **6** contains one cationic molecule of the metal complex, one BF$_4$-anion and two dichloromethane molecules. One of the dichloromethane molecules is disordered in two positions with a ratio of 60:40. The measured sample is formed by a minimum of two crystals with a ratio of 71:29. The collected data were processed with TWINABS taking into account overlapping reflections.

[5] (a) Data collection with APEX II v2014.9-0. Bruker (2014). Bruker AXS Inc., Madison, Wisconsin, USA. (b) Data reduction with Bruker SAINT+ version V8.35A. Bruker (2013). Bruker AXS Inc., Madison, Wisconsin, USA. (c) SADABS: V2014/5 Bruker (2001). Bruker AXS Inc., Madison, Wisconsin, USA. Blessing, Acta Cryst. (1995) A51 33-38. (d) TWINABS Version 2008/4 Bruker AXS; Blessing, Acta Cryst. (1995) A51 33-38. (e) Data collection with CrystalClear-SM Expert 2.1 b29. Rigaku 2013. (f) Data reduction with CrysAlisPro 1.171.38.37f (Rigaku OD, 2015). (g) Empirical absorption correction using spherical harmonics implemented in Scale3 Abspack scaling algorithm, CrysAlisPro 1.171.38.37f (Rigaku OD, 2015). (h) SHELXT; Sheldrick, G.M. *Acta Cryst*. **2015** A71, 3-8. (i) SHELXle; C.B. Huebschle, G.M. Sheldrick & B. Dittrich; J.Appl.Cryst. (2011) 44, 1281-1284. (j) SHELXL; Sheldrick, G.M. *Acta Cryst*. **2015** C71, 3-8. SHELXT

Table S2: Crystal data for compounds **3-I, 3-MeCN,** and **6**.

Compound	3-I	3-MeCN	6
Formula	$C_{22}H_{24}Cl_3Co_1I_1O_1N_1$	$C_{24}H_{28}B_1Cl_2Co_1F_4N_2$	$C_{39}H_{40}B_1Cl_4Co_1F_4N_2$
Solvents	$1 \times CH_1Cl_3$	$2 \times CH_2Cl_2$	$2 \times CH_2Cl_2$
Formula weight	594.60	561.12	824.27
Crystal size (mm³)	0.15 x 0.10 x 0.05	0.15 x 0.12 x 0.04	0.10 x 0.10 x 0.04
Crystal color	red	red	red
Temp (K)	90	100	100
Crystal system	orthorhombic	monoclinic	monoclinic
Space group	$Pca2_1$	$P2_1/c$	$P2_1/c$
A (Å)	13.2003(10)	15.7322(12)	18.274(3)
B (Å)	14.5076(12)	12.8138(9)	14.107(2)
C (Å)	12.1182(7)	24.8722(16)	14.908(3)
α (deg)	90	90	90
β (deg)	90	91.821(4)	96.949(6)
γ (deg)	90	90	90
V (Å³)	2320.7(3)	5011.4(6)	3815.0(11)
Z	4	8	4
ρ (g/cm³)	1.702	1.487	1.435
μ (mm⁻¹)	2.424	0.944	0.781
θ_{max} (°)	30.796	25.143	29.018
Reflec. measured	25084	9296	9622
Unique reflections	5048 [R_{int} = 0.0636]	7170 [R_{int} = 0.0817]	7651 [R_{int} = 0.0610]
Absorpt. correct.	empirical	Empirical, multicomponent	Empirical, multicomponent
Trans. min/max	0.738/0.975	0.741/0.963	0.659/0.969
Parameters/restrains	258/1	794/564	494/35
R1/wR2 [I>2σ(I)]	0.0511/0.1177	0.0514/0.1095	0.0500/0.1383
R1/wR2 [all data]	0.0774/0.1287	0.0763/0.1230	0.7040.1596
Goodness-of-fit (F²)	1.046	1.024	1.103
Peak/hole (e/Å³)	1.866/-1.457	0.614/-0.531	0.563/-0.637

3.6.12 NMR Characterization of Complex 3-I

¹H NMR spectrum of **3-I** at 25 °C (CD₂Cl₂)
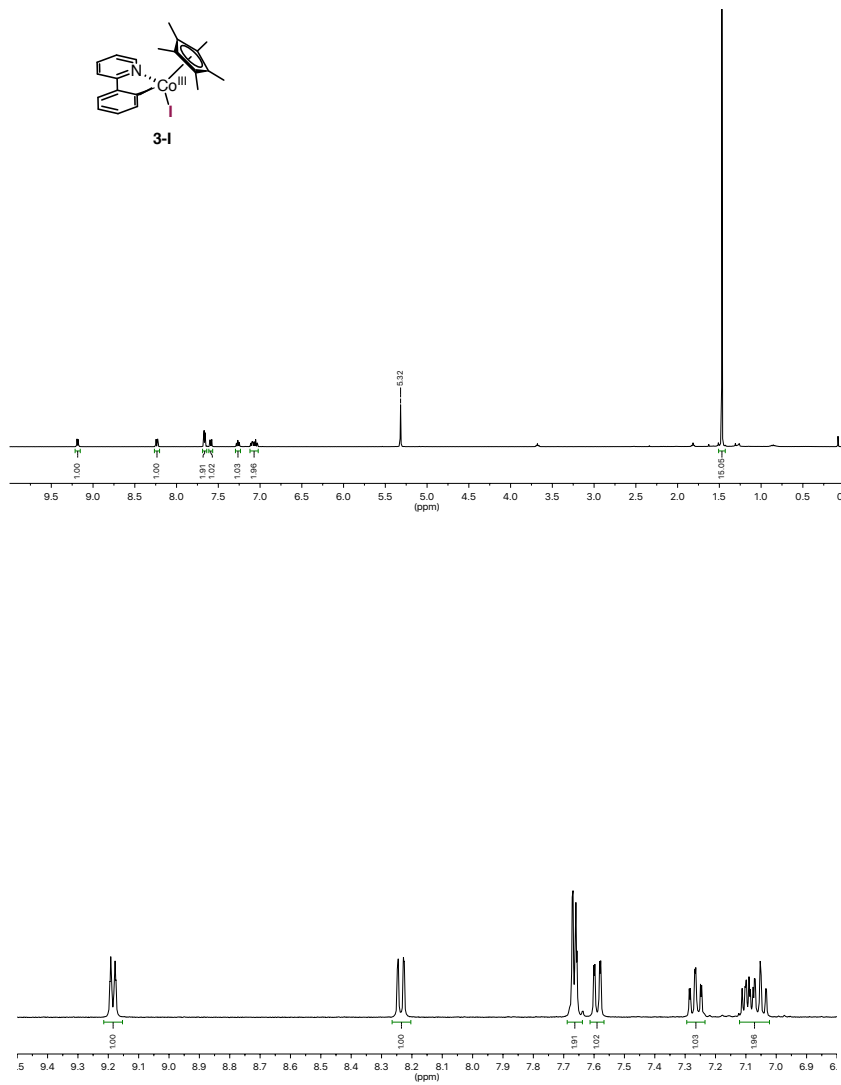
13C NMR spectrum of **3-I** at 25 ºC (CD₂Cl₂)
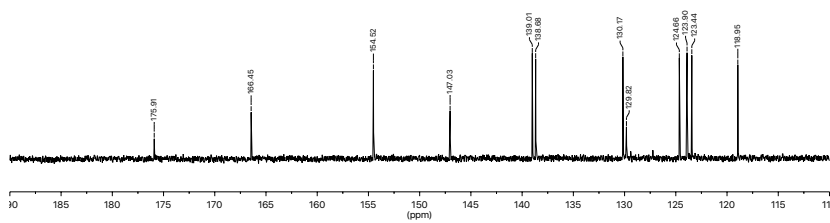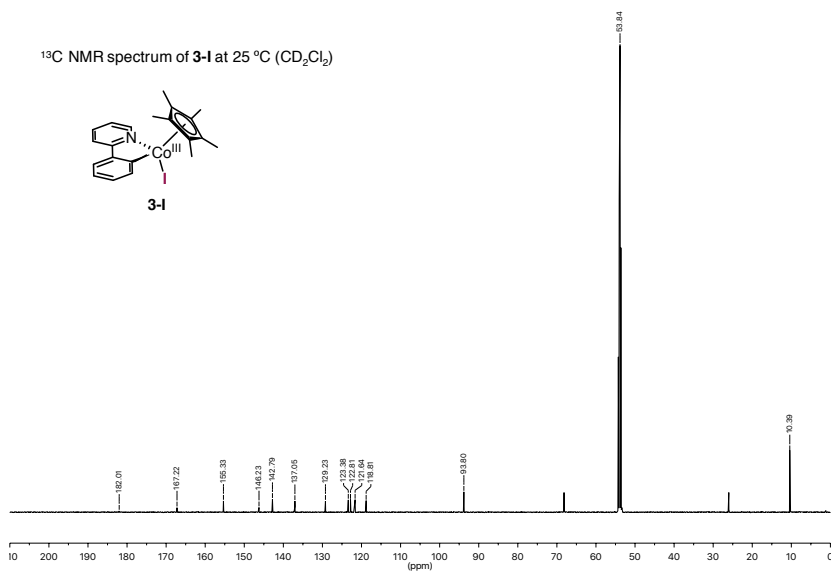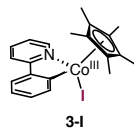
3-I

¹H-¹H COSY NMR spectrum of **3-I** at 25 ºC (CD₂Cl₂)

¹H-¹H TOCSY NMR spectrum of **3-I** at 25 °C (CD₂Cl₂)
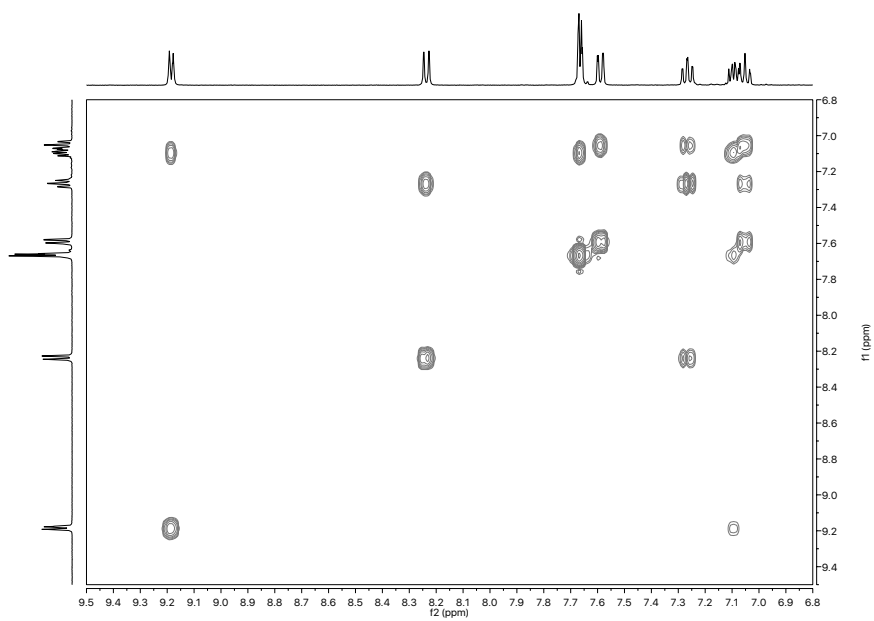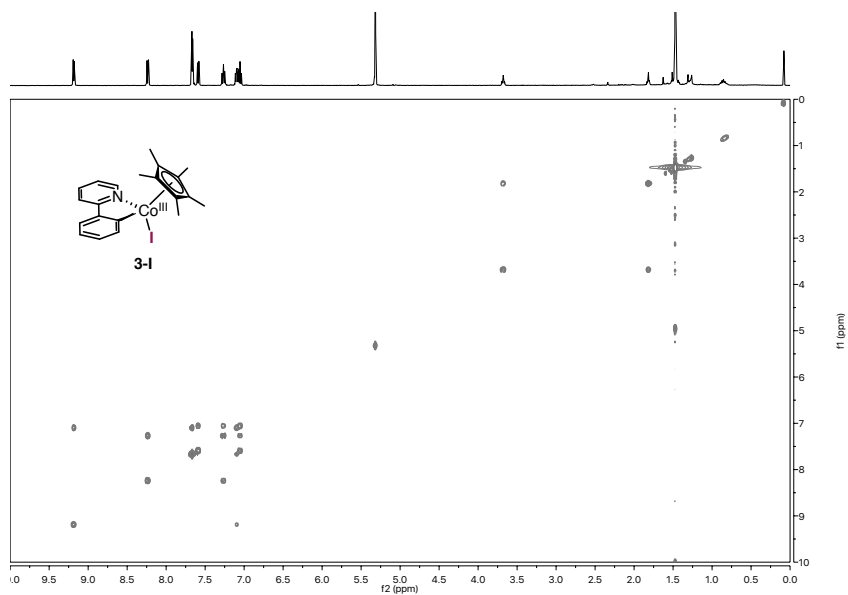
¹H-¹³C HSQC NMR spectrum of **3-I** at 25 ºC (CD₂Cl₂)

^{1}H-^{13}C HMBC NMR spectrum of **3-I** at 25 ºC (CD$_2$Cl$_2$)
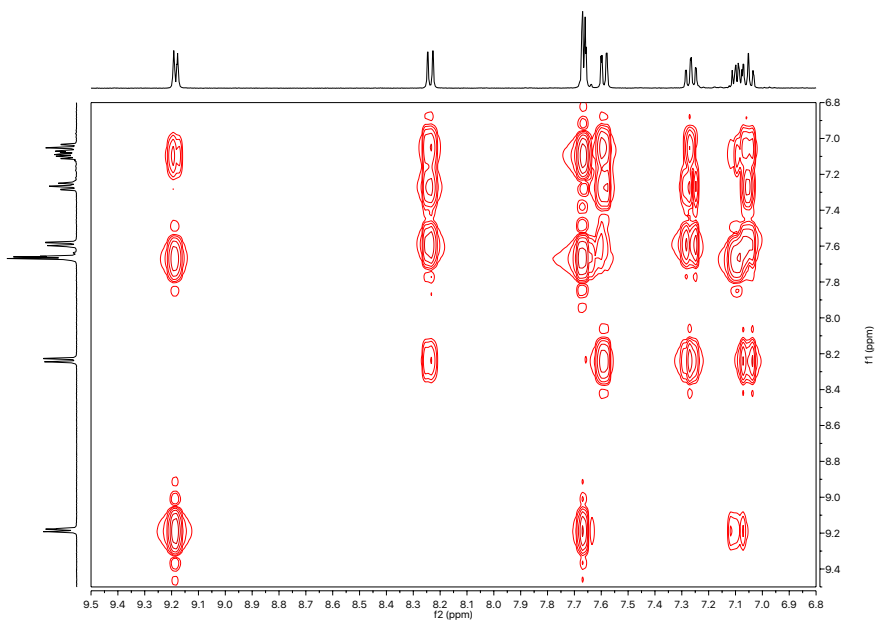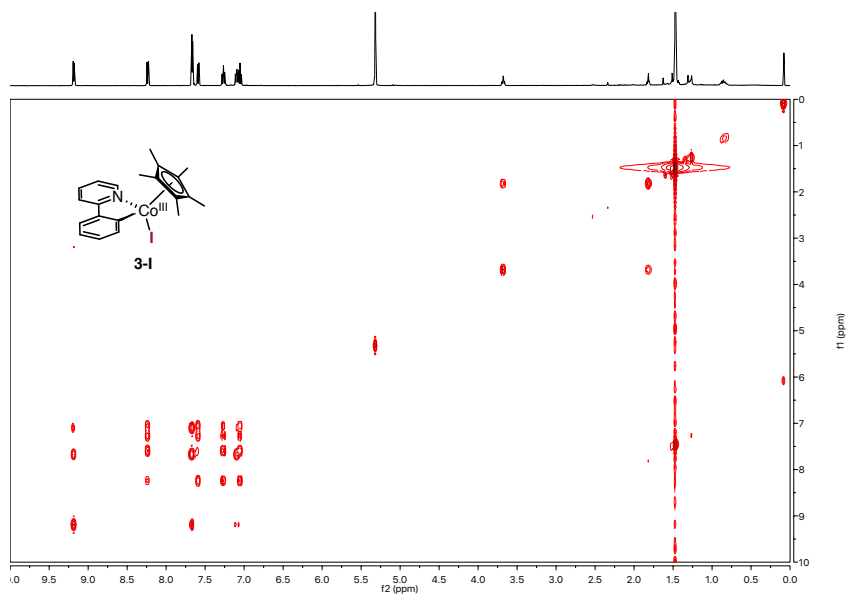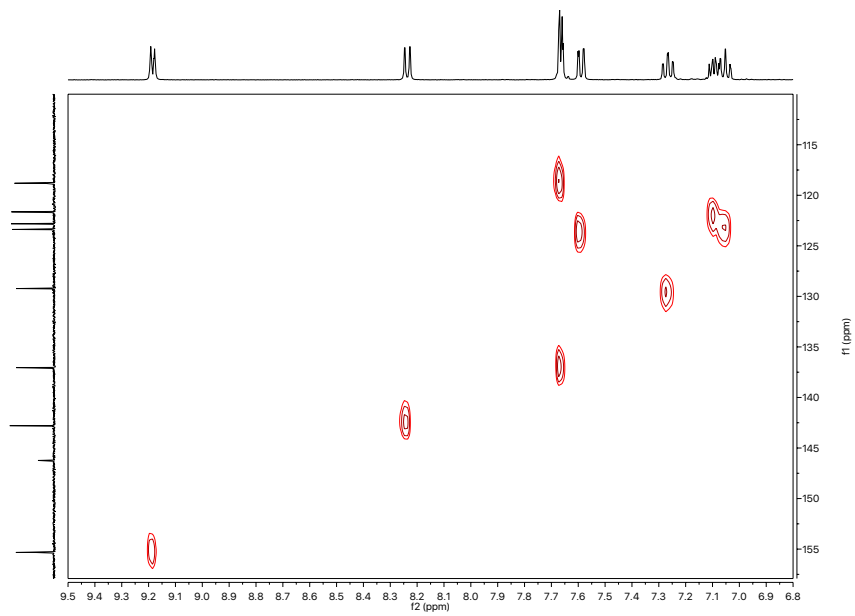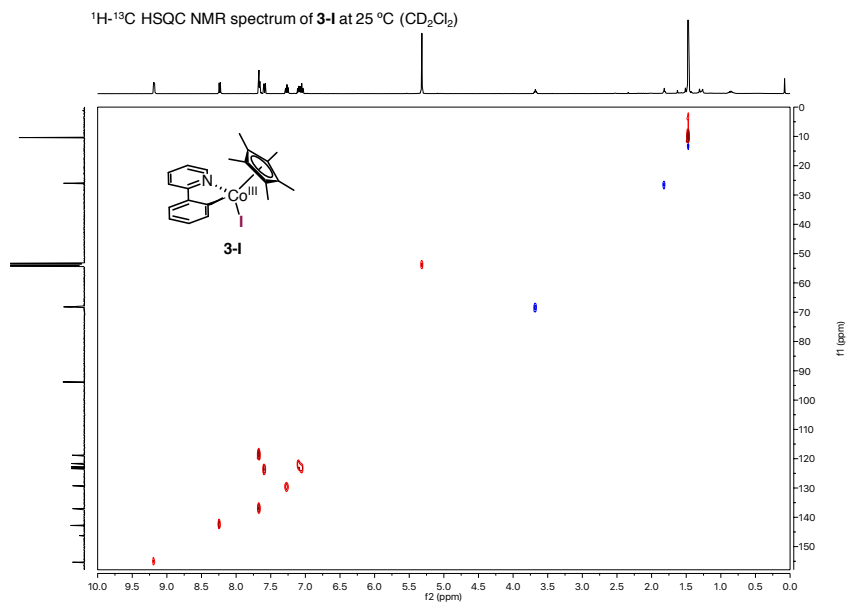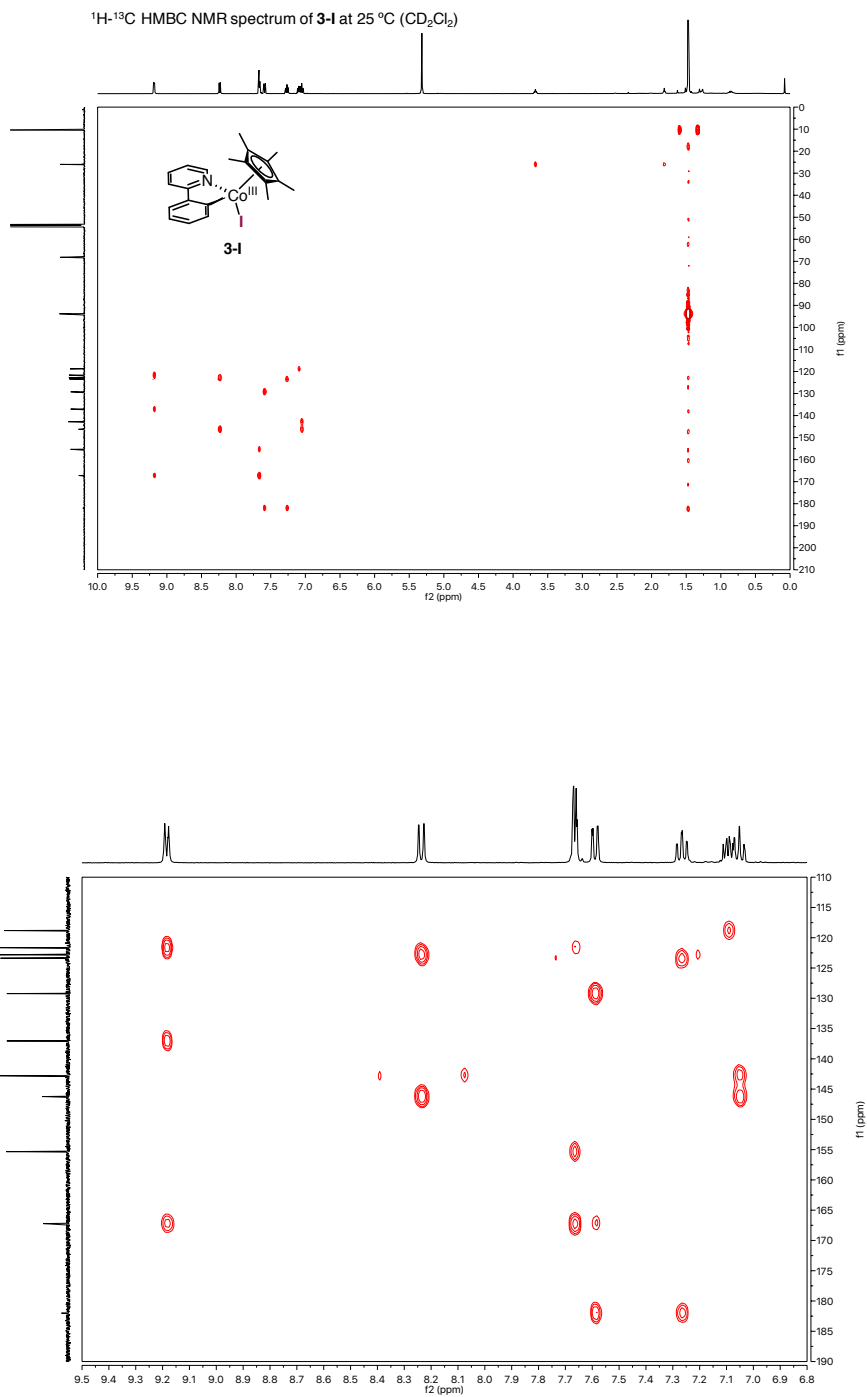
3.6.13 NMR Characterization of Complex 3-MeCN

^{1}H NMR spectrum of **3-MeCN** at 25 °C (CDCl$_3$)
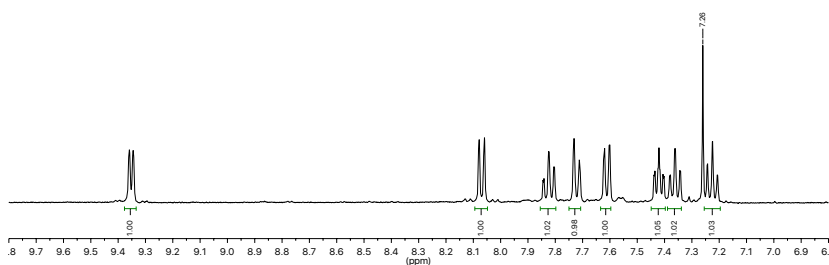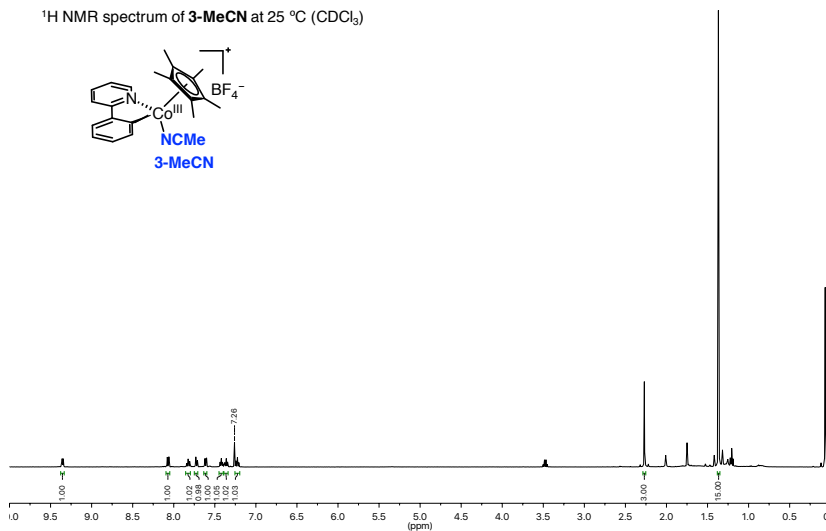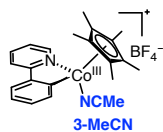
^{13}C NMR spectrum of **3-MeCN** at 25 ºC (CDCl$_3$)
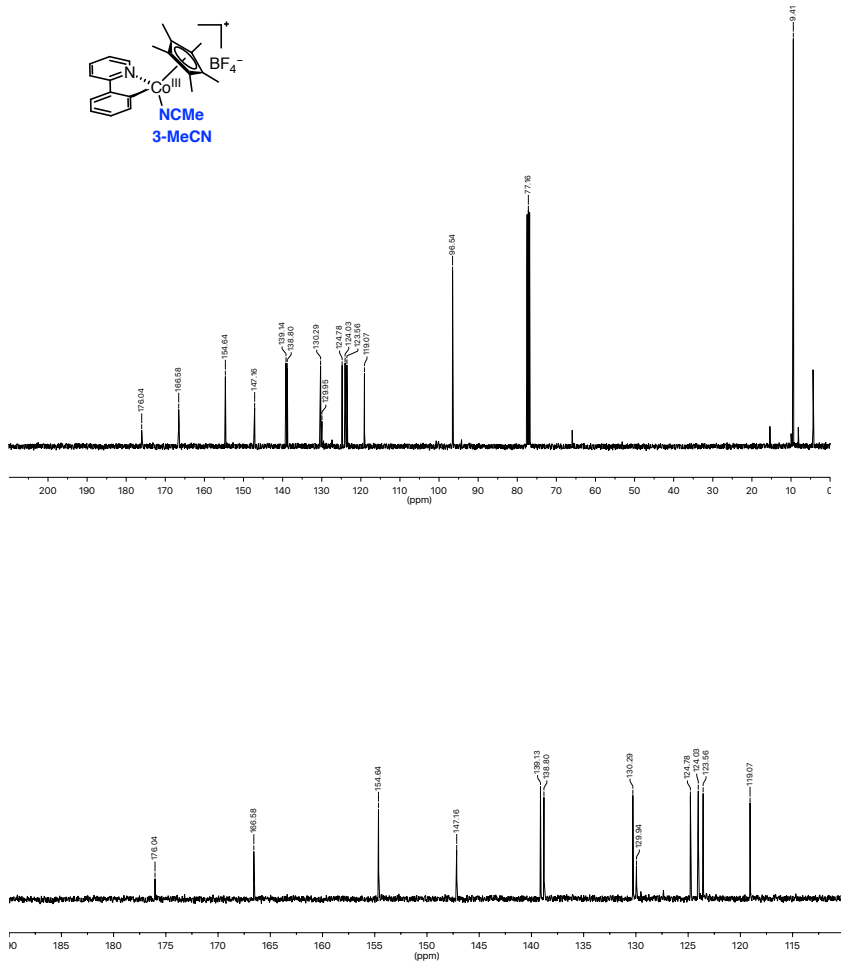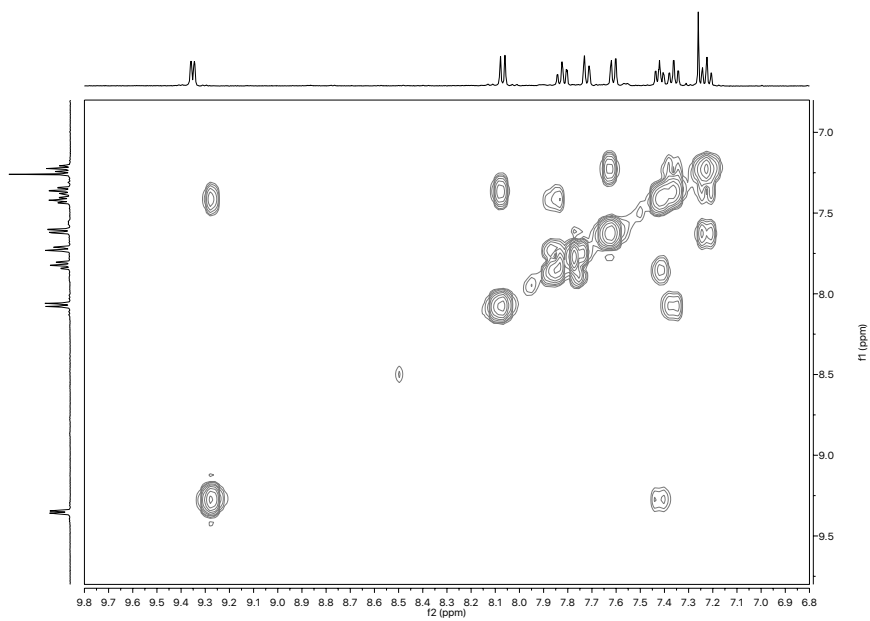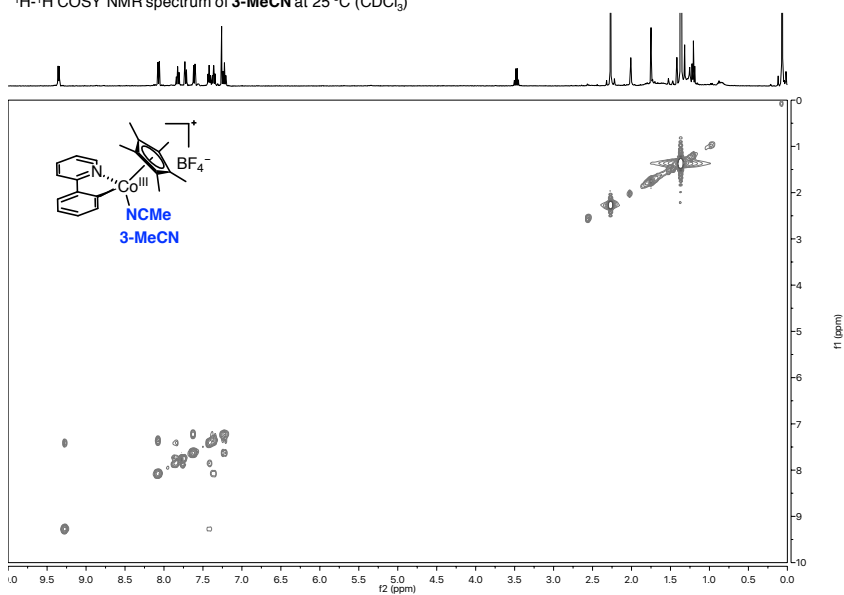
¹H-¹H COSY NMR spectrum of **3-MeCN** at 25 ºC (CDCl₃)

¹H-¹H TOCSY NMR spectrum of **3-MeCN** at 25 ºC (CDCl$_3$)

^{1}H-^{13}C HSQC NMR spectrum of **3-MeCN** at 25 ºC (CDCl$_3$)
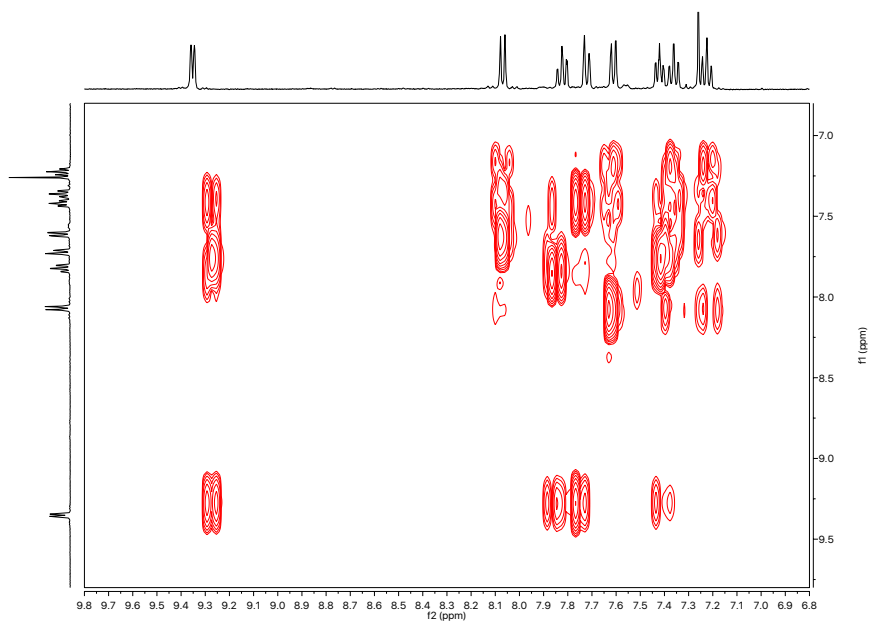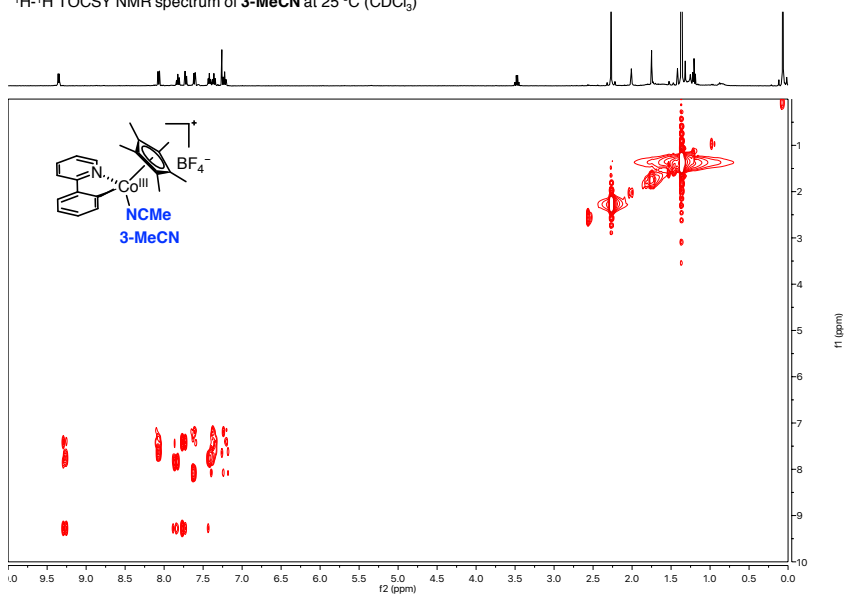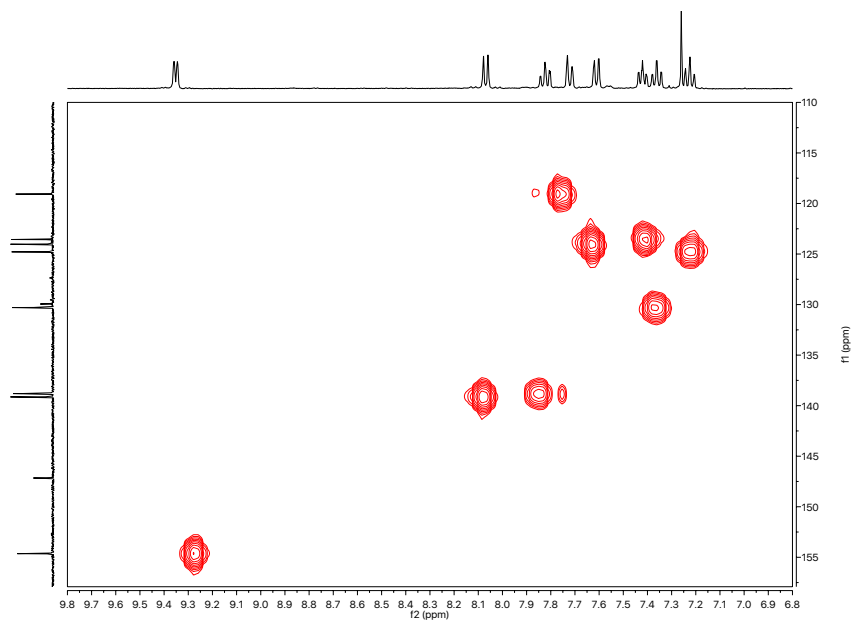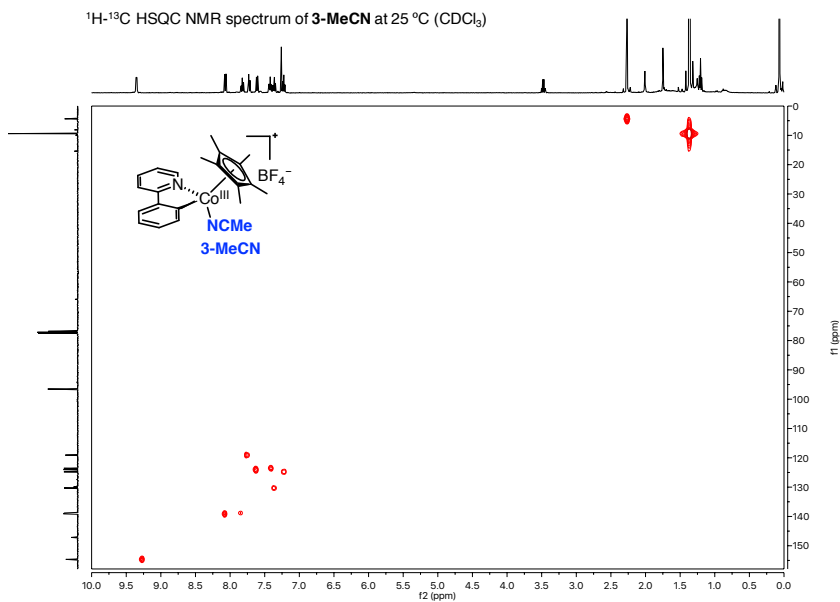
¹H-¹³C HMBC NMR spectrum of **3-MeCN** at 25 °C (CDCl₃)
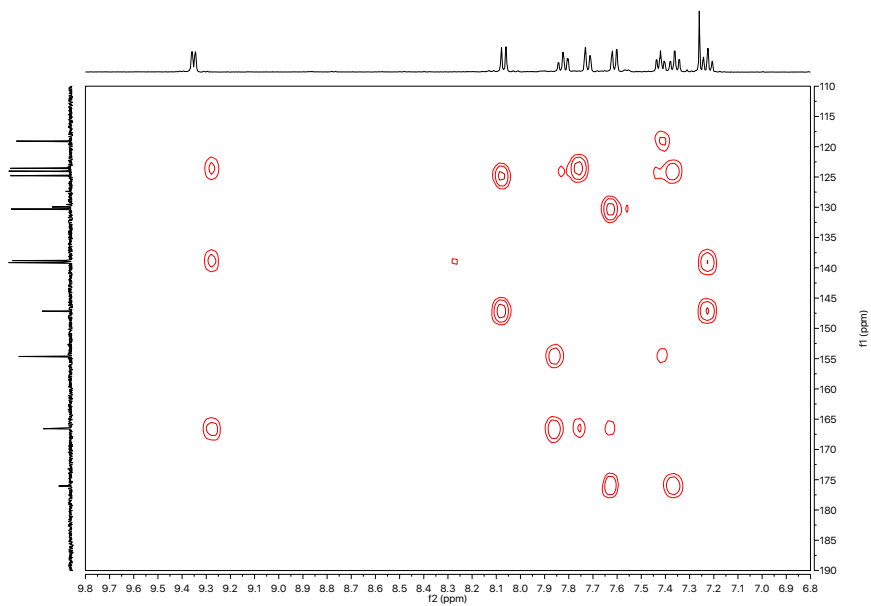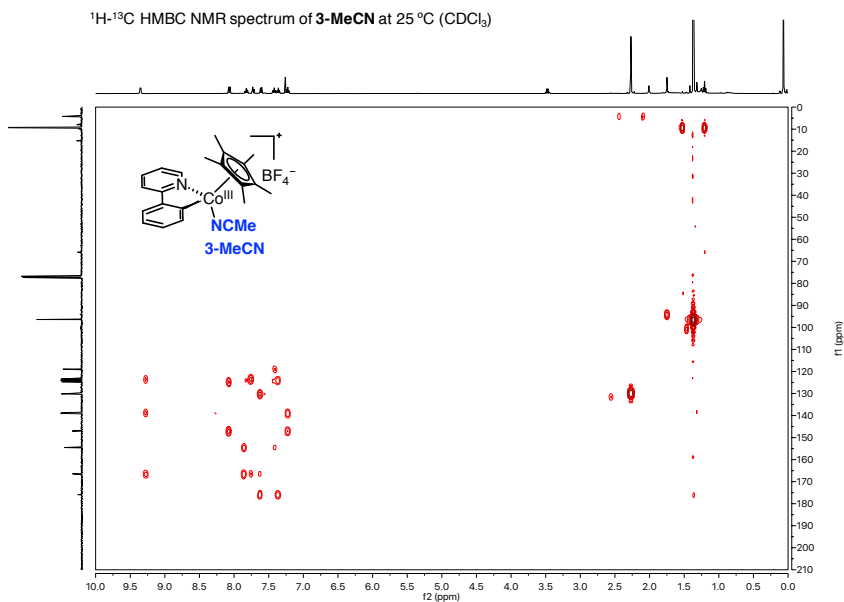
¹⁹F NMR spectrum of **3-MeCN** at 25 °C (CDCl₃)
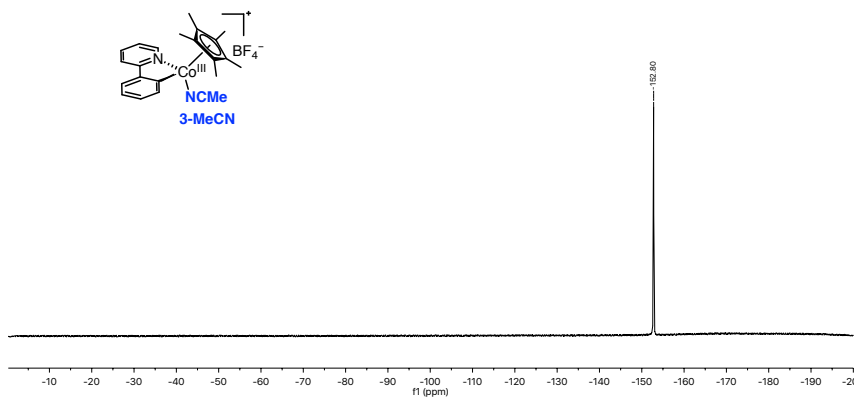
3.6.14 NMR Characterization of Complex 6

^{1}H NMR spectrum of **6** at –20 ºC (CD$_2$Cl$_2$)
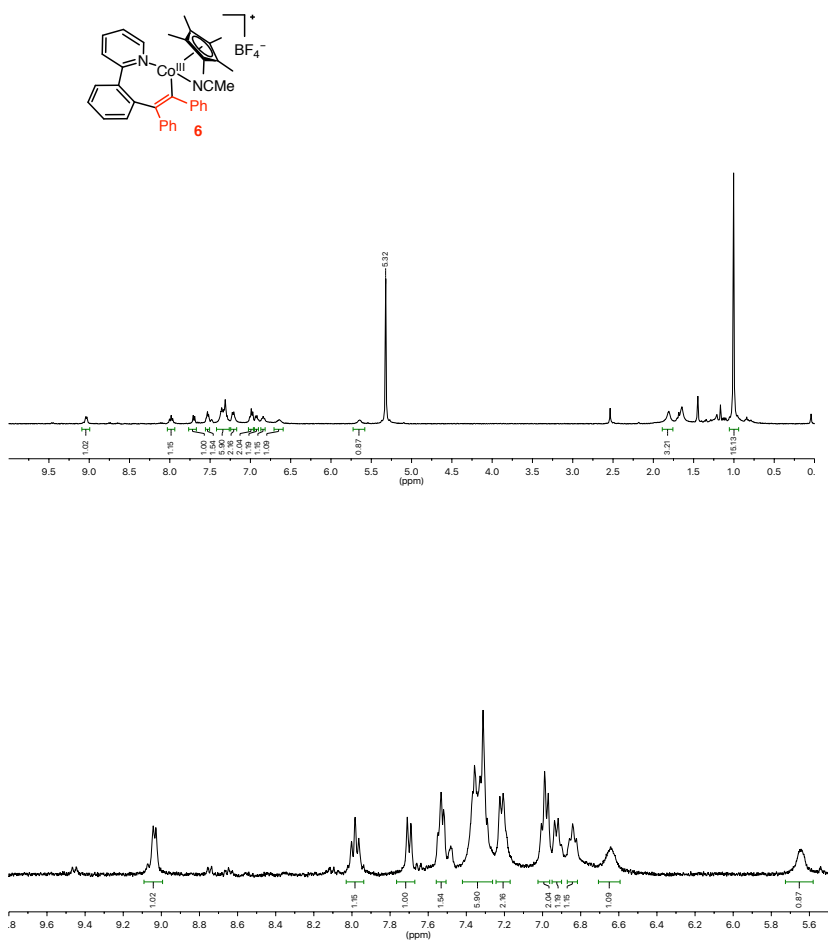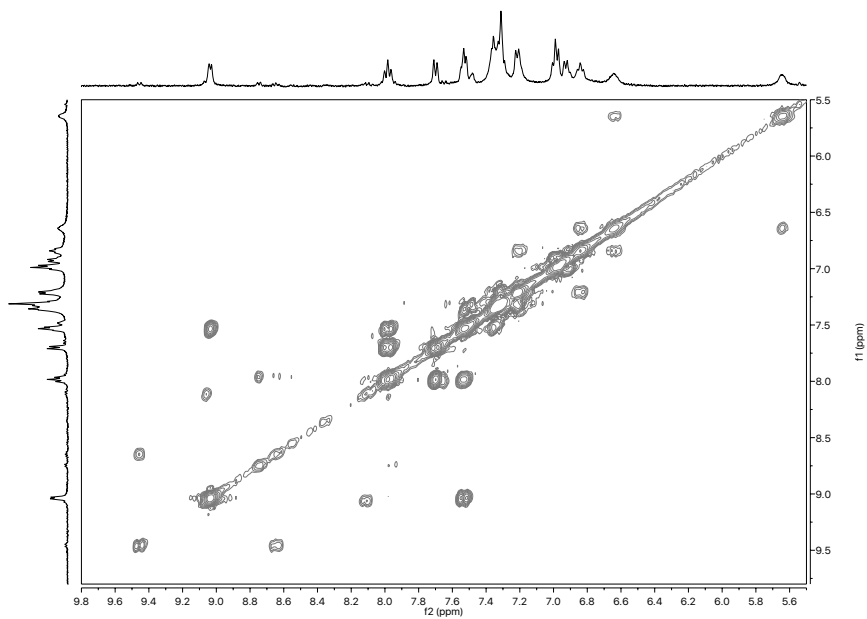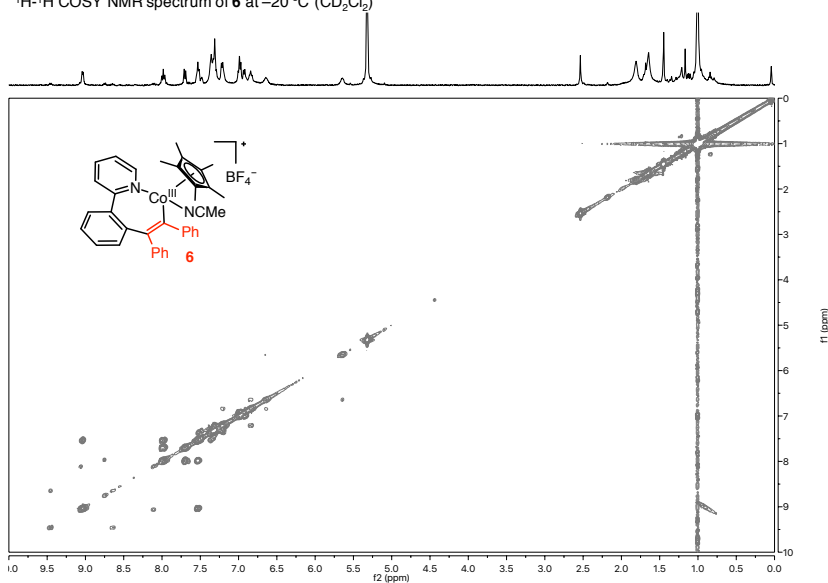
¹H-¹H COSY NMR spectrum of **6** at −20 ºC (CD₂Cl₂)

¹H-¹H TOCSY NMR spectrum of **6** at –20 ºC (CD₂Cl₂)

¹⁹F NMR spectrum of **6** at −20 ºC (CD$_2$Cl$_2$)
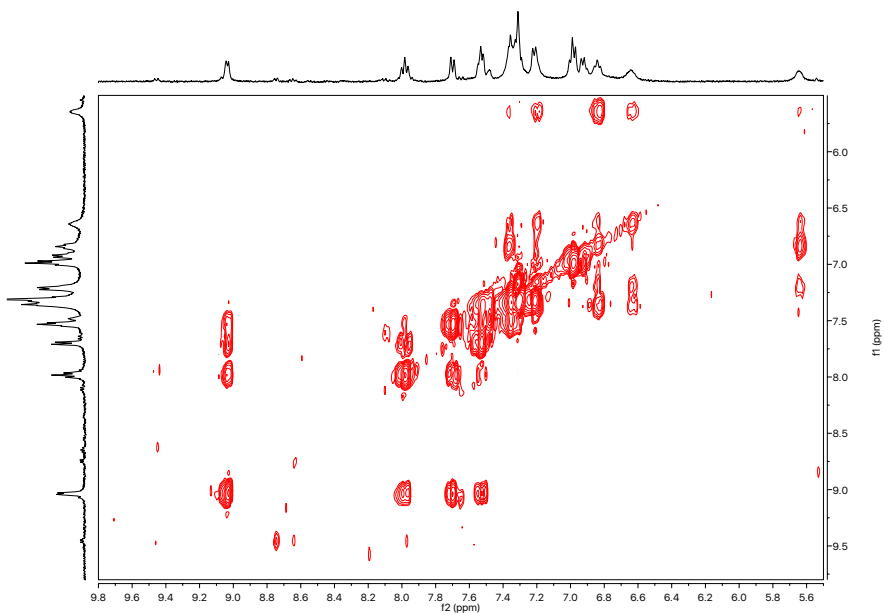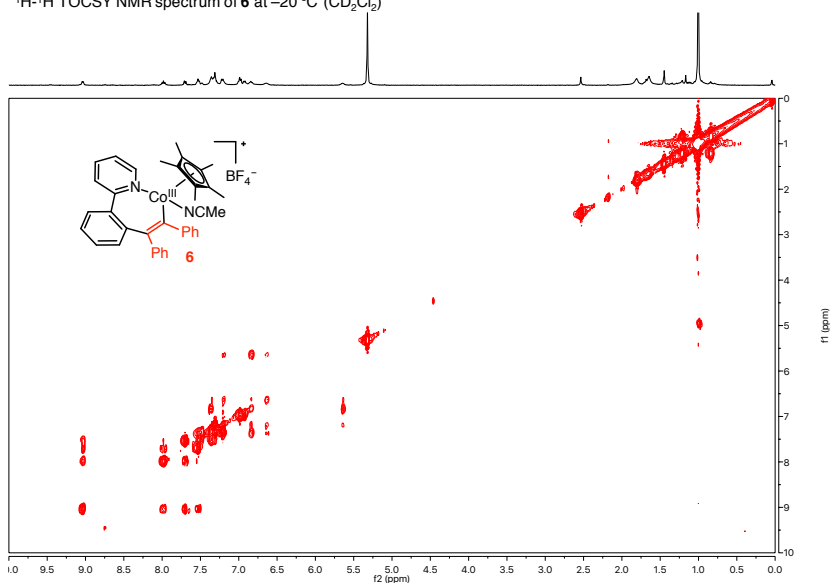
[1,2]-insertion   *[1,1]-insertion*   *[1,2]-insertion*
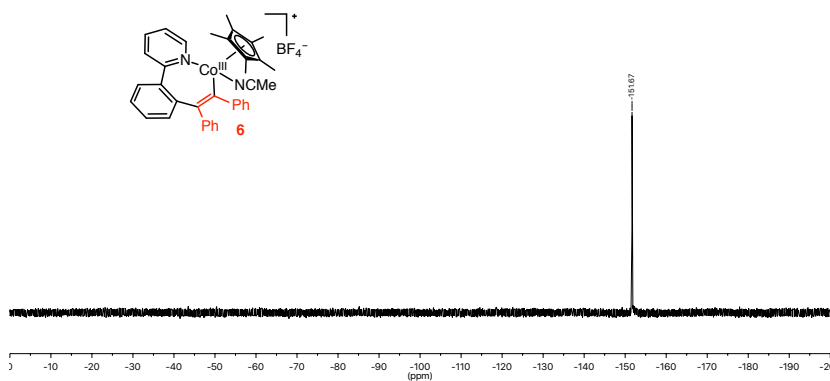
Unravelling Molecular Aspects of the Migratory Insertion Step in Cp*Co(III) Metallacyclic Systems

Jesús Sanjosé-Orduna,[†,‡] Jordi Benet-Buchholz,[†] and Mónica H. Pérez-Temprano[*,†]

[†]Institute of Chemical Research of Catalonia (ICIQ), The Barcelona Institute of Science and Technology (BIST), Avenida Països Catalans 16, 43007 Tarragona, Spain

[‡]Departament de Química Analítica i Química Orgànica, Universitat Rovira i Virgili, C/Marcel·li Domingo s/n, 43007 Tarragona, Spain

S Supporting Information

ABSTRACT: This Forum Article describes the reactivity and regioselectivity of the insertion of electrophiles, such as alkynes and alkenes, into Co−C bonds in the context of Cp*Co-catalyzed C−H functionalization reactions. The mechanistic investigation, using diphenylacetylene as the model system, reveals that the rate-determining step of the insertion process depends on the temperature. The reaction of a catalytically relevant cobaltacycle, [Cp*Co(III)(2-ppy)(MeCN)](BF$_4$), with selected terminal electrophiles, such as phenylacetylene, styrene, and vinyl acetate, unravels different insertion modes depending on the nature of the unsaturated molecule. The inserted products were fully characterized by NMR spectroscopy, electrospray ionization mass spectrometry, and single-crystal X-ray diffraction. In addition, we performed a kinetic study to establish their relative reactivity.

[1,2]-insertion   *[1,1]-insertion*   *[1,2]-insertion*
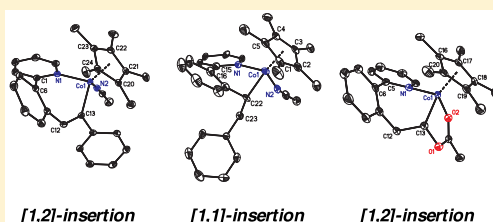
INTRODUCTION

Over the past few years, cobalt catalysts have emerged as a potential alternative to precious metals in directed C−H functionalization reactions.[1] Compared to noble metals, cobalt catalysts offer obvious advantages, including being earth-abundant and cheaper. However, the most interesting feature of cobalt catalysts is the potential rich manifold of reactivity patterns that they can provide, not only mimicking precious metals but also exhibiting a unique and versatile reactivity. This is likely due to cobalt low electronegativity, small radius, and facile access to multiple oxidation states through one- or two-electron processes. Surprisingly, the first example of chelation-assisted transition-metal-catalyzed C−H functionalization was reported by Murahashi, as early as in the 1950s, using a cobalt catalyst (Scheme 1).[2] However, it took more than 50 years to rediscover the potential of cobalt-catalyzed directed C−H functionalization in organic synthesis.[1]

In this context, the employment of Cp*Co(III) complexes, known since the mid-1970s[3] and analogous to active ruthenium(III) catalysts for C−H activation,[4] has represented a tremendous advance in cobalt catalysis over the past 5 years.[1,5] Despite the growth of this field, there are relatively few

mechanistic insights into these transformations even when using well-established electrophilic coupling partners such as alkenes or alkynes.[1,5,6] One of the main reasons for the lack of fundamental knowledge is the difficulty in detecting/characterizing/isolating relevant reactive species in these systems.[7] This is likely due to the proposed reversible nature of the C−H metalation step and/or the high reactivity of the transient cobalt intermediates after their reaction with the corresponding coupling partner (Scheme 2).[8] In most cases, the mechanistic knowledge available is limited to hydrogen/deuterium exchange experiments, kinetic isotope effect values, or the detection of cobalt intermediates by electrospray ionization mass spectrometry (ESI-MS).[1,5,8] These data do not provide

Scheme 1. First Ligand-Assisted Transition-Metal-Catalyzed C−H Functionalization Reaction
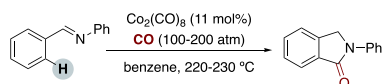
Scheme 2. Cp*Co-Catalyzed Directed C−H Functionalization Reactions

structural information, at the molecular level, of the cobalta-cycle intermediates involved in these transformations.

As part of our interest in understanding the reaction mechanisms of Cp*Co[III]-catalyzed directed C−H functional-ization reactions, we recently designed two different synthetic strategies for accessing a direct analogue of one the most widely invoked C−H-activated cationic Cp*Co[III] metallacycles (Scheme 3).[7b,f] Initially, because of the proposed reversibility

Scheme 3. Designed Synthetic Routes for Accessing 1-MeCN
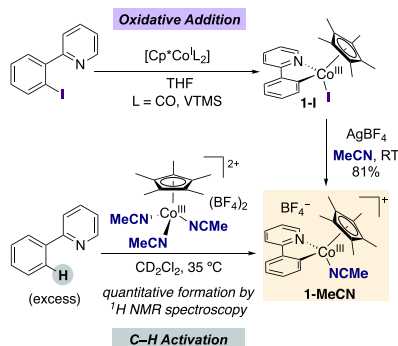
of the C−H activation step, we explored one of the preferred routes to afford cyclometalated products: oxidative addition reactions.[9] Although the oxidative addition of perfluoroalkyl iodides (R$_f$-I) to [Cp*Co[I](CO)$_2$] to form stable [Cp*Co[III](CO)R$_f$I] complexes has been known since pioneer-ing studies by Stone and co-workers,[10] the preparation of cobaltacycles using this approach was unprecedented at that time. The heteroatom-assisted oxidative addition of 2-(2-iodophenyl)pyridine to [Cp*Co[I]L$_2$] (L = CO, vinyltrimethyl-silane), followed by halide abstraction with AgBF$_4$ in acetonitrile (MeCN), produced the desired cationic cobalta-cycle [Cp*Co[III](2-ppy)(MeCN)][BF$_4$] (1-MeCN).[7b] It is worth mentioning that the employment of noncoordinating solvents such as dichloromethane (DCM) in salt metathesis led to decomposition. Inspired by these results, we took advantage of the stabilizing capability of MeCN to overcome the reversible nature of the C−H bond cleavage by Cp*Co[III] and capture otherwise inaccessible cobalt intermediates via C−H activation.[7f] We observed the smooth formation of 1-MeCN by ^{1}H NMR spectroscopy upon the reaction of [Cp*Co[III](MeCN)$_3$](BF$_4$)$_2$ with 10 equiv of 2-ppyH, using the substrate also as a surrogate base.

We have used 1-MeCN to describe, for the first time, a comprehensive mechanistic picture of the most explored reactivity with Cp*Co[III] catalysts: C−H oxidative alkyne annulations.[7b] Using diphenylacetylene (dpa) as the model coupling partner, we were able to detect and characterize in situ the catalyst resting state, a seven-membered ring cobaltacycle (2a-MeCN) stabilized by MeCN. This highly reactive intermediate was formed by the alkyne coordination and migratory insertion of dpa into the Co−C bond of 1-MeCN. Stoichiometric reactions of 1-MeCN with 3 equiv of dpa revealed that the presence of an excess of MeCN slows not only the formation of 2a-MeCN but also the reductive elimination step that affords the annulated product. This suggests that the stabilized 18-electron cobaltacycles (1-MeCN

and 2a-MeCN) are off-cycle species in equilibrium with the 16-electron complexes (1 and 2a) with a vacant coordination site, which are the reactive ones (Scheme 4). Importantly,

Scheme 4. Mechanistic Investigation of Cp*Co[III]-Catalyzed Oxidative Alkyne Annulation
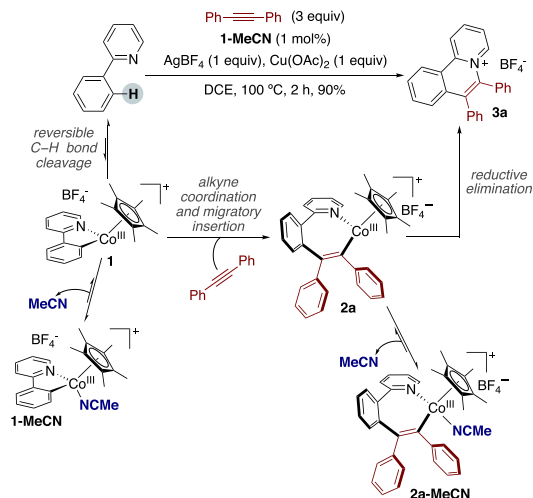
under stoichiometric conditions, the formation of [Cp*Co[I]] after the reductive elimination step could be indirectly corroborated by the subsequent addition of 2-(2-iodophenyl)-pyridine, resulting in the clean formation of 1-I. Under catalytic conditions, the copper and/or silver salts present in the reaction mixture are presumably responsible for reoxidation of the cobalt(I) species. The resulting [Cp*Co[III]] would be the active species in the C−H activation step.[7a,11]

Despite our contributions[7b,f] and the recent observation of analogous insertion products,[7d,e,g] there are still important fundamental questions regarding the insertion step, funda-mental in different Cp*Co-catalyzed C−H functionalization reactions (Scheme 5), that need to be addressed. In sharp contrast to analogous iridium- and rhodium-based systems,[12] to date, there is a dearth of fundamental information on the reactivity and regioselectivity of the insertion of alkynes or

Scheme 5. Mechanistic Proposal of Cp*Co-Catalyzed C−H Functionalization Involving Insertion Reactions as Key Steps
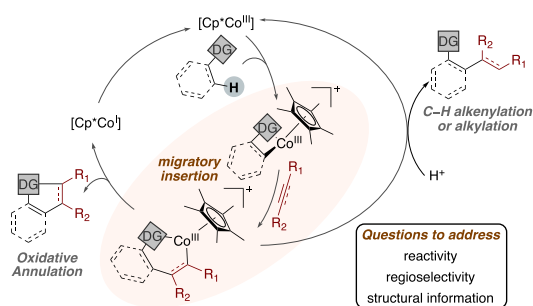
alkenes into Co—C bonds of Cp*Co^{III} cyclometalated complexes.

Inspired by our previous results, in this Forum Article, we employ **1-MeCN** as the platform to explore previously inaccessible mechanistic intricacies of the migratory insertion step using dpa as the model system. Our kinetic study reveals that the rate-determining step of the alkyne insertion process can vary depending on the reaction conditions. Moreover, we investigated the reactivity of selected unsaturated molecules with different stereoelectronic properties: dpa, phenylacetylene, styrene, and vinyl acetate. The molecular structures by X-ray diffraction of the inserted products unravel multiple insertion modes depending on the nature of the unsaturated molecule. Elucidation of this structural information at the molecular level, along with the observed reactivity, is unprecedented in cobalt chemistry.

■ RESULTS AND DISCUSSION

Mechanistic Study on the Insertion Reaction Using dpa as the Model Coupling Partner. First, we sought to gain a detailed mechanistic understanding of the insertion of internal alkynes into the Co—C of Cp*Co^{III} cyclometalated complexes. These electrophiles are the most widely used coupling partners in Cp*Co-catalyzed C—H functionalization reactions.[1,5,6] As shown above, our previous investigation using dpa as the model alkyne system showed that its insertion involves multiple elementary steps when starting from coordinatively saturated cationic cobaltacycles (see Scheme 4).[7b] However, these preliminary studies left several open questions, including determination of the rate-limiting step of the insertion process or reactivity of neutral Cp*Co^{III} cobaltacycles, such as **1-I**, toward dpa.

1.1. Influence of the Cp*Co^{III} Cobaltacycle Precursor. We first investigated the impact of the coordination sphere of the metal center on the outcome of the insertion reaction. It is well-known that the rate of alkyne insertion is highly dependent on the coordination number of the starting metalacyclic complex.[13] We used our previous results, the reaction of **1-MeCN** with 3 equiv of dpa in DCM-d_2, as benchmark for evaluating these effects in our cobalt system. Under these reaction conditions, we observed the formation of **2a-MeCN** along with the annulated product (**3a**) after 25 min at 35 °C (Figure 1a). Next, we explored the reactivity of **1-I**. Different literature precedents have shown that neutral cyclometalated complexes [Cp*M(C^N)X] (M = Ir, Rh; C^N = 2-ppy; X = halide) readily undergo alkyne insertion reactions.[12c] Traces of neither a seven-membered ring cobaltacycle nor **3a** were detected by ^{1}H NMR spectroscopy upon the treatment of **1-I** with 3 equiv of dpa at 35 °C for 2 h in DCM-d_2 (Figure 1b). In sharp contrast, upon performing the same reaction but in the presence of AgBF$_4$ (1.5 equiv), we observed the instantaneous formation of the annulated product (Figure 1c). Under these reaction conditions, in the absence of a stabilizing ligand such as MeCN, **2a** cannot be observed directly because of its highly reactive nature. This reactivity trend clearly indicates that facile access to a cationic 16-electron intermediate with a vacant coordination site accelerates the rate of insertion and the reductive elimination process (Scheme 6).

1.2. MeCN Effect. We next determined the order of the alkyne insertion reaction with respect to MeCN using **1-MeCN**. Because the reductive elimination product, **3a**, exhibits solubility issues in DCM, the initial rate method was used to
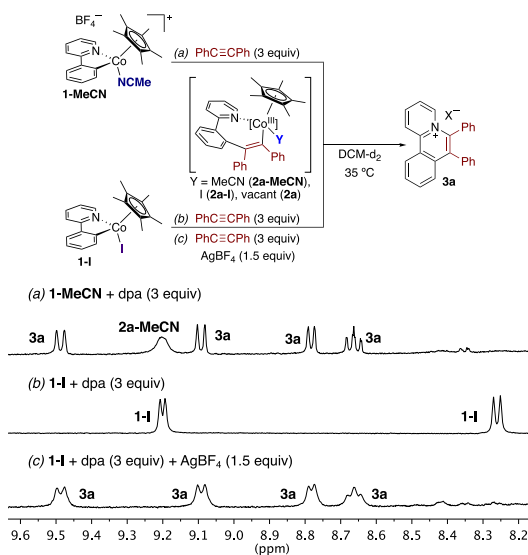
Figure 1. Comparative study on the reactivity of **1-MeCN** and **1-I** toward dpa. Reaction conditions: 0.01 mmol of **1-MeCN** or **1-I**, 0.03 mmol of dpa in 0.5 mL of CD$_2$Cl$_2$, 35 °C, 25 min. For part c, 0.015 mmol of AgBF$_4$ was added.

Scheme 6. Reactivity Trend of Cobaltacycle Complexes toward Alkyne Insertion
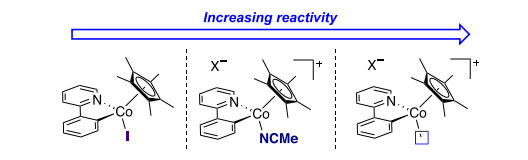
determine the insertion rate at each [MeCN] in DCM-d_2 at 25 °C. The experimental data employed to determine r_0 were obtained within reaction times in which the amount of **3a** did not affect the concentration of the complexes under study. Under these conditions, the concentrations of **1-MeCN** and **2a-MeCN**, were monitored by ^{1}H NMR spectroscopy. As expected, increasing amounts of MeCN dramatically slowed the reaction rate.[14] The plot of the initial reaction rate (r_0) versus [MeCN]$^{-1}$ was linear, indicating an inverse order on MeCN (Figure 2). This result confirms that dissociation of MeCN is crucial for generating the reactive unsaturated cobalt species involved in the alkyne insertion process.

1.3. Influence of dpa. We next investigated the dependence of the reaction rate of alkyne insertion on the concentration of dpa. We monitored the reaction between **1-MeCN** and different amounts of added dpa (3 or 10 equiv), in the presence of 5 equiv of MeCN, in DCM-d_2 at 35 °C.[15] Despite the solubility problems associated with the formation of **3a** under these reactions conditions, which hamper NMR monitoring,[16] we observed that the reaction rate clearly depends on the concentration of dpa, as shown in Figure 3, accelerating the formation of **2a-MeCN**.

Next, we carried out these reactions at lower temperature, 0 °C, in the absence of added MeCN. Under these reaction conditions, the product formation is sufficiently slow to allow
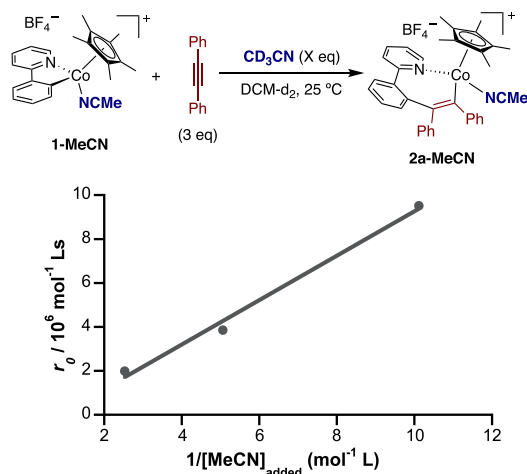
Figure 2. Plot of initial rates versus $[MeCN]^{-1}$ showing inverse order kinetics in MeCN. Reaction conditions: 0.01 mmol of **1-MeCN**, 0.03 mmol of dpa in 0.5 mL of CD_2Cl_2, 25 °C. A total of 2.5, 5, and 10 μL of CD_3CN were added, respectively.
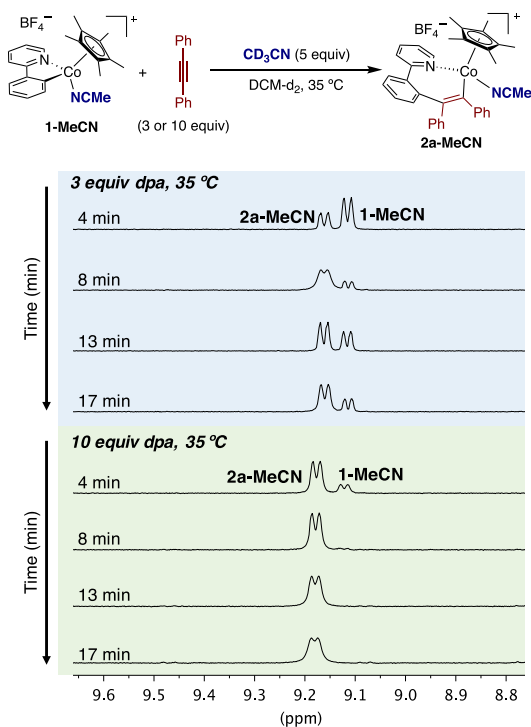
Figure 3. Influence of dpa on the alkyne insertion process at 35 °C. Reaction conditions: 0.01 mmol of **1-MeCN**, 0.03 or 0.1 mmol of dpa in 0.5 mL of CD_2Cl_2, 35 °C.

the study of the alkyne insertion step independently. Surprisingly, the formation of **2a-MeCN** is zero-order-dependent on $[dpa]$ (Figure 4). Similar values of r_0 were found for

$[dpa]_0 = 0.06$ or 0.2 mol L^{-1}, resulting in $r_0 = 2.7 \times 10^6$ and 3.0×10^6 mol L^{-1} s^{-1}, respectively.
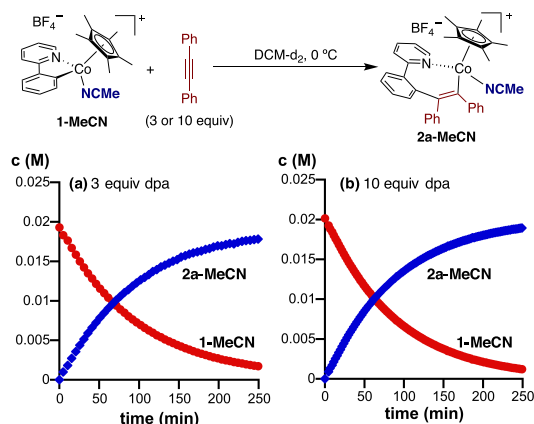
Figure 4. Alkyne insertion process at 0 °C in the presence of different amounts of dpa. Reaction conditions: 0.01 mmol of **1-MeCN**, 0.03 or 0.1 mmol of dpa in 0.5 mL of CD_2Cl_2, 0 °C.

Although the reaction conditions are slightly different at 0 and 35 °C, the effect of $[dpa]$ on the alkyne reaction rate suggests a temperature-dependent change in the rate-determining step in the alkyne insertion process. At 35 °C, insertion of the alkyne into the Co–C bond is presumably the rate-determining step, while at 0 °C, the alkyne seems not to be involved.

1.4. Eyring Plot. In order to gain further insights into the rate-determining step of the alkyne insertion process at low temperature, we calculated the activation parameters. We monitored the reaction of **1-MeCN** with 3 equiv of dpa in the temperature range from −10 to 10 °C by ^{1}H NMR spectroscopy. The rate constants (k_1) were obtained by fitting the concentration versus time data to the kinetic model shown in Figure 5, by nonlinear least-squares regression,[17] considering that the reaction is zero-order with respect to dpa. This figure shows the data at −10 °C as a representative example.

The activation parameters were determined using the Eyring equation, affording the following values: $\Delta H^{\ddagger} = 21.0 \pm 1.95$ kcal mol^{-1}; $\Delta S^{\ddagger} = 1.61 \pm 0.24$ cal K^{-1} mol^{-1} (Figure 6). Although the calculated $\Delta S^{\ddagger}$ is not large, its positive value, along with the zero-order dependence on alkyne, suggests that, at low temperature, dissociation of MeCN, prior to migratory insertion, could be the rate-determining step.

Reactions of 1-MeCN with Terminal Unsaturated Electrophiles. Next, we aimed to unravel the reactivity and insertion modes of selected unsaturated model molecules such as phenylacetylene, styrene and vinyl acetate. For dpa, we have reported the formation of a seven-membered cobaltacycle, **2a-MeCN**, through the traditional 1,2-insertion mode. However, other types of products could be potentially formed whether the corresponding electrophile inserts into the Co–C bond multiple times or insertion occurs in a 1,1-fashion (Figure 7). We have targeted these terminal alkynes and alkenes for our reactivity study because different literature reports have shown these nontraditional insertion modes with analogous Cp*Ir^{III}- and Cp*Rh^{III}-based systems.[12]
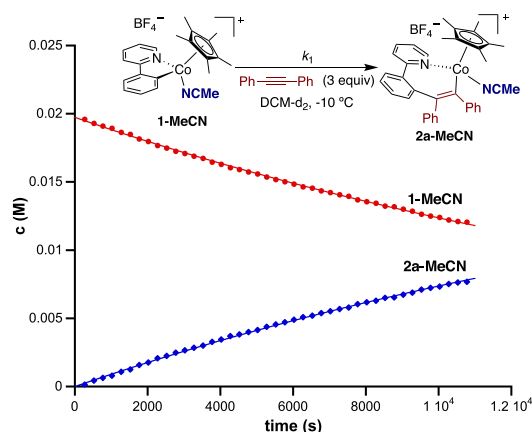
Figure 5. Alkyne insertion process at −10 °C. The solid lines are the best fit using GEPASI. Reaction conditions: 0.01 mmol of **1-MeCN**, 0.03 mmol of dpa in 0.5 mL of CD$_2$Cl$_2$, −10 °C.
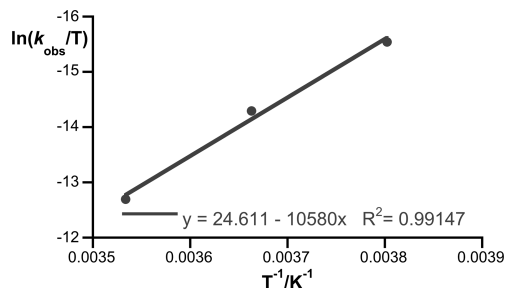
Figure 6. Eyring plot for the determination of $\Delta H^{\ddagger}$ and $\Delta S^{\ddagger}$ for alkyne insertion at low temperature.
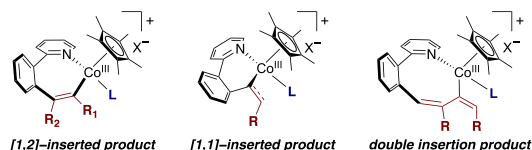
Figure 7. Potential insertion modes.

On the basis of our previous knowledge, we attempted to access the inserted products following an procedure analogous to that previously described for dpa, using **1-MeCN** as the starting complex (Scheme 7). As for **2a-MeCN**, the corresponding inserted products when using phenylacetylene and styrene were not isolable. However, inspired by our mechanistic insights, we added a high excess of MeCN to enable full characterization of **2b-MeCN** (CCDC 1909808) and **2c-MeCN** (CCDC 1909807) by NMR spectroscopy (1D and 2D experiments) and ESI-MS.[18] In sharp contrast, **2d** (CCDC 1909809) exhibits high stability and was isolated in a quantitative manner. In all cases, we observed a single inserted product. Phenylacetylene and vinyl acetate insert into the Co−C bond of **1-MeCN** in a completely regiospecific 1,2-manner. For analogous rhodium systems, Jones and co-workers have reported the formation of double-insertion products when using phenylacetylene as the electrophile.[12c] In our case, we

Scheme 7. Reactivity of 1-MeCN with Terminal Electrophiles
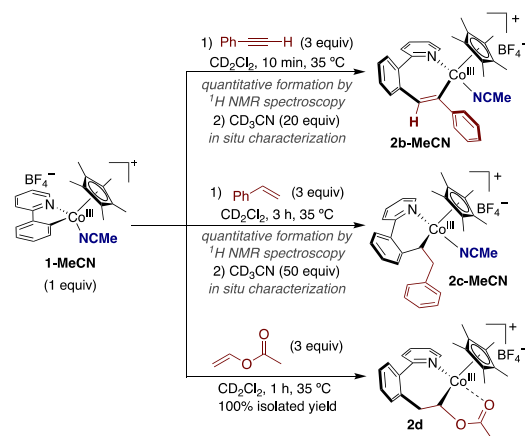
did not observe the formation of these types of products. A rhodacycle analogous to **2d** has been described by Ellman and co-workers as a catalyst resting state of the Cp*Rh^{III}-catalyzed directed C−H vinylation using vinyl acetate as the vinyl source.[19] Surprisingly, the [1,1]-insertion product is obtained when using styrene. The observation and characterization of **2c-MeCN** is particularly relevant because, to date, the formation of this type of inserted product had not been proposed in Cp*Co-catalyzed C−H functionalization products.[11a,20] The preference for six-membered-ring metallacycles over seven-membered-ring ones when using alkenes as coupling partners has been reported for Cp*Rh^{III} cyclometalated complexes.[12c]

The structural and spectroscopic characterization of these cobalt complexes displayed interesting features at the molecular level. As observed for **2a-MeCN**, the ^{1}H NMR spectra of the inserted products show an upfield displacement of the chemical shift of the Cp* ligand compared to **1-MeCN**. This can be explained as due to the anisotropic action of a ring current of the cyclometalated phenyl. When using the terminal alkenes, the coupling patterns of the resulting alkylic protons are analogous. In both cases, we observed three different signals because the protons of the methylene group are diastereotopic. However, the chemical shift of the alkylic CH varies dramatically, 4.73 and 7.86 ppm for **2c-MeCN** and **2d**, respectively.

The structures of the inserted products were unequivocally confirmed by single-crystal X-ray diffraction (see Table 1 and Figure 8). As **1-MeCN** and **2a-MeCN**, all three structures show a three-legged piano-stool geometry. For **2b-MeCN**, the phenyl group of PhC≡CH is preferentially located adjacent to the metal center after alkyne insertion, indicating dominance of the electronic effects. The solid-state structures of **2c-MeCN** and **2d** show that a subtle modification on the nature of the terminal alkene can induce different insertion modes. While styrene affords a six-membered-ring cobaltacycle via [1,1] insertion, vinyl acetate undergoes a traditional [1,2] mode. In this case, acetate is coordinated to the cobalt metal center instead of a molecule of MeCN.

The C$_A$−Co−N$_{Ppy}$ bite angle of the inserted products is larger than that for **1-MeCN** [82.39(15)°]. The phenyl rings

Table 1. Selected Bonds and Angles for the Single-Crystal Structures Measured

distance [Å]/angle [deg]	1-MeCN[a]	2a-MeCN[a]	2b-MeCN	2c-MeCN	2d
Co−N$_{ppy}$	1.959(3)	2.011(2)	1.9822(10)	1.980(8)	1.991(3)
Co−N$_{ACN}$	1.905(4)	1.928(3)	1.9242(11)	1.917(11)	
Co−C$_A$[b]	1.936(4)	1.984(3)	1.9775(12)	2.051(7)	1.960(3)
N$_{ppy}$−Co−N$_{ACN}$[c]	91.46(13)	89.47(10)	91.85(4)	92.2(6)	90.61(11)
N$_{ppy}$−Co−C$_A$	82.39(15)	90.49(10)	90.60(4)	86.93(9)	97.13(14)
Co−N$_{ACN}$−C$_{1ACN}$	173.6(3)	175.7(2)	170.55(10)	166.38(9)	
Torsion 1[d]	0.6(5)	61.2(4)	55.18(17)	33.9(13)	45.6(5)

[a]From ref 7b. [b]C$_A$ is the carbon atom attached to the cobalt. [c]In **2d**, it corresponds to the angle between N$_{ppy}$, cobalt, and the oxygen corresponding to acetate. [d]Torsion angle at 2-ppy.
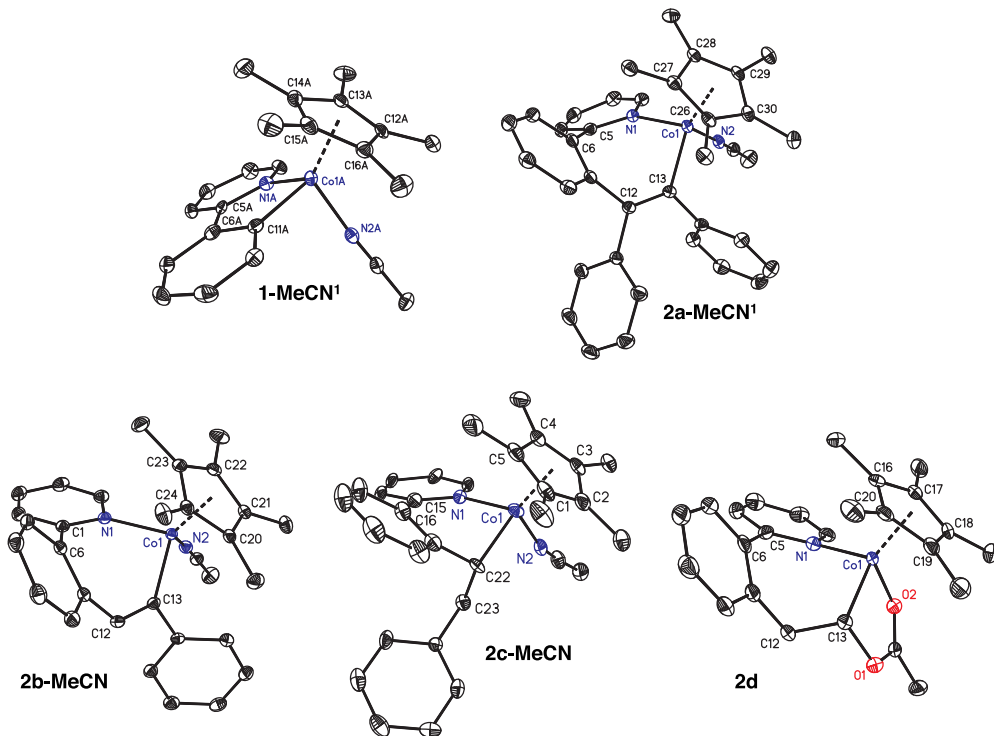
Figure 8. ORTEP plots of **2a-MeCN**, **2b-MeCN**, **2c-MeCN**, and **2d**, respectively. Thermal ellipsoids were drawn at 50% probability, and hydrogen atoms, BF$_4$ anions, and additional molecules in the unit cell were omitted for clarity.

are rotated out of the plane of the pyridine with a dihedral angle, ranging from 33.9(13)° for **2c-MeCN** to 61.2(4)° for **2a-MeCN**, which are much larger than that observed for **1-MeCN** [0.6(5)°]. It is worth mentioning that the Co−N$_{ppy}$, Co−N$_{ACN}$, and Co−C$_A$ bond lengths for the inserted products are longer than those for **1-MeCN**.

2.1. Reactivity of Terminal versus Internal Alkyne. With this structural information in hand, we compared the behavior of terminal and internal alkynes. We monitored the reaction of **1-MeCN** with 3 equiv of alkyne, PhC≡CPh or PhC≡CH, in DCM-d_2 at 35 °C, in the presence of 5 equiv of MeCN, in order to establish their relative reactivity. We selected these reaction conditions, where formation of the annulation product is very slow, to simplify the systematic study by ^{1}H NMR spectroscopy. When the kinetic experiments of PhC≡CPh

and PhC≡CH are compared, it is found that PhC≡CH reacts faster than the internal alkyne (Figure 9). Although we did not quantify formation of the reductive elimination products because they exhibit low solubility in DCM, we detected the formation of **3a** at longer reaction times, while the seven-membered-ring cobaltacycle **2b-MeCN** does not undergo reductive elimination under our reaction conditions. These results suggest that alkyne insertion is favored for phenyl-acetylene, while the reductive elimination process is facilitated using dpa.

2.2. Reactivity of Phenylacetylene versus Styrene. We monitored the reaction of **1-MeCN** with 3 equiv of styrene in DCM-d_2 at 35 °C, in the presence of 5 equiv of MeCN, in order to establish its relative reactivity toward phenylacetylene, the analogous terminal alkyne. Under these reaction
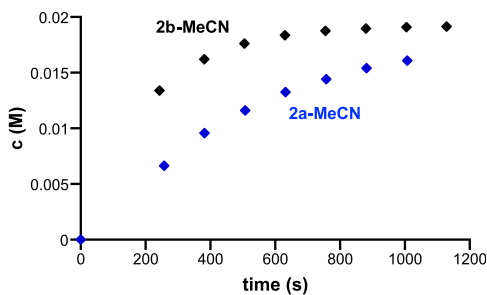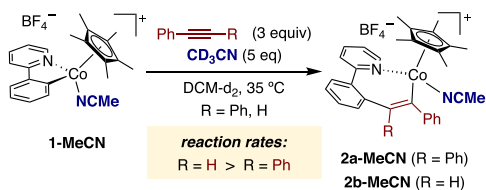
Figure 9. Reactivity of terminal versus internal alkynes. Reaction conditions: 0.01 mmol of **1-MeCN**, 0.03 of dpa or phenylacetylene, 0.05 mmol of CD_3CN in 0.5 mL of CD_2Cl_2, 35 °C.

conditions, we observed a dramatic difference in the insertion rate. While **2b-MeCN** formed quantitatively after 20 min, we only observed traces of the corresponding inserted product with styrene (Figure 10). These experimental results could be explained by taking into account the nature of the electrophile and the resulting inserted product. It is well-known that alkene insertions into M−C bonds are thermodynamically disfavored compared to alkyne ones because of the challenging C−C π-
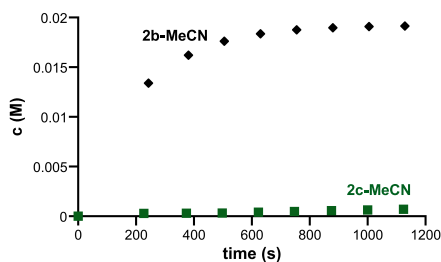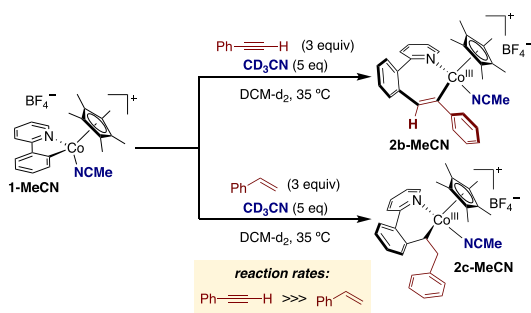
Figure 10. Reactivity of phenylacetylene versus styrene. Reaction conditions: 0.01 mmol of **1-MeCN**, 0.03 of dpa or styrene, 0.05 mmol of CD_3CN in 0.5 mL of CD_2Cl_2, 35 °C.

bond cleavage of the olefin. Moreover, the strength of the new M−C_{sp^2} bond on the alkyne insertion product is higher than the M−C_{sp^3} bond for olefins.[13]

2.3. Reactivity of Styrene versus Vinyl Acetate. Finally, we determined the relative reactivity between the two targeted terminal alkenes. As shown in Figure 11, the insertion of
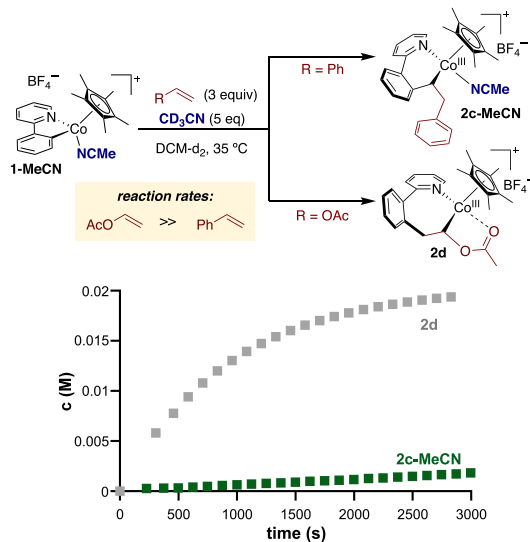
Figure 11. Reactivity of styrene versus vinyl acetate. Reaction conditions: 0.01 mmol of **1-MeCN**, 0.03 of styrene or vinyl acetate, 0.05 mmol of CD_3CN in 0.5 mL of CD_2Cl_2, 35 °C.

styrene to afford **2c-MeCN** occurs at extreme slowness compared to vinyl acetate. Under analogous reaction conditions, we observed almost quantitative formation of **2d** after 50 min, while at that time, less than 10% of the six-membered-ring cobaltacycle was detected by ^{1}H NMR spectroscopy. A plausible hypothesis that explains these experimental data is that acetate might facilitate an assisted alkene insertion acting as a chelating ligand. In alignment with this assumption, when we tried the insertion reaction with vinyl ethyl ether, we did not observe the inserted product, even in the absence of added CD_3CN.

■ **CONCLUDING REMARKS**

In conclusion, this work explores one of the fundamental steps in Cp*Co-catalyzed C−H functionalization reactions: the migratory insertion. We have used a direct analogue of a C−H-activated Co^{III} metallacycle, **1-MeCN**, for providing previously inaccessible mechanistic intricacies on the reactivity and regioselectivity of the insertion of selected alkynes and alkenes into the Co−C bond. Our initial mechanistic study, using dpa as a model electrophile, revealed a temperature dependence of the rate-determining step. At 35 °C, insertion of the alkyne into the Co−C bond seems to be the rate-determining step. In sharp contrast, at low temperature, 0 °C, the insertion reaction is zero-order in electrophile, suggesting that dissociation of MeCN from **1-MeCN**, to generate a reactive 16-electron complex, is the rate-determining step.

The reaction of our cobalt platform with terminal electrophiles unraveled different insertion modes depending on the

nature of the unsaturated molecule. The reactions with phenylacetylene and vinyl acetate afford the expected seven-membered-ring cobaltacycles via a traditional [1,2] insertion. However, the treatment of **1-MeCN** with styrene provides a six-membered-ring complex, presumably due to [1,1] insertion. The inserted products were fully characterized by NMR spectroscopy, ESI-MS, and single-crystal X-ray diffraction. The reactivity comparison between the tested electrophiles shows that phenylacetylene provides the fastest alkyne insertion, while styrene provides the slowest one.

The results provided herein not only reveal mechanistic information on the migratory insertion process in the context of Cp*Co-catalyzed C−H functionalization reactions but also demonstrate that subtle modifications of the structure of the employed electrophile can produce a significant change in the nature of the transient cobalt species at the molecular level.

■ ASSOCIATED CONTENT

ⓢ Supporting Information

The Supporting Information is available free of charge on the ACS Publications website at DOI: 10.1021/acs.inorg-chem.9b01111.

> Complete experimental details, including general con-siderations, kinetic studies, and full characterization of the new compounds, including NMR spectra and X-ray diffraction analysis (PDF)

Accession Codes

CCDC 1909807−1909809 contain the supplementary crys-tallographic data for this paper. These data can be obtained free of charge via www.ccdc.cam.ac.uk/data_request/cif, or by emailing data_request@ccdc.cam.ac.uk, or by contacting The Cambridge Crystallographic Data Centre, 12 Union Road, Cambridge CB2 1EZ, UK; fax: +44 1223 336033.

■ AUTHOR INFORMATION

Corresponding Author
*E-mail: mperez@iciq.es.

ORCID ⊙
Jesús Sanjosé-Orduna: 0000-0002-9942-502X
Mónica H. Pérez-Temprano: 0000-0003-4815-7990

Author Contributions

The manuscript was written through contributions of all authors. All authors have given approval to the final version of the manuscript.

Notes

The authors declare no competing financial interest.

■ ACKNOWLEDGMENTS

■ REFERENCES

(1) For selected recent reviews on cobalt-catalyzed directed C−H functionalization reactions, see: (a) Gao, K.; Yoshikai, N. Low-valent cobalt catalysis: New opportunities for C−H functionalizations. *Acc. Chem. Res.* **2014**, 47, 1208−1219. (b) Tilly, D.; Dayaker, G.; Bachu, P.

Cobalt mediated C−H bond functionalization: emerging tools for organic synthesis. *Catal. Sci. Technol.* **2014**, 4, 2756−2777. (c) Ackermann, L. Cobalt-catalyzed C−H arylations, benzylations, and alkylations with organic electrophiles and beyond. *J. Org. Chem.* **2014**, 79, 8948−8954. (d) Su, B.; Cao, Z.-C.; Shi, Z.-J. Exploration of earth-abundant transition metals (Fe, Co, and Ni) as catalysts in unreactive chemical bond activations. *Acc. Chem. Res.* **2015**, 48, 886−896. (e) Moselage, M.; Li, J.; Ackermann, L. Cobalt-catalyzed C−H activation. *ACS Catal.* **2016**, 6, 498−525. (f) Pototschnig, G.; Maulide, N.; Schnürch, M. Direct Functionalization of C−H bonds by Iron, Nickel, and Cobalt catalysis. *Chem. - Eur. J.* **2017**, 23, 9206−9232. (g) Gandeepan, P.; Müller, T.; Zell, D.; Cera, G.; Warratz, S.; Ackermann, A. 3d transition metals for C−H activation. *Chem. Rev.* **2019**, 119, 2192−2452.

(2) Murahashi, S. Synthesis of phthalimidines from Schiff bases and carbon monoxide. *J. Am. Chem. Soc.* **1955**, 77, 6403−6404.

(3) (a) King, R. B.; Efraty, A.; Douglas, W. M. Pentamethylcyclo-pentadienyl Derivatives of Transition Metals. III. Some Reactions of Pentamethylcyclopentadienyl-metal Carbonyl Derivatives of Cobalt and Manganese. *J. Organomet. Chem.* **1973**, 56, 345−355. (b) Fair-hurst, G.; White, C. Syntheses of Pentamethylcyclopentadienylcobalt-(III) Compounds and Reactions of $[Co(C_5Me_5)(solvent)_3]X_2$ (solvent = acetonitrile or acetone, X = BF_4 or PF_6). *J. Chem. Soc., Dalton Trans.* **1979**, 1524−1530. (c) Fairhurst, G.; White, C. Cyclopentadienyl- or Pentamethylcyclopentadienyl-(arene)cobalt-(III) Complexes: arene = indole, benzene, mesitylene, hexamethyl-benzene, 1,4-dihydroxy- and 1-hydroxy-4-methoxytetramethylben-zene. *J. Chem. Soc., Dalton Trans.* **1979**, 1531−1538. (d) Loginov, D. A.; Shul'pina, L. S.; Muratov, D. V.; Shul'pin, G. B. Cyclo-pentadienyl cobalt(III) complexes: Synthetic and catalytic chemistry. *Coord. Chem. Rev.* **2019**, 387, 1−31.

(4) For selected reviews, see: (a) Satoh, T.; Miura, M. Oxidative coupling of aromatic substrates with alkynes and alkenes under rhodium catalysis. *Chem. - Eur. J.* **2010**, 16, 11212−11222. (b) Song, G.; Wang, F.; Li, X. C−C, C−O and C−N bond formation via rhodium(III)-catalyzed oxidative C−H activation. *Chem. Soc. Rev.* **2012**, 41, 3651−3678. (c) Colby, D. A.; Tsai, A. S.; Bergman, R. G.; Ellman, J. Rhodium catalyzed chelation-assisted C−H bond functionalization reactions. *Acc. Chem. Res.* **2012**, 45, 814−825. (d) Patureau, F. W.; Wencel-Delord, J.; Glorius, F. Cp*Rh-catalyzed C−H activations. Versatile dehydrogenative cross-couplings of Csp2 C−H positions with olefins, alkynes, and arenes. *Aldrichim. Acta* **2012**, 45, 31−41. (e) Kuhl, N.; Schröder, N.; Glorius, F. Formal SN-type reactions in rhodium(III)-catalyzed C−H bond activation. *Adv. Synth. Catal.* **2014**, 356, 1443−1460. (f) Song, G.; Li, X. Substrate activation strategies in rhodium(III)-catalyzed selective functionalization of arenes. *Acc. Chem. Res.* **2015**, 48, 1007−1020. (g) Shin, K.; Kim, H.; Chang, S. Transtion-metal-catalyzed C−N bond forming reactions using organic azides as the nitrogen source: a journey for the mild and versatile C−H amination. *Acc. Chem. Res.* **2015**, 48, 1040.

(5) For selected recent reviews on Cp*Co-catalyzed directed C−H functionalization reactions, see: (a) Wei, D.; Zhu, X.; Niu, J.-L.; Song, M.-P. *ChemCatChem* **2016**, 8, 1242−1263. (b) Yoshino, T.; Matsunaga, S. (Pentamethylcyclopentadienyl)cobalt(III)-catalyzed C−H bond functionalization: from discovery to unique reactivity and selectivity. *Adv. Synth. Catal.* **2017**, 359, 1245−1262. (c) Wang, S.; Chen, S.-Y.; Yu, X.-Q. C−H functionalizations by high-valent Cp*Co(III) catalysis. *Chem. Commun.* **2017**, 53, 3165−3180. (d) Chirila, P. G.; Whiteoak, C. J. *Dalton. Trans.* **2017**, 46, 9721−9739. (e) Ghorai, J.; Anbarasan, P. Developments in Cp*Co^III-catalyzed C−H bond functionalizations. *Asian J. Org. Chem.* **2019**, 8, 430−455.

(6) (a) Prakash, S.; Kuppusamy, R.; Cheng, C.-H. Cobalt-catalyzed annulation reactions via C−H activation. *ChemCatChem* **2018**, 10, 683−705. (b) Santhoshkumar, R.; Cheng, C.-H. Hydroarylaitons by cobalt-catalyzed C−H activation. *Beilstein J. Org. Chem.* **2018**, 14, 2266−2288. (c) Peneau, A.; Guillou, C.; Chabaud, L. Recent advances in $[Cp*M^{III}]$ (M = Co, Rh, Ir)-catalyzed intramolecular annulation through C−H activation. *Eur. J. Org. Chem.* **2018**, 2018,

5777−5794. (d) Ujwaldev, S. M.; Harry, N. A.; Divakar, M. A.; Anilkumar, G. Cobalt-catalyzed C−H activation: recent progress in heterocyclic chemistry. *Catal. Sci. Technol.* **2018**, *8*, 5983−6018.

(7) (a) Ikemoto, H.; Yoshino, T.; Sakata, K.; Matsunaga, S.; Kanai, M. Pyrroloindolone synthesis via a Cp*Co[III]-catalyzed redox-neutral directed C−H alkenylation/annulation sequence. *J. Am. Chem. Soc.* **2014**, *136*, 5424−5431. (b) Sanjosé-Orduna, J.; Gallego, D.; Garcia-Roca, A.; Martin, E.; Benet-Buchholz, J.; Pérez-Temprano, M. H. Capturing elusive cobaltacycle intermediates: a real-time snapshot of the Cp*Co[III]-catalyzed oxidative alkyne annulation. *Angew. Chem., Int. Ed.* **2017**, *56*, 12137−12141. (c) Sen, M.; Dahiya, P.; Premkumar, J. R.; Sundararaju, B. Dehydrative Cp*Co(III)-catalyzed C−H bond allenylation. *Org. Lett.* **2017**, *19*, 3699−3702. (d) Yu, X.; Chen, K.; Guo, S.; Shi, P.; Song, C.; Zhu, J. Direct access to cobaltacycles via C−H activation: N-chloroamide-enable room-temperature synthesis of heterocycles. *Org. Lett.* **2017**, *19*, 5348−5351. (e) Sen, M.; Rajesh, N.; Emayavaramban, B.; Premkumar, J. R.; Sundararaju, B. Isolation of Cp*Co(III)-alkenyl intermediate in efficient cobalt catalyzed C−H bond alkenylation with alkynes. *Chem. - Eur. J.* **2018**, *24*, 342−346. (f) Sanjosé-Orduna, J.; Sarria Toro, J. M.; Pérez-Temprano, M. H. HFIP-assisted C−H functionalization by Cp*Co[III]: access to key reactive cobaltacycles and implication in catalysis. *Angew. Chem., Int. Ed.* **2018**, *57*, 11369−11373. (g) Boerth, J. A.; Maity, S.; Williams, S. K.; Mercado, B. Q.; Ellman, J. A. Selective and synergistic cobalt(III)-catalysed three-component C−H bond addition to dienes and aldehydes. *Nat. Catal.* **2018**, *1*, 673−679.

(8) (a) Gallego, D.; Baquero, E. A. Recent advances on mechanistic studies on C−H activation catalyzed by base metals. *Open. Chem.* **2018**, *16*, 1001−1058. (b) Planas, O.; Chirila, P. G.; Whiteoak, C. J.; Ribas, X. Current mechanistic understanding of cobalt-catalyzed C−H functionalization. *Adv. Organomet. Chem.* **2018**, *69*, 209−282.

(9) Albrecht, M. Cyclometalation using d-block transition metals: fundamental aspects and recent trends. *Chem. Rev.* **2010**, *110*, 576−623.

(10) King, R. B.; Treichel, P. M.; Stone, F. G. A. Chemistry of the Metal Carbonyls. XII. New Complexes Derived from Cyclopentadienylcobalt Dicarbonyl. *J. Am. Chem. Soc.* **1961**, *83*, 3593−3597.

(11) Under catalytic conditions, the presence of acetate in the reaction mixture presumably facilitates the C−H metalation step. See: (a) Zell, D.; Bursch, M.; Müller, V.; Grimme, S.; Ackermann, L. Full selectivity control in cobalt(III)-catalyzed C−H alkylations by switching of the C−H activation mechanism. *Angew. Chem., Int. Ed.* **2017**, *56*, 10378−10382. (b) Qu, S.; Cramer, C. J. Mechanistic study of Cp*Co[III]/Rh[III]-catalyzed directed C−H functionalization with diazo compounds. *J. Org. Chem.* **2017**, *82*, 1195−1204. (c) Wang, W.; Huang, F.; Jiang, L.; Zhang, C.; Sun, C.; Liu, J.; Chen, D. Comprehensive Mechanistic Insight into cooperative Lewis acid/Cp*Co[III]-catalyzed C−H/N−H activation for the synthesis of isoquinolin-3-ones. *Inorg. Chem.* **2018**, *57*, 2804−2814. (d) Lorion, M. M.; Kaplaneris, N.; Son, J.; Kuniyil, R.; Ackermann, L. Late-stage peptide diversification through cobalt-catalyzed C−H activation: sequential multicatalysis for stapled peptides. *Angew. Chem., Int. Ed.* **2019**, *58*, 1684−1688.

(12) (a) Li, L.; Brennessel, W. W.; Jones, W. D. An efficient low-temperature route to polycyclic isoquinoline salt synthesis via C−H activation with [Cp*MCl₂]₂ (M = Rh, Ir). *J. Am. Chem. Soc.* **2008**, *130*, 12414−12419. (b) Davies, D. L.; Al-Duaij, O.; Fawcett, J.; Singh, K. Reactions of cyclometalated oxazoline half-sandwich complexes of iridium and ruthenium with alkynes and CO. *Organometallics* **2010**, *29*, 1413−1420. (c) Li, L.; Jiao, Y.; Brennessel, W. W.; Jones, W. D. Reactivity and regioselectivity of insertion of unsaturated molecules into M−C (M = Ir, Rh) bonds of cyclometalated complexes. *Organometallics* **2010**, *29*, 4593−4605. (d) Boutadla, Y.; Davies, D. L.; Al-Duaij, O.; Fawcett, J.; Jones, R. C.; Singh, K. Alkyne insertion into cyclometallated pyrazole and imine complexes of iridium, rhodium and ruthenium; relevance to catalytic formation of carbo- and heterocycles. *Dalton Trans.* **2010**, *39*, 10447−10457. (e) Espada, M. F.; Poveda, M. L.; Carmona, E. Reactivity of a cationic (C₅Me₅)Ir[III]-

cyclometalated phosphine complex with alkynes. *Organometallics* **2014**, *33*, 7164−7175. (f) Sun, R.; Zhang, S.; Chu, X.; Zhu, B. Synthesis, structures, and reactivity of cyclometalated complexes formed by insertion of alkynes into M−C (M = Ir and Rh) bonds. *Organometallics* **2017**, *36*, 1133−1141. (g) Giner, E. A.; Gómez-Gallego, M.; Merinero, A. D.; Casarrubios, L.; Ramírez de Arellano, C.; Sierra, M. A. Sequential Reactions of alkynes on an iridium(III) single site. *Chem. - Eur. J.* **2017**, *23*, 8941−8948.

(13) Hartwig, J. F. Migratory insertion reactions. In *Organotransition Metal Chemistry: From Bonding to Catalysis*; University Science Books: Sausalito, CA, 2010; pp 349−396.

(14) We have determined the kinetic order in MeCN, adding 5, 10, and 20 equiv of the stabilizing ligand.

(15) We added an excess of MeCN to slow down formation of the annulated product and observe the conversion of **1-MeCN** into **2a-MeCN**.

(16) Under these reaction conditions, at longer reaction times, we observed a mass balance problem associated with the low solubility of **3a**.

(17) (a) Mendes, P. GEPASI: a software package for modelling the dynamics, steady states and control of biochemical and other systems. *Bioinformatics* **1993**, *9*, 563−571. (b) Mendes, P. Biochemistry by numbers: simulation of biochemical pathways with Gepasi 3. *Trends Biochem. Sci.* **1997**, *22*, 361−363. (c) Mendes, P.; Kell, D. B. Non-linear optimization of biochemical pathways: applications to metabolic engineering and parameter estimation. *Bioinformatics* **1998**, *14*, 869−883. (d) Martins, A. M.; Mendes, P.; Cordeiro, C.; Freire, A. P. In situ kinetic analysis of glyoxalase I and glyoxalase II in Saccharomyces cerevisiae. *Eur. J. Biochem.* **2001**, *268*, 3930−3936.

(18) To enable full characterization by NMR spectroscopy of **2b-MeCN** and **2c-MeCN**, we added different amounts of MeCN depending on their reactivity. Because **2c-MeCN** turned out to be more unstable, instead of 20 equiv, we added 50 equiv.

(19) (a) Otley, K. D.; Ellman, J. A. An efficient method for the preparation of styrene derivatives via Rh(III)-catalyzed direct C−H vinylation. *Org. Lett.* **2015**, *17*, 1332−1335.

(20) Zell, D.; Müller, V.; Dhawa, U.; Bursch, M.; Presa, R. R.; Grimme, S.; Ackermann, L. Mild cobalt(III)-catalyzed allylative C−F/C−H functionalizations at room temperature. *Chem. - Eur. J.* **2017**, *23*, 12145−12148.

3.8 Supporting Information for Article 2

Table of Contents

3.8.1 General Procedures

All experiments were conducted under an argon-filled glove box (mBraun Unilab 4420) with concentrations of O_2 and H_2O < 0.1 ppm or using Schlenk techniques under argon atmosphere. All the glassware was oven-dried at 100 ºC overnight and cooled under vacuum prior use. NMR spectra were obtained on a Bruker 400 MHz or a 500 MHz cryoprobe spectrometers. ^1H, ^{13}C and ^{19}F NMR chemical shifts are reported in parts per million (ppm), relative to tetramethylsilane (TMS) for ^1H and ^{13}C with the residual solvent peak used as an internal reference, and relative to CCl_3F (Freon) for ^{19}F. Multiplicities are reported as follows: singlet (s), doublet (d), doublet of doublets (dd), triplet of doublets (td), triplet (t), and multiplet (m). High Resolution Mass Spectrometry (HRMS) data was recorded on a LCT-Premier (Waters) or a MicroTOF Focus (Bruker Daltonics) mass spectrometers using ESI ionization technique and acetonitrile as solvent. Details for X-ray structure determination can be found on page 129.

3.8.2 Materials and Methods

Commercially available reagents diphenylacetylene, phenylacetylene, vinyl acetate, $AgBF_4$, were used without further purification directly as received from the commercial supplier, and stored under inert gas and/or low temperature when required.

The solvents (^{n}hexane, Et_2O, CH_2Cl_2, MeCN) were used from a solvent purification system *pure-solv* (SPS-400, Innovative Technology) and stored under argon with activated 4 Å molecular sieves.

Deuterated solvents (CD_3CN, CD_2Cl_2) were stored under argon with activated 4 Å molecular sieves.

1−MeCN was synthesized according to previous literature procedures.[1]

---

[1] J. Sanjosé-Orduna, D. Gallego, A. Garcia-Roca, E. Martin, J. Benet-Buchholz, M. H. Pérez-Temprano, *Angew. Chem. Int. Ed.* **2017**, *56*, 12137−12141.

3.8.3 Procedure for the Synthesis of Inserted Cobaltacycles

3.8.3.1 Formation and Characterization of 2b-MeCN
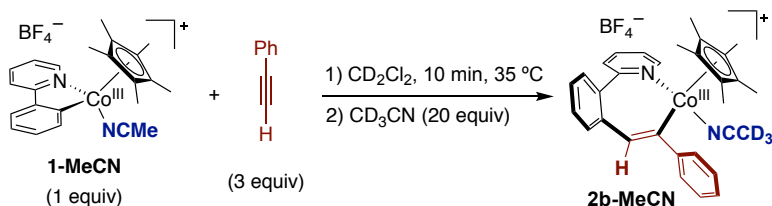
Inside the glovebox an NMR tube was loaded with **1-MeCN** (4.7 mg, 0.01 mmol). The tube was then taken out and connected to the Schlenk line *via* an adaptor and then the solid was dissolved in 0.5 mL of CD_2Cl_2. After that, phenylacetylene (3.3 µL, 0.03 mmol) was added. After 10 min at 35 ºC, excess of CD_3CN (10 µL, 0.19 mmol) was added to stabilize this reactive intermediate. Full characterization of this mixture by NMR was performed afterwards.

Characterization of **2b-MeCN**
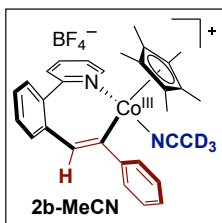
¹H NMR (500 MHz, CD_2Cl_2/CD_3CN (50:1), 25 °C): δ 9.10 (d, J = 4.9 Hz, 1H), 7.91 (t, J = 7.6 Hz, 1H), 7.53 − 7.46 (m, 5H), 7.21 (t, J = 7.4 Hz, 2H), 7.16 (d, J = 7.3 Hz, 1H), 7.06 (s, 1H), 6.94 (d, J = 7.2 Hz, 2H), 1.97 (s, 3H), 1.02 (s, 15H). One proton is missing due to overlapping peaks.

¹³C NMR (126 MHz, CD_2Cl_2/CD_3CN (50:1), 25 °C) δ 167.54, 165.84, 155.23, 154.64, 139.94, 138.82, 135.66, 135.35, 133.89, 132.20, 129.93, 129.56, 129.25, 127.91, 127.09, 126.46, 125.60, 124.78, 122.44, 96.73, 9.54.

¹⁹F NMR (376 MHz, CD_2Cl_2/CD_3CN (50:1), 25 °C): δ −152.16 (s).

HRMS-ESI (m/z): [M−MeCN]⁺ calcd for $C_{29}H_{29}CoN$, 450.1632; Found, 450.1629.

3.8.3.2 Formation and Characterization of 2c-MeCN
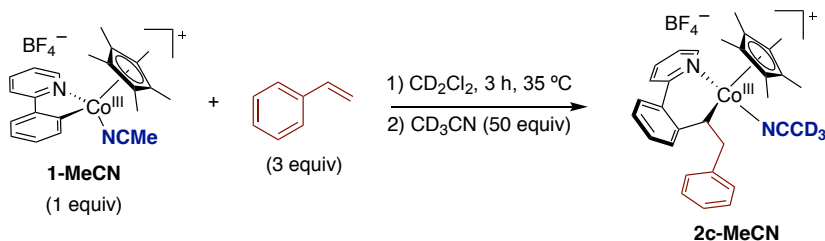
Inside the glovebox an NMR tube was loaded with **1-MeCN** (4.7 mg, 0.01 mmol). The tube was then taken out and connected to the Schlenk line *via* an adaptor and then the solid was dissolved in 0.5 mL of CD_2Cl_2. After that, styrene (3.7 µL, 0.03 mmol) was added. After 3 h at 35 °C, excess of CD_3CN (28 µL, 0.53 mmol) was added to stabilize this reactive intermediate, and then filtered with a PTFE syringe filter. Full characterization of this reaction mixture by NMR was done afterwards.

Characterization of **2c-MeCN**
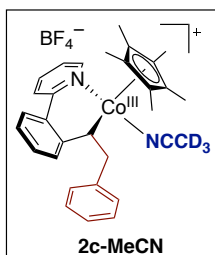
¹H NMR (500 MHz, CD_2Cl_2/CD_3CN (20:1), 25 °C): δ 9.37 (d, J = 5.9 Hz, 1H), 7.98 (t, J = 7.7 Hz, 1H), 7.91 (d, J = 8.0 Hz, 1H), 7.56 (t, J = 6.7 Hz, 1H), 7.51 (d, J = 7.7 Hz, 1H), 7.17 (t, J = 7.7 Hz, 1H), 7.11 − 7.00 (m, 4H), 6.98 (t, J = 8.4 Hz, 1H), 6.66 (d, J = 7.2 Hz, 2H) 4.73 (dd, J = 11.1, 5.4 Hz, 1H), 2.53 (dd, J = 13.7, 5.4 Hz, 1H), 1.96 (s, 3H), 1.15 (t, J = 12.3 Hz, 1H), 1.03 (s, 15H).

¹³C NMR (126 MHz, CD_2Cl_2/CD_3CN (20:1), 25 °C): δ 160.36, 156.66, 146.70, 142.24, 139.50, 137.17, 130.12, 129.53, 128.95, 128.65, 128.56, 127.93, 126.84, 126.34, 125.64, 124.68, 123.58, 95.25, 44.23, 38.84, 8.43.

¹⁹F NMR (376 MHz, CD_2Cl_2/CD_3CN (20:1), 25 °C): δ −151.24 (s).

HRMS-ESI (m/z): [M−MeCN]⁺ calcd for $C_{29}H_{31}CoN$, 452.1789; Found, 452.1783.

3.8.3.3 Isolation and Characterization of 2d

1-MeCN
(1 equiv)

(3 equiv)

2d

100% isolated yield
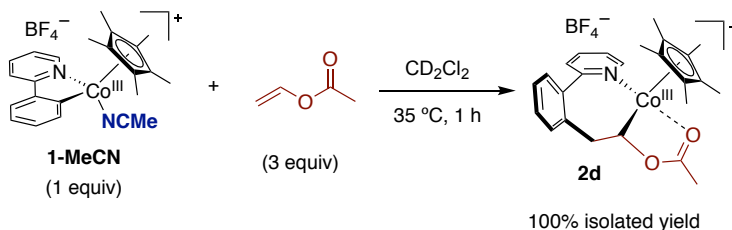
Inside the glovebox an NMR tube was loaded with **1-MeCN** (15.2 mg, 0.03 mmol). The tube was then taken out and connected to the Schlenk line *via* an adaptor and then the solid was dissolved in 1.5 mL of CD_2Cl_2. After that, vinyl acetate (8.7 μL, 0.09 mmol) was added. After 1 h at 35 °C, the reaction mixture was filtered with a PTFE syringe filter and the solvent was removed in vacuo. Further washings with Et_2O (3x5 mL), gave rise the desired inserted cobaltacycle **2d** in quantitative yield (16.4 mg, 100%) as a pure brown solid.

Characterization of **2d**
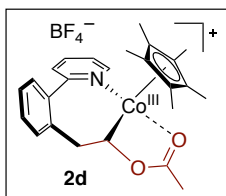
¹H NMR (500 MHz, CD_2Cl_2, 25 °C): δ 9.23 (d, J = 4.9 Hz, 1H), 8.07 (td, J = 7.8, 1.6 Hz, 1H), 7.86 (dd, J = 12.0, 5.3 Hz, 1H), 7.71 (d, J = 7.9 Hz, 1H), 7.61 (t, J = 6.0 Hz, 2H), 7.54 (t, J = 6.9 Hz, 2H), 7.51 − 7.42 (m, 1H), 3.23 (dd, J = 12.1, 5.3 Hz, 1H), 2.23 (s, 3H), 1.86 (t, J = 12.1 Hz, 1H), 0.89 (s, 15H).

¹³C NMR (126 MHz, CD_2Cl_2, 25 °C) δ 186.27, 165.01, 154.52, 139.69, 138.26, 135.65, 131.37, 131.34, 130.84, 129.67, 128.17, 124.37, 106.00, 94.27, 43.69, 19.39, 8.70.

¹⁹F NMR (376 MHz, CD_2Cl_2, 25 °C): δ −151.20 (s).

HRMS-ESI (m/z): [M]⁺ calcd for $C_{25}H_{29}CoNO_2$, 434.1530; Found, 434.1533.

3.8.4 Mechanistic Study on the Insertion Reaction using Diphenylacetylene as Model Coupling Partner

3.8.4.1 Influence of the Cp*Co^{III} Cobaltacycles
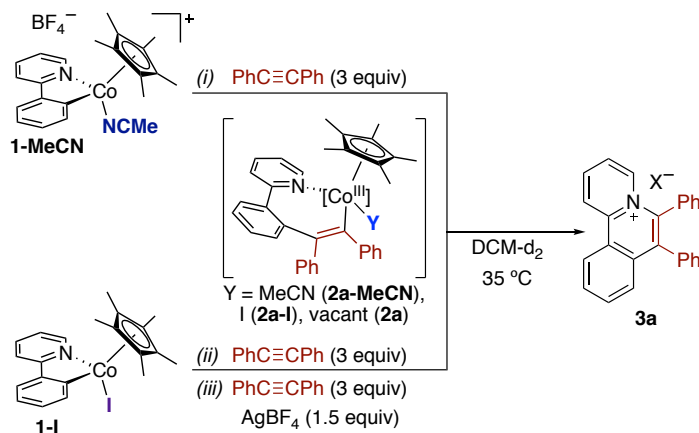
Inside the glovebox an NMR tube was loaded with **1-MeCN** (4.7 mg, 0.01 mmol) or **1-I** (4.8 mg, 0.01 mmol), diphenylacetylene (5.3 mg, 0.03 mmol) and AgBF$_4$ (2.9 mg, 0.015 mmol) if required. The tube was then taken out and connected to the Schlenk line via an adaptor and cooled down to −35 °C. The solid was then dissolved in 0.5 mL of CD$_2$Cl$_2$. The reaction was kept at this temperature until transferred to the NMR instrument for measurement at 35 °C.
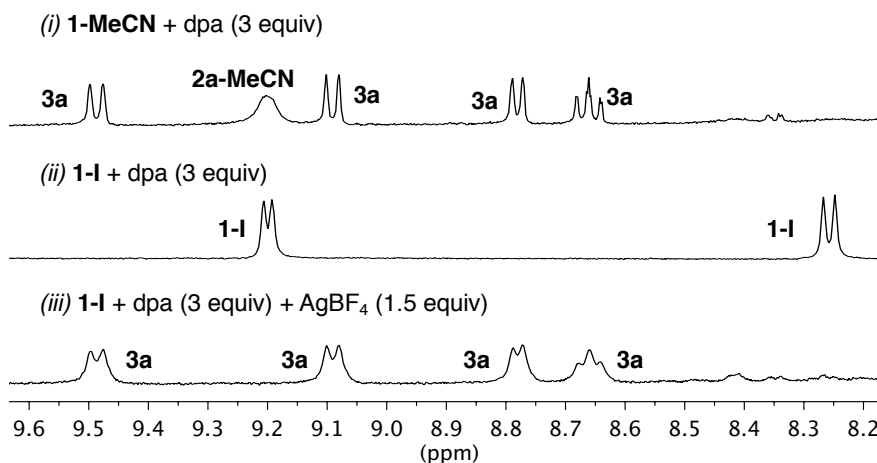
Figure S1. Sequences of ^{1}H NMR spectra corresponding to the insertion of dpa to different cobaltacycles, after 25 min at 35 °C.

3.8.4.2 MeCN Effect
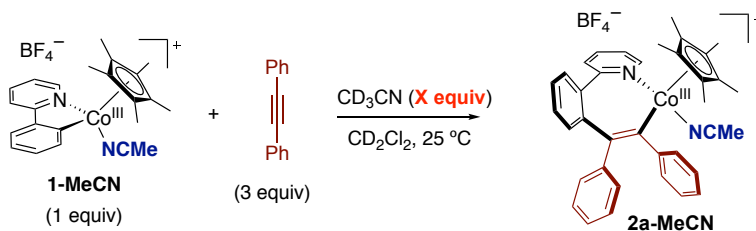
Inside the glovebox an NMR tube was loaded with **1-MeCN** (4.7 mg, 0.01 mmol) and diphenylacetylene (5.3 mg, 0.03 mmol). The tube was then taken out and connected to the Schlenk line *via* an adaptor and cooled down to −35 °C. The solid was then dissolved in 0.5 mL of CD_2Cl_2. After that, the proper amount of CD_3CN was added (see table S1). The reaction was kept at this temperature until transferred to the NMR instrument for measurement at 25 °C. 1,3,5-trimetoxybencene was used as internal standard.

Table S1. Initial rates for the formation of 2a-MeCN in CD_2Cl_2 at 25 °C, in the presence of added CD_3CN.[a]

CD_3CN amount	$[CD_3CN]_{added}$ mol L^{-1}	$r_0/10^{-6}$ mol L^{-1} s^{-1}
5 equiv / 2.5 µL	0.1	10.1
10 equiv / 5 µL	0.2	4.36
20 equiv /10 µL	0.4	2.22

[a] Up to 30% conversion
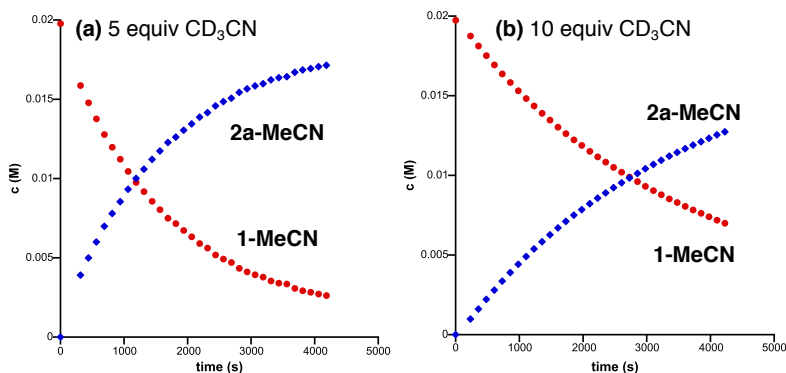
Figure S2.1. Concentration vs time plots for the formation of **2a-MeCN**. Starting conditions $[1\text{-MeCN}]_0$ = 0.02 M, $[dpa]_0$ = 0.06 M. a) 5 equiv of MeCN. b) 10 equiv of MeCN.
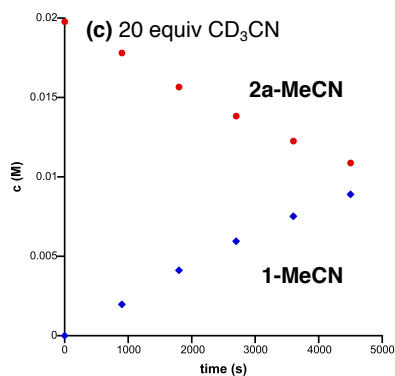
Figure S2.2. Concentration vs time plots for the formation of **2a-MeCN**. Starting conditions [1-MeCN]$_0$ = 0.02 M, [dpa]$_0$ = 0.06 M. c) 20 equiv of MeCN.
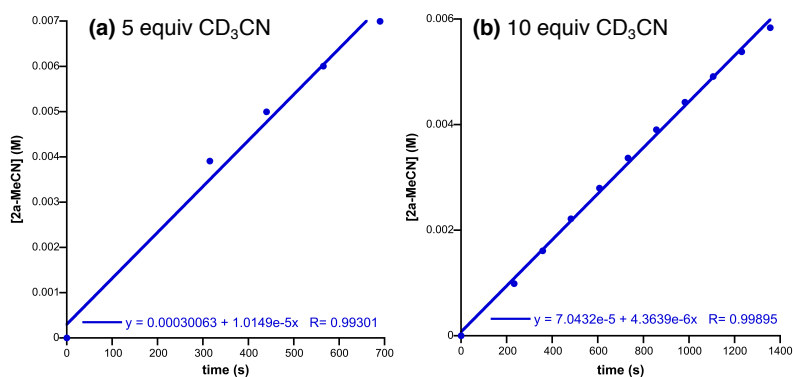
Figure S3.1. Obtention of the initial rates, from the slope of the 30% conversion for every reaction. a) 5 equiv of MeCN. b) 10 equiv of MeCN.
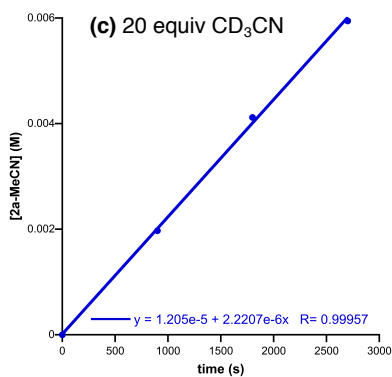
Figure S3.2. Obtention of the initial rates, from the slope of the 30% conversion for every reaction. c) 20 equiv of MeCN.
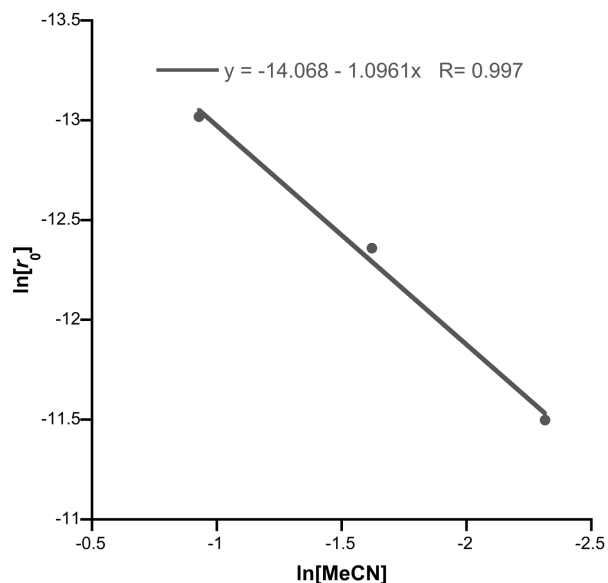
Figure S4. Plot of $\ln(r_0)$ vs. $\ln[MeCN]$. The slope of the straight line is -1.

3.8.4.3 Influence of the Diphenylacetylene at Variable T

3.8.4.3.1 High Temperature
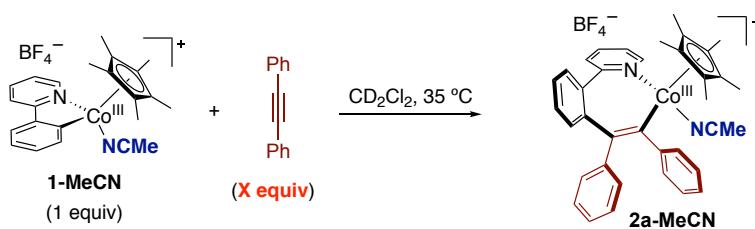
Inside the glovebox an NMR tube was loaded with **1-MeCN** (4.7 mg, 0.01 mmol) and the proper amount of diphenylacetylene (5.3 mg, 0.03 mmol or 17.8 mg, 0.1 mmol). The tube was then taken out and connected to the Schlenk line via an adaptor and cooled down to −35 °C. The solid was then dissolved in 0.5 mL of CD_2Cl_2. The reaction was kept at this temperature until transferred to the NMR instrument for measurement at 35 °C. 1,3,5-trimetoxybencene was used as internal standard.
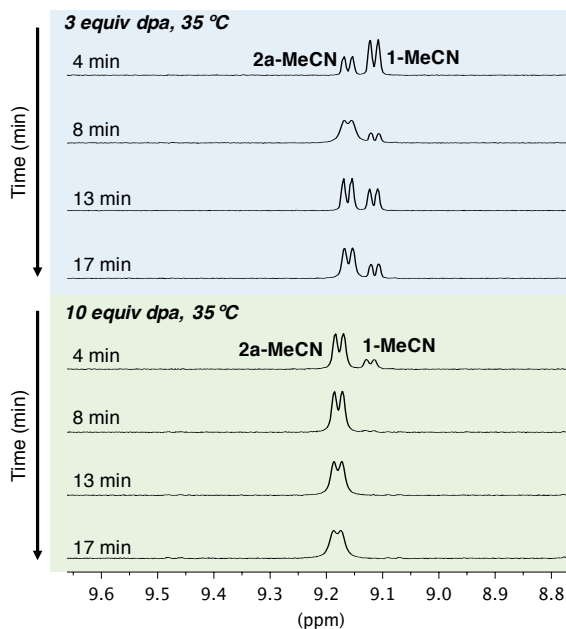
**Figure S5**. Sequences of ¹H NMR spectra corresponding to the insertion of dpa to **1-MeCN**. Blue spectra are using 3 equiv of dpa. Green spectra are using 10 equiv of dpa.

3.8.4.3.2 Low Temperature
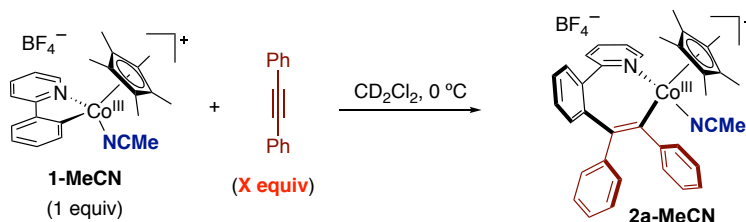
Inside the glovebox an NMR tube was loaded with **1-MeCN** (4.7 mg, 0.01 mmol) and the proper amount of diphenylacetylene (see Table S2). The tube was then taken out and connected to the Schlenk line via an adaptor and cooled down to −35 °C. The solid was then dissolved in 0.5 mL of CD$_2$Cl$_2$. The reaction was kept at this temperature until transferred to the NMR instrument for measurement at 0 °C. 1,3,5-trimetoxybencene was used as internal standard.

Table S2. Initial rates for the formation of 2a-MeCN in CD_2Cl_2 at 0 °C, with varying amounts of dpa.[a]

DPA equiv	$[dpa]_{added}$ mol L^{-1}	$r_0/10^{-6}$ mol L^{-1} s^{-1}
3 equiv / 5.3 mg	0.06	2.77
10 equiv / 17.8 mg	0.2	3.04

[a] Up to 30% conversion
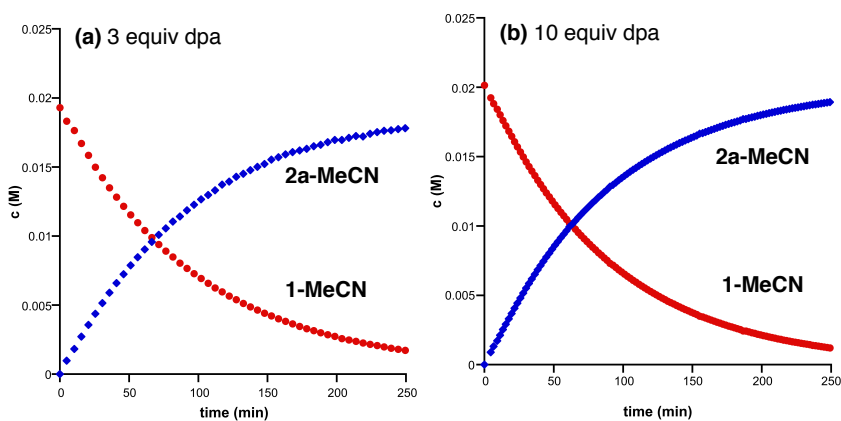
Figure S6. Concentration vs time plots for the formation of **2a-MeCN**. Starting conditions $[1\text{-MeCN}]_0 = 0.02$ M. a) 3 equiv of dpa. b) 10 equiv of dpa.
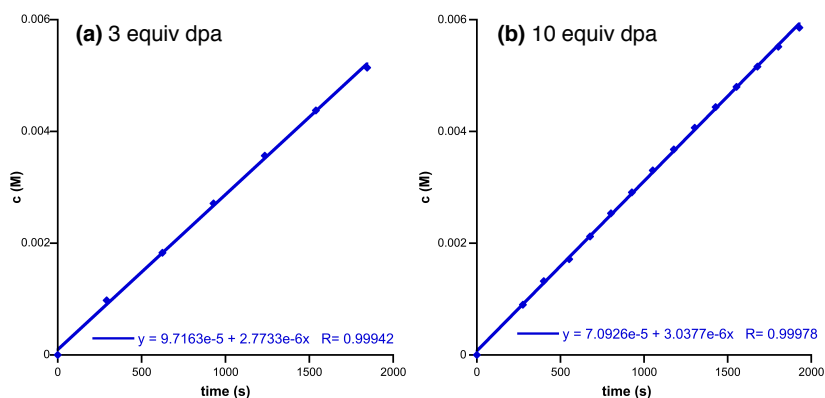
Figure S7. Obtention of the initial rates, from the slope of the 30% conversion for every reaction. a) 3 equiv of dpa. b) 10 equiv of dpa.

3.8.4.4 Eyring Analysis for the Alkyne Insertion at Low Temperature
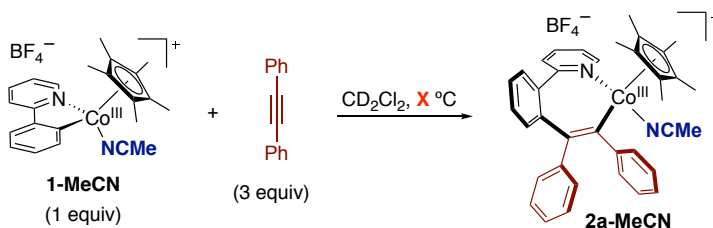
Inside the glovebox an NMR tube was loaded with **1-MeCN** (4.7 mg, 0.01 mmol) and diphenylacetylene (5.3 mg, 0.03 mmol). The tube was then taken out and connected to the Schlenk line via an adaptor and cooled down to −35 ºC. The solid was then dissolved in 0.5 mL of CD_2Cl_2. The reaction was kept at this temperature until transferred to the NMR instrument for measurement at the temperature indicated in Table S3. 1,3,5-trimetoxybencene was used as internal standard. The rate constants (k_1) were obtained by fitting the kinetic data to the kinetic model shown in Figure S8, by nonlinear least-squares (NLLS) regression using the program GEPASI.[2]
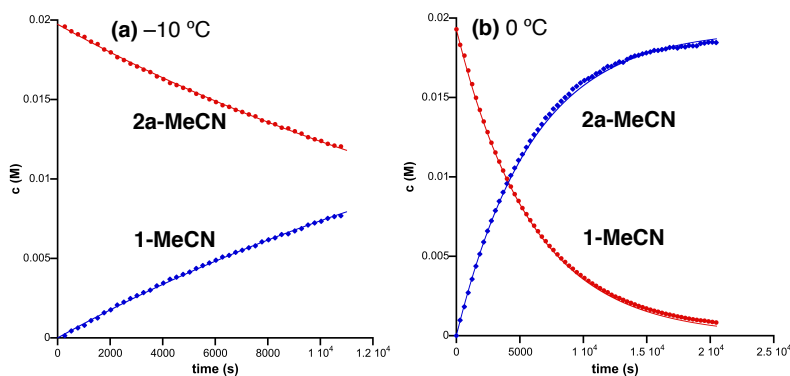
Fig S8.1. Concentration vs time plots for the formation of **2a-MeCN**. Starting conditions [1-MeCN]$_0$ = 0.02 M, [dpa]$_0$ = 0.06 M. Solid lines are the best fit using Gepasi. (a) −10 ºC. (b) 0 ºC.

[2] (a) Mendes, P. *Bioinformatics* **1993**, *9*, 563. (b) Mendes, P. *Trends Biochem. Sci.* **1997**, *22*, 361. (c) Mendes, P.; Kell, D. B. *Bioinformatics* **1998**, *14*, 869. (d) Martins, A. M.; Mendes, P.; Cordeiro, C.; Freire, A. P. *Eur. J. Biochem.* **2001**, *268*, 3930.
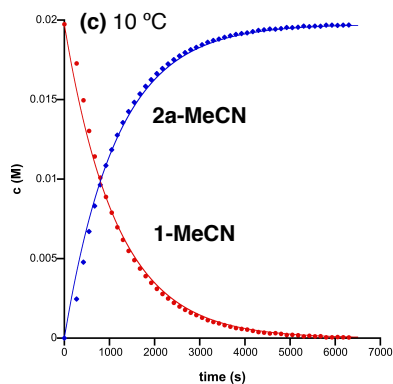
Fig S8.2. Concentration vs time plots for the formation of **2a-MeCN**. Starting conditions [1-MeCN]$_0$ = 0.02 M, [dpa]$_0$ = 0.06 M. Solid lines are the best fit using Gepasi. (c) 10 ºC.

Table S3. Rate constants for the dpa insertion to 1-MeCN in CD$_2$Cl$_2$ at variable temperatures.

T/K	k_1 x 10^{-5} s^{-1}
263	4.67
273	16.98
283	86.8

y = 24.611 - 10580x   R^2= 0.99147
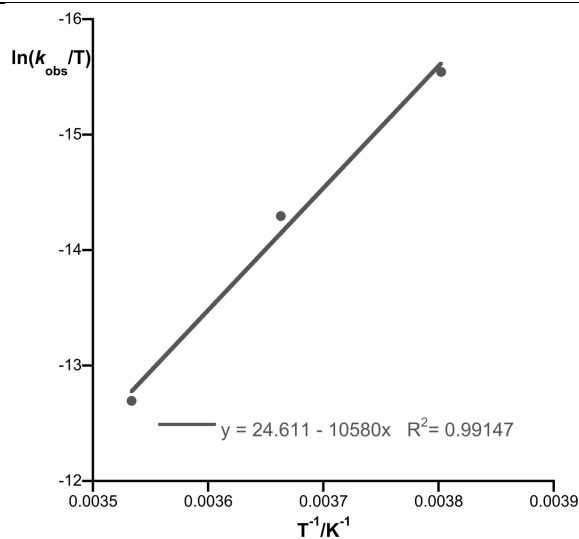
Figure S9. Eyring plot for the determination of ΔH‡ and ΔS‡ for the dpa insertion to obtain **2a-MeCN**.

Activation parameters:
ΔH‡ = 21.0 kcal mol^{-1}
ΔS‡ = 1.63 cal K^{-1} mol^{-1}

3.8.5 Reaction of 1-MeCN Towards Other Unsaturated Molecules

3.8.5.1 Phenylacetylene
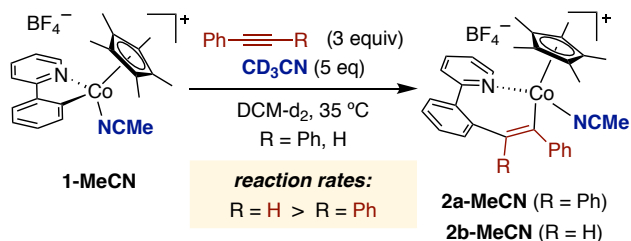
1-MeCN

Ph━━━R (3 equiv)
CD₃CN (5 eq)
DCM-d₂, 35 °C
R = Ph, H

reaction rates:
R = H > R = Ph

2a-MeCN (R = Ph)
2b-MeCN (R = H)

Inside the glovebox an NMR tube was loaded with **1-MeCN** (4.7 mg, 0.01 mmol). The tube was then taken out and connected to the Schlenk line via an adaptor and cooled down to −35 °C. The solid was then dissolved in 0.5 mL of CD₂Cl₂. After that, CD₃CN (2.5 µL, 0.05 mmol) and phenylacetylene (3.3 µL, 0.03 mmol) were added successively. The reaction was kept at this temperature until transferred to the NMR instrument for measurement at 35 °C. In the dpa reaction, diphenylacetylene (5.3 mg, 0.03 mmol) was weighted in the glovebox. 1,3,5-trimetoxybencene was used as internal standard.
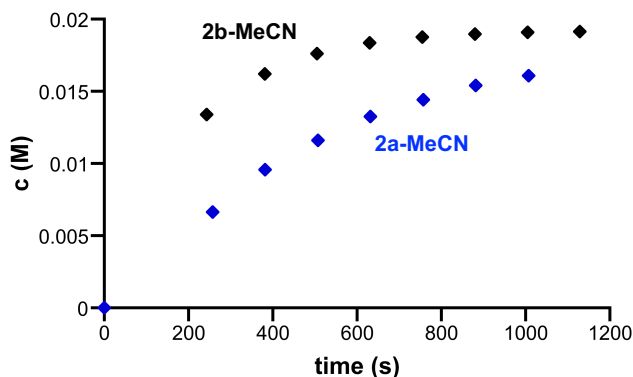
Figure S10. Concentration vs time plots comparison for the formation of **2a-MeCN** and **2b-MeCN**.

3.8.5.2 Styrene
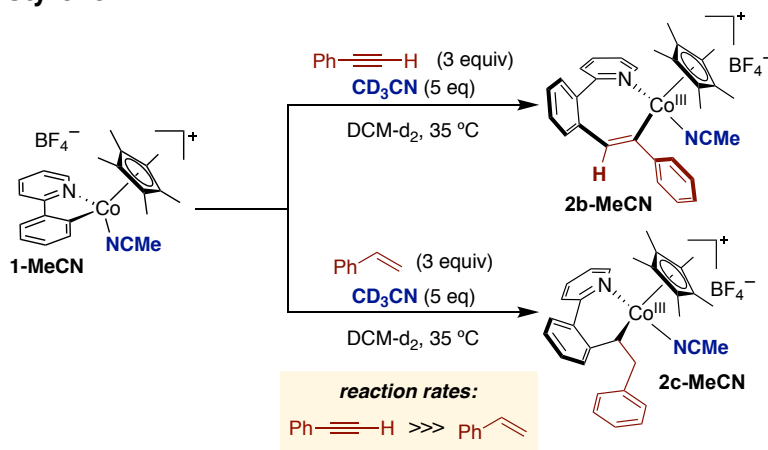
Inside the glovebox an NMR tube was loaded with **1-MeCN** (4.7 mg, 0.01 mmol). The tube was then taken out and connected to the Schlenk line *via* an adaptor and cooled down to −35 ºC. The solid was then dissolved in 0.5 mL of CD_2Cl_2. After that, CD_3CN (2.5 µL, 0.05 mmol) and styrene (3.7 µL, 0.03 mmol) were added successively. The reaction was kept at this temperature until transferred to the NMR instrument for measurement at 35 ºC. 1,3,5-trimetoxybencene was used as internal standard.

This reaction was compared with the reaction prepared in the section 3.8.5.1 with phenylacetylene.
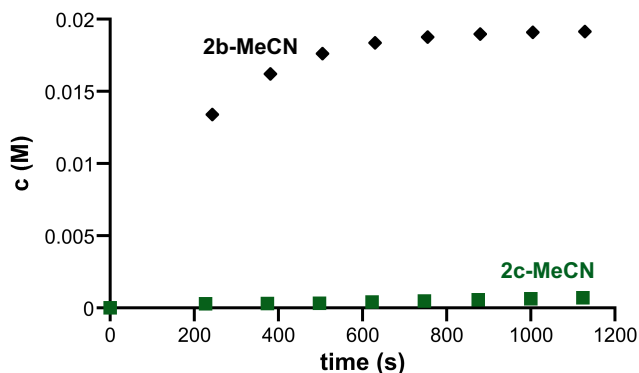
Figure S11. Concentration vs time plots comparison for the formation of **2b-MeCN** and **2c-MeCN**.

3.8.5.3 Vinyl Acetate
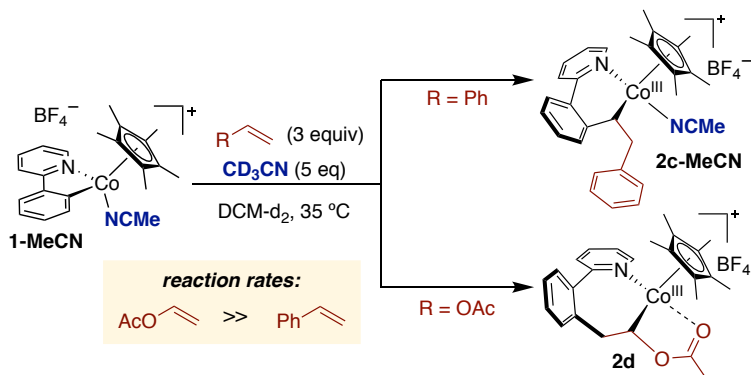
Inside the glovebox an NMR tube was loaded with **1-MeCN** (4.7 mg, 0.01 mmol). The tube was then taken out and connected to the Schlenk line *via* an adaptor and cooled down to −35 °C. The solid was then dissolved in 0.5 mL of CD_2Cl_2. After that, CD_3CN (2.5 μL, 0.05 mmol) and vinyl acetate (2.8 μL, 0.03 mmol) were added successively. The reaction was kept at this temperature until transferred to the NMR instrument for measurement at 35 °C. 1,3,5-trimetoxybencene was used as internal standard.

This reaction was compared with the reaction prepared in the section 3.8.5.2 with styrene.
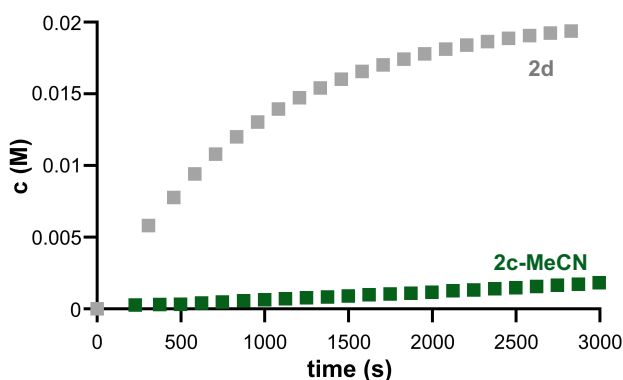
Figure S12. Concentration vs time plots comparison for the formation of **2c-MeCN** and **2d**.

5.4.   Ethyl vinyl ether
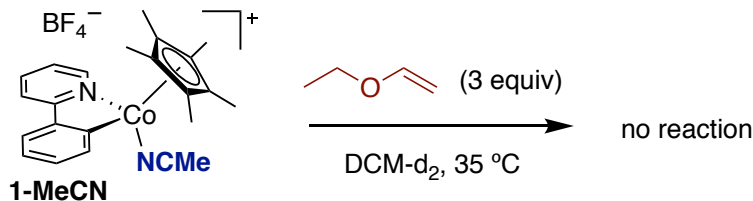
Inside the glovebox an NMR tube was loaded with **1-MeCN** (4.7 mg, 0.01 mmol). The tube was then taken out and connected to the Schlenk line via an adaptor and was dissolved in 0.5 mL of CD₂Cl₂. After that, ethyl vinyl ether (2.9 μL, 0.03 mmol) was added. The reaction mixture was transferred to the NMR instrument for measurement at 35 °C immediately. 1,3,5-trimetoxybencene was used as internal standard.

After 2 hours at this temperature, no reaction was observed (see Figure S13).
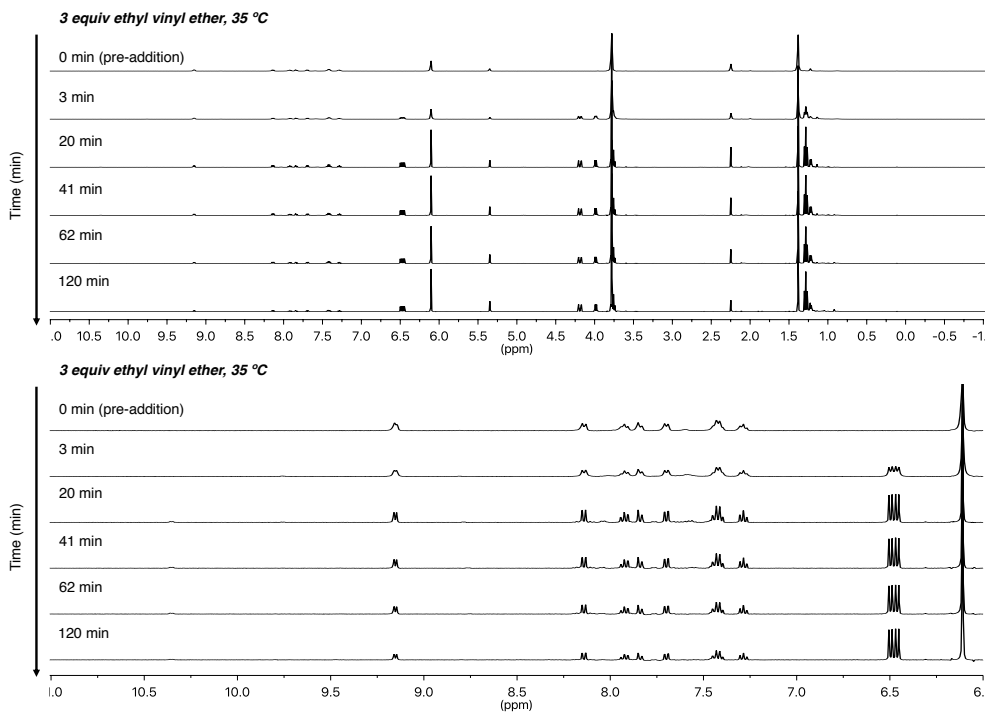
Figure S13. Stacked plot of the reaction of 1-**MeCN** and ethyl vinyl ether.

3.8.6 Single Crystal X-Ray Structure Determinations
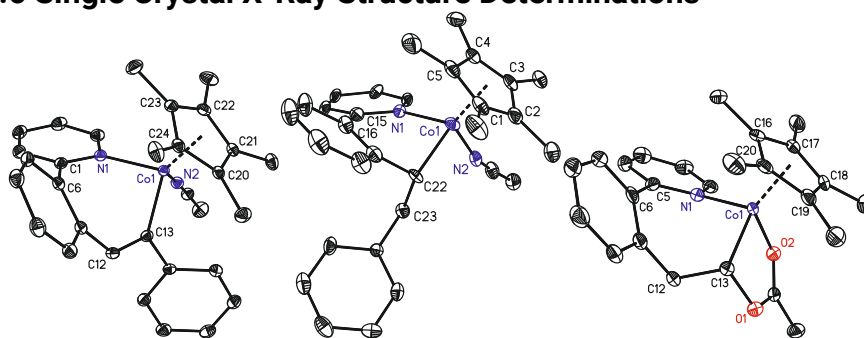
Figure 1. ORTEP drawing (thermal ellipsoids 50 %) of **2b-MeCN, 2c-MeCN and 2d**.

Crystal preparation: Crystals of **2b-MeCN, 2c-MeCN and 2d** were grown at −32 ºC by liquid/liquid diffusion of *n*-hexane into a solution of the corresponding complex in CD_2Cl_2. The measured crystals were prepared under inert conditions immersed in perfluoropolyether as protecting oil for manipulation.

Data collection: Crystal structure determination for **2b-MeCN** was carried out using a Apex DUO Kappa 4-axis goniometer equipped with an APPEX 2 4K CCD area detector, a Microfocus Source E025 IuS using MoK$_\alpha$ radiation (0.71073 Å), Quazar MX multilayer Optics as monochromator and a Oxford Cryosystems low temperature device Cryostream 700 plus (*T* = -173 ˚C). Full-sphere data collection was used with *ω* and *φ* scans. *Programs used:* Data collection APEX-2,[3] data reduction Bruker Saint[4] V/.60A and absorption correction SADABS.[5]

Crystal structure determination for compounds **2c-MeCN** and **2d** were carried out using a Rigaku diffractometer equipped with a Pilatus 200K area detector, a Rigaku MicroMax-007HF microfocus rotating anode with MoKα radiation, Confocal Max Flux optics and an Oxford Cryosystems low temperature device Cryostream 700 plus (T = -173 °C). Full-sphere data collection was used with ω and φ scans. Programs used: Data collection and reduction with CrysAlisPro[6] V/.60A and absorption correction with Scale3 Abspack scaling algorithm.[7]

---

[3] Data collection with APEX II v2014.9-0. Bruker (2014). Bruker AXS Inc., Madison, Wisconsin, USA.

[4] Data reduction with Bruker SAINT+ version V8.35A. Bruker (2013). Bruker AXS Inc., Madison, Wisconsin, USA.

[5] SADABS: V2014/5 Bruker (2001). Bruker AXS Inc., Madison, Wisconsin, USA. Blessing, Acta Cryst. (1995) A51 33-38.

[6] Data collection and reduction with CrysAlisPro 1.171.39.12b (Rigaku OD, 2015).

[7] Empirical absorption corrrection using spherical harmonics implemented in Scale3 Abspack scaling algorithm, CrysAlisPro 1.171.39.12b (Rigaku OD, 2015).

Structure Solution and Refinement: Crystal structure solution was achieved using the computer program SHELXT.[8] Visualization was performed with the program SHELXle[9]. Missing atoms were subsequently located from difference Fourier synthesis and added to the atom list. Least-squares refinement on F^2 using all measured intensities was carried out using the program SHELXL 2015.[10] All non-hydrogen atoms were refined including anisotropic displacement parameters.

Comments to the structures: 2b-MeCN: The asymmetric unit contains one molecule of the metal complex, one BF_4 anion and two dichloromethane molecules. The main molecule is disordered in two shifted positions with a ratio of 51:49. The dichloro-methane molecules are disordered in two orientations with ratios of approximately 50:50. **2c-MeCN:** The asymmetric contains one cationic molecule of the metal complex, one BF_4 anion and two dichloromethane molecules. Both dichloromethane molecules are disordered in two orientations with a ratio of respectively 90:10 and 85:15. **2d:** The asymmetric unit contains one molecule of the metal complex and one BF_4 anion. This compound crystallized as a twin following the Twin law (1 0 0) [1 0 0]. A HKLF 5 file was generated using the operation TwinRotMat in Platon (A.L. Spek (2009) Acta Cryst. D65, 148-155. Platon –A Multipurpose Crystallographic Tool, Utrecht University, Utrecht, The Netherlands A.L. Spek (2011)). The BASF value refined to 0.228.

[8] SHELXT; Sheldrick, G.M. *Acta Cryst.* **2015** A71, 3-8.
[9] SHELXle; C.B. Huebschle, G.M. Sheldrick & B. Dittrich; *J.Appl.Cryst.* (2011) 44, 1281-1284.
[10] SHELXL; Sheldrick, G.M. *Acta Cryst.* **2015** C71, 3-8. SHELXT.

Table S3: Crystal data for compounds **2b-MeCN, 2c-MeCN and 2d.**

Compound	2b-MeCN	2c-MeCN	2d
Formula	$C_{66}H_{76}B_2Cl_8Co_2F_8N_4$	$C_{33}H_{36}B_1Cl_4Co_1F_4N_2$	$C_{25}H_{29}B_1Co_1F_4N_1O_2$
Solvents	2 x CH_2Cl_2	2 x CH_2Cl_2	
Formula weight	1500.38	748.18	1360.51
Crystal size (mm³)	0.05 x 0.10 x 0.15	0.20 x 0.30 x 0.40	0.30 x 0.06 x 0.04
Crystal color	brown	yellow	red
Chem. Formula	$C_{66}H_{76}B_2Cl_8Co_2F_8N_4$	$C_{33}H_{36}B_1Cl_4Co_1F_4N_2$	$C_{25}H_{29}B_1Co_1F_4N_1O_2$
Temp (K)	100	100	100
Crystal system	Triclinic	Monoclinic	Monoclinic
Space group	*P*-1	*P*2_1/c	*P*2_1/c
A (Å)	11.1562(7)	14.3896(3)	8.4860(5)
B (Å)	12.1685(8)	16.4231(3)	20.2522(12)
C (Å)	13.5568(8)	14.5526(3)	13.7940(8)
α (deg)	76.8852(18)	90	90
β (deg)	89.9460(18)	105.647(2)	98.879(6)
γ (deg)	74.3783(18)	90	90
V (Å³)	1722.63(19)	3311.64(13)	2342.2(2)
Z	1	4	4
ρ (g/cm³)	1.446	1.501	1.478
μ (mm^{-1})	0.856	0.891	0.788
θ_{max} (°)	31.416	32.488	28.35
Reflec. measured	17651	38540	11473
Unique reflections	7390 [R_{int} = 0.0419]	9261 [R_{int} = 0.0403]	6612 [R_{int} = 0.1025]
Absorpt. correct.	SADABS	Scale3 Abspack	Scale3 Abspack
Trans. min/max	0.5812/0.7462	0.828/0.985	1.000/0.890
Parameters/Restrains	776/712	459/102	314/0
R1/wR2 [I>2σ(I)]	0.0472/0.1235	0.0350/0.0888	0.0568/0.1346
R1/wR2 [all data]	0.0647/0.1362	0.0429/0.0915	0.1043/0.1500
Goodness-of-fit (F²)	1.038	1.061	0.955
Special refinement	---	---	2-component twin; Twin Law (1 0 0)[1 0 0]
Peak/hole (e/Å³)	0.729/-0.581	0.515/-0.366	0.720/-0.449

3.8.7 NMR Characterization

3.8.7.1 NMR Characterization of Complex 2b-MeCN

^{1}H NMR spectra of 2b-MeCN at 25 °C (CD$_2$Cl$_2$/CD$_3$CN (50:1))
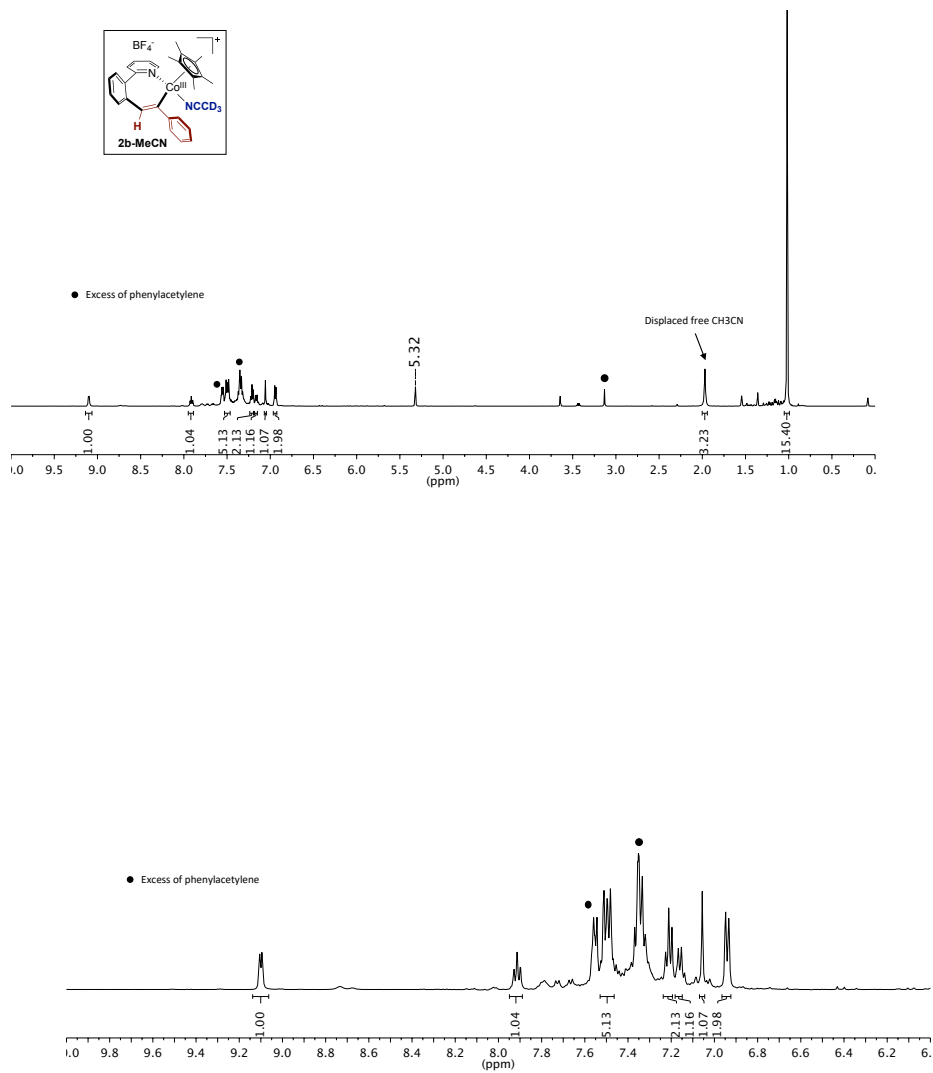
13C NMR spectra of 2b-MeCN at 25 °C (CD$_2$Cl$_2$/CD$_3$CN (50:1))
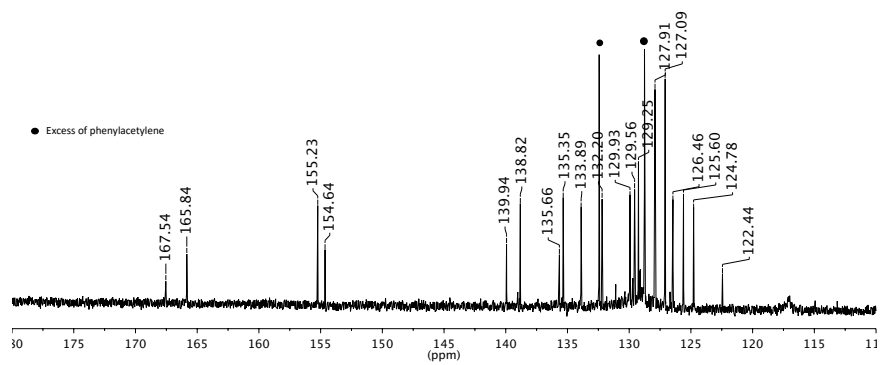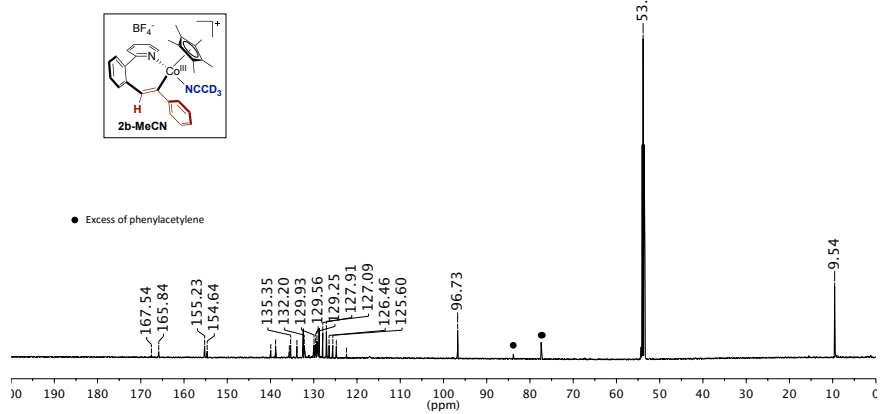
● Excess of phenylacetylene

● Excess of phenylacetylene
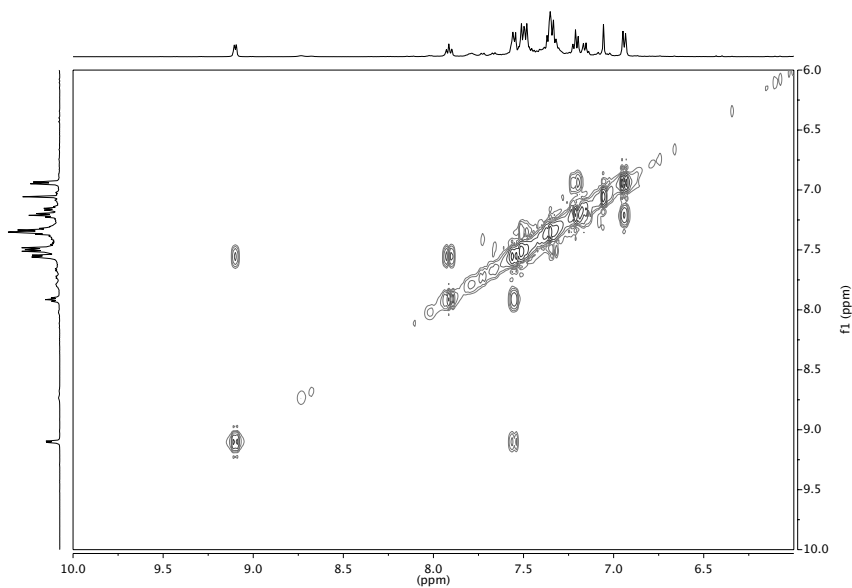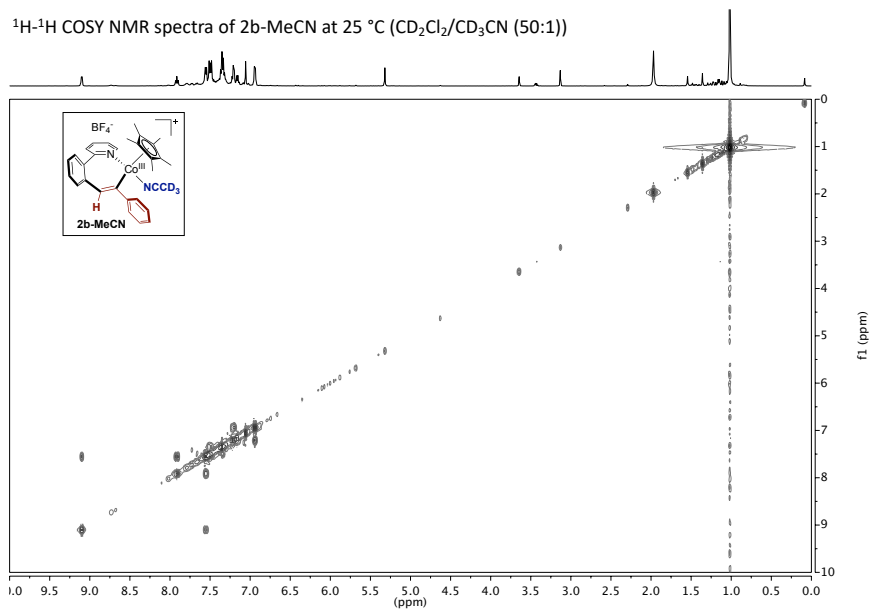
¹H-¹H COSY NMR spectra of 2b-MeCN at 25 °C (CD₂Cl₂/CD₃CN (50:1))

¹H-¹H TOCSY NMR spectra of 2b-MeCN at 25 °C (CD$_2$Cl$_2$/CD$_3$CN (50:1))
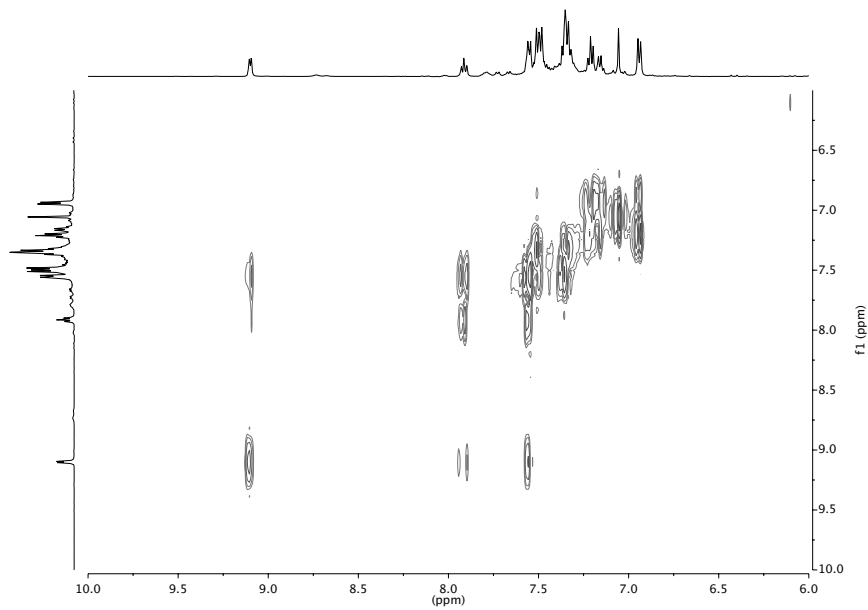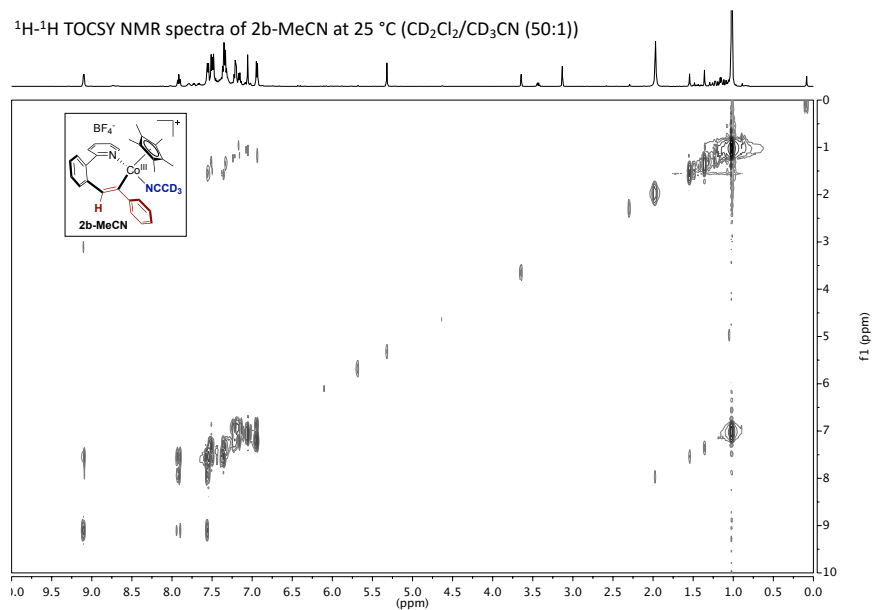
¹H-¹H NOESY NMR spectra 2b-MeCN at 25 °C (CD₂Cl₂/CD₃CN (50:1))
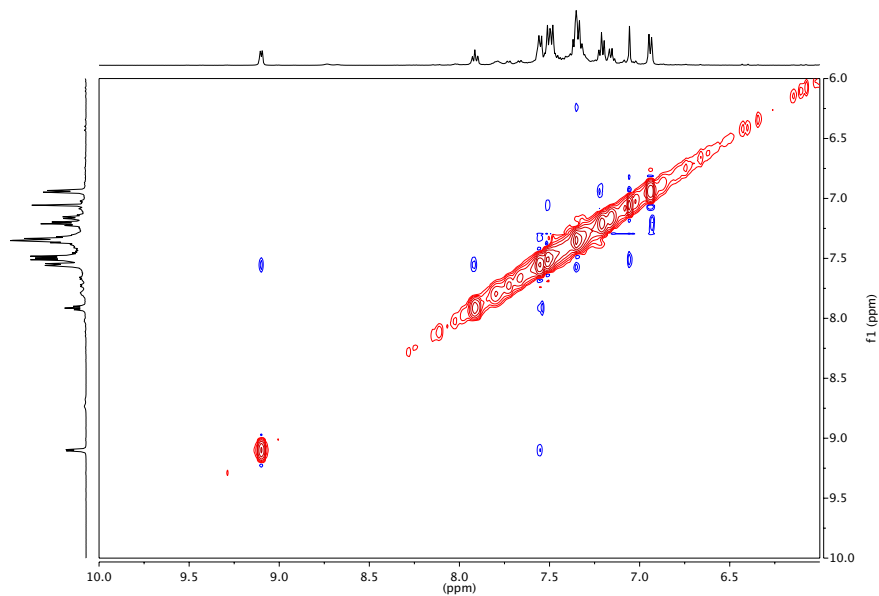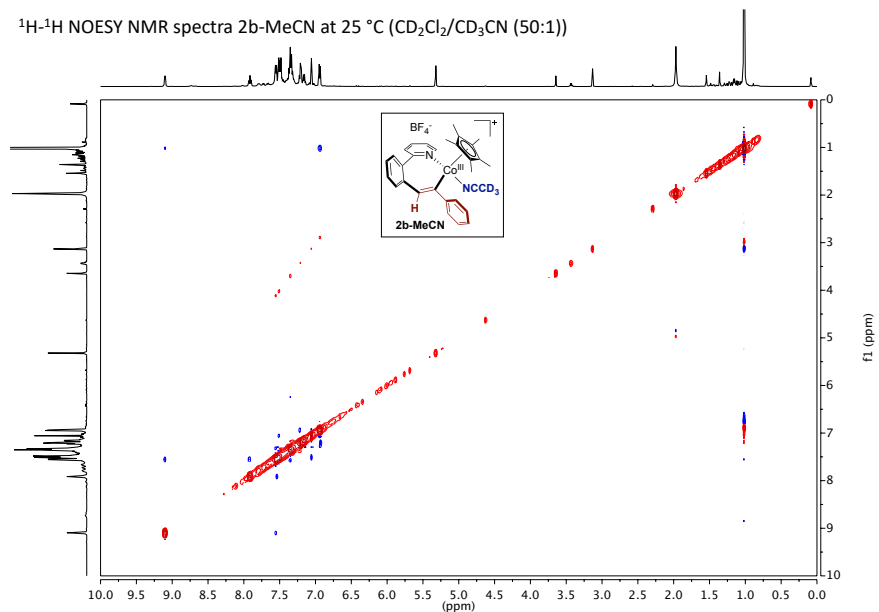
¹H-¹³C HSQC NMR spectra 2b-MeCN at 25 °C (CD$_2$Cl$_2$/CD$_3$CN (50:1))
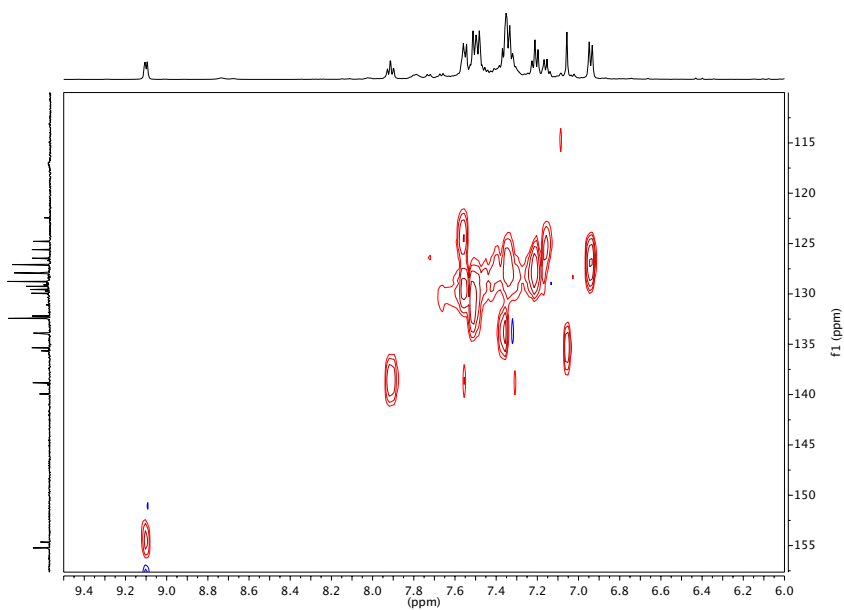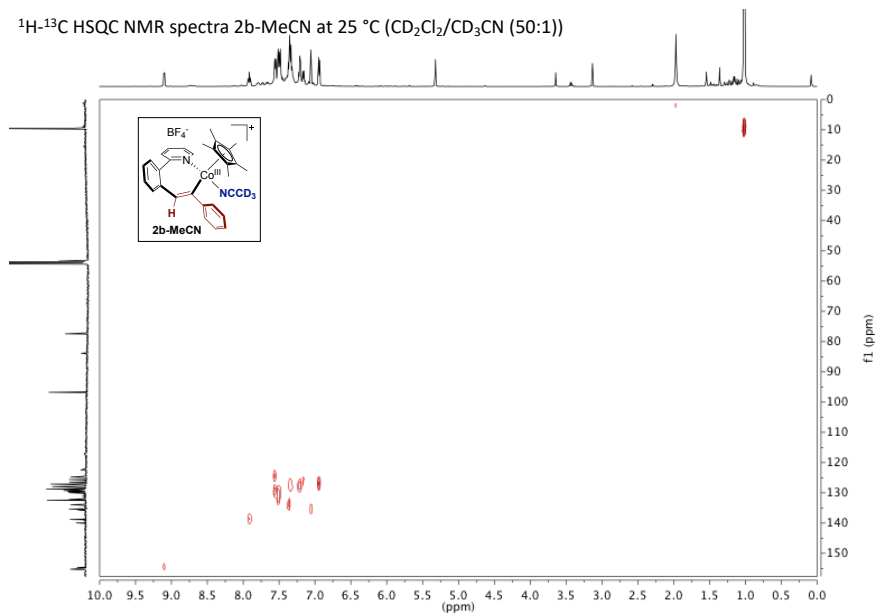
^{1}H-^{13}C HMBC NMR spectra of 2b-MeCN at 25 °C (CD$_2$Cl$_2$/CD$_3$CN (50:1))
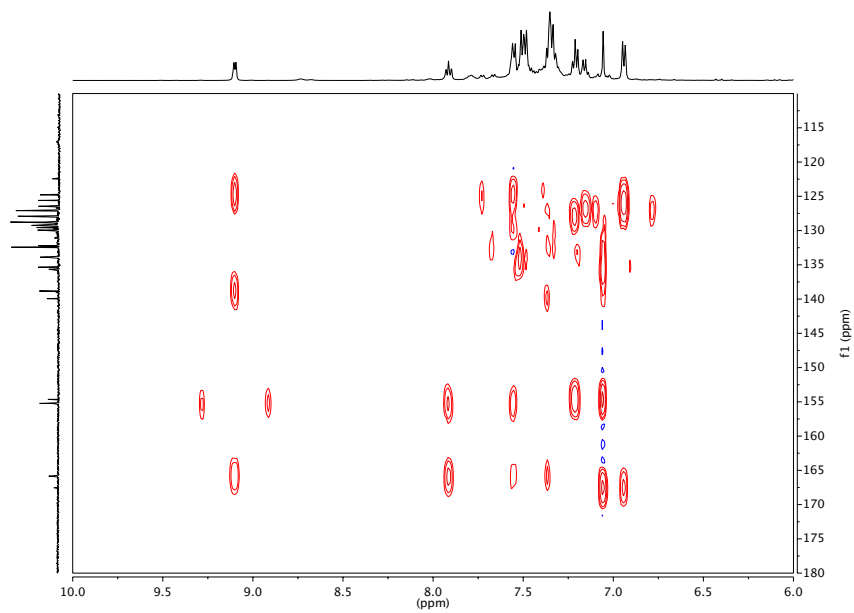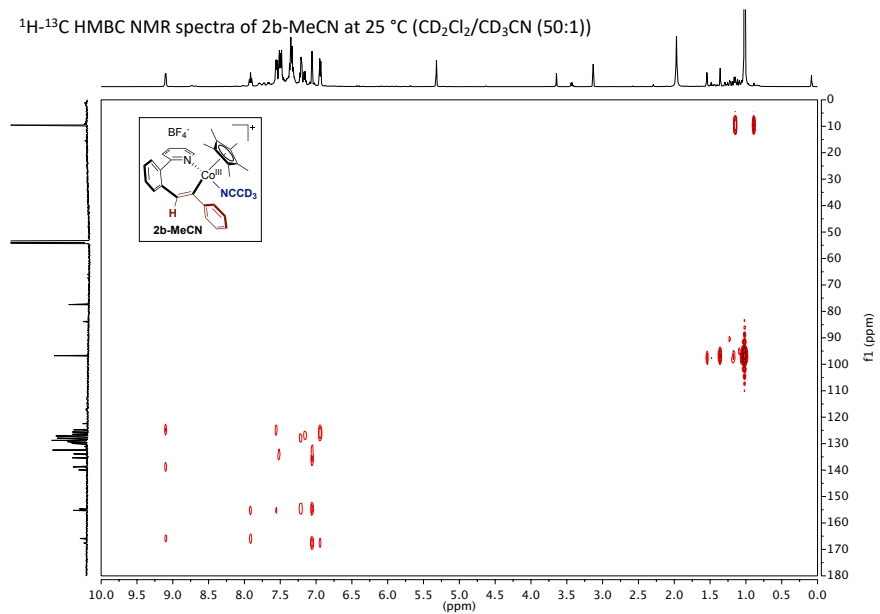
¹⁹F NMR spectra of 2b-MeCN at 25 °C (CD$_2$Cl$_2$/CD$_3$CN (50:1))
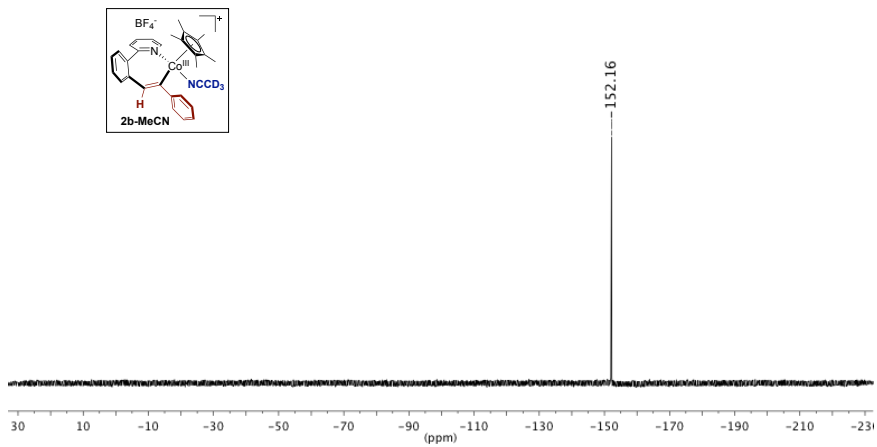
3.8.7.2 NMR Characterization of Complex 2c-MeCN

^{1}H NMR spectra of 2c-MeCN at 25 °C (CD$_2$Cl$_2$/CD$_3$CN (20:1))
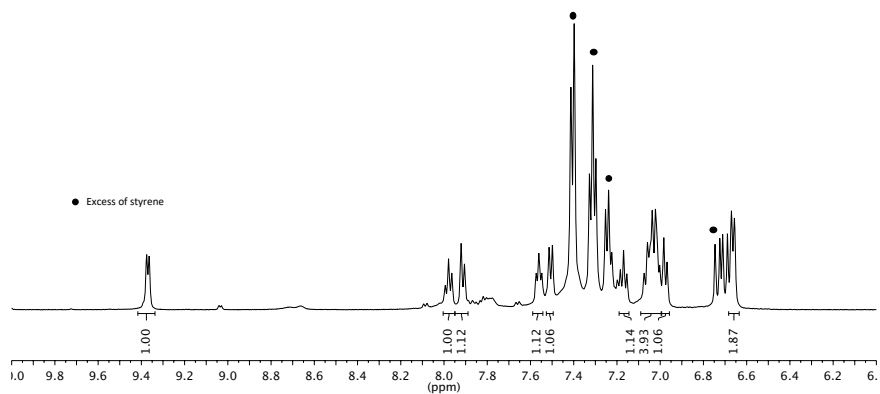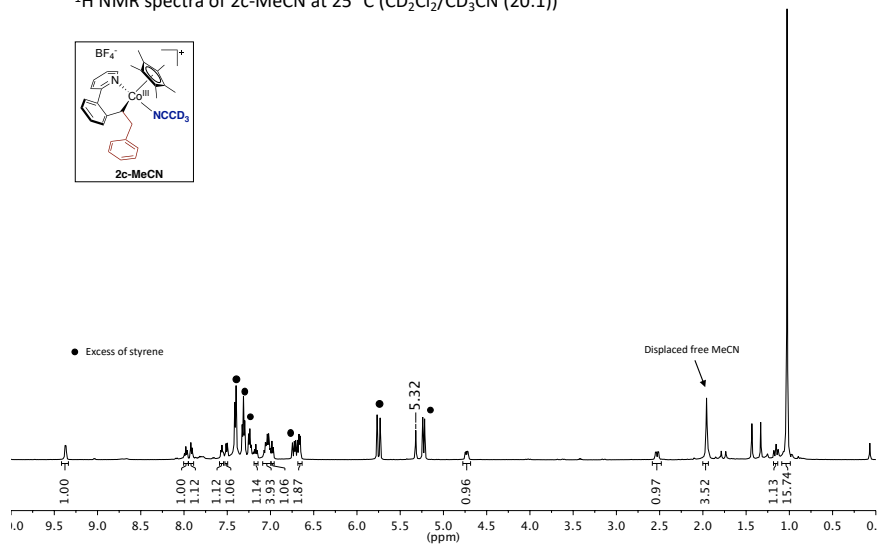
^{13}C NMR spectra of 2c-MeCN at 25 °C (CD$_2$Cl$_2$/CD$_3$CN (20:1))
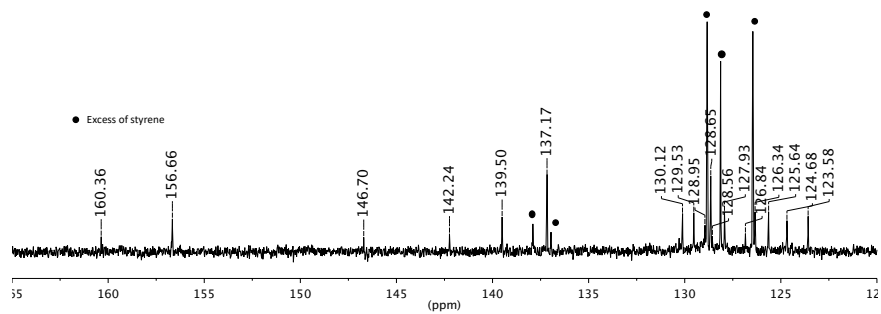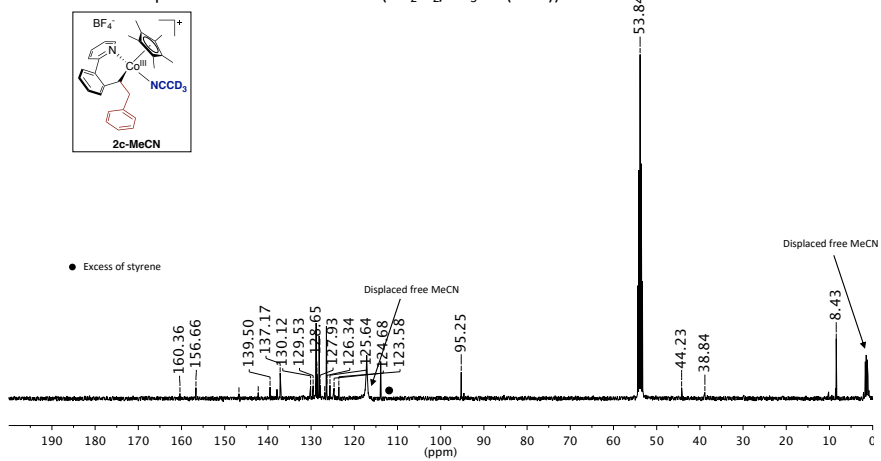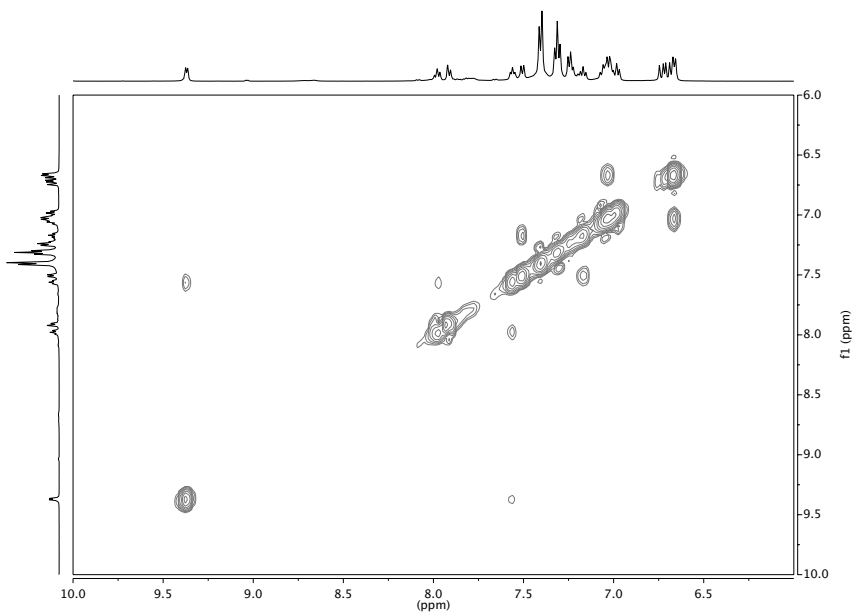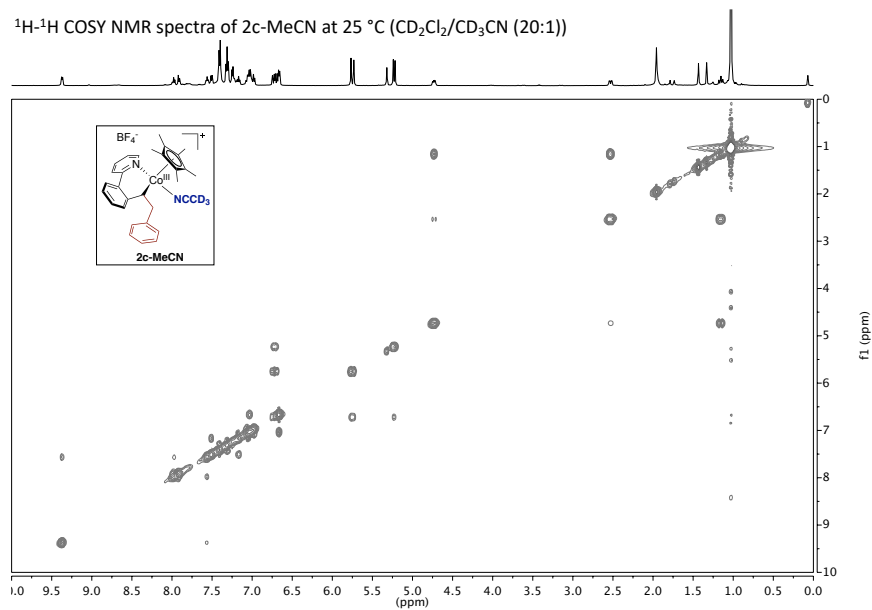
¹H-¹H COSY NMR spectra of 2c-MeCN at 25 °C (CD₂Cl₂/CD₃CN (20:1))

^{1}H-^{1}H TOCSY NMR spectra of 2c-MeCN at 25 °C (CD$_2$Cl$_2$/CD$_3$CN (20:1))
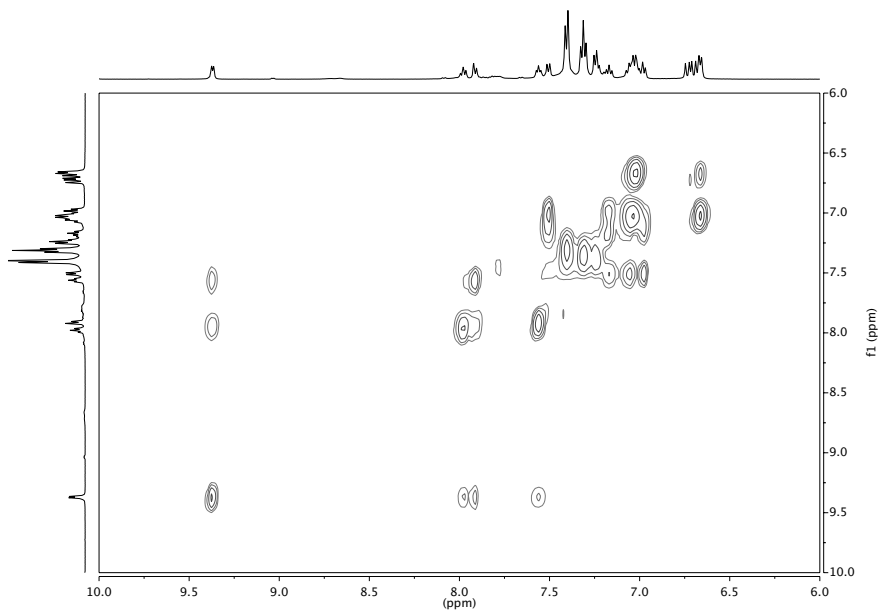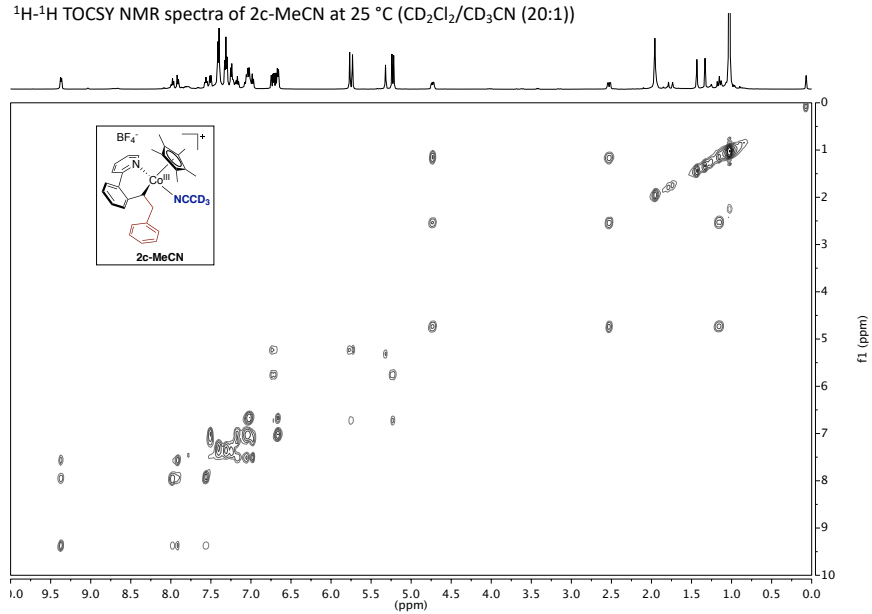
^{1}H-^{1}H NOESY NMR spectra of 2c-MeCN at 25 °C (CD$_2$Cl$_2$/CD$_3$CN (20:1))
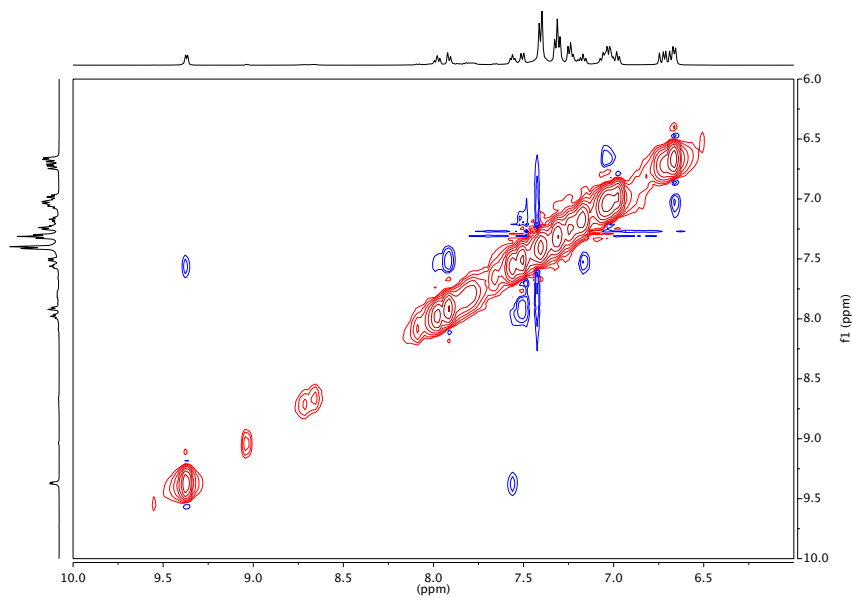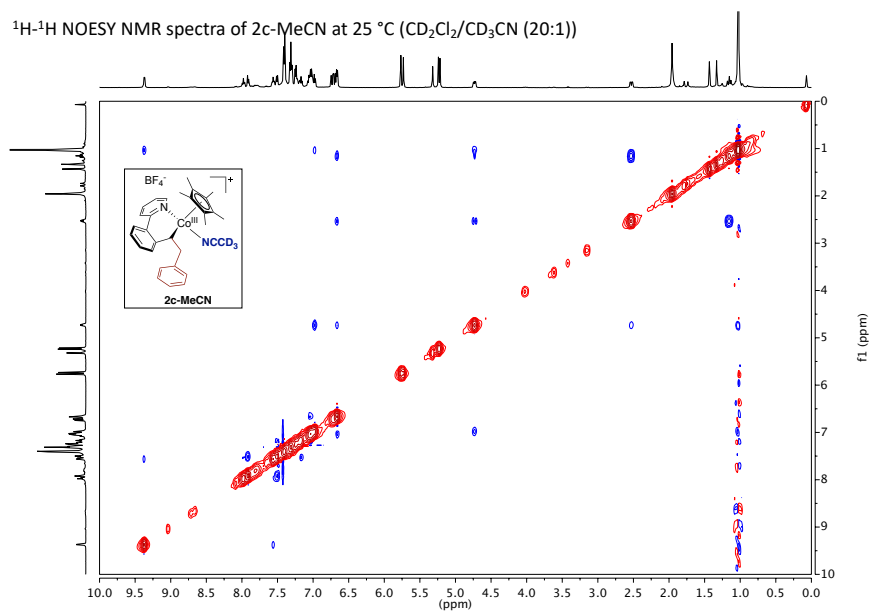
^{1}H-^{13}C HSQC NMR spectra 2c-MeCN at 25 °C (CD$_2$Cl$_2$/CD$_3$CN (20:1))
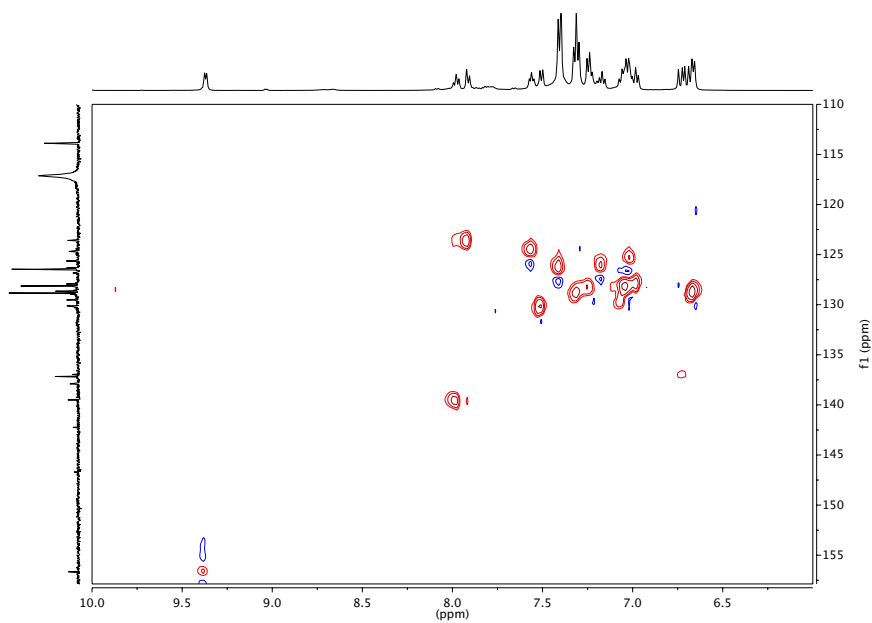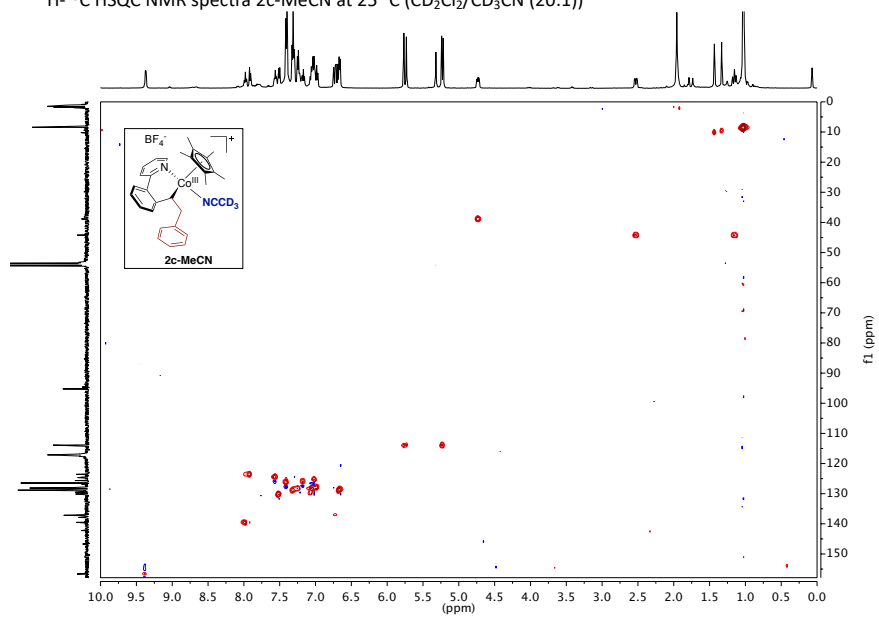
^{1}H-^{13}C HMBC NMR spectra of 2c-MeCN at 25 °C (CD$_2$Cl$_2$/CD$_3$CN (20:1))
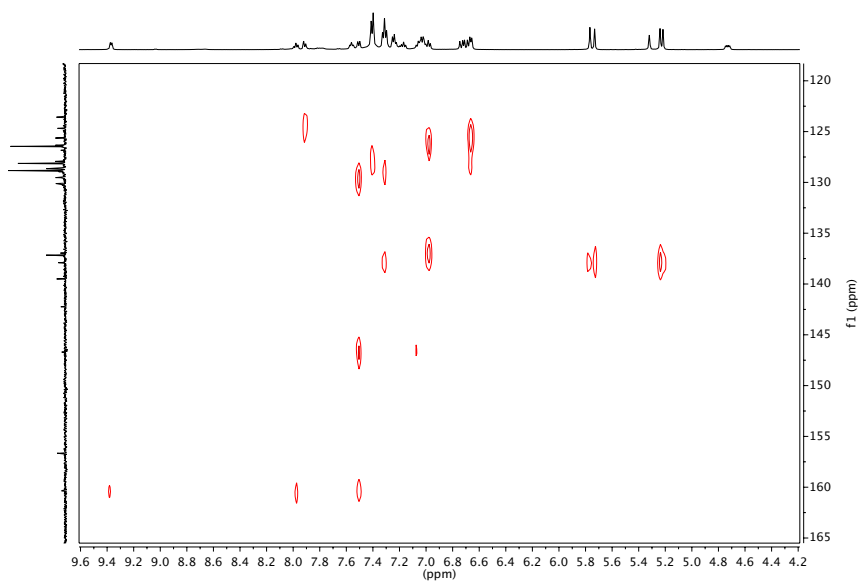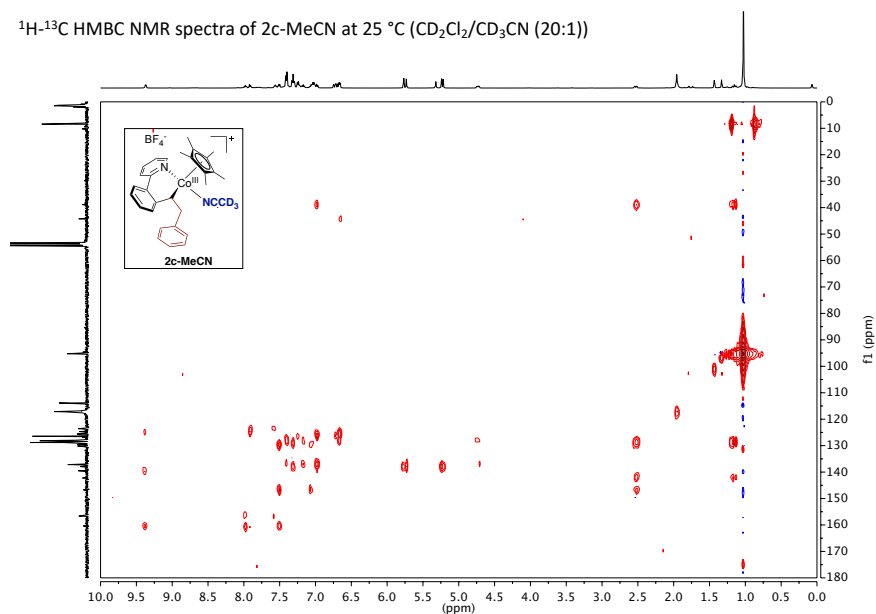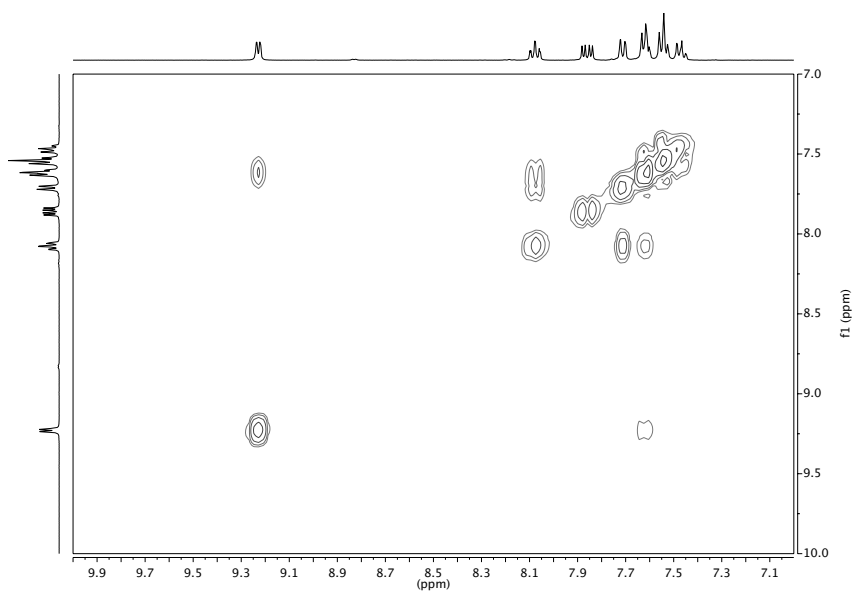
^{19}F NMR spectra of 2c-MeCN at 25 °C (CD$_2$Cl$_2$/CD$_3$CN (20:1))
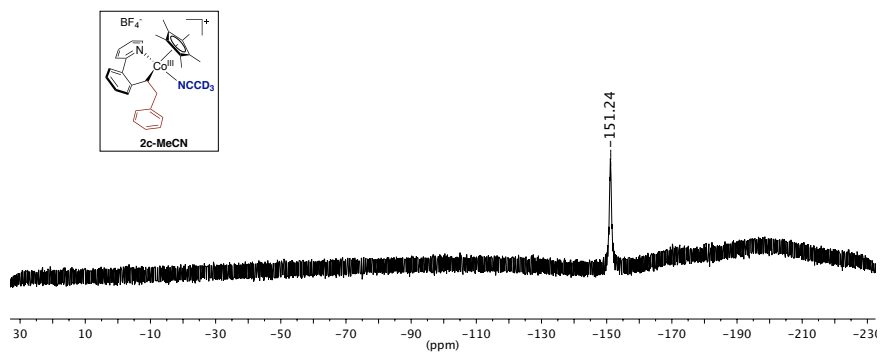
3.8.7.3. NMR Characterization of Complex 2d

^{1}H NMR spectra of 2d at 25 °C (CD$_2$Cl$_2$)
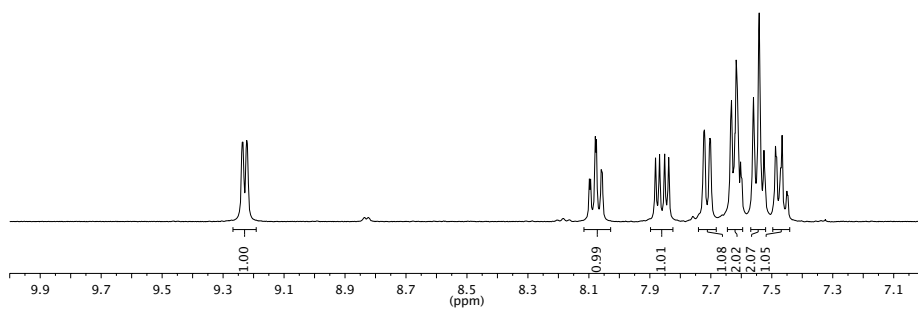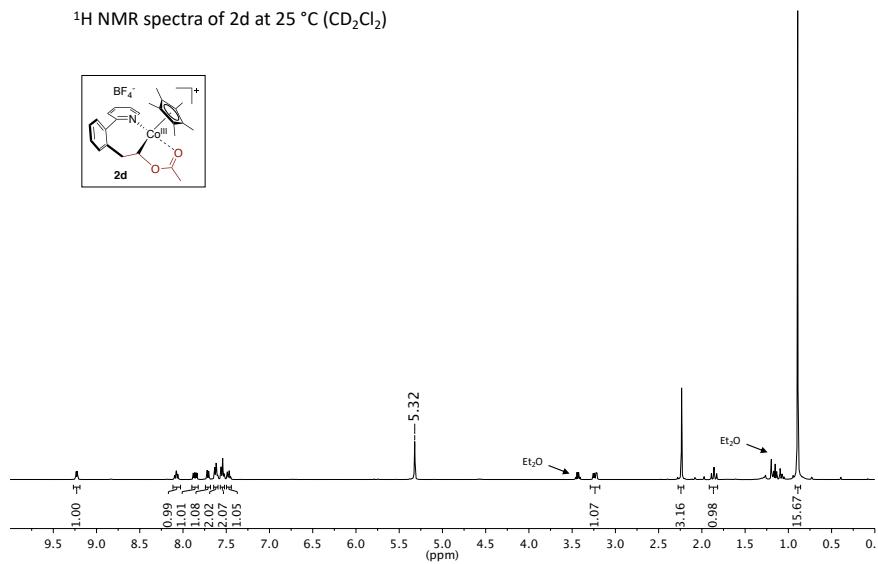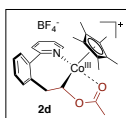
¹³C NMR spectra of 2d at 25 °C (CD$_2$Cl$_2$)
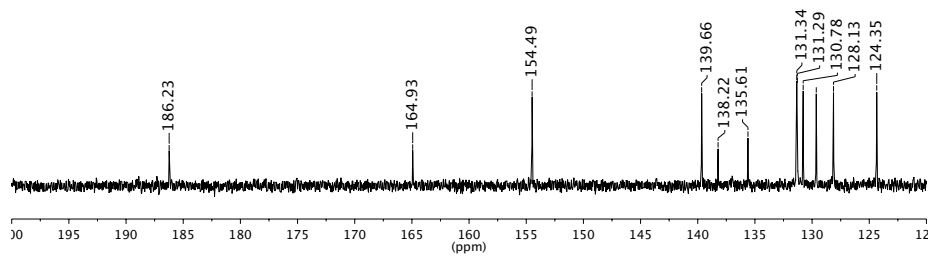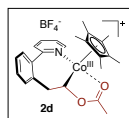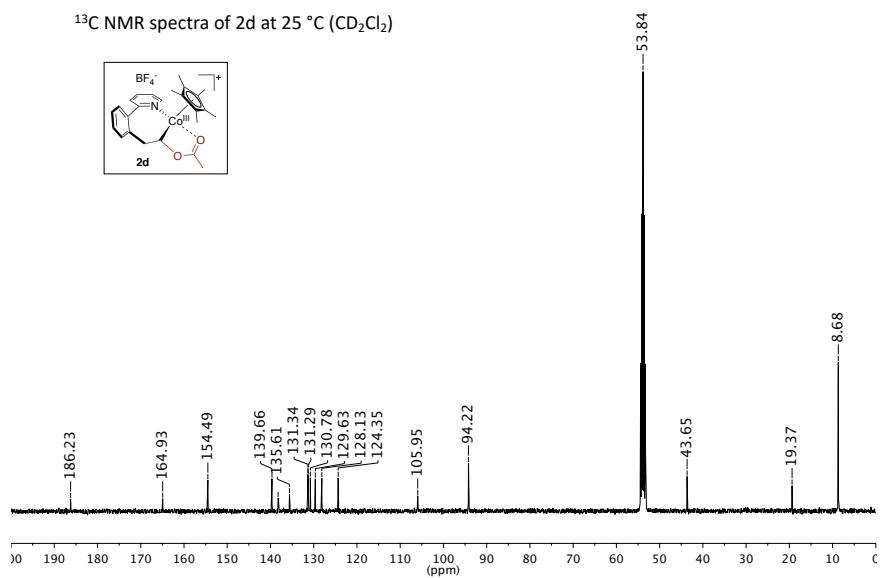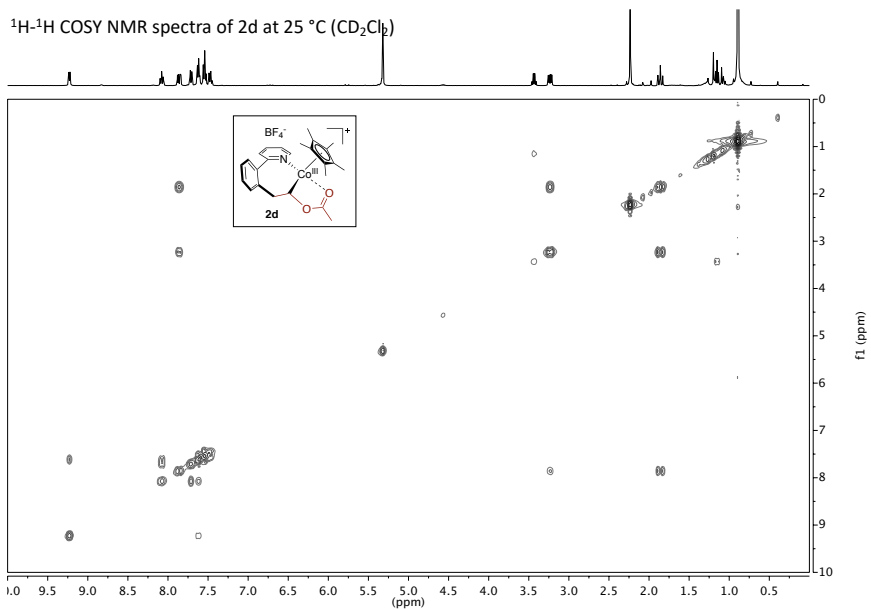
^{1}H-^{1}H COSY NMR spectra of 2d at 25 °C (CD$_2$Cl$_2$)

¹H-¹H TOCSY NMR spectra of 2d at 25 °C (CD₂Cl₂)

^{1}H-^{1}H NOESY NMR spectra of 2d at 25 °C (CD$_2$Cl$_2$)

^{1}H-^{13}C HSQC NMR spectra 2d at 25 °C (CD$_2$Cl$_2$)
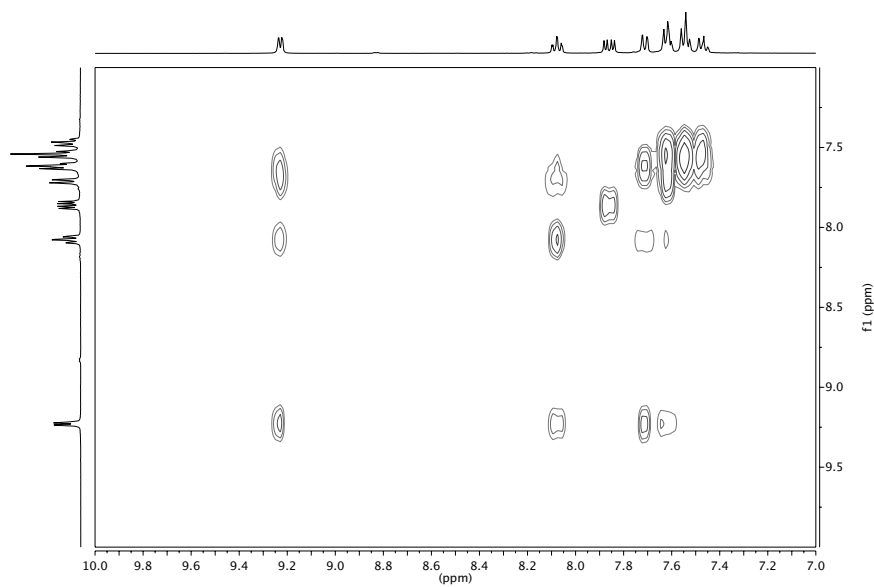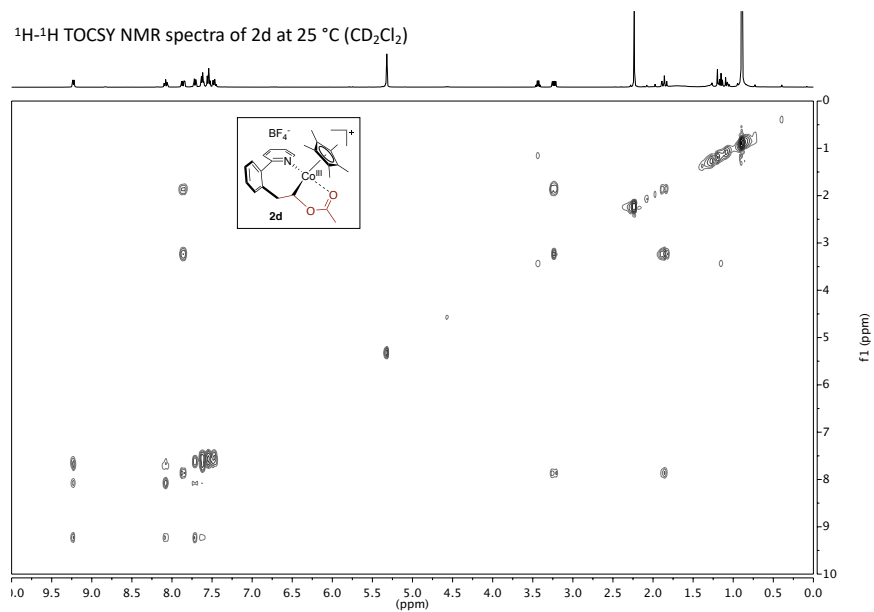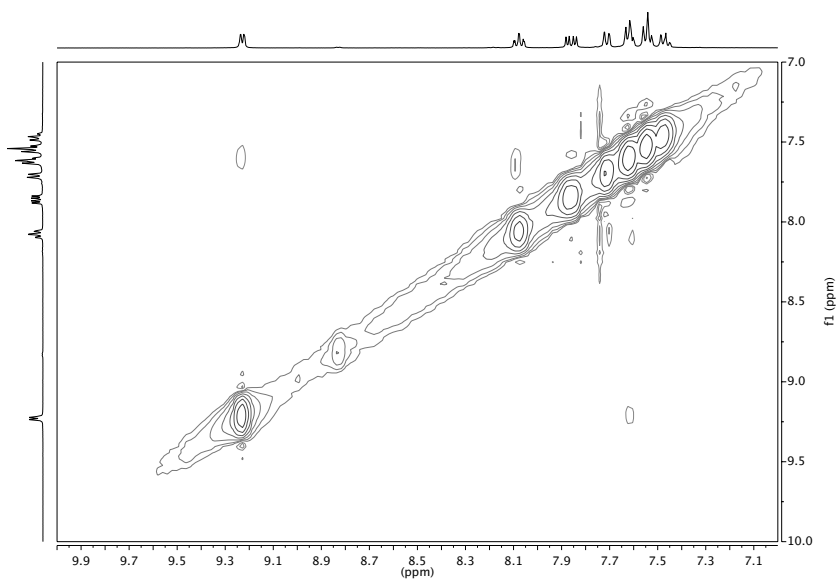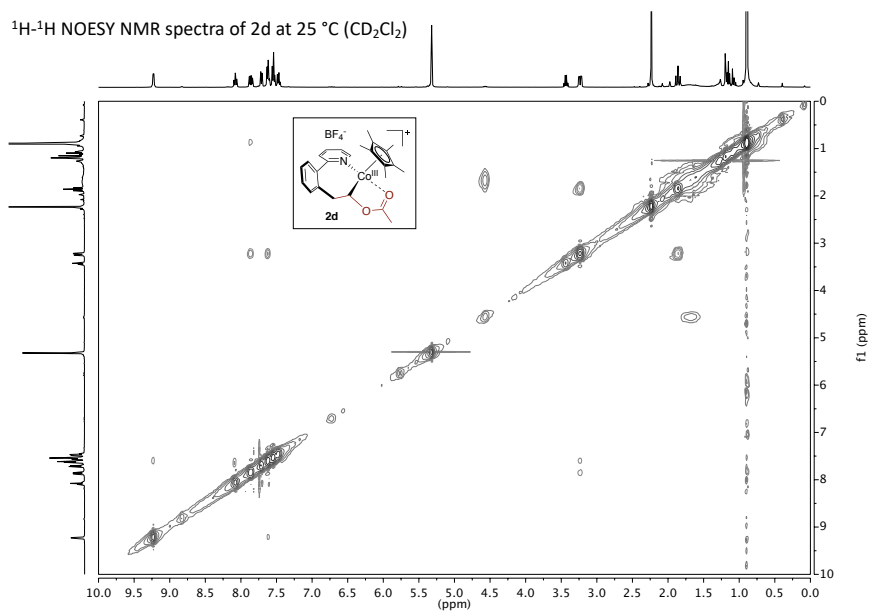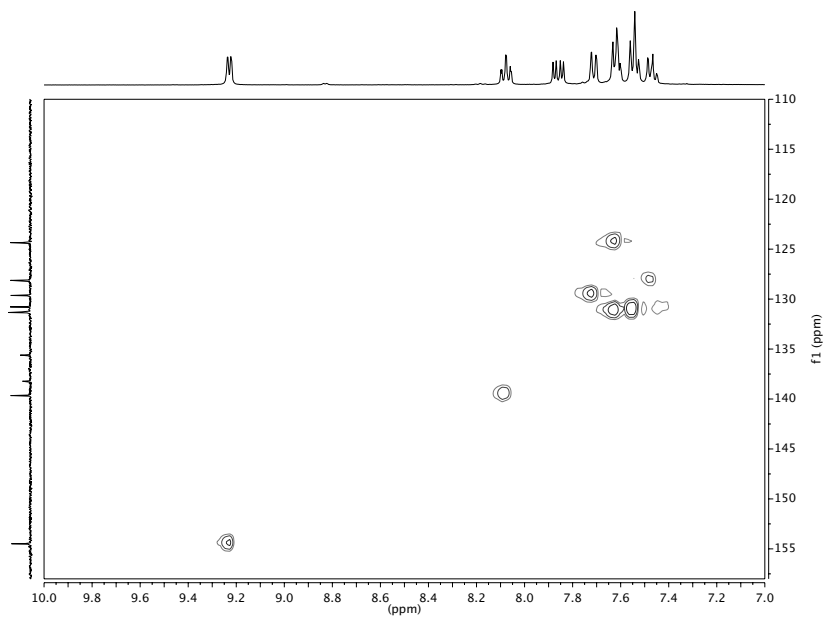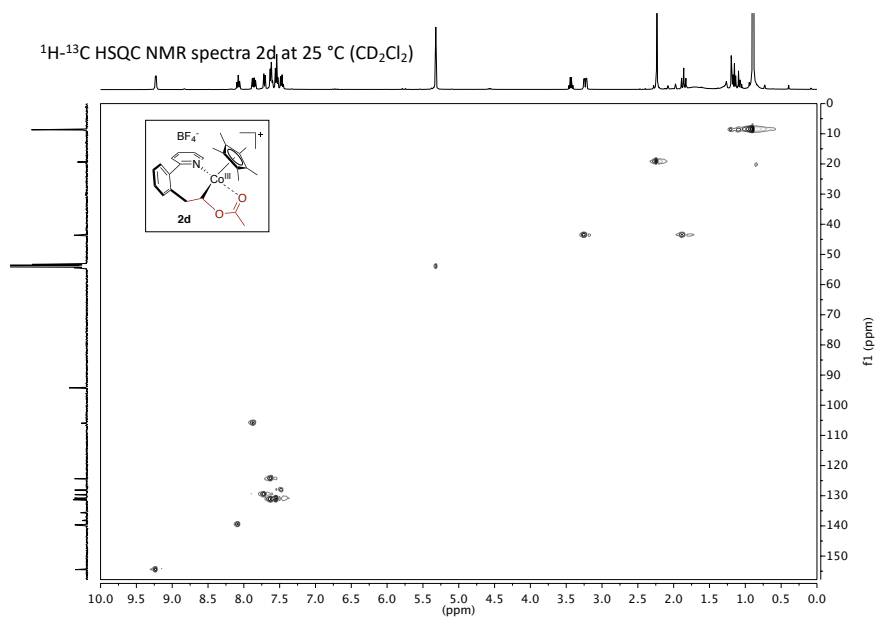
^{1}H-^{13}C HMBC NMR spectra of 2d at 25 °C (CD$_2$Cl$_2$)
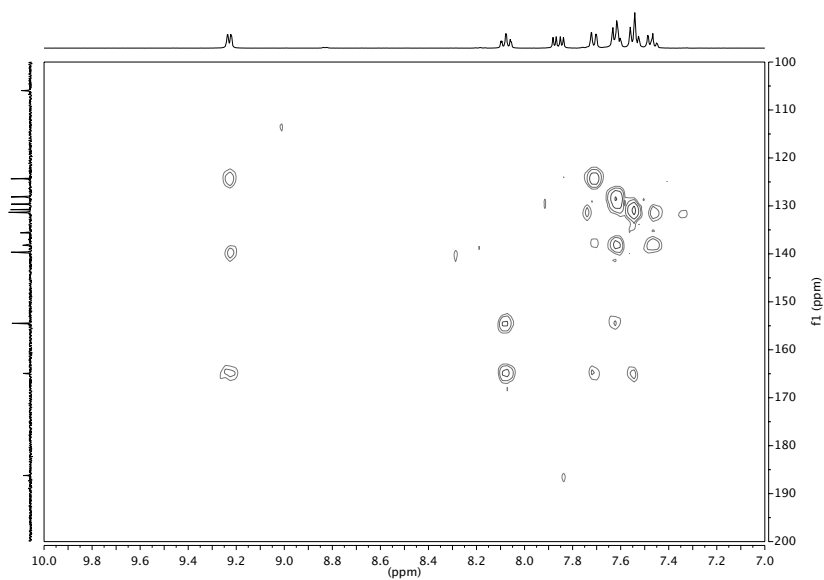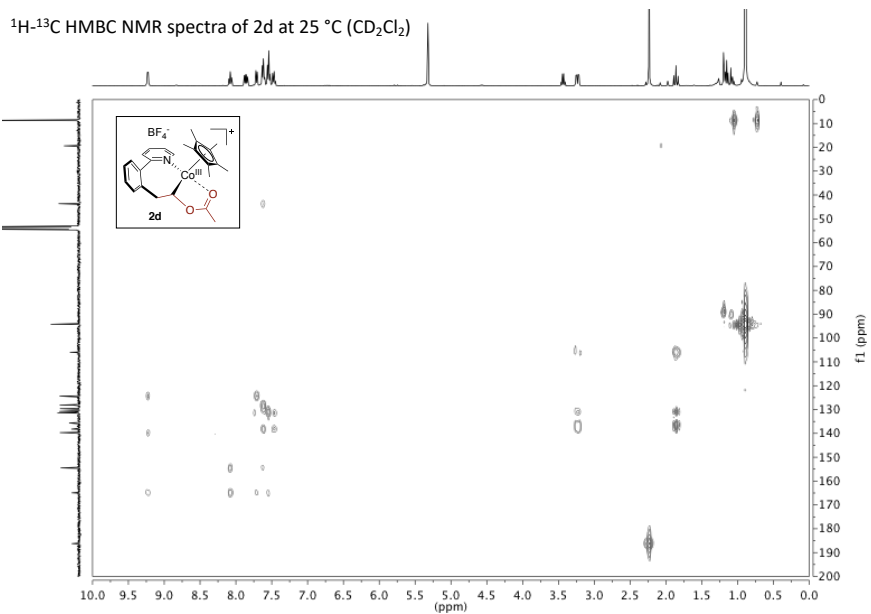
^{19}F NMR spectra of 2d at 25 °C (CD$_2$Cl$_2$)
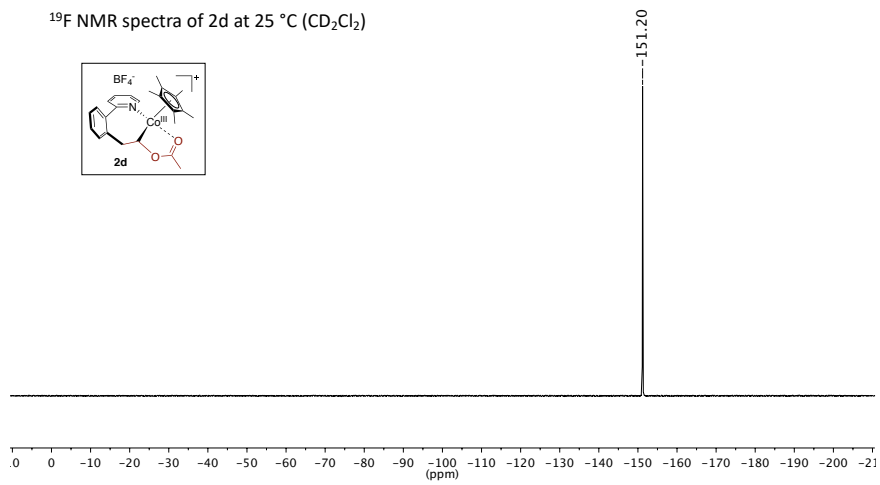
Chapter 4

C–H Activation in Cp*Co^{III} Systems and the Effect of Fluorinated Additives
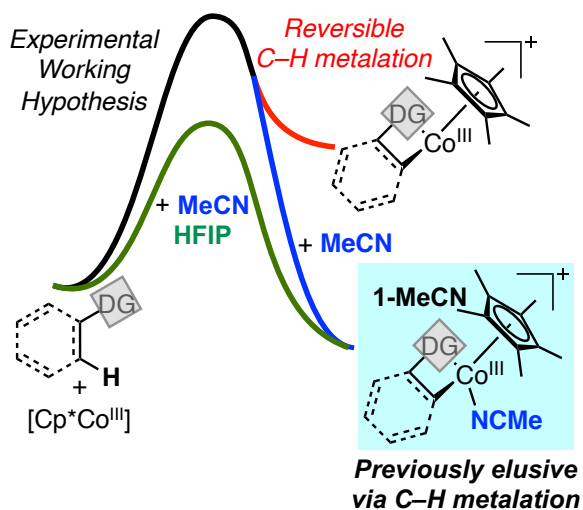
Aims

1) Design of a direct synthetic route, via C−H bond cleavage, for accessing Cp*Co^{III} metallacycles.
2) Investigate the effect of 1,1,1,3,3,3-hexafluoroisopropanol (HFIP) not only in this elementary step but also in catalysis.

Strategies

1) Use of stabilizing ligands for overcoming the reversible nature of the C−H metalation step in Cp*Co^{III} systems.
2) Exploration of the influence of HFIP in orthogonal benchmark catalytic reactions.

4.1 Synthesis of Cp*M^{III}(C^N) Metallacycles *via* C−H Activation

As previously discussed, the C−H bond cleavage mediated by Cp*Co^{III} complexes is proposed to be a reversible process. Several experimental (e.g. H/D scrambling) and computational investigations supported this hypothesis. This, in combination with the lack of use of the proper stabilizing ligands, has hampered the isolation of cobaltacyclic species using C−H activation approaches.

In sharp contrast, the synthesis of half-sandwich metallacyclic iridium and rhodium complexes by C−H activation is well-precedented in the literature.[1] Although the term "metallacycle" refers to complexes that contain (at least) one metal-carbon bond stabilized by (at least) one donor atom (e.g. N, C, O, P), during this doctoral thesis we focused our attention into Cp*M^{III}(C^N) cyclometalated complexes exclusively.[2] In the following section we will disclose some of the most relevant of group 9 half-sandwich metallacycles synthesized through C−H bond cleavage.

4.1.1 *N,C*-Chelated Half-Sandwich Iridium and Rhodium Metallacycles

The first synthesis of a *N,C*-chelated Cp*Ir^{III} metallacycle through a C−H bond activation was described in 1998.[3] In this pioneer work, Beck and co-workers described the cyclometalation of [Cp*IrCl₂]₂ with phenyl oxazolones in the presence of a carboxylate additive (Scheme 4.1).
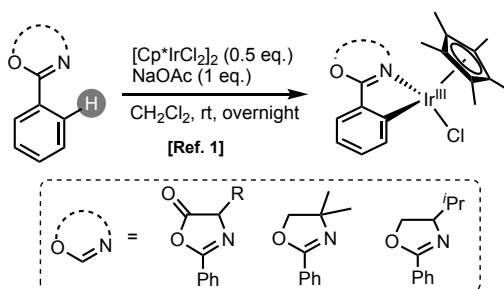
Scheme 4.1. First Cp*Ir^{III} C−H cyclometallation reaction.

[1] Han, Y.-F.; Jin, G.-X. "Cyclometalated [Cp*M(C^X)] (M = Ir, Rh; X = N, C, O, P) complexes" *Chem. Soc. Rev.* **2014**, *43*, 2799−2823.

[2] In parallel to this doctoral thesis, in our research group we have also been interested in the isolation of Cp*Co^{III}(C^O) complexes. See Annex I for further information.

[3] Bauer, W.; Prem, M.; Polborn, K.; Sünkel, K.; Steglich, W.; Beck, W. "Organometallic Complexes of Iridium, Palladium, Chromium and Iron from 2-Phenyl-5(4*H*)-oxazolones − Organometallic Labelled Dipeptides" *Eur. J. Inorg. Chem.* **1998**, 485−493.

Not long after that, Davies expanded the scope of this reaction to *N,N*-dimethylbenzylamine, alkyl and aryl imines.[4] They also achieved, for the first time, the C−H cyclometalation of rhodium species in the presence of aryl imines (Scheme 4.2).

M = Ir, Rh
R = (CH₂)₂OMe, (CH₂)₃OMe, Ph
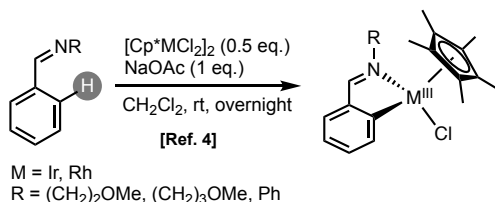
Scheme 4.2. Imine C−H cyclometalation with Cp*Ir^{III} and Cp*Rh^{III} complexes.

Having a reliable synthetic route in hand for accessing this type of complexes, the same group, in collaboration with Macgregor, performed competition experiments to compare the reactivity of different substrates when using Cp*Ir^{III} or Cp*Rh^{III} systems (Scheme 4.3).[5]
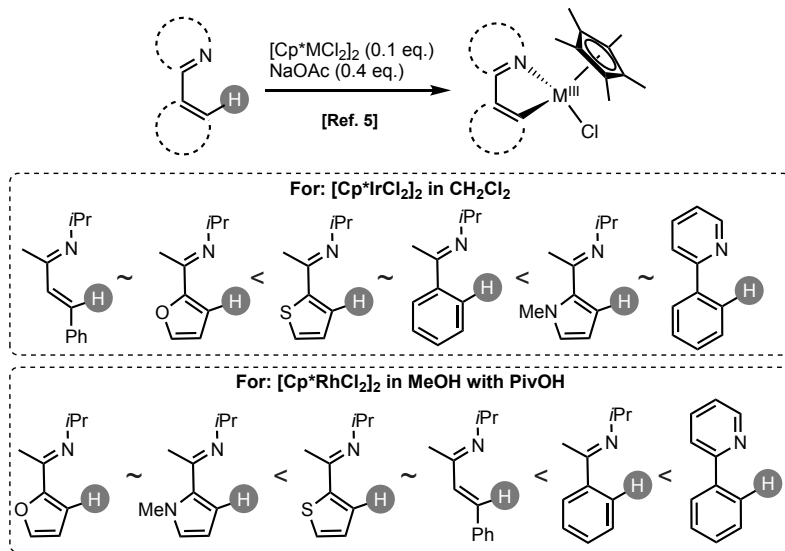
Scheme 4.3. Relative reactivity of N-based ligands in the Cp*M^{III} C−H cyclometalation.

[4] Davies, D. L.; Al-Duaij, O.; Fawcett, J.; Giardiello, M.; Hilton, S. T.; Russel, D. R. "Room-temperature cyclometalation of amines, imines and oxazolines with [MCl₂Cp*]₂ (M = Rh, Ir) and [RuCl₂(*p*-cymene)]₂" *Dalton Trans*. **2003**, 4132−4138.

[5] Carr, K. J. T.; Davies, D. L.; Macgregor, S. A.; Singh, K.; Villa-Marcos, B. "Metal control of selectivity in acetate-assisted C−H bond activation: an experimental and computational study of heterocyclic, vinylic and phenylic C(sp²)−H bonds at Ir and Rh" *Chem. Sci.* **2014**, *5*, 2340−2346.

Interestingly, Ellman and Bergman discovered that the C−H metalation of 2-phenylpyridine, using [Cp*RhCl₂]₂ as rhodium source, did not required the addition of external carboxylates when the reaction was performed in presence of a silver salt and excess of the substrate (Scheme 4.4).[6] By ^{1}H NMR spectroscopy, along with the corresponding cationic rhodacycle, the authors observed the formation of a pyridinium salt. This new cationic species turned out to be a Cp*Rh[III] metallacycle where one 2-phenylpyridine was acting as a *N,C* bidentate ligand and a second one was saturating the free coordination vacant of the metal as a monodentate nitrogenated ligand. After some mechanistic investigations, they discovered that this compound is the resting state of in a Cp*Rh[III]-catalyzed protocol of arylation of imines. In this work, the dissociation of the second molecule of substrate from the metal inner sphere was proposed to be the rate-determining step in the overall catalytic cycle.
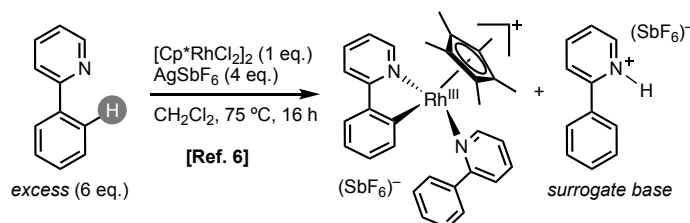
Scheme 4.4. Cp*Rh[III] C−H cyclometalation without carboxylates.

Having in hand reliable reactions conditions to form, isolate and characterize metallacycles through C−H activation stoichiometrically is the basis for the understanding of the C−H cyclometalation step. The examples shown here are just a flavor of all the mechanistic investigations that have been performed in the last twenty years.[7]

[6] Tauchert, M. E.; Incarvito, C. D.; Rheingold, A. L.; Bergman, R. G.; Ellman, J. A. "Mechanism of the Rhodium(III)-Catalyzed Arylation of Imines via C−H Bond Functionalization: Inhibition by Substrate" *J. Am. Chem. Soc.* **2012**, *134*, 1482−1485.

[7] (a) Li, L.; Brennessel, W. W.; Jones, W. D. "C−H Activation of Phenyl Imines and 2-Phenylpyridines with [Cp*MCl₂]₂ (M = Ir, Rh): Regioselectivity, Kinetics and Mechanism" *Organometallics* **2009**, *28*, 3492−3500. (b) Walsh, A. P.; Jones, W. D. "Mechanistic Insights of a Concerted Metalation-Deprotonation Reaction with [Cp*RhCl₂]₂" *Organometallics* **2015**, *34*, 3400−3407. (c) VanderWeide, A. I.; Brennessel, W. W.; Jones, W. D. "Reversible Concerted Metalation-Deprotonation C−H Bond Activation by [Cp*RhCl₂]₂" *J. Org. Chem.* **2019**, *84*, 12960−12965.

4.1.2 Isolation of Cp*Co^{III} Metallacycles *via* C−H Activation

As shown above, over the past two decades, a wide variety of half-sandwich iridium and rhodium metallacycles, synthesized through a C−H bond-cleavage, have been reported in the literature. In stark contrast, at the beginning of this doctoral thesis, there was not a single example of a Cp*Co^{III}-mediated C−H cyclometalation reaction. The proposed reversibility of the C−H activation precluded at that time the isolation and characterization of the corresponding highly unstable 16-electron Cp*Co^{III} cyclometalated species. As described in **Article 1**, we were able to trap this elusive cobaltacycle species by addition of acetonitrile as stabilizing ligand. Nevertheless, the Co−C bond was formed by an alternative oxidative addition reaction instead by a C−H bond cleavage.

Due to the popularity of the field, during the development of this dissertation, several research groups kept studying these reactions in parallel. In 2017, Zhu and co-workers described the first Cp*Co^{III} C−H cyclometalation reaction (Scheme 4.5).[8] They took advantage of the physical properties of *N*-chlorobenzamides and a carbonyl as stabilizing ligand to isolate in low yield the corresponding neutral cobaltacycle.
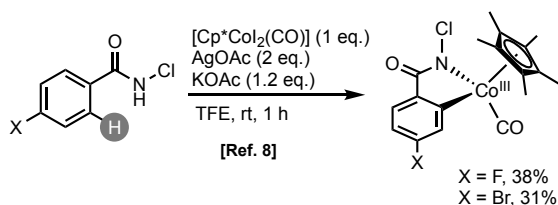
Scheme 4.5. First cobaltacycle synthesized by C−H activation.

In this literature precedent, the authors hypothesized that the carbonyl group present in the precatalyst is responsible of stabilizing this otherwise elusive species. However, they did not disclosed the behavior of this ligand in the catalytic cycle.

Due to the low yield and reproducibility of this methodology for the isolation of cobalt metallacycles through C−H activation, our group decided to search for alternative strategies. In this process, we discovered that perfluorinated alcohols could play a decisive role in the success of a reliable and efficient Cp*Co^{III} C−H cyclometalation reaction.

---

[8] Yu, X.; Chen, K.; Guo, S.; Shi, P.; Song, C.; Zhu, J. "Direct Access to Cobaltacycles via C−H Activation: *N*-Chloroamide-Enabled-Room-Temperature Synthesis of Heterocycles" *Org. Let.* **2017**, *19*, 5348−5351.

4.2 The Beneficial Effect of Perfluorinated Alcohols in Cp*M^{III}-Mediated C−H Activation Reactions

Over the past years, perfluorinated alcohols have exhibited an extraordinary capability for facilitating transition metal-catalyzed directed C−H functionalization reactions. Among them, 1,1,1,3,3,3-hexafluoroisopropanol (HFIP) is probably the most remarkable solvent in this category, next to trifluoroethanol (TFE). Presumably their beneficial effects can be attributed to a combination of their unique features, such as high polarity (for an organic solvent), combining both a hydrophobic as well as a hydrophilic side, mildly acidic OH group (pK$_A$ analogous to that of a phenol) and excellent single H-bond donor properties (Figure 4.1).[9] In this section we will discuss some selected examples, in the context of site-selective Cp*M^{III}-catalyzed C−H functionalization reactions (M = group 9 transition metals).


Physical properties

- *No UV light absorption.*
- *Thermally stable.*
- *Miscible in water and common polar solvents.*
- *Low boiling point = 59 °C*
- *pK$_A$ = 9.3 (in H$_2$O)*
- *Dielectric constant ε = 15.7*

H-bond donor ability

- *Single-crystal X-ray structure of HFIP shows infinite helices of H-bonded aggregates.*
- *Stable HFIP:THF complex with a bp = 100 °C reported.*
- *Proton shuttle in some C−H activation reactions.*

Redox stability

- *High redox stability, ideal solvent for electrochemical investigations.*
- *Stable under highly oxidizing environments*
- *Greater electrochemical domain than H$_2$O.*

HFIP

Cation stabilization

- *The combination of a high dielectric constant and low nucleophilicity makes HFIP an ideal solvent for the stabilization of cations.*

Figure 4.1. Key properties of 1,1,1,3,3,3-hexafluoroisopropanol (HFIP).

4.2.1 C(*sp^2*)−C Bond Forming Reactions

One of the pioneering groups in harnessing HFIP properties as a solvent for the Cp*M^{III} C−H functionalization reaction was Rovis group. In 2014, they used this fluorinated alcohol for the decarboxylative coupling of acrylic acids with

[9] (a) Wencel-Delord, J.; Colobert, F. "A remarkable solvent effect of fluorinated alcohols on transition metal catalysed C−H functionalizations" *Org. Chem. Front*. **2016**, *3*, 394−400. (b) Colomer, I.; Chamberlain, A. E. R.; Haughey, M. B.; Donohoe, T. J. "Hexafluoroisopropanol as a highly versatile solvent" *Nat. Rev. Chem*. **2017**, *1*, 0088, 1−12. (c) Sinha, S. K.; Bhattacharya, T.; Maiti, D. "Role of hexafluoroisopropanol in C−H activation" *React. Chem. Eng*. **2019**, *4*, 244−253. (d) Yu, C.; Sanjosé-Orduna, J.; Patureau, F. W.; Pérez-Temprano, M. H. "Emerging unconventional organic solvents for C−H bond and related functionalizations reactions" *Chem. Soc. Rev*. **2020**, DOI: 10.1039/c8cs0083c.

unsaturated oxime esters.[10] After a slightly modification of the Cp ligand, they were able to describe an excellent methodology for the obtention of substituted pyridines (Scheme 4.6).
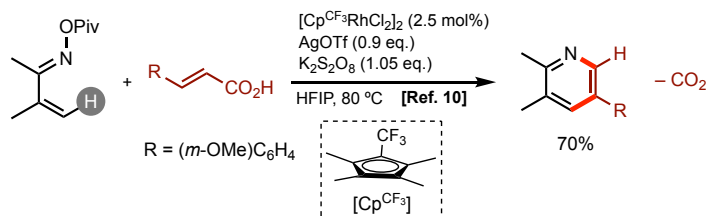
Scheme 4.6. Rhodium-catalyzed decarboxylative synthesis of pyridines.

Loh and co-workers have reported selective Cp*Co^{III}-catalyzed C−H aminomethylation/hydroxymethylation of heteroarenes using 1,2-oxadetidine as coupling partner.[11] The formation of the aminomethylated product was favoured when using PhCF$_3$ as solvent, while 2,2,2-Trifluoroethanol (TFE) was the best choice for developing the hydromethylation protocol (Scheme 4.7).
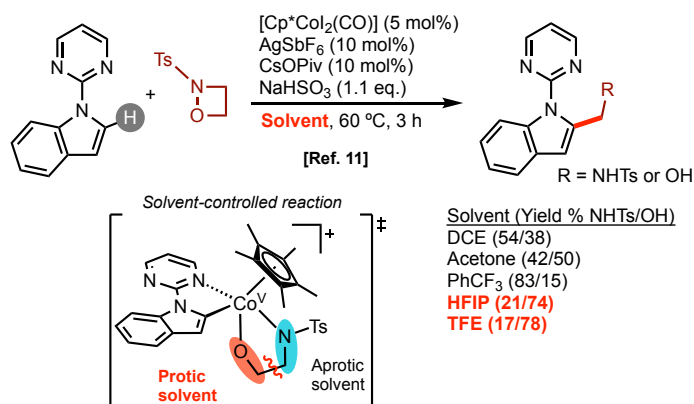

Scheme 4.7. Cp*Co^{III} C−H chemodivergent transformation *via* a proposed Co^V intermediate.

Very recently, Miura and co-workers have demonstrated the chemodivergent C−H functionalization of 2-pyridones with acrylates depending on the solvent choice (Scheme 4.8). Using DMF, the authors observed the expected formation of the C6-

[10] Neely, J. M.; Rovis, T. "Rh(III)-Catalyzed Decarboxylative Coupling of Acrylic Acids with Unsaturated Oxime Esters: Carboxylic Acids Serve as Traceless Activators" *J. Am. Chem. Soc.* **2014**, *136*, 2735−2738.
[11] Li, S.; Shi, P.; Liu, R.-H.; Hu, X.-H.; Loh, T.-P. "Cobalt-Catalyzed N−O and C−C Bond Cleavage in 1,2-Oxazetidines: Solvent-Controlled C−H Aminomethylation and Hydroxymethylation of Heteroarenes" *Org. Lett.* **2019**, *21*, 1602−1606.

alkenylated product. In sharp contrast, HFIP promoted the alkylation processes due to its capability to act as a proton source.[12]
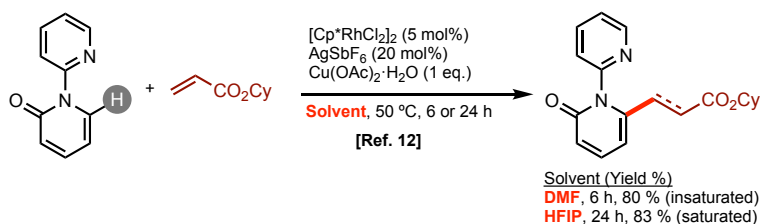
Scheme 4.8. Rhodium-catalyzed alkenylation of 2-pyridones.

Interestingly, Rovis *et al.* have reported a regiodivergent Cp*Ir[III]-catalyzed alkene diamination protocol.[13] The authors observed the formation of five- or six-membered ring lactams by the employment of HFIP and TFE, respectively. They hypothesized that the higher acidity of HFIP compared to TFE is the responsible of the regioselectivity (Scheme 4.9).
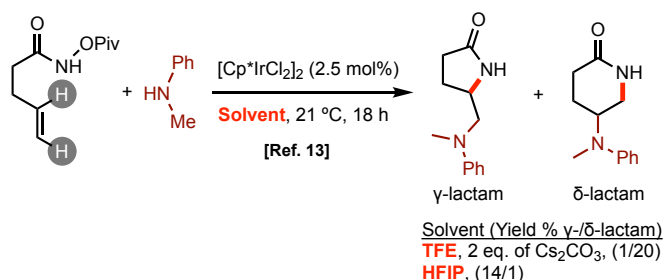
Scheme 4.9. Cp*Ir[III]-catalyzed regiodivergent synthesis of γ- or δ-lactams.

4.2.1.1 C(sp^2)−C Bond-Forming Enantioselective Transformations
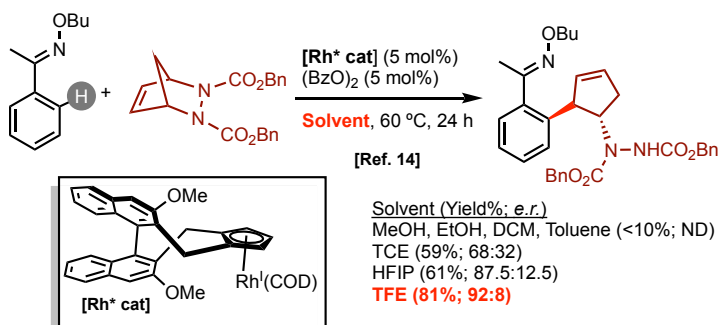
These protic perfluorinated solvents have also been exploited to develop novel stereoselective transformations. In this regard, Cramer *et al.* have disclosed the highly efficient enantioselective synthesis of cyclopentenylamines, using a chiral Cp[x]Rh(cod) precatalyst and TFE as solvent (Scheme 4.10).[14] The authors proposed that the strong ionizing ability of the perfluorinated alcohol favors the generation of the active rhodium(III) species involved in the C−H activation step. This is supported

---

[12] Hazra, S.; Hirano, K.; Miura, M. "Solvent-Controlled Rhodium-Catalyzed C6-Selective C−H Alkenylation and Alkylation of 2-Pyridones with Acrylates" *Asian J. Org. Chem.* **2019**, *8*, 1097−1101.
[13] Conway Jr, J. H.; Rovis, T. "Regiodivergent Iridium(III)-Catalyzed Diamination of Alkenyl Amides with Secondary Amines: Complementary Access to γ- or δ-Lactams" *J. Am. Chem. Soc.* **2018**, *140*, 135−138.
[14] Wang, S.-G.; Cramer, N. "An Enantioselective Cp[X]Rh(III)−Catalyzed C−H Functionalization/Ring-Opening Route to Chiral Cyclopentenylamines" *Angew. Chem. Int. Ed.* **2019**, *58*, 2514−2518.

by the low conversions observed in less polar solvents such as dichloromethane or toluene.

Solvent (Yield%; *e.r.*)
MeOH, EtOH, DCM, Toluene (<10%; ND)
TCE (59%; 68:32)
HFIP (61%; 87.5:12.5)
TFE (81%; 92:8)

Scheme 4.10. Cp^XRh^III-catalyzed enantioselective synthesis of cyclopentenylamines.

More recently, the same group has exploited their chiral pentamethylcyclopentadienyl ligands to develop another enantioselective transformation, this time harnessing chiral Cp^XCo^III complexes (Scheme 4.11).[15] After an intensive scope of chiral cyclopentadienyl ligands, they were able to design an enantio- and regioselective synthesis of dihydroisoquinolones from *N*-chlorobenzamides and alkenes, out-performing an analogous rhodium precatalyst in this, and giving rise to opposite regioselectivity.


96% yield (99.5:0.5 *e.r.*)
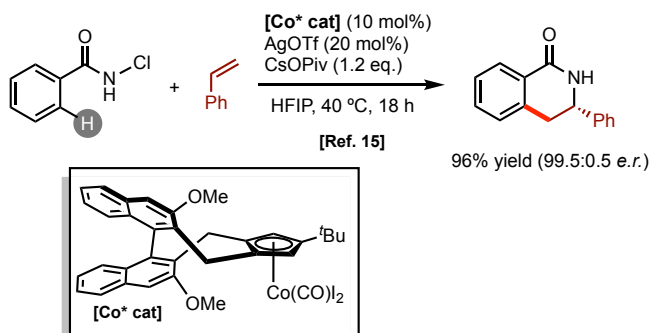
Scheme 4.11. Cp^XCo^III-catalyzed enantioselective synthesis of dihydroisoquinolones.

[15] Ozols, K.; Jang, Y.-S.; Cramer, N. "Chiral Cyclopentadienyl Cobalt(III) Complexes Enable Highly Enantioselective 3d-Metal-Catalyzed C−H Functionalizations" *J. Am. Chem. Soc.* **2019**, *141*, 5675–5680.

4.2.2 C(*sp²*)−Heteroatom Bond-Forming Reactions

In 2017, Martín-Matute and co-workers used HFIP for the development of a Cp*Ir^{III}-catalyzed *ortho*-iodination of benzoic acids.[16] After screening a range of solvents, they found that only TFE and HFIP rendered the desired coupling product in excellent and quantitative yields, respectively. Other solvents like acetone, DCE, THF or ^{i}PrOH performed poorly under these reaction conditions. After some DFT calculations, they proposed an electron withdrawing H-bond interaction of HFIP with an Ir^{V} intermediate, destabilizing it, and therefore accelerating the reaction (Scheme 4.12).

Scheme 4.12. Iridium-catalyzed *ortho*-iodination of benzoic acids.
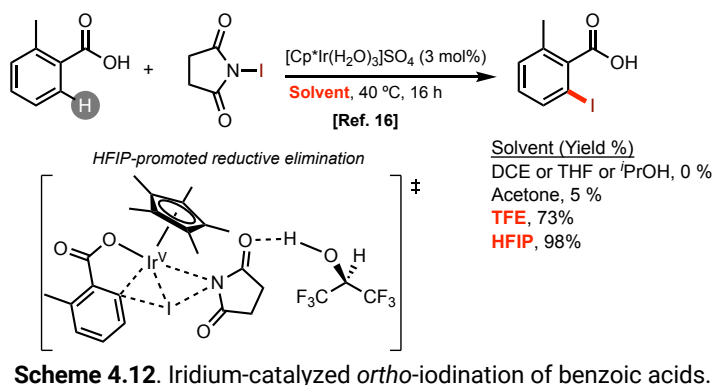
These examples are just a flavor of the potential that perfluorinated alcohols have in promoting new and unprecedented C−H functionalization reactions. Therefore, prompted by this extraordinary literature precedents, we aimed to study more in detail the effect of 1,1,1,3,3,3-hexafluoroisopropanol in the reversible C−H cyclometalation reaction with Cp*Co^{III}-complexes. In **Article 3** are disclosed the results obtained in this direction.

Further information about the effect of these perfluorinated alcohols in the Cp*Co^{III} C−H cyclometalation reaction can be found in **Annex II**.

---

[16] Erbing, E.; Sanz-Marco, A.; Vázquez-Romero, A.; Malmberg, J.; Johansson, M. J.; Gómez-Bengoa, E.; Martín-Matute, B. "Base- and Additive-Free Ir-Catalyzed *ortho*-Iodination of Benzoic Acids: Scope and Mechanistic Investigations" *ACS Catal.* **2018**, *8*, 920−925.
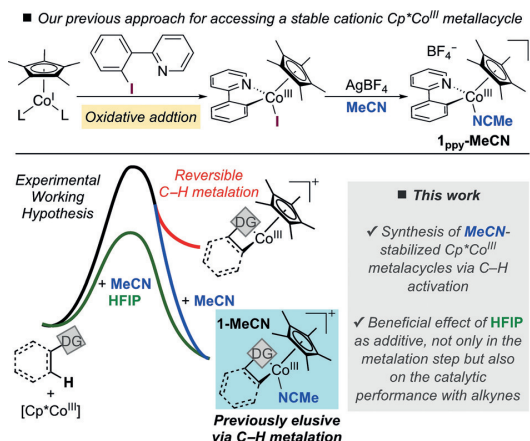
4.3 References

[1] Han, Y.-F.; Jin, G.-X. "Cyclometalated [Cp*M(C^X)] (M = Ir, Rh; X = N, C, O, P) complexes" *Chem. Soc. Rev.* **2014**, *43*, 2799−2823.

[2] In parallel to this doctoral thesis, in our research group we have also been interested in the isolation of Cp*Co^{III}(C^O) complexes. See Annex I for further information.

[3] Bauer, W.; Prem, M.; Polborn, K.; Sünkel, K.; Steglich, W.; Beck, W. "Organometallic Complexes of Iridium, Palladium, Chromium and Iron from 2-Phenyl-5(4*H*)-oxazolones − Organometallic Labelled Dipeptides" *Eur. J. Inorg. Chem.* **1998**, 485−493.

[4] Davies, D. L.; Al-Duaij, O.; Fawcett, J.; Giardiello, M.; Hilton, S. T.; Russel, D. R. "Room-temperature cyclometalation of amines, imines and oxazolines with [MCl₂Cp*]₂ (M = Rh, Ir) and [RuCl₂(p-cymene)]₂" *Dalton Trans*. **2003**, 4132−4138.

[5] Carr, K. J. T.; Davies, D. L.; Macgregor, S. A.; Singh, K.; Villa-Marcos, B. "Metal control of selectivity in acetate-assisted C−H bond activation: an experimental and computational study of heterocyclic, vinylic and phenylic C(sp2)−H bonds at Ir and Rh" *Chem. Sci*. **2014**, *5*, 2340−2346.

[6] Tauchert, M. E.; Incarvito, C. D.; Rheingold, A. L.; Bergman, R. G.; Ellman, J. A. "Mechanism of the Rhodium(III)-Catalyzed Arylation of Imines via C−H Bond Functionalization: Inhibition by Substrate" *J. Am. Chem. Soc*. **2012**, *134*, 1482−1485.

[7] (a) Li, L.; Brennessel, W. W.; Jones, W. D. "C−H Activation of Phenyl Imines and 2-Phenylpyridines with [Cp*MCl₂]₂ (M = Ir, Rh): Regioselectivity, Kinetics and Mechanism" *Organometallics* **2009**, *28*, 3492−3500. (b) Walsh, A. P.; Jones, W. D. "Mechanistic Insights of a Concerted Metalation-Deprotonation Reaction with [Cp*RhCl₂]₂" *Organometallics* **2015**, *34*, 3400−3407. (c) VanderWeide, A. I.; Brennessel, W. W.; Jones, W. D. "Reversible Concerted Metalation-Deprotonation C−H Bond Activation by [Cp*RhCl₂]₂" *J. Org. Chem*. **2019**, *84*, 12960−12965.

[8] Yu, X.; Chen, K.; Guo, S.; Shi, P.; Song, C.; Zhu, J. "Direct Access to Cobaltacycles via C−H Activation: *N*-Chloroamide-Enabled-Room-Temperature Synthesis of Heterocycles" *Org. Let.* **2017**, *19*, 5348−5351.

[9] (a) Wencel-Delord, J.; Colobert, F. "A remarkable solvent effect of fluorinated alcohols on transition metal catalysed C−H functionalizations" *Org. Chem. Front*. **2016**, *3*, 394−400. (b) Colomer, I.; Chamberlain, A. E. R.; Haughey, M. B.; Donohoe, T. J. "Hexafluoroisopropanol as a highly versatile solvent" *Nat. Rev. Chem*. **2017**, *1*, 0088, 1−12. (c) Sinha, S. K.; Bhattacharya, T.; Maiti, D. "Role of hexafluoroisopropanol in C−H activation" *React. Chem. Eng*. **2019**, *4*, 244−253. (d) Yu, C.; Sanjosé-Orduna, J.; Patureau, F. W.; Pérez-Temprano, M. H. "Emerging unconventional organic solvents for C−H bond and related functionalizations reactions" *Chem. Soc. Rev.* **2020**, DOI: 10.1039/c8cs0083c.

[10] Neely, J. M.; Rovis, T. "Rh(III)-Catalyzed Decarboxylative Coupling of Acrylic Acids with Unsaturated Oxime Esters: Carboxylic Acids Serve as Traceless Activators" *J. Am. Chem. Soc.* **2014**, *136*, 2735−2738.

[11] Li, S.; Shi, P.; Liu, R.-H.; Hu, X.-H.; Loh, T.-P. "Cobalt-Catalyzed N−O and C−C Bond Cleavage in 1,2-Oxazetidines: Solvent-Controlled C−H Aminomethylation and Hydroxymethylation of Heteroarenes" *Org. Lett*. **2019**, *21*, 1602−1606.

[12] Hazra, S.; Hirano, K.; Miura, M. "Solvent-Controlled Rhodium-Catalyzed C6-Selective C−H Alkenylation and Alkylation of 2-Pyridones with Acrylates" *Asian J. Org. Chem.* **2019**, *8*, 1097−1101.

[13] Conway Jr, J. H.; Rovis, T. "Regiodivergent Iridium(III)-Catalyzed Diamination of Alkenyl Amides with Secondary Amines: Complementary Access to γ- or δ-Lactams" *J. Am. Chem. Soc*. **2018**, *140*, 135−138.

[14] Wang, S.-G.; Cramer, N. "An Enantioselective Cp^XRh(III)−Catalyzed C−H Functionalization/Ring-Opening Route to Chiral Cyclopentenylamines" *Angew. Chem. Int. Ed.* **2019**, *58*, 2514−2518.

[15] Ozols, K.; Jang, Y.-S.; Cramer, N. "Chiral Cyclopentadienyl Cobalt(III) Complexes Enable Highly Enantioselective 3d-Metal-Catalyzed C−H Functionalizations" *J. Am. Chem. Soc.* **2019**, *141*, 5675−5680.

[16] Erbing, E.; Sanz-Marco, A.; Vázquez-Romero, A.; Malmberg, J.; Johansson, M. J.; Gómez-Bengoa, E.; Martín-Matute, B. "Base- and Additive-Free Ir-Catalyzed ortho-Iodination of Benzoic Acids: Scope and Mechanistic Investigations" *ACS Catal.* **2018**, *8*, 920−925.

Article 3
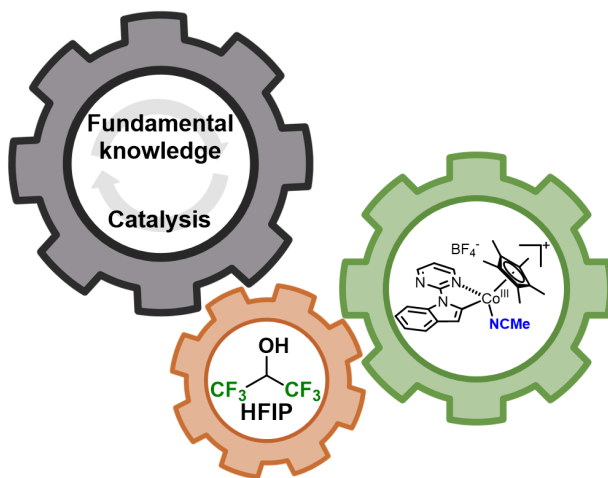
HFIP-Assisted C−H Functionalization by Cp*Co(III): Access to Key Reactive Cobaltacycles and Implication in Catalysis

Jesús Sanjosé-Orduna[+], Juan Manuel Sarria Toro[+], and Mónica H. Pérez-Temprano*

Abstract: *Described here is a synthetic approach to access two of the most widely invoked cationic cobaltacycles in Cp*Co(III)-catalyzed C−H functionalization reactions by C−H activation. The unique stabilizing capability of MeCN was used to surmount the previously proposed reversible nature of the C−H metalation step. Moreover, it is revealed the boosting effect of 1,1,1,3,3,3-hexafluoroisopropanol in the metalation step and in the reaction between N-pyrimidinylindole and diphenylacetylene under catalytic conditions.*

Over the past few years, Cp*Co(III) complexes have emerged as a potential alternative to noble metals in one of the cornerstones of modern organic synthesis: ligand-directed C−H functionalization reactions.[1] These cobalt catalysts can not only emulate the same reaction patterns of analogous rhodium and iridium systems, but also exhibit a unique reactivity because of the inherent properties of this first-row metal, properties such as its low electronegativity, hard nature, or small radius.[1] Despite the remarkable progress achieved in this field since the seminal work by Kanai, Matsunaga, and co-workers in 2013,[2] there is still a lack of fundamental understanding of these Cp*Co(III)-catalyzed transformations. In sharp contrast to analogous rhodium systems,[3] the investigation of the underlying reaction mechanisms of Cp*Co-catalyzed directed C−H functionalizations has been hampered by the difficulty of capturing transient key reaction intermediates, since, in most cases, the formation of C−H activated Cp*Co(III) metallacycles is proposed to be reversible.[1,4] To tackle this situation, our group has recently reported the employment of acetonitrile as a stabilizing ligand to access a direct analogue of a long-sought cyclometalated cobalt(III) complex (**1_ppy**-MeCN; Figure 1), by a ligand-assisted oxidative addition,[5] to bring light into the mechanistic insights of C−H oxidative alkyne annulations. Inspired by these results, we wondered whether it would be possible to overcome the reversibility of the C−H cobaltation by taking advantage of the unique ability of MeCN to stabilize

[*] J. Sanjosé-Orduna,[+] Dr. J. M. Sarria Toro,[+]
Dr. M. H. Pérez-Temprano
Institute of Chemical Research of Catalonia (ICIQ), The Barcelona
Institute of Science and Technology (BIST)
Avgda. Països Catalans 16, 43007 Tarragona (Spain)
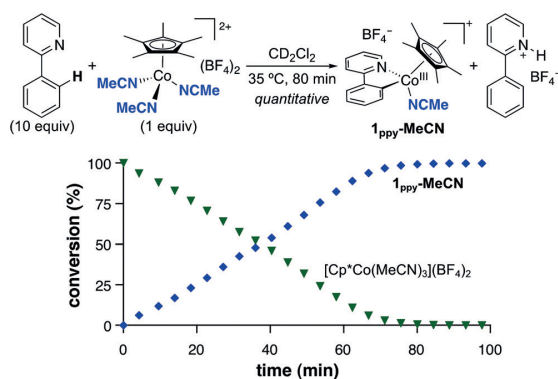E-mail: mperez@iciq.es

J. Sanjosé-Orduna[+]
Departament de Química Analítica i Química Orgànica, Universitat
Rovira i Virgili, 43007 Tarragona (Spain)

[+] These authors contributed equally to this work.

Supporting information and the ORCID identification number(s) for
the author(s) of this article can be found under:
https://doi.org/10.1002/anie.201806847.

Figure 1. Proposed synthetic approach for accessing the long-sought after key reactive Cp*Co(III) intermediates by C−H activation.

otherwise highly reactive cobalt species. Herein, we provide a direct synthetic route to two of the most widely invoked cationic metalacyclic intermediates in Cp*Co(III)-catalyzed C−H functionalization reactions by C−H bond cleavage. Our studies not only demonstrate the intermediacy of this type species in the oxidative alkyne annulation and alkyne insertion benchmark transformations, but also reveal the crucial role of fluorinated alcohols, such as 1,1,1,3,3,3-hexa-fluoroisopropanol (HFIP), to improve the efficiency, not only of the C−H activation step, but also of catalytic transformations using diphenylacetylene as coupling partner.

We started our investigations by targeting the synthesis of **1_ppy**-MeCN through a C−H metalation step using [Cp*Co(III)-(MeCN)₃]X₂ as the cobalt source. We selected this Cp*Co(III) complex to test our working hypothesis because: a) it is commonly used as catalyst in Cp*Co-catalyzed C−H func-tionalizations,[1] b) the cationic nature of this Cp*Co(III) system simplifies the reaction conditions, avoiding the use of silver salts to generate the active species, and c) it already contains our desired stabilizing ligand. Gratifyingly, the reaction of [Cp*Co(III)(MeCN)₃](BF₄)₂ with 10 equivalents of 2-ppyH, used not only as substrate but also as surrogate base,[6] afforded the smooth formation of the targeted acetonitrile-stabilized cobaltacycle **1_ppy**-MeCN along with the protonated substrate as determined by ¹H NMR spectroscopic analysis (Figure 2).[7,8]

Despite this promising result, we surmised that this synthetic strategy could not be effective when exploring substrates containing less basic directing groups. This assump-tion proved correct since the metalation of one of the most

Figure 2. Conversion versus time plot for the reaction of [Cp*Co-(MeCN)$_3$](BF$_4$)$_2$ + 2-ppyH in CD$_2$Cl$_2$ at 35 °C as monitored by ^{1}H NMR spectroscopy.

commonly used substrates in Cp*Co-catalyzed transformations, *N*-pyrimidinylindole (pmiH),[1] was rather slow, under the reaction conditions described above for accessing **1$_{ppy}$-MeCN**, when monitored by ^{1}H NMR spectroscopy (Figure 3a). After some experimentation, this limitation was addressed by the use of 2,6-di-*tert*-butylpyridine (DTBP) as an external base,[9] which provided the quantitative formation of **1$_{pmi}$-MeCN**, in CH$_2$Cl$_2$ at 35 °C after 20 hours as determined
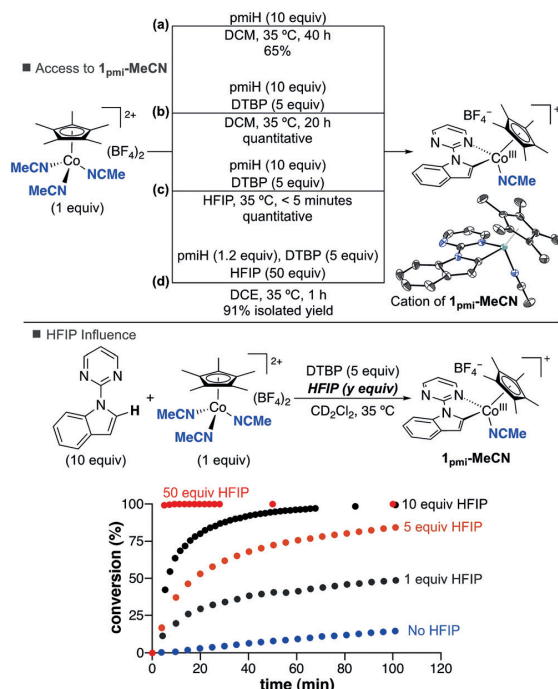
Figure 3. Stoichiometric experiments for accessing **1$_{pmi}$-MeCN**. ORTEP plot of **1$_{pmi}$-MeCN**. Thermal ellipsoids drawn at 50% probability, and the hydrogen atoms, BF$_4$ anion, and additional molecules in the unit cell are omitted for clarity. DCM = dichloromethane.

by ^{1}H NMR spectroscopy (Figure 3b).[10] The structure of **1$_{pmi}$-MeCN** was unequivocally confirmed by NMR spectroscopy and single-crystal X-ray diffraction.[11] The use of HFIP as solvent caused a dramatic increase in the reaction efficiency,[12] reducing the reaction time to less than 5 minutes (Figure 3c). Although the beneficial effect of this fluorinated solvent is commonly acknowledged in transition metal catalyzed C−H functionalization processes,[13] its real role still remains unclear. To gain insights into this unique capability, we performed ^{1}H NMR spectroscopic titrations of [Cp*Co^{III}(MeCN)$_3$](BF$_4$)$_2$ with HFIP to test whether the accelerating effect during the metalation step is due to an initial ligand displacement. Importantly, in these experiments, we do not observe MeCN replacement by the perfluorinated alcohol.[14] Furthermore, we conducted a series of preliminary experiments, monitoring the formation of **1$_{pmi}$-MeCN** by ^{1}H NMR spectroscopy, using HFIP as an additive. Addition of even just 1 equivalent of HFIP accelerated the C−H metalation step, suggesting that the polarity of solvent alone is not responsible for the dramatic effect on the reaction rate. These results along with literature precedents may hint at HFIP acting as proton shuttle during the C−H activation step.[15] Indeed, in the presence of 50 equivalents of the fluorinated alcohol, we observed the quantitative formation of **1$_{pmi}$-MeCN** in less than 5 minutes (Figure 3).[16] We were able to isolate **1$_{pmi}$-MeCN** in 91% yield in the presence of 50 equivalents of HFIP at 35 °C, after 1 hour using DCE as solvent (Figure 3d).

Encouraged by the dramatic effect of HFIP on the C−H activation step, we next sought to explore the influence of this fluorinated alcohol on subsequent elementary steps involved in a potential catalytic cycle. In particular, we targeted as a benchmark the reactivity of **1$_{pmi}$-MeCN** with diphenylacetylene in the context of Cp*Co-catalyzed hydroarylation and oxidative annulation reactions. Based on the mechanistic proposals found in the literature, at the beginning both reactions share identical reactive intermediates, as is depicted in Scheme 1. However, the two pathways differ in the steps that follow the migratory insertion: protodemetalation in the presence of a protic source[17] versus reductive elimination/reoxidation sequence.[1f,5] Therefore, the comparison of the HFIP effect on these two reactivity patterns represents
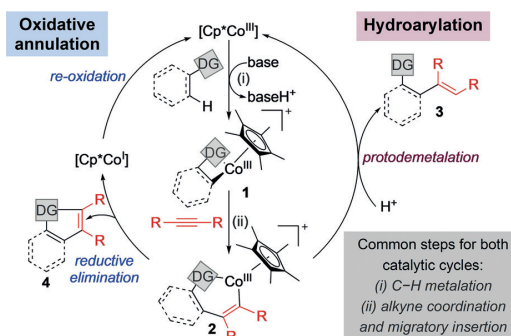
Scheme 1. Mechanistic proposals for Cp*Co-catalyzed hydroarylation and oxidative annulation reactions. DG = directing group.

a particular interesting case, since a priori, the fluorinated alcohol could affect them differently.

On this basis, our first objective was to confirm the formation of **2**-type complexes. The treatment of **1**$_{pmi}$**-MeCN** with 2 equivalents of diphenylacetylene in CD$_2$Cl$_2$ at −20°C resulted in the quantitative formation of **2**$_{pmi}$**-MeCN** within 1 hour, as determined by ^{1}H NMR spectroscopy. This compound, whose structure was also characterized by single-crystal X-ray diffraction, is analogous to seven-membered cationic cobaltacycles reported by our group and that of Sundararaju (see Scheme 2).[5,11,17c] We then carried out
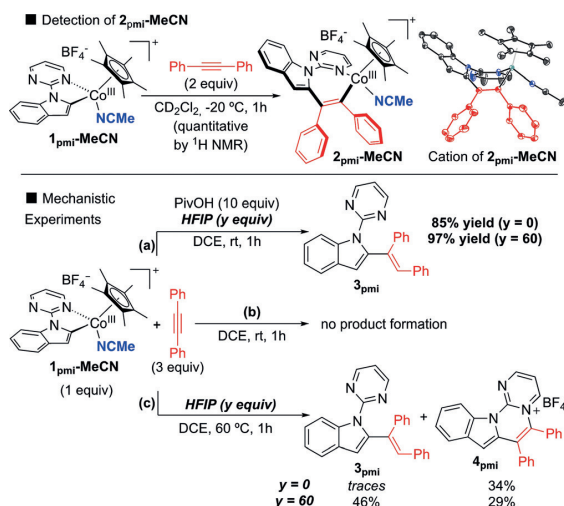
Scheme 2. Stoichiometric experiments. The yields were obtained by ^{1}H NMR spectroscopy, using 1,3,5-trimethoxybenzene as an internal standard. ORTEP plot of **2**$_{pmi}$**-MeCN**. Thermal ellipsoids drawn at 50% probability, and the hydrogen atoms, BF$_4$ anion and additional molecules in the unit cell were omitted for clarity. DCE = 1,2-dichloroethane.

a series of stoichiometric studies, not only to provide consistent experimental evidence of the proposed divergent reactivities from **2**$_{pmi}$, but also to unravel the potential impact of HFIP as additive on both reaction pathways.[18] We first studied the hydroarylation process using PivOH as proton source (Scheme 2a). The reaction of **1**$_{pmi}$**-MeCN** with 3 equivalents of diphenylacetylene in the presence of 10 equivalents of PivOH at room temperature for 1 hour in DCE resulted in the selective formation of **3**$_{pmi}$ in 85% yield as determined by ^{1}H NMR spectroscopy. Gratifyingly, under these reaction conditions, the presence of HFIP as an additive led to a higher yield of the desired product (97%). This increase in yield could be consistent with the potential role of the fluorinated alcohol as a proton shuttle.[15] Following a similar strategy, we next investigated the annulation reaction. Neither traces of **3**$_{pmi}$ nor **4**$_{pmi}$ were detected by ^{1}H NMR spectroscopy upon treatment of **1**$_{pmi}$**-MeCN** with 3 equivalents of diphenylacetylene at room temperature for 1 hour in DCE (Scheme 2b).[19] At 60°C (Scheme 2c), we observed the formation of **4**$_{pmi}$ in 34% yield along with traces (<5%) of **3**$_{pmi}$, indicating that the

reductive elimination is accelerated at higher temperature. In this system, the addition of HFIP resulted in competing hydroarylation and annulation processes, favoring the formation of the hydroarylated product (**3**$_{pmi}$/**4**$_{pmi}$ = 46:29). This result strongly suggests HFIP can act as proton source.[20]

With these mechanistic insights in hand, we explored the global effect of HFIP under catalytic conditions. In alignment with our stoichiometric experiments, when we used HFIP as an additive in the hydroarylation of diphenylacetylene with pmiH in DCE at room temperature using [Cp*Co(MeCN)$_3$]-(BF$_4$)$_2$ (5 mol%) as the catalyst and 0.5 equivalents of PivOH as proton source, we observed a significant increase in yield (Table 1, entries 1 and 2).[21] The efficiency of the reaction was

Table 1: Hydroarylation of diphenylacetylene.[a]

Entry	Catalyst	PivOH (equiv)	Yield [%][b]
1	[Cp*Co(MeCN)$_3$][BF$_4$]$_2$	0.5	12[c]
2	[Cp*Co(MeCN)$_3$][BF$_4$]$_2$	0.5	50[d]
3	[Cp*Co(MeCN)$_3$][BF$_4$]$_2$	1.5	86[d]
4	**1**$_{pmi}$**-MeCN**	1.5	98[e]

[a] NMR-scale reactions: 0.025 mmol scale. See the Supporting Information for details. [b] Yield determined by ^{1}H NMR spectroscopy. [c] No HFIP used. [d] Given sufficiently long times, these two reactions reach quantitative yields. [e] Yield of product isolation from a reaction run on a 0.20 mmol scale.

improved in the presence of higher amounts of PivOH (1.5 equiv), obtaining the desired product in 86% yield (entry 3). Interestingly, the use of **1**$_{pmi}$**-MeCN** as a catalyst provided **3**$_{pmi}$ in 98% yield upon isolation (entry 4).[22] This result confirms not only the catalytic competence of this type of cobaltacycle species, formed by C−H metalation from [Cp*Co(MeCN)$_3$](BF$_4$)$_2$, but also their excellent efficiency.

Surprisingly, when we investigated the impact of HFIP in the formation of the annulated product **4**$_{pmi}$, under catalytic oxidative conditions in DCE at 60°C, we observed a dramatic and quite unexpected positive effect (Table 2).[23] In the

Table 2: Oxidative annulation of diphenylacetylene.[a]

Entry	catalyst	HFIP/DCE (ratio)	Yield [%][b]
1	[Cp*Co(MeCN)$_3$][BF$_4$]$_2$	no HFIP	4
2	[Cp*Co(MeCN)$_3$][BF$_4$]$_2$	1:100	13
3	[Cp*Co(MeCN)$_3$][BF$_4$]$_2$	1:10	83
4	**1**$_{pmi}$**-MeCN**	1:10	91
5	**1**$_{pmi}$**-MeCN**	1:10	97[c]

[a] Reactions run at 0.20 mmol scale and 0.1 M concentration. [b] Yield of isolated product. [c] Stoichiometric NMR experiment.

absence of HFIP and using 1 mol% of [Cp*Co(MeCN)$_3$]-(BF$_4$)$_2$, the reaction of pmiH with diphenylacetylene afforded less than 5% of the desired product after 8 hours (entry 1). As shown in entries 2 and 3, we found that the ratio of HFIP/DCE plays a crucial role in the efficiency of this transformation. Only a modest increase in yield was obtained when the reaction was conducted in the presence of small amount of HFIP (13% as compared to 4% in the absence of HFIP). Notably, the catalytic performance was further improved by increasing the concentration of HFIP, obtaining **4$_{pmi}$** in 83% yield upon isolation (entry 3).[24] In alignment with the results obtained in the hydroarylation process, using **1$_{pmi}$-MeCN** as catalyst provided the best result, giving **4$_{pmi}$** in 91% yield upon isolation (entry 4). As mentioned before, a priori, this trend clearly argues against the HFIP effect observed in the stoichiometric studies. However, revisiting those experiments with **1$_{pmi}$-MeCN**, we found that the reaction of **1$_{pmi}$-MeCN** with 3 equivalents of diphenylacetylene at 60°C in a HFIP/DCE (1:10) solvent mixture, this time in the presence of the salts employed under catalytic conditions, AgBF$_4$ and Cu-(OAc)$_2$, affords the annulated product in 97% yield (entry 5). This result along with the catalytic experiments shown in Table 2 suggest that the increased polarity of the solvent mixture in the presence of HFIP may play a crucial beneficial effect on the formation of **4$_{pmi}$** by enhancing the solubility of the required Cu/Ag salts.[25]

In summary, we have designed a new strategy for circumventing the reversible nature of the C−H metalation step when using Cp*Co complexes to access two of the most widely invoked cationic cobaltacyclic intermediates. Our work reveals the boosting effect of HFIP as an additive, not only in the C−H activation step, but also on benchmark catalytic processes involving alkynes as coupling partners, presumably because of its capability as a proton shuttle and polar nature.[26] Further investigations into the role of fluorinated alcohols in catalysis are currently underway.

Acknowledgements

Conflict of interest

The authors declare no conflict of interest.

[1] a) M. Moselage, J. Li, L. Ackermann, *ACS Catal.* **2016**, *6*, 498; b) D. Wei, X. Zhu, J.-L. Niu, M.-P. Song, *ChemCatChem* **2016**, *8*, 1242; c) P. G. Chirila, C. J. Whiteoak, *Dalton Trans.* **2017**, *46*, 9721; d) S. Wang, S. Y. Chen, X. Q. Yu, *Chem. Commun.* **2017**, *53*, 3165; e) T. Yoshino, S. Matsunaga, *Adv. Synth. Catal.* **2017**, *359*, 1245; f) S. Prakash, R. Kuppusamy, C.-H. Cheng, *ChemCatChem* **2018**, *10*, 683.

[2] a) T. Yoshino, H. Ikemoto, S. Matsunaga, M. Kanai, *Angew. Chem. Int. Ed.* **2013**, *52*, 2207; *Angew. Chem.* **2013**, *125*, 2263.

[3] For selected mechanistic investigations on Cp*Rh^{III}-catalyzed C−H functionalization, see: a) M. E. Tauchert, C. D. Incarvito, A. L. Rheingold, R. G. Bergman, J. A. Ellman, *J. Am. Chem. Soc.* **2012**, *134*, 1482; b) M. Brasse, J. Campora, J. A. Ellman, R. G. Bergman, *J. Am. Chem. Soc.* **2013**, *135*, 6427; c) N. Wang, B. Li, H. Song, S. Xu, B. Wang, *Chem. Eur. J.* **2013**, *19*, 358; d) S. H. Park, J. Kwak, K. Shin, J. Ryu, Y. Park, S. Chang, *J. Am. Chem. Soc.* **2014**, *136*, 2492; e) Y. Park, K. T. Park, J. G. Kim, S. Chang, *J. Am. Chem. Soc.* **2015**, *137*, 4534; f) Y. Park, J. Heo, M.-H. Baik, S. Chang, *J. Am. Chem. Soc.* **2016**, *138*, 14020; g) R. Thenarukandiyil, S. K. Gupta, J. Choudhury, *ACS Catal.* **2016**, *6*, 5132; h) S. Y. Hong, J. Jeong, S. Chang, *Angew. Chem. Int. Ed.* **2017**, *56*, 2408; *Angew. Chem.* **2017**, *129*, 2448.

[4] Zhu and co-workers reported the low yielding (31–38%) formation of two neutral Cp*Co metallacycles by C−H activation: X. Yu, K. Chen, S. Guo, P. Shi, C. Song, S. Zhu, *Org. Lett.* **2017**, *19*, 5348.

[5] J. SanJosé-Orduna, D. Gallego, A. Garcia-Roca, E. Martin, J. Benet-Buchholz, M. H. Pérez-Temprano, *Angew. Chem. Int. Ed.* **2017**, *56*, 12137; *Angew. Chem.* **2017**, *129*, 12305.

[6] Analogue metalations promoted by the substrate using Cp*Rh^{III} complexes have been observed by Bergman, Ellman, and co-workers see Ref. [3a].

[7] Unlike the analogue rhodium-based systems, the formation of a cationic cobaltacycle stabilized by a second molecule of 2-ppyH is not observed. This is presumably due to the smaller atomic radius of cobalt which prevents its coordination. See Ref. [3a,d–e].

[8] We also tested the use of carboxylic bases, such as NaOAc, to promote the base-assisted cyclometalation of 2-ppyH by [Cp*Co^{III}(MeCN)$_3$]X$_2$. Under these reaction conditions, we observed a complex mixture of products, including **1$_{ppy}$-MeCN** and an inactive dimeric cobalt species (**S1**) containing bridging acetate groups. See p. S2–4 in the Supporting Information for further details.

[9] We discarded the use of carboxylic bases based on the preliminary results described in Ref. [8] and in the Supporting Information.

[10] This result along with the use of 2-ppyH as an external base support a base-assisted intermolecular C−H metalation step.

[11] CCDC 1846807, 1846808, and 1846809 (**S1, 1$_{pmi}$-MeCN, 2$_{pmi}$-MeCN**) contain the supplementary crystallographic data for this paper. These data can be obtained free of charge from The Cambridge Crystallographic Data Centre.

[12] For recent examples of the use of HFIP in Cp*Co^{III} catalysis, see: a) L. Kong, X. Yang, X. Zhou, S. Yu, X. Li, *Org. Chem. Front.* **2016**, *3*, 813; b) Y. Bunno, N. Murakami, Y. Suzuki, M. Kanai, T. Yoshino, S. Matsunaga, *Org. Lett.* **2016**, *18*, 2216; c) H. Wang, M. Moselage, M. J. González, L. Ackermann, *ACS Catal.* **2016**, *6*, 2705; d) A. Lerchen, S. Vásquez-Céspedes, F. Glorius, *Angew. Chem. Int. Ed.* **2016**, *55*, 3208; *Angew. Chem.* **2016**, *128*, 3261; e) M. Yoshida, K. Kawai, R. Tanaka, T. Yoshino, S. Matsunaga, *Chem. Commun.* **2017**, *53*, 5974.

[13] J. Wencel-Delord, F. Colobert, *Org. Chem. Front.* **2016**, *3*, 394.

[14] During the titration and metalation experiments, we do not observe, by ^{1}H NMR spectroscopy, the formation of additional

[15] a) A. Berkessel, J. A. Adrio, D. Hüttenhain, J. M. Neudörfl, *J. Am. Chem. Soc.* **2006**, *128*, 8421; b) D. Vuluga, J. Legros, B. Crousse, A. M. Z. Slawin, C. Laurence, P. Nicolet, D. Bonnet-Delpon, *J. Org. Chem.* **2011**, *76*, 1126.

[16] The same trend is observed when using 2-ppyH as substrate. See the Supporting Information for further details.

[17] For selected examples of Cp*Co[III]-catalyzed hydroarylation with alkynes, invoking cationic cobaltacycles as reactive intermediates, see: a) M. Sen, B. Emayavaramban, N. Barsu, J. R. Premkumar, B. Sundararaju, *ACS Catal.* **2016**, *6*, 2792; b) X. Zhou, Y. Luo, L. Kong, Y. Xu, G. Zheng, Y. Lan, Z. Li, *ACS Catal.* **2017**, *7*, 7296; c) M. Sen, N. Rajesh, B. Emayavaramban, J. R. Premkumar, B. Sundararaju, *Chem. Eur. J.* **2018**, *24*, 342.

[18] In alignment with the previous titration experiments, we do not observe the displacement of MeCN ligand when we treated **1**[pmi]**-MeCN** with variable amounts of HFIP. See the Supporting Information for further details.

[19] Under these reaction conditions, we only observed the formation of **2**[pmi]**-MeCN**.

[20] See the Supporting Information for further details on the stoichiometric experiments.

[21] Under the reaction conditions shown in entries 1 and 2 of Table 1, we have also tested [Cp*CoI$_2$(CO)], the most widely used Cp*Co[III] precatalyst, in combination with AgBF$_4$, observing **3**[pmi] in low yields. See the Supporting Information for more details.

[22] For literature precedents on the synthesis of **3**[pmi] (33% yield upon isolation) using Cp*Co catalysts see Ref. [16c].

[23] Cp*Co[III]-catalyzed synthesis of **4**[pmi] has been reported to proceed in DCE at 130°C for 24 h in 64% yield upon isolation. See: Y. Yang, B. Li, W. Liu, R. Zhang, L. Yu, Q.-G. Ma, R. Lv, D. Du, T. Li, *J. Org. Chem.* **2016**, *81*, 11335.

[24] We have also tested [Cp*CoI$_2$(CO)] as a precatalyst under the reaction conditions shown in entries 1 and 3 of Table 2. In the absence of HFIP, we did not observe any trace of the desired product. In the solvent mixture HFIP/DCE (1:10), **4**[pmi] was formed in low yield (31%). See the Supporting Information for more details.

[25] For a cooperative reductive elimination step in oxidative couplings, see: a) I. Funes-Ardoiz, F. Maseras, *Angew. Chem. Int. Ed.* **2016**, *55*, 2764; *Angew. Chem.* **2016**, *128*, 2814; b) I. Funes-Ardoiz, F. Maseras, *ACS Catal.* **2018**, *8*, 1161; c) I. Funes-Ardoiz, F. Maseras, *Chem. Eur. J.* **2018**, https://doi.org/10.1002/chem.201800627.

[26] Apart from increasing the solubility of ionic additives, the polar nature of HFIP could potentially contribute to facilitating MeCN dissociation to access reactive unsaturated species involved in the catalytic cycle.

4.5 Supporting Information for Article 3

Table of Contents

4.5.1 General Procedures

All experiments were conducted under an argon-filled glove box (mBraun Unilab 4420) with concentrations of O_2 and H_2O < 0.1 ppm or using Schlenk techniques under argon atmosphere. All the glassware was oven-dried at 100 °C overnight and cooled under vacuum prior use. NMR spectra were obtained on a Bruker 400 MHz or a 500 MHz cryoprobe spectrometers. ^{1}H, ^{13}C and ^{19}F NMR chemical shifts are reported in parts per million (ppm), relative to tetramethylsilane (TMS) for ^{1}H and ^{13}C with the residual solvent peak used as an internal reference, and relative to CCl_3F (Freon) for ^{19}F. Multiplicities are reported as follows: singlet (s), doublet (d), doublet of doublets (dd), triplet of doublets (td), triplet (t), broad signal (br) and multiplet (m). High Resolution Mass Spectrometry (HRMS) data was recorded on a LCT-Premier (Waters) or a MicroTOF Focus (Bruker Daltonics) mass spectrometers using ESI ionization technique and acetonitrile as solvent. Details for X-ray structure determination can be found on page 198.

4.5.2 Materials and Methods

Commercially available reagents 2-phenylpyridine, indole, 2-chloropyrimidine, diphenylacetylene, 2,6-di-*tert*-butylpyridine, 1,2,3,4,5-pentamethylcyclopentadiene, 1,3-cyclohexadiene, ^{n}BuLi, $Co_2(CO)_8$, $AgBF_4$, $Pd(OAc)_2$, $Cu(OAc)_2$, pivalic acid, NaOAc, ethyl acetate, ^{n}hexane, and acetone were used without further purification directly as received from the commercial supplier, and stored under inert gas and/or low temperature when required. 1,2-dichloroethane (DCE) and 1,1,1,3,3,3-hexafluoroisopropanol (HFIP) were stored under argon with activated 4 Å molecular sieves.

If necessary, the solvents (*n*-hexane, Et_2O, CH_2Cl_2, MeCN) were used from a solvent purification system *pure-solv* (SPS-400, Innovative Technology) and stored under argon with activated 4 Å molecular sieves.

Solvents were degassed (when necessary) by bubbling an argon stream at 0 °C for at least 2 h.

Deuterated solvents ($CDCl_3$, CD_2Cl_2) were stored under argon with activated 4 Å molecular sieves. [Cp*Co(MeCN)$_3$][BF$_4$]$_2$,[1] *N*-pyrimidinylindole,[2] were synthesized according to previous literature procedures.

[1] Yu, D.-G.; Gensch, T.; de Azambuja, F.; Vásquez-Céspedes, S.; Glorius, F. *J. Am. Chem. Soc.* **2014**, *136*, 17722.

[2] Ackermann, L.; Lygin, A. V. *Org. Lett*. **2011**, *13*, 3332.

4.5.3 Access to 1-MeCN-type Complexes *via* C−H Activation

### 4.5.3.1 From 2-phenylpyridine (1$_{ppy}$-MeCN)

4.5.3.1.1 Using Carboxylate Bases

We initially attempted to generate **1$_{ppy}$-MeCN** by reacting 2 equiv of 2-phenylpyridine (2-ppyH) with 1 equiv of [Cp*Co(MeCN)$_3$](SbF$_6$)$_2$ in DCM at room temperature in the presence of excess NaOAc (10 equiv), in order to promote a base-assisted cyclometalation and mimic previously reported catalytic conditions (Figure S1). In a glass vial, [Cp*Co(MeCN)$_3$](SbF$_6$)$_2$ (10.0 mg, 0.013 mmol), NaOAc (10.4 mg, 0.127 mmol) and 2-phenylpyridine (3.6 µL, 0.025 mmol or 18 µL, 0.127 mmol) were stirred in 1.0 mL CD$_2$Cl$_2$ for 60 minutes. The obtained solution was filtered directly into an NMR tube for characterization. Under these reaction conditions, we detected the formation of the desired cobaltacycle (**1$_{ppy}$-MeCN**) by ^{1}H NMR spectroscopy along with a mixture of products including **S1**,[3,4] a dimeric cobalt species containing bridging acetate groups (**1$_{ppy}$-MeCN/S1** 7:1, Figure S1a). The structure of **S1** was confirmed by X-ray analysis and ESI-MS. The formation of **1$_{ppy}$-MeCN** was significantly favored over **S1** when the reaction was performed with 10 equiv of 2-ppyH (**1$_{ppy}$-MeCN/2** 25:1, Figure S1b).

---

[3] This type of acetate-bridged structure has been proposed only once for a [Cp*Co] system, see: U. Kölle, B. Fuss, *Chem. Ber.* **1984**, *117,* 743.

[4] Similar structures supported by nitrogen ligands have been structurally characterized, see: (a) P. Chaudhuri, J. Querbach, K. Wieghardt, B. Nuber, J. Weiss, *J. Chem. Soc., Dalton Trans.* **1990**, 271-278; (b) D. A. Brown, W. Errington, W. K. Glass, W. Haase, T. J. Kemp, H. Nimir, S. M. Ostrovsky, R. Werner, *Inorg. Chem.* **2001**, *40*, 5962-5971; (c) V. B. Romakh, B. Therrien, G. Labat, H. Stoekli-Evans, G. B. Shul'pin, G. Süss-Fink, *Inorg. Chim. Acta* **2006**, *359*, 3297.
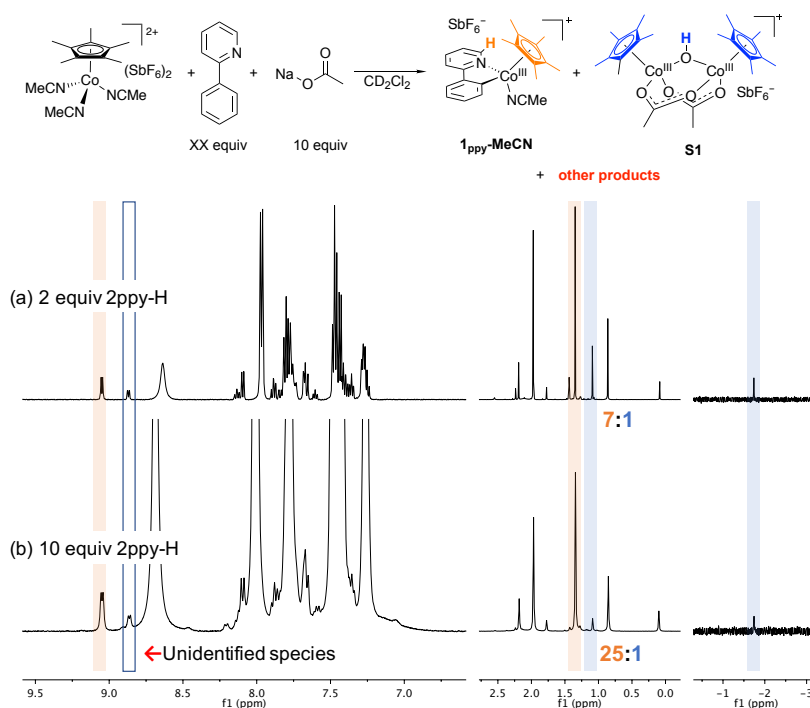
**Figure S1.** Formation of 1ppy-MeCN in presence of carboxylate bases.

It is noteworthy that no C−H metalation was observed when isolated **S1** was reacted with 2ppy-H in CH₂Cl₂ even upon prolonged heating (Figure S2).
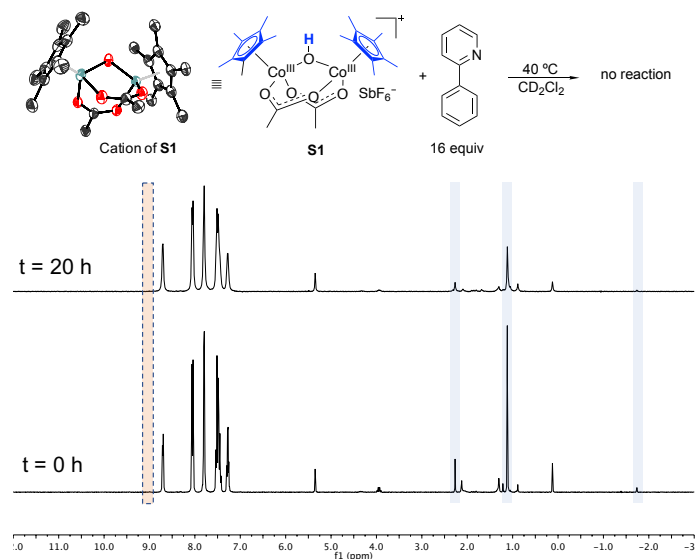
Figure S2. Attempted reaction between **S1** and 2-phenylpyridine.

*Experimental Procedure for the synthesis of [(Cp*Co)₂(OAc)₂OH]SbF₆ (**S1**)*

In a glass vial, [Cp*Co(MeCN)₃](SbF₆)₂ (10.0 mg, 0.013 mmol) and NaOAc (10.4 mg, 0.127 mmol) were stirred in 1.0 mL CD₂Cl₂ for 30 minutes. The obtained deep blue solution was filtered directly into an NMR tube for characterization, the spectrum indicated complete conversion into the product.
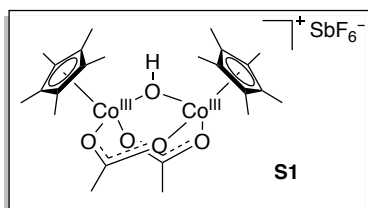
¹H NMR: ¹H NMR (500 MHz, CD₂Cl₂) δ 2.24 (s, 6H), 1.09 (s, 30H), -1.75 (s, 1H)

¹³C NMR: ¹³C NMR (126 MHz, CD₂Cl₂) δ 185.0, 90.3, 28.4, 9.0

HRMS-ESI (m/z): [M⁺]: Calcd for C₂₄H₃₇Co₂O₅, 523.129941; Found, 523.127824.

*Experimental procedure for the reaction of **S1** with 2-ppyH*

A solution of **S1** (3.25 μmol) in 0.7 mL of CD₂Cl₂ was prepared as described. Excess acetonitrile was removed by evaporation and re-dissolution. The solution was mixed with 2-ppyH (7.95 μL, 0.051 mmol) in an NMR tube. An initial ¹H spectrum was measured, then the tube was heated to 40 °C for 20 h. A second ¹H NMR was taken. No cobaltacycle was observed.

4.5.3.1.2 Using the Substrate as Surrogate Base
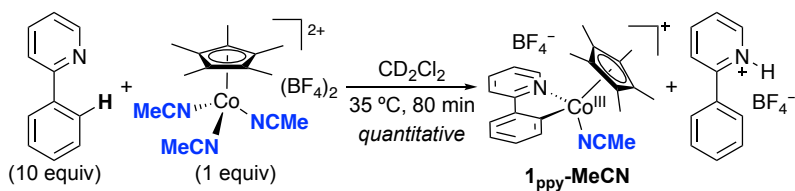
Inside the glovebox an NMR tube was loaded with [Cp*Co(MeCN)₃](BF₄)₂ (4.9 mg, 0.01 mmol). The tube was then taken out and connected to the Schlenk like via an adaptor and cooled down to −35 °C. The solid was then dissolved in 0.5 mL of CD₂Cl₂ and 2-ppyH was added (14.3 μL, 0.10 mmol) The reaction was kept at this temperature until transferred to the NMR instrument for measurement at 35 °C. The formation of **1ₚₚy-MeCN** from [Cp*Co(MeCN)₃](BF₄)₂ was monitored by ¹H NMR spectroscopy (Figure S3).
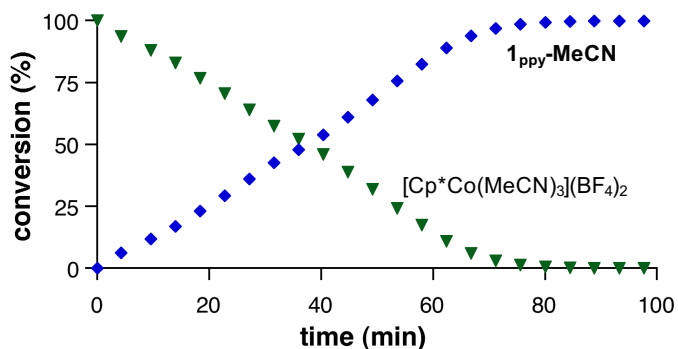
Figure S3. Conversion vs. time plot for the formation of **1_{ppy}-MeCN** via C−H activation using the substrate as surrogate base.

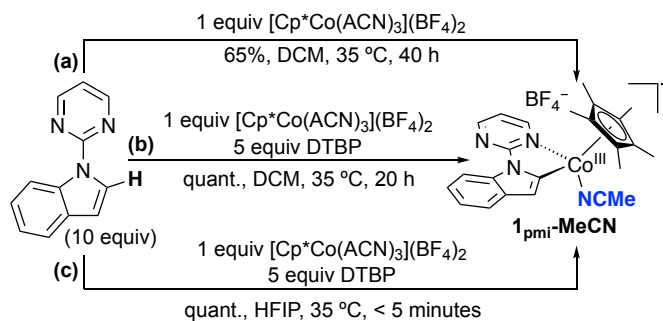### 4.5.3.1.3 Using the Substrate as Surrogate Base in Presence of HFIP

Inside the glovebox an NMR tube was loaded with [Cp*Co(MeCN)₃](BF₄)₂ (5.0 mg, 0.01 mmol). The tube was then taken out and connected to the Schlenk like via an adaptor and cooled down to −35 ºC. The solid was then dissolved in 0.5 mL of CD₂Cl₂. 2-ppyH (14.3 µL, 0.10 mmol) and HFIP (52 µL, 50 equiv) were added. The reaction was kept at this temperature until transferred to the NMR instrument for measurement at 35 ºC. As observed in Figure S4, after just 6 minutes [Cp*Co(ACN)₃](BF₄)₂ is barely detectable. After 15 minutes full conversion into **1_{ppy}-MeCN** has been reached.
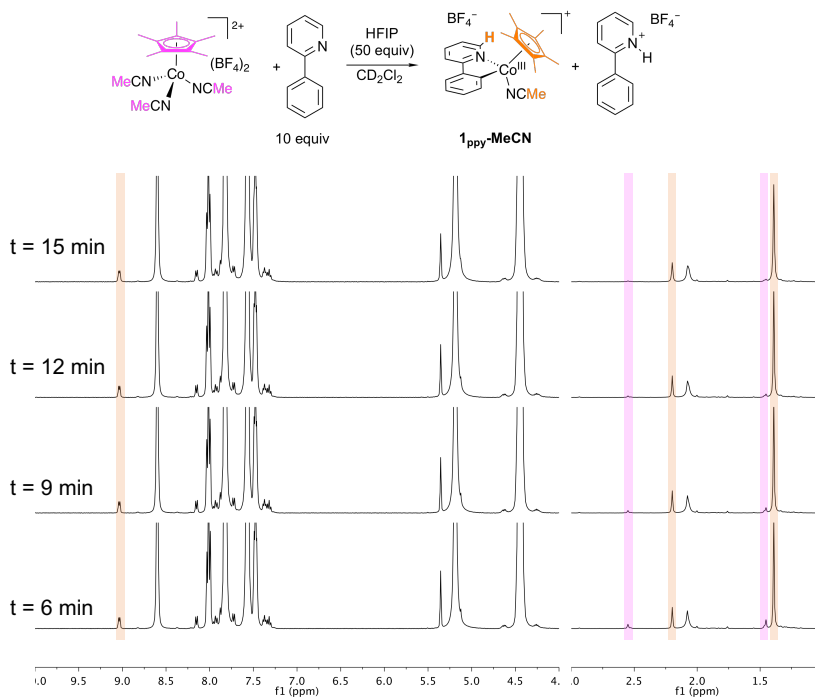
Figure S4. Monitoring of the formation of **1_{ppy}-MeCN** in presence of HFIP.

4.5.3.2 From N-pyrimidinylindole (1$_{pmi}$-MeCN)

Scheme S1. Conditions explored for the synthesis of **1$_{pmi}$-MeCN**.

In the following experiments the ratio of ^{1}H signals of the Cp* ligand from starting material and product were taken as measure of reaction progress.

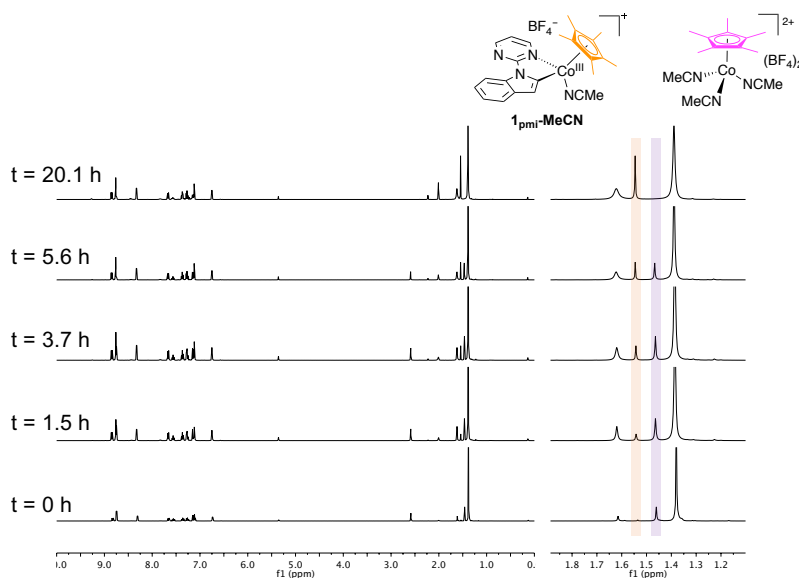### 4.5.3.2.1 Using the Substrate as Surrogate Base (Scheme S1a)

Inside the glovebox an NMR tube was loaded with [Cp*Co(MeCN)$_3$](BF$_4$)$_2$ (3 mg, 6.11 µmol) and *N*-pyrimidinylindole (11.9 mg, 61.1 µmol). The mixture was then dissolved in 0.6 mL of CD$_2$Cl$_2$. A ^{1}H NMR was measured right after preparation, then the sample was heated to 35 ºC in a water bath and additional spectra were acquired at intervals (Figure S5).
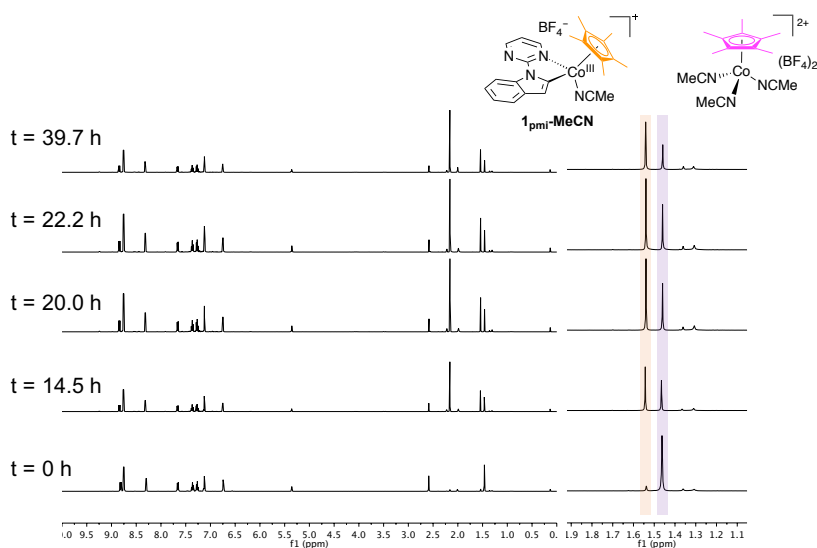
Figure S5. ^{1}H NMR spectra for conditions in Scheme S1a.

4.5.3.2.2 Using 2,6-Di-*tert*-butylpyridine (DTBP) as Base (Scheme S1b)

Inside the glovebox an NMR tube was loaded with [Cp*Co(MeCN)$_3$](BF$_4$)$_2$ (3 mg, 6.11 µmol), *N*-pyrimidinylindole (11.9 mg, 61.1 µmol) and 2,6-Di-*tert*-butylpyridine (6.6 µL, 30.6 µmol). The mixture was then dissolved in 0.6 mL of CD$_2$Cl$_2$. A ^{1}H NMR was measured right after preparation, then the sample was heated to 35 °C in a water bath and additional spectra were acquired at intervals (Figure S6).

Figure S6. ^{1}H NMR spectra for conditions in Scheme S1b.

4.5.3.2.3 Using DTBP in HFIP (Scheme S1c)

Inside the glovebox an NMR tube was loaded with [Cp*Co(MeCN)$_3$](BF$_4$)$_2$ (3 mg, 6.11 μmol), *N*-pyrimidinylindole (11.9 mg, 61.1 μmol) and 2,6-Di-*tert*-butylpyridine (6.6 μL, 30.6 μmol). The tube was then taken out and connected to the Schlenk like via an adaptor and cooled down to −35 ºC. The mixture was then dissolved in 0.6 mL of HFIP and an acetone-d_6 insert was placed inside the NMR. The reaction was kept at this temperature until transferred to the NMR instrument for measurement at 35 ºC (Figure S7).
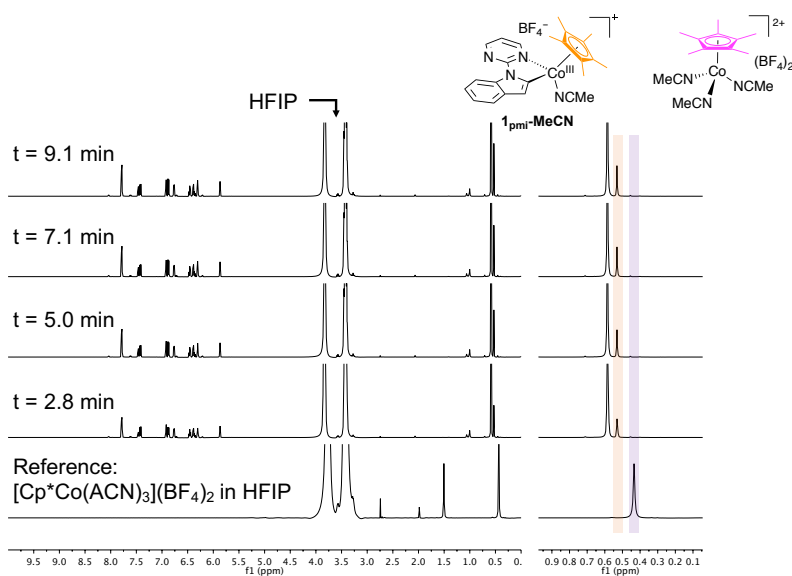
Figure S7. ^{1}H NMR spectra for conditions Scheme S1c.

4.5.3.2.4 Titration Experiment of [Cp*Co(MeCN)$_3$](BF$_4$)$_2$ with HFIP

Inside the glovebox, a glass vial was loaded with [Cp*Co(MeCN)$_3$](BF$_4$)$_2$ (10.1 mg, 0.020 mmol) and dissolved in 1.00 mL of anhydrous CD$_2$Cl$_2$. Of this solution 0.50 mL (0.01 mmol) were transferred to a screw-cap NMR tube and 2 µL of MeCN were added. The tube was sealed with a cap with septum (titration tube). The remaining of the parent solution was transferred to a regular NMR tube and 50 µL of HFIP were added before closing the tube (Co-blank tube). A third tube was filled with 0.50 mL of CD$_2$Cl$_2$, 2 µL MeCN and 50 µL of HFIP and then closed (MeCN-blank tube). The ^{1}H NMR spectrum at RT of the solutions contained in all tubes were measured. HFIP was added to the titration tube in steps with a microsyringe and the spectrum of the resulting mixtures were measured (Figure S8).
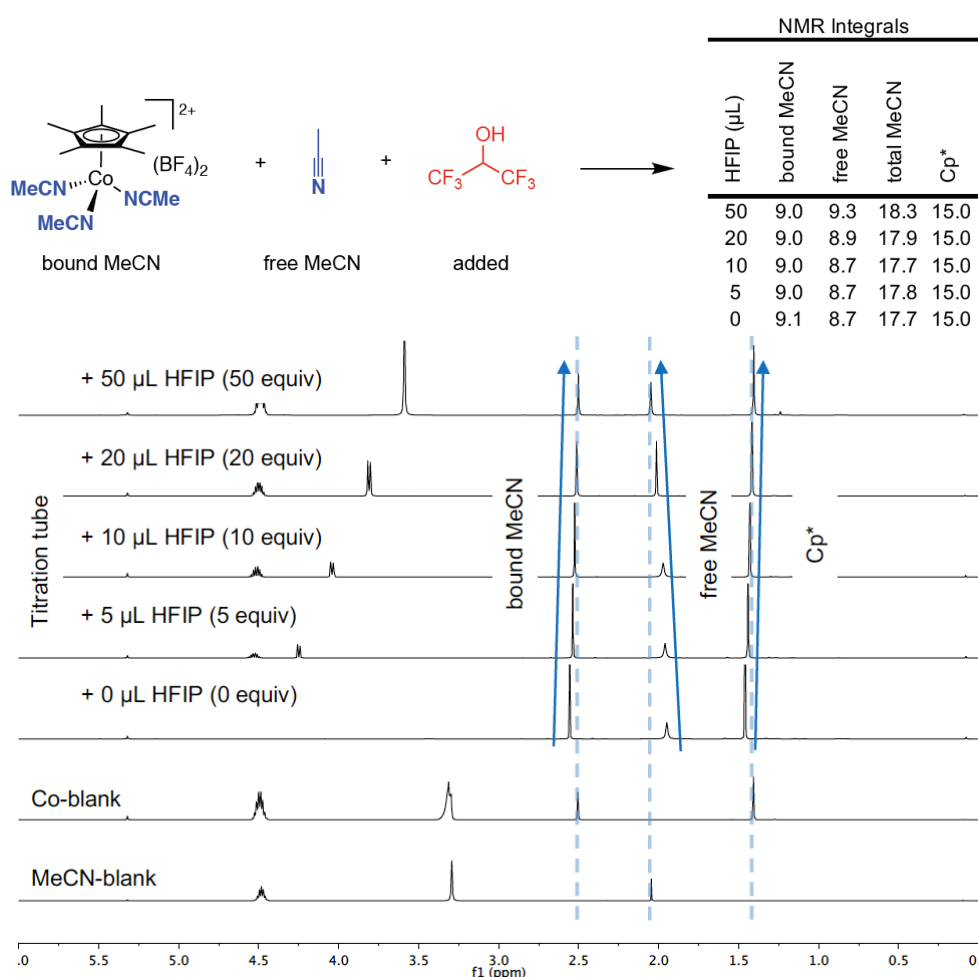

HFIP (µL)	bound MeCN	free MeCN	total MeCN	Cp*
50	9.0	9.3	18.3	15.0
20	9.0	8.9	17.9	15.0
10	9.0	8.7	17.7	15.0
5	9.0	8.7	17.8	15.0
0	9.1	8.7	17.7	15.0

Figure S8. ^{1}H NMR of the titration experiment of [Cp*Co(MeCN)$_3$](BF$_4$)$_2$.

The titration experiment shows no evidence of replacement of MeCN by HFIP in the cobalt complex. Moreover, the chemical shift of the signals in the titration tube after adding 50 μL of HFIP match the shifts observed in the blank tubes for both MeCN and [Cp*Co(MeCN)$_3$](BF$_4$)$_2$.

4.5.3.2.5 Effect of HFIP Concentration in the Formation of 1$_{pmi}$-MeCN Using DTBP as Base
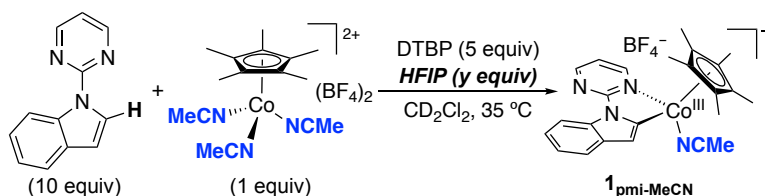
A crimped vial was loaded with [Cp*Co(MeCN)$_3$](BF$_4$)$_2$ (29.26 mg, 0.059 mmol) and 1,3,5-trimethoxybenzene (10.1 mg, 0.06 mmol). The solids were then dissolved in 3 mL of 1,2-dichloroethane to obtain a [0.02 M] stock solution. Then, outside the glove box, under argon atmopshere, *N*-pyrimidinylindole (19.4 mg, 0.099 mmol), was charged into 5 different NMR tubes. Then, 0.5 mL of the stock solution, followed by 2,6-Di-*tert*-butylpyridine (10.8 μL, 0.05 mmol) were added to each NMR tube. Then different amounts of HFIP (Table S1) were added to each NMR tube at −32 °C. The reaction was kept at this temperature until transferred to the NMR instrument for measurement at 35 °C. The formation of **1$_{pmi}$-MeCN** was monitored by ^{1}H NMR spectroscopy (Figure S9).

Table S1.

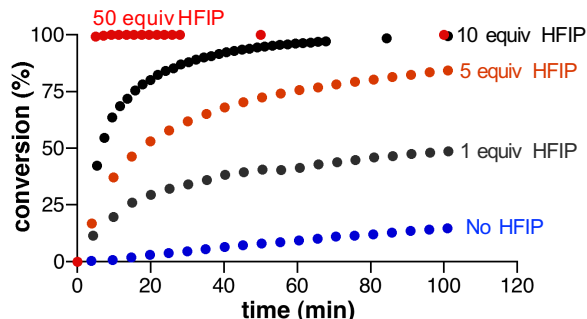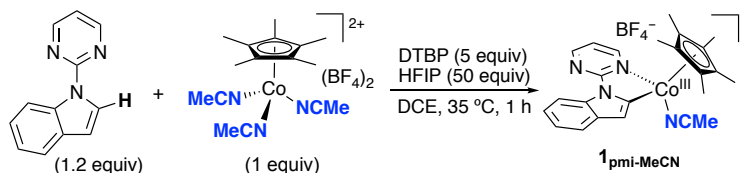| Tube	HFIP (μL)	HFIP (equiv)
1	52	50
2	10.5	10
3	5.2	5
4	1.1	1
5	0	0

Figure S9. Conversion vs. time plot for studying the effect of HFIP in the access of **1$_{pmi}$-MeCN** using DTBP as base.

4.5.3.2.6 Isolation of 1$_{pmi}$-MeCN

Under an argon atmosphere, [Cp*Co(MeCN)$_3$](BF$_4$)$_2$ (0.122 mmol) is placed inside a Schlenk flask together with *N*-pyrimidinylindole (0.244 mmol, 2 equiv) and 2,6-Di-*tert*-butylpyridine (137 µL, 0.611 mmol, 5 equiv). The mixture is suspended in 6 mL of DCE and then HFIP (643 µL, 6.11 mmol) is added. After closing the Schlenk flask, the mixture is heated at 35 °C for 1 h. The reaction is then cooled down and concentrated to about 2 mL under reduced pressure followed by addition of 20 mL of diethylether causing the precipitation of an orange solid, which was washed once with 10 mL of diethylether and dried under high vacuum. Sodium acetate (10.53 mg, 0.128 mmol) was added followed by 6 mL of acetonitrile. The mixture was stirred for 30 minutes, then concentrated to about 2 mL under reduced pressure followed by addition of 20 mL of diethylether causing the precipitation of an orange solid, the supernatant is then filtered off. The solid is then disolved in dichloromethane, filtered and precipitated again with another 20 mL of diethylether. The obtained orange solid was washed three times with 10 mL of diethylether and dried under high vacuum affording 54.4 mg (91%) of the pure product as an orange solid.

4.5.3.2.7 Characterization of 1$_{pmi}$-MeCN
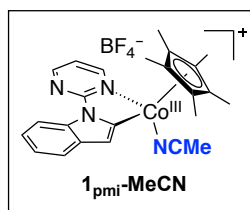
^{1}H NMR (500 MHz, CDCl$_3$, 25 °C): δ 9.45 (dd, J = 5.7, 2.2 Hz, 1H), 8.69 (dd, J = 4.6, 2.2 Hz, 1H), 8.43 (dd, J = 8.1, 0.9 Hz, 1H), 7.55 − 7.51 (m, 1H), 7.32 (dd, J = 5.8, 4.7 Hz, 1H), 7.24 (td, J = 7.9, 1.5 Hz, 1H), 7.16 (ddd, J = 8.3, 7.2, 1.2 Hz, 1H), 7.12 (d,8 J = 0.8 Hz, 1H), 2.24 (s, 3H), 1.53 (s, 15H).
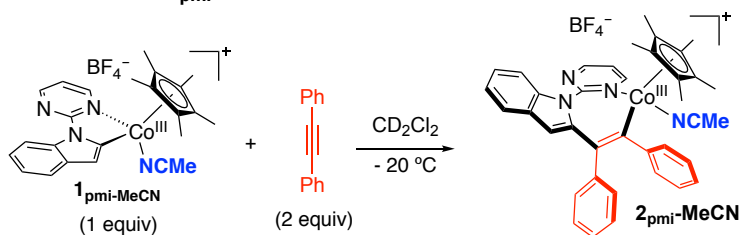
^{13}C NMR (126 MHz, CDCl$_3$, 25 °C): δ 163.1, 160.9, 160.4, 157.9, 137.7, 135.0, 130.0, 123.0, 121.4, 117.8, 116.6, 116.4, 113.6, 97.2, 9.7, 4.4.

^{19}F NMR (376 MHz, CDCl$_3$, 25 °C): δ −152.2 (s).

**HRMS-ESI** (m/z): [M−MeCN]$^+$ calcd for C$_{22}$H$_{23}$CoN$_3$, 388.1218; Found, 388.1205.

4.5.4 Stoichiometric Reactions Using 1$_{pmi}$-MeCN

4.5.4.1 Formation of 2$_{pmi}$-MeCN

Inside the glovebox an NMR tube was loaded with **1$_{pmi}$-MeCN** (5.1 mg, 0.01 mmol) and diphenylacetylene (3.5 mg, 0.02 mmol). The tube was then taken out and connected to the Schlenk like *via* an adaptor and cooled down to −35 °C. Then the solid was then dissolved in 0.5 mL of CD$_2$Cl$_2$. The reaction was kept at this temperature until transferred to the NMR instrument for measurement at −20 °C. After 1h at this temperature, total conversion to **2$_{pmi}$-MeCN** was observed.

4.5.4.2 Characterization of 2$_{pmi}$-MeCN
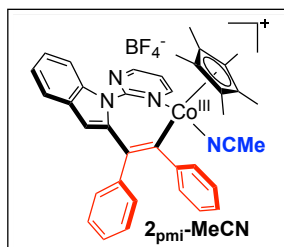
**^{1}H NMR** (500 MHz, CDCl$_3$, − 20 °C): δ 9.49 (dd, J = 6.0, 2.2 Hz, 1H), 8.95 (dd, J = 4.6, 2.2 Hz, 1H), 7.74 (t, J = 5.2 Hz, 1H), 7.50 (overlapped peak, 1H), 7.43 (d, J = 7.6, 1H), 7.40 − 7.23 (overlapped peak, 2H), 7.25 − 7.18 (m, 3H), 7.09-7.00 (m, 4H), 6.88 (t, J = 7.4 Hz, 1H), 6.74 (t, J = 7.5 Hz, 1H), 6.19 (s, 1H), 5.95 (d, J = 7.7 Hz, 1H), 1.88 (s, 3H), 1.08 (s, 15H).

^{13}C NMR (126 MHz, CD$_2$Cl$_2$, −20 °C) δ 165.2, 164.9, 161.3, 160.3, 153.0, 145.6, 143.5, 139.5, 139.0, 132.6, 129.4, 127.8, 127.6, 127.6, 127.5, 127.1, 124.5, 123.8, 123.2, 120.8, 120.7, 113.8, 110.8, 97.1, 9.4, 3.8.

^{19}F NMR (376 MHz, CDCl$_3$, −20 °C): δ −151.67 (s).

HRMS-ESI (m/z): [M−MeCN]$^+$ calcd for C$_{36}$H$_{33}$CoN$_3$, 566.2006; Found, 566.2009.

4.5.4.3 Stoichiometric Formation of 3$_{pmi}$ and 4$_{pmi}$
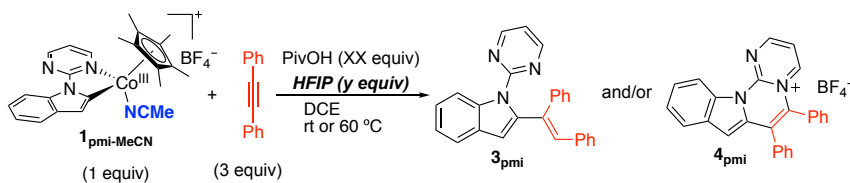
Stock solutions were prepared inside the glovebox as follows: **Solution A**: A glass vial was loaded with **1$_{pmi}$-MeCN** (45.5 mg, 0.088 mmol) and 1,3,5-trimethoxybenzene as internal standard (15.6 mg, 0.093 mmol). The solids were then dissolved in 3.6 mL of DCE. **Solution B:** A glass vial was loaded with diphenylacetylene (48.1 mg, 0.324 mmol) and dissolved in 1.80 mL of DCE. **Solution C:** A glass vial was loaded with pivalic acid (51.0 mg, 0.485 mmol) and dissolved in 1 mL of DCE. NMR tubes, containing an acetone-d_6 capillary for NMR lock, were prepared according to **Table S2**. Then the tubes were sealed and taken out of the glovebox for monitoring by ^{1}H NMR. At times longer than 1 h, we started to observe a complex mixture by ^{1}H NMR, therefore compositions after 1h are used for analysis (Figures S10-12).

Table S2

Tube	Solution A (mL)	Solution B (mL)	Solution C (mL)	Temperature (° C)	DCE (mL)	HFIP (mL)
1	0.40	0.2	0.2	rt	0	0
2	0.40	0.2	0.2	rt	0	0.06
3	0.40	0.2	0	rt	0.2	0
4	0.40	0.2	0	60 °C	0.2	0
5	0.40	0.2	0	60 °C	0.2	0.06

The composition of the reaction (Table S3) at a given time was calculated with the ratio of integrals for signals corresponding to the internal standard and the substance to be quantified.

Table S3   Yield of **3$_{pmi}$** and **4$_{pmi}$** (%) after 1 h.

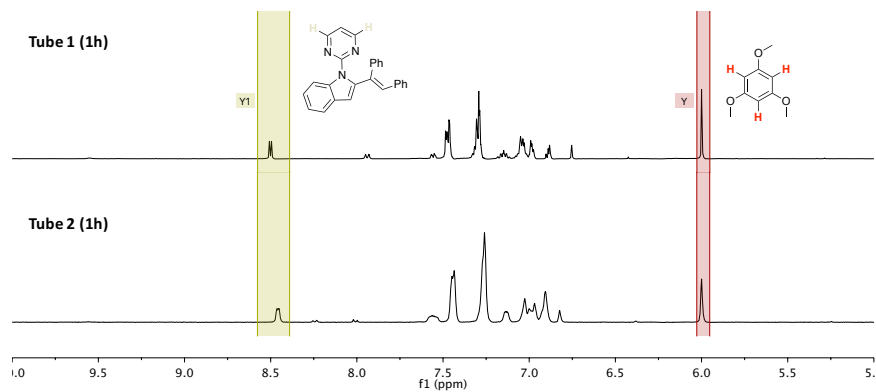| Product	Tube 1	Tube	Tube 3	Tube 4	Tube 5
3$_{pmi}$	85	97	0	6	46
4$_{pmi}$	0	0	0	34	29

Figure S10. ^{1}H NMR spectra measured for Tube 1 and Tube 2.
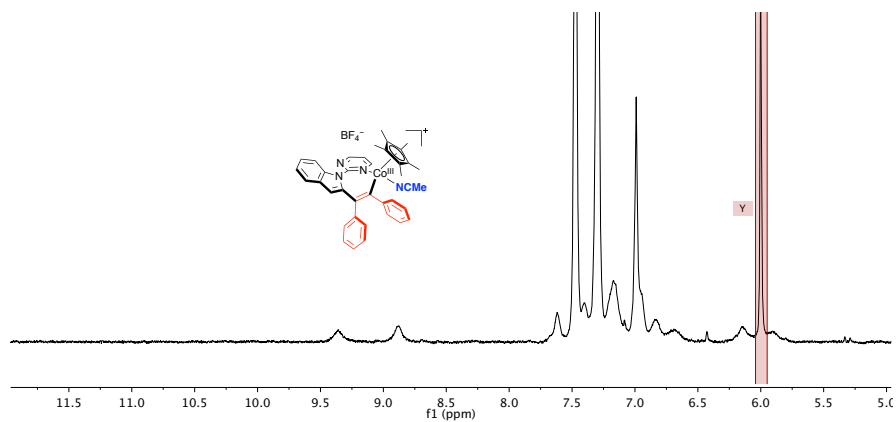

Figure S11. ^{1}H NMR spectrum measured for Tube 3.
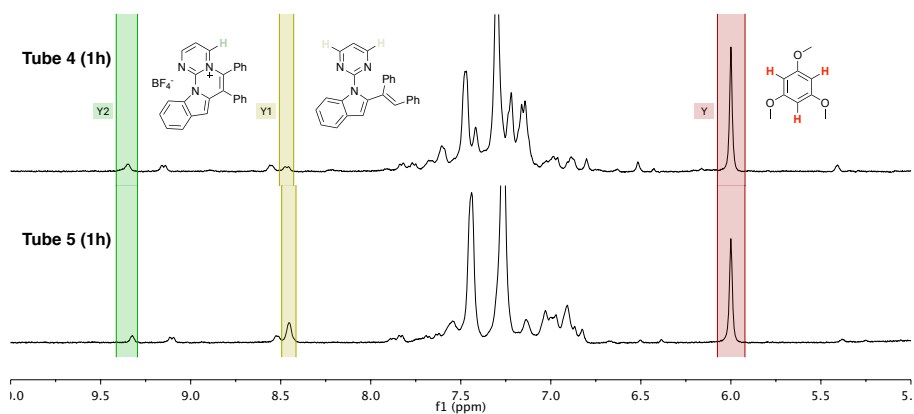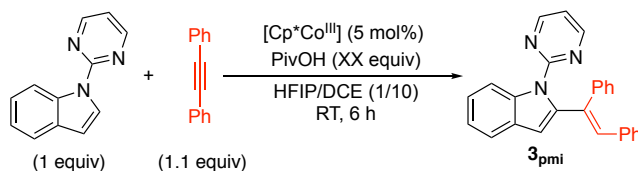

Figure S12. ^{1}H NMR spectra measured for Tube 4 and Tube 5.

4.5.5 Effect of HFIP Under Catalytic Conditions

4.5.5.1 Hydroarylation of Diphenylacetylene

4.5.5.1.1 NMR Monitored Reactions

Stock solutions were prepared inside the glovebox as follows: **Solution A**: A glass vial was loaded with *N*-pyrimidinylindole (29.2 mg, 0.149 mmol), diphenylacetylene (30.1 mg, 0.169 mmol), 1,3,5-trimethoxybenzene as internal standard (24.8 mg, 0.147 mmol) and [Cp*Co(ACN)$_3$](BF$_4$)$_2$ (3.5 mg, 0.007 mmol). The solids were then dissolved in 1.80 mL of DCE. **Solution B:** A glass vial was loaded with pivalic acid (22.6 mg, 0.221 mmol) and dissolved in 1.80 mL of DCE. NMR tubes containing an insert of acetone-d_6 were prepared according to **Table S4**. Then the tubes were sealed and taken out of the glovebox for monitoring by ^{1}H NMR at intervals (Figures S13-16).

Table S4

Tube	Solution A (mL)	Solution B (mL)	DCE (mL)	HFIP (mL)	PivOH (equiv)
1	0.30	0.00	0.30	0.06	0.00
2	0.30	0.10	0.26	0.00	0.49
3	0.30	0.10	0.20	0.06	0.49
4	0.30	0.30	0.00	0.06	1.48

The composition of the reaction (Table S5) at a given time was calculated with the ratio of integrals for signals corresponding to the internal standard and the substance to be quantified.

Table S5. Yield of **3$_{pmi}$** (%)

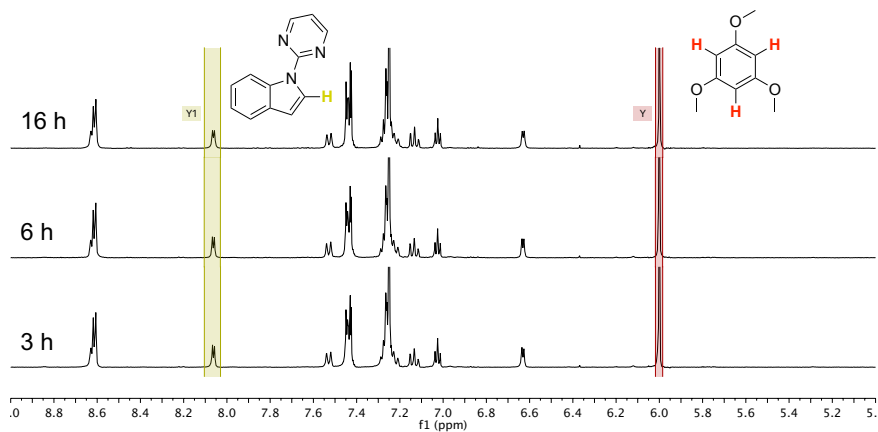| Tube	Time (h)		
	3	**6**	**16**
1	0	0	0
2	5	12	29
3	22	50	97
4	48	86	97

Figure S13. ^{1}H NMR spectra measured for Tube 1.

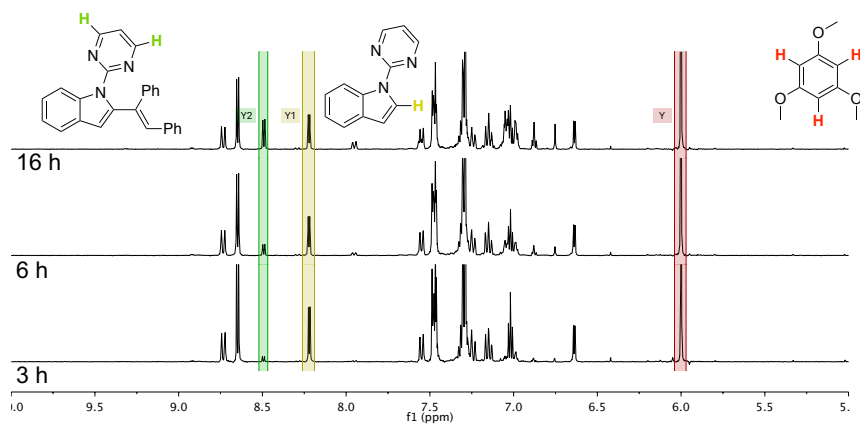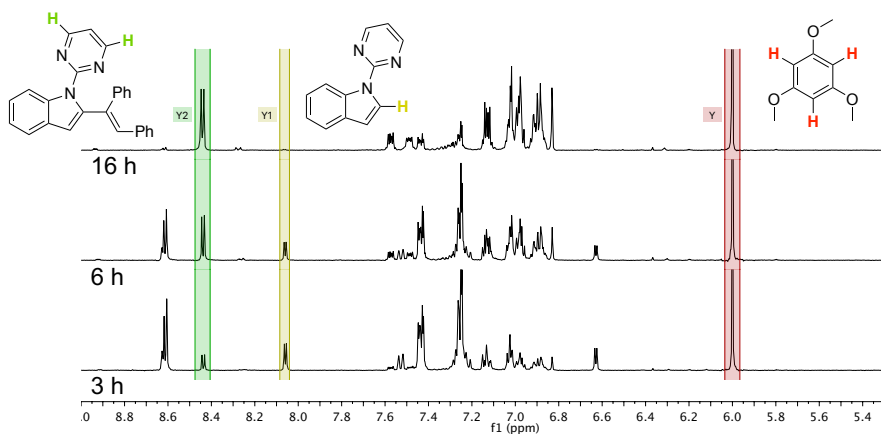**Figure S14.** ^{1}H NMR spectra measured for Tube 2.
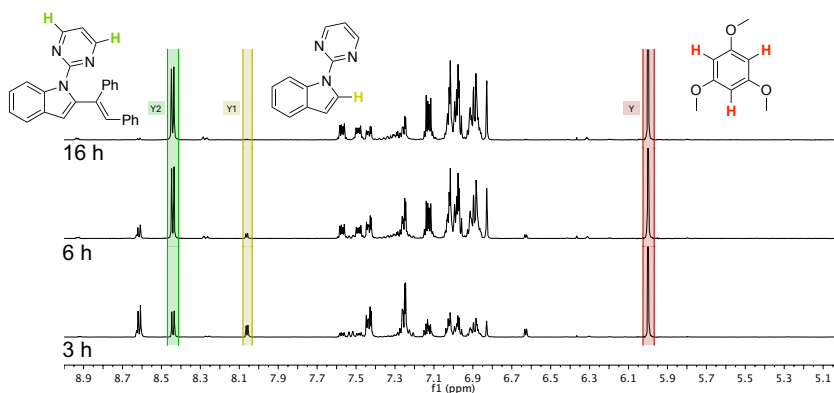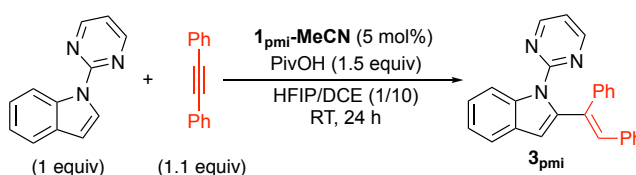

Figure S15. ^{1}H NMR spectra measured for Tube 3.

Figure S16. ^{1}H NMR spectra measured for Tube 4.

4.5.5.1.2 Preparative Scale Reaction

In a glass vial were weighed *N*-pyrimidinylindole (39.2 mg, 0.2 mmol), diphenylacetylene (39.7 mg, 0.22 mmol) and pivalic acid (30.8 mg, 0.3 mmol). The vial was transferred to the glovebox and **1**$_{pmi}$-**MeCN** (5.3 mg, 0.01 mmol) and DCE (2mL) were added to the mixture. The vial was crimped inside the box. Outside the glovebox, HFIP (200 µL) was added with a Hamilton syringe and the vial was left stirring at room temperature. After 24 h, the solution was removed with a rotatory evaporator and the remaining crude was purified by column chromatography on silica (Hexane:Ethyl acetate 90/10) to yield 72.6 mg (98%) of a yellow solid.

4.5.5.2 Oxidative Annulation
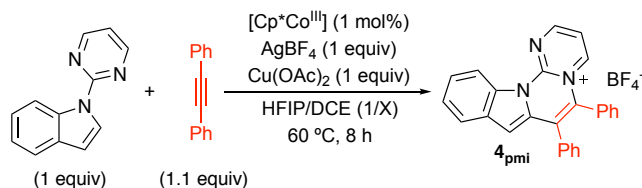
The reported procedure by Lao *et al.*[5] was adapted for the synthesis of the annulated product, with some changes: In a glass vial were weighted *N*-pyrimidinylindole (39.0 mg, 0.2 mmol) and diphenylacetylene (39.2 mg, 0.22 mmol). The vial was transferred to the glovebox and Cu(OAc)$_2$ (36.3 mg, 0.2 mmol), the [Cp*Co^{III}] catalyst (0.002 mmol) and AgBF$_4$ (38.9 mg, 0.2 mmol) were added to the mixture. The vial was crimped and outside the glove box DCE (2.0 mL) and HFIP were added. The resulting reaction mixture was stirred outside the glove box at the temperature and time described in **Table S6**. After cooling down to room temperature, the reaction mixture was then purified by passing it through a silica pad and washed with DCE. After removing the solvent, the remaining crude was washed with hexane (3 x 10 mL) and decantated to yield the desired product as a red solid.
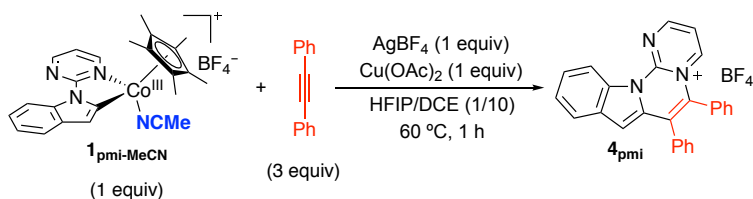
Table S6. Oxidative alkyne annulation reactions.

Entry	Catalyst	HFIP/DCE (ratio)	Yield (%)[a]
1	[Cp*Co(MeCN)$_3$][BF$_4$]$_2$	No HFIP	4
2	[Cp*Co(MeCN)$_3$][BF$_4$]$_2$	1/100	13
3	[Cp*Co(MeCN)$_3$][BF$_4$]$_2$	1/10	83
4	**1$_{pmi}$-MeCN**	1/10	91

[a] Isolated product.

[5] Lao, Y.-X.; Zhang, S.-S.; Liu, X.-G.; Jiang, C.-Y.; Wu, J.-Q.; Li, Q.; Huang, Z.-S.; Wang, H. *Adv. Synth. Catal.* **2016**, *358*, 2186–2191.

4.5.5.2.1 Stoichiometric Oxidative Annulation

Inside the glovebox an NMR tube was loaded with **1$_{pmi}$-MeCN** (5.1 mg, 0.01 mmol), diphenylacetylene (5.3 mg, 0.03 mmol), 1,3,5-trimethoxybenzene (3.68 mg, 0.02 mmol), AgBF$_4$ (1.9 mg, 0.01 mmol) and Cu(OAc)$_2$ (1.8 mg, 0.01 mmol). The mixture was dissolved in 0.5 mL of DCE followed by 60 µL of HFIP. The tube was then taken out and heated to 60 ºC. After 1h at this temperature, 97% yield was obtained. (measured by ^{1}H NMR).
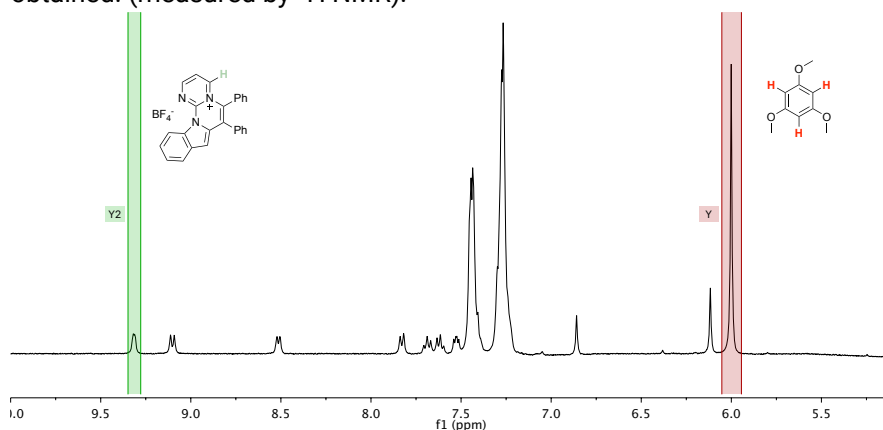

Figure S17. ^{1}H NMR spectrum for stoichiometric oxidative alkyne annulation.

4.5.6 Single Crystal X-Ray Structure Determinations

Crystal preparation: Crystals of **1$_{pmi}$-MeCN**, **2$_{pmi}$-MeCN** and **S1** were grown at −32 °C by liquid/liquid diffusion of *n*-hexane into a solution of the corresponding complex in CD_2Cl_2 or $CDCl_3$. The measured crystals were prepared under inert conditions immersed in perfluoropolyether as protecting oil for manipulation.

Data collection: Crystal structure determination of **S1** was carried out using a Apex DUO Kappa 4-axis goniometer equipped with an APPEX 2 4K CCD area detector, a Microfocus Source E025 IuS using MoK$_\alpha$ radiation (0.71073 Å), Quazar MX multilayer Optics as monochromator and a Oxford Cryosystems low temperature device Cryostream 700 plus (*T* = -173 °C). Full-sphere data collection was used with ω and φ scans. *Programs used:* Data collection APEX-2,[6] data reduction Bruker Saint[7] V/.60A and absorption correction SADABS.[8]

Crystal structure determination for compounds **1$_{pmi}$-MeCN** and **2$_{pmi}$-MeCN** were carried out using a Rigaku diffractometer equipped with a Pilatus 200K area detector, a Rigaku MicroMax-007HF microfocus rotating anode with MoK$_\alpha$ radiation, Confocal Max Flux optics and an Oxford Cryosystems low temperature device Cryostream 700 plus (*T* = -173 °C). Full-sphere data collection was used with ω and φ scans. *Programs used:* Data collection and reduction with CrysAlisPro[9] V/.60A and absorption correction with Scale3 Abspack scaling algorithm.[10]

Structure Solution and Refinement: Crystal structure solution was achieved using the computer program SHELXT.[11] Visualization was performed with the program SHELXle.[12] Missing atoms were subsequently located from difference Fourier synthesis and added to the atom list. Least-squares refinement on F^2 using all measured intensities was carried out using the program SHELXL 2015.[13] All non-hydrogen atoms were refined including anisotropic displacement parameters.

Comments to the structures: Complex **1$_{pmi}$-MeCN:** The asymmetric unit contains one molecule of the metal complex coordinated to an acetonitrile molecule and one BF_4^- anion. The Cp*-ligand is disordered in two orientations (ratio: 55:45). The BF_4^- anion is disordered in three orientations (ratio: 69:19:12). **2$_{pmi}$-MeCN:** The asymmetric unit contains one molecule of the metal complex coordinated to an acetonitrile molecule, two disordered chloroform molecules

[6] Data collection with APEX II v2014.9-0. Bruker (2014). Bruker AXS Inc., Madison, Wisconsin, USA.

[7] Data reduction with Bruker SAINT+ version V8.35A. Bruker (2013). Bruker AXS Inc., Madison, Wisconsin, USA.

[8] SADABS: V2014/5 Bruker (2001). Bruker AXS Inc., Madison, Wisconsin, USA. Blessing, Acta Cryst. (1995) A51 33-38.

[9] Data collection and reduction with CrysAlisPro 1.171.39.12b (Rigaku OD, 2015).

[10] Empirical absorption corrrection using spherical harmonics implemented in Scale3 Abspack scaling algorithm, CrysAlisPro 1.171.39.12b (Rigaku OD, 2015).

[11] SHELXT; Sheldrick, G.M. *Acta Cryst*. **2015** A71, 3-8.

[12] SHELXle; C.B. Huebschle, G.M. Sheldrick & B. Dittrich; *J.Appl.Cryst.* (2011) 44, 1281-1284.

[13] SHELXL; Sheldrick, G.M. *Acta Cryst*. **2015** C71, 3-8.

(ratios of disorder: 53:24:23 and 75:25) and one BF_4^- anion. Complex **S1:** The asymmetric contains two molecules of the metal complex (1:0.5:0.5) and two SbF_6^- anions. The Cp* ligands are in all cases disordered in two orientations. The atoms located between the Cobalt atoms were identified after refinement as OH anions.

Table S7. Crystal Data and Structure Refinement for **1$_{pmi}$-MeCN**, **2$_{pmi}$-MeCN** and **S1**

| Compound	1$_{pmi}$-MeCN	2$_{pmi}$-MeCN	S1
Formula	$C_{24}H_{26}BCoF_4N_4$	$C_{80}H_{75.49}B_2Cl_{12}Co_2F_8N$	$C_{48}H_{74}Co_4F_{12}O_{10}Sb_2$
Solvents	None	2 x $CDCl_3$	None
Formula weight	516.23	1865.83	1518.29
Crystal size (mm³)	0.30 x 0.20 x 0.02	0.40 x 0.20 x 0.10	0.15 x 0.03 x 0.01
Crystal color	Blue	Brown	Blue
Temp (K)	100	100	100
Crystal system	monoclinic	orthorhombic	orthorhombic
Space group	*P2(1)/n*	*Pbca*	*P 2 2ab$_1$*
A (Å)	7.84710(10)	10.6146(2)	21.479(3)
B (Å)	15.3914(3)	19.1718(4)	35.804(4)
C (Å)	19.0890(3)	42.3233(7)	7.5313(9)
α (deg)	90	90	90
β (deg)	96.025(2)	90	90
γ (deg)	90	90	90
V (Å³)	2292.79(6)	8612.8(3)	5791.8(12)
Z	4	4	8
ρ (g/cm³)	1.495	1.439	1.741
μ (mm⁻¹)	0.801	0.822	2.129
θ_{max} (°)	32.176	30.520	30.188
Reflec. measured	24849	139258	75626
Unique reflection	6426 [R_{int} = 0.0186]	11381 [R_{int} = 0.0322]	11597 [R_{int} = 0.0959]
Absorpt. correct.	Multi-scan	Multi-scan	Empirical
Trans. min/max	0.757/0.984	0.709/0.922	0.753/0.979
Parameters/ restrains	502/1018	583/349	1286/2016
R1/wR2 [I>2σ(I)]	0.0301/0.0813	0.0472/0.1340	0.0535/0.0971
R1/wR2 [all data]	0.0366/0.0843	0.0542/0.1388	0.0995/0.1147
Goodness-of-fit (F²)	1.052	1.024	1.028
Peak/hole (e/Å³)	0.413/-0.432	0.740/-0.756	1.232/-0.921
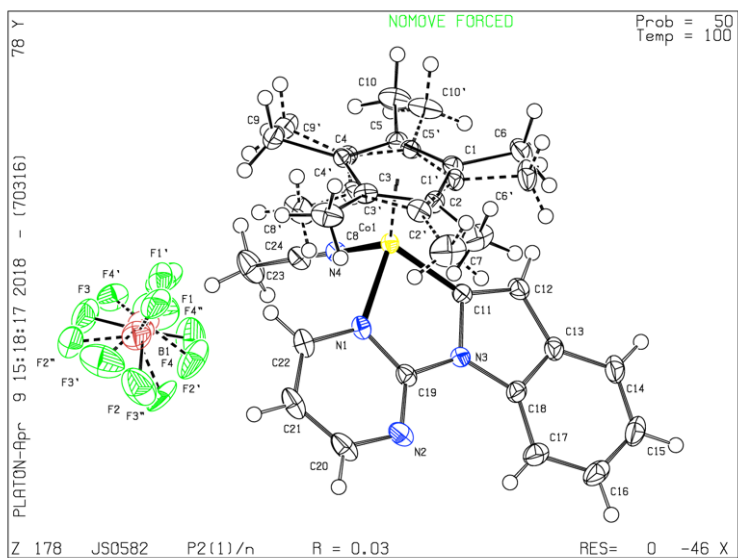
Figure S18. Solid state molecular structure of complex **1pmi-MeCN**.
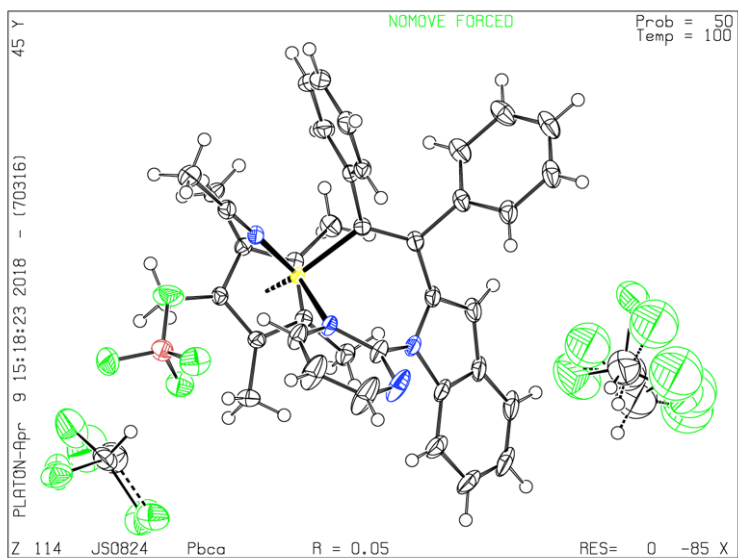
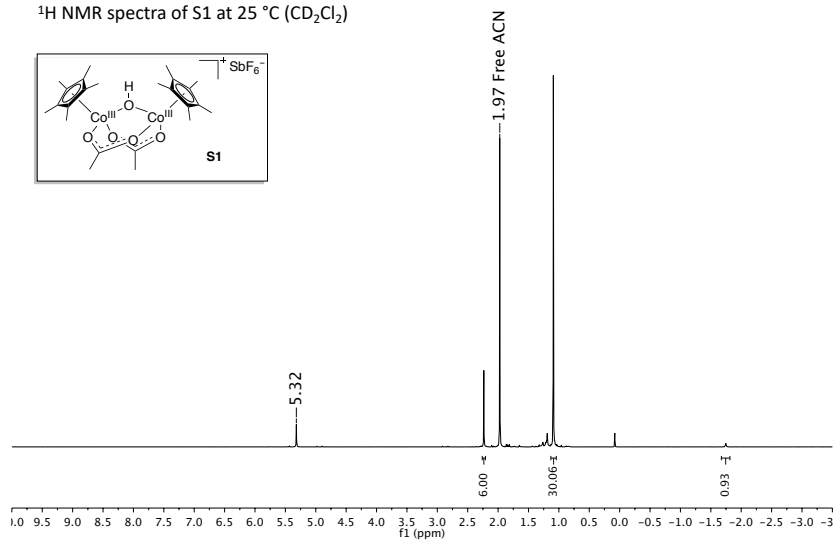**Figure S19.** Solid state molecular structure of cobaltacyle **2pmi-MeCN**.
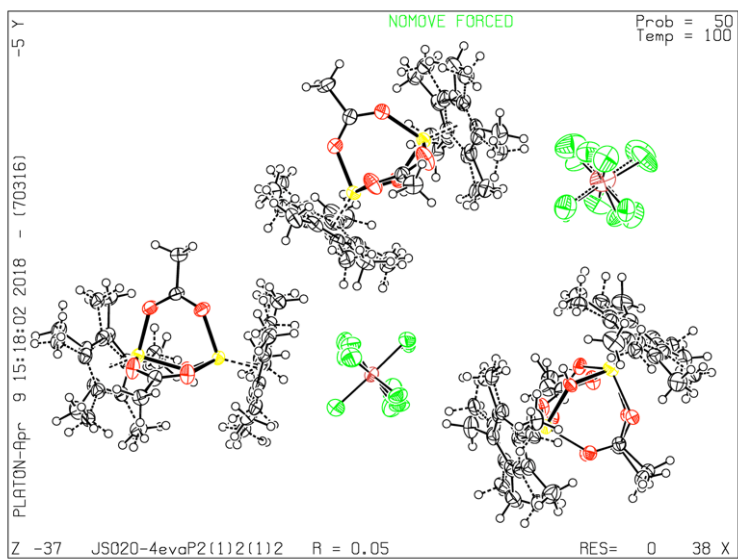
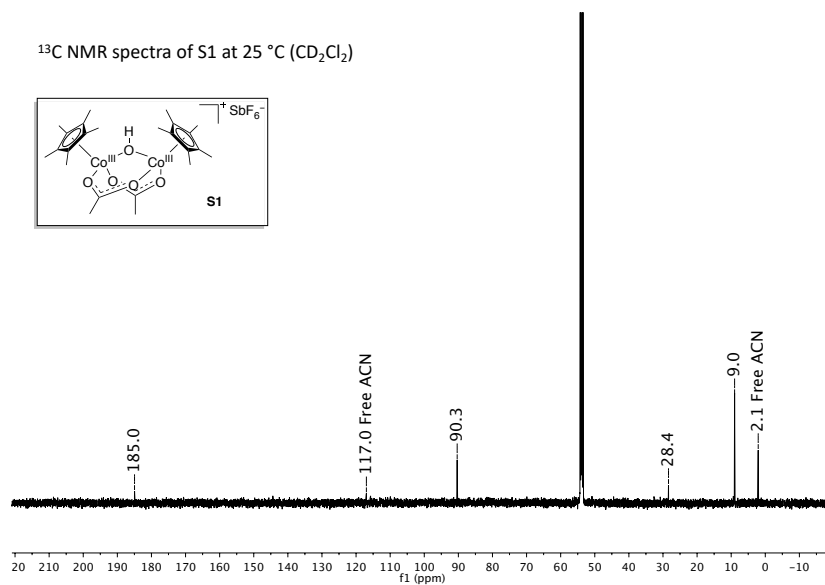**Figure S20.** Solid state molecular structure of cobaltacycle **S1**.

4.5.7 NMR Spectra

4.5.7.1 Complex S1
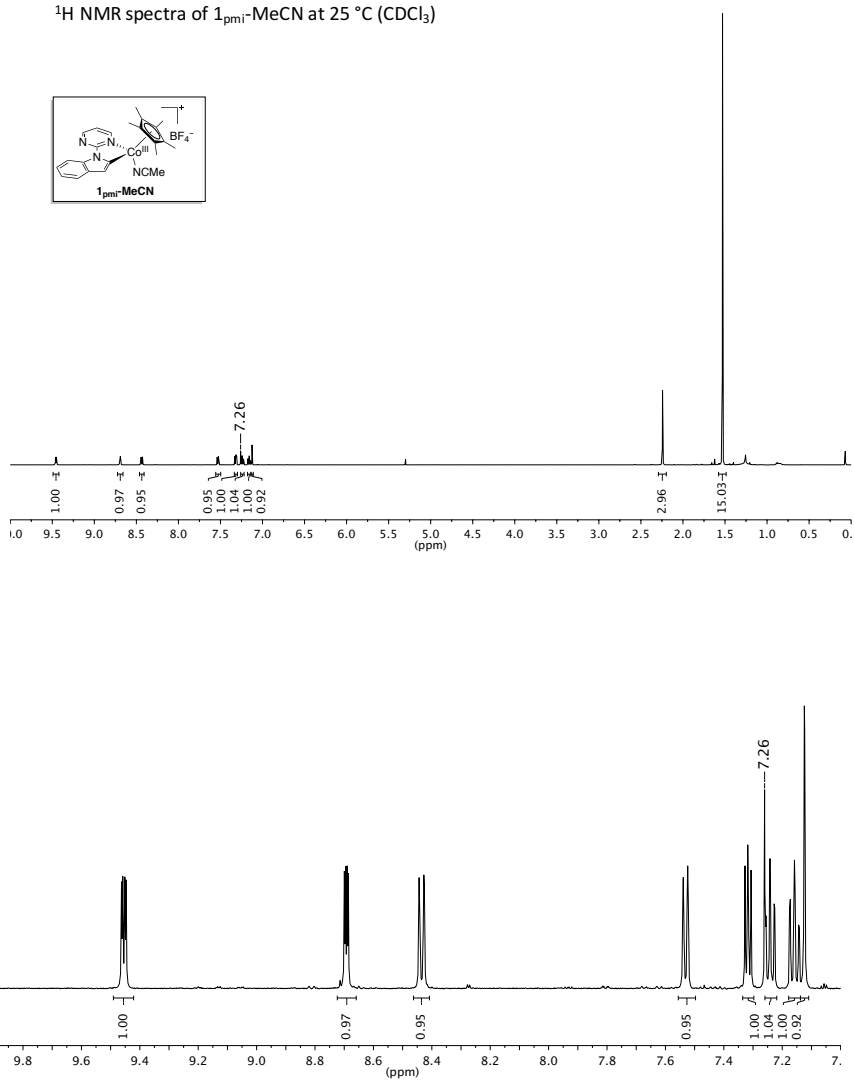
^{1}H NMR spectra of S1 at 25 °C (CD$_2$Cl$_2$)

^{13}C NMR spectra of S1 at 25 °C (CD$_2$Cl$_2$)

4.5.7.2 Complex 1$_{pmi}$-MeCN

¹H NMR spectra of 1$_{pmi}$-MeCN at 25 °C (CDCl₃)

^{13}C NMR spectra of 1$_{pmi}$-MeCN at 25 °C (CDCl$_3$)
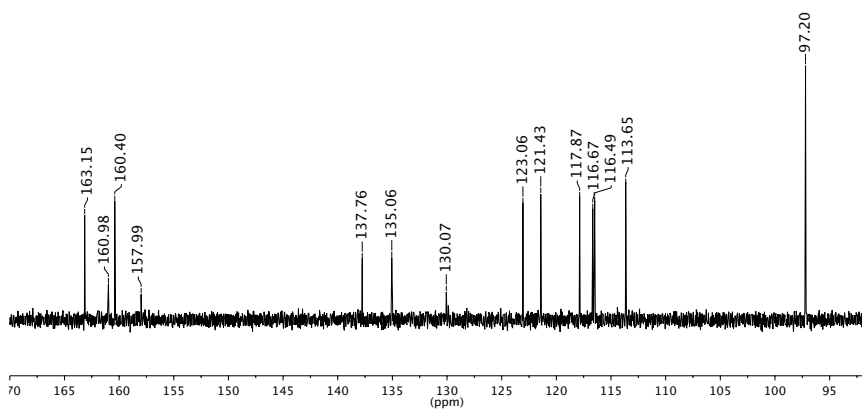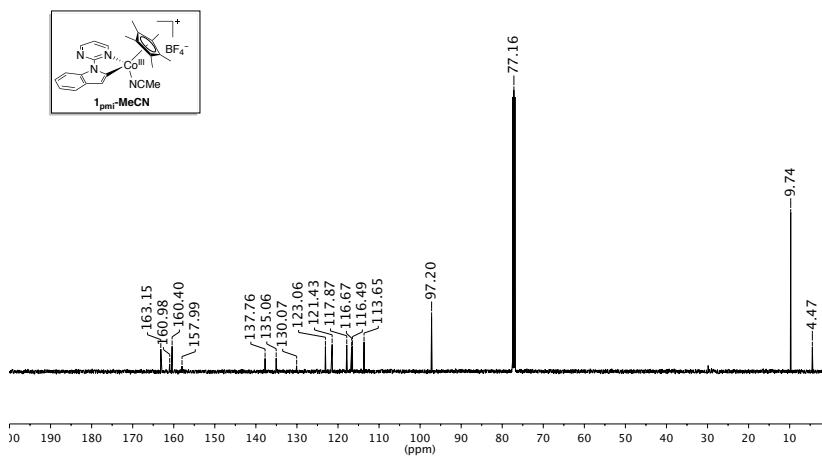
¹H-¹H COSY NMR spectra of 1_{pmi}-MeCN at 25 °C (CDCl₃)
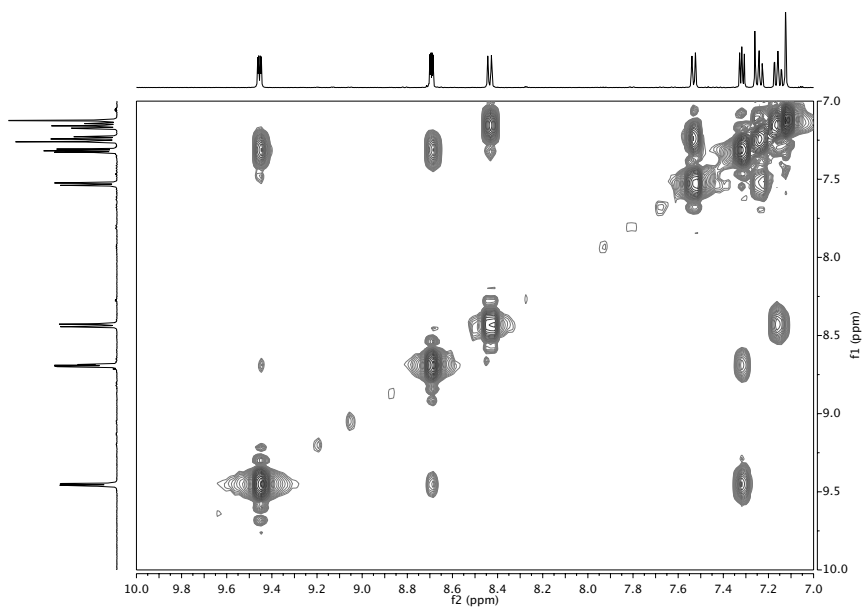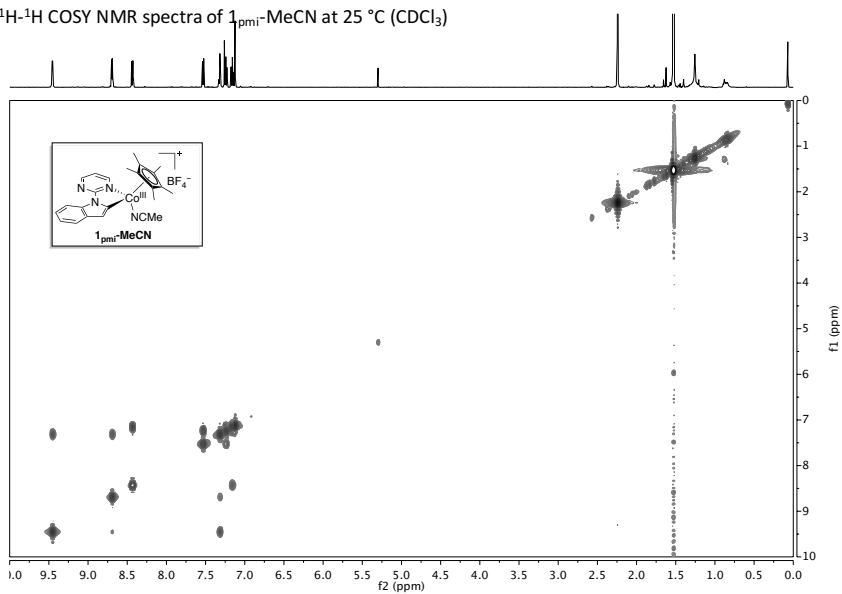
^{1}H-^{1}H TOCSY NMR spectra of 1_{pmi}-MeCN at 25 °C (CDCl$_3$)
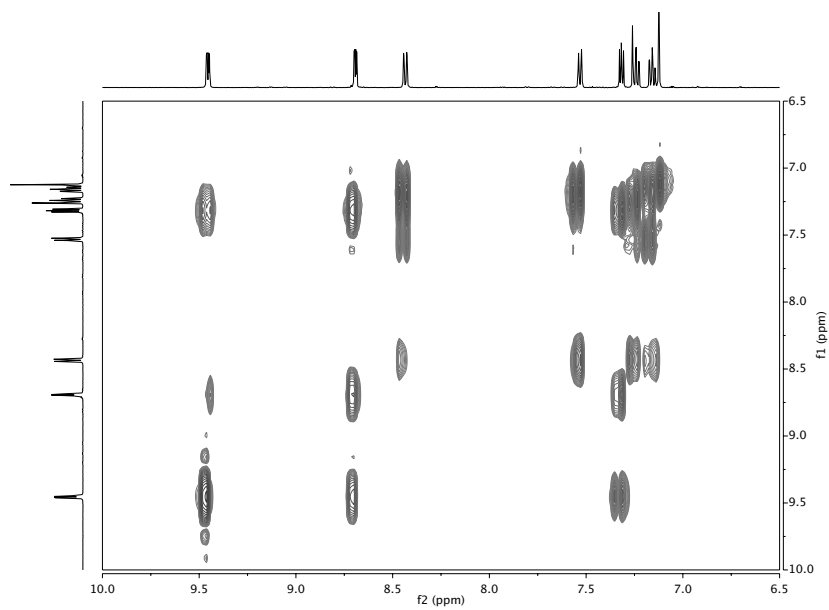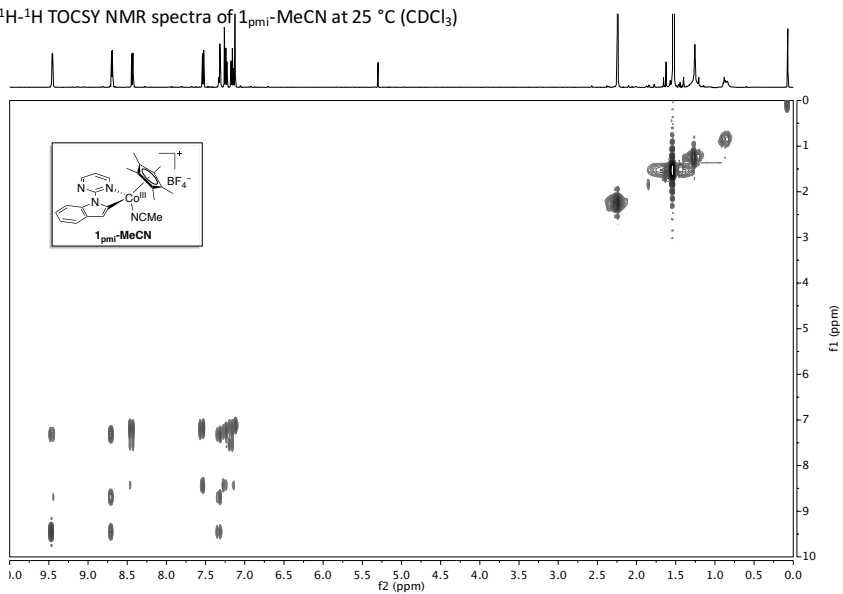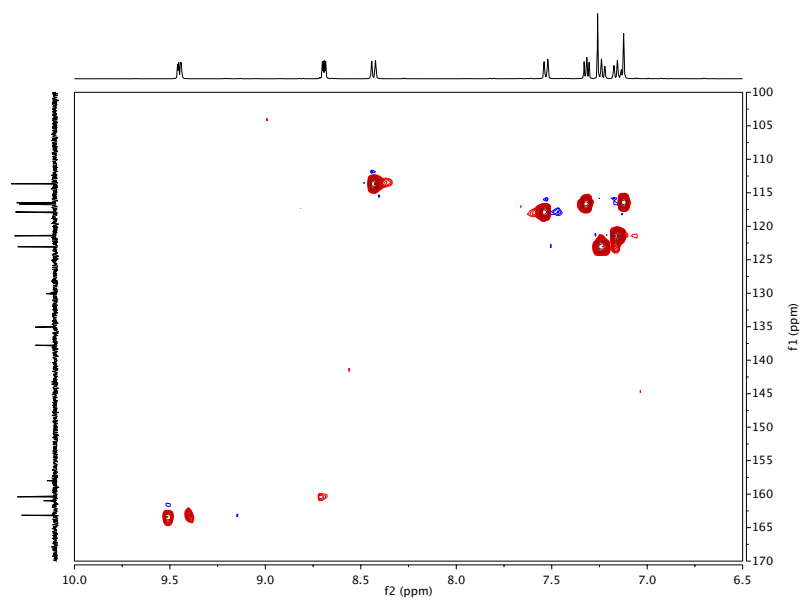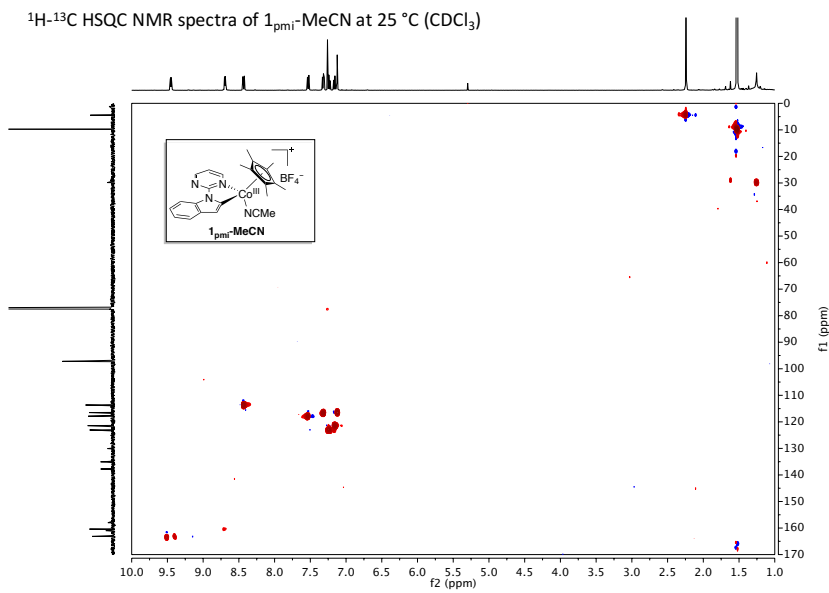
^{1}H-^{13}C HSQC NMR spectra of 1$_{pmi}$-MeCN at 25 °C (CDCl$_3$)

¹H-¹³C HMBC NMR spectra of 1$_{pmi}$-MeCN at 25 °C (CDCl₃)
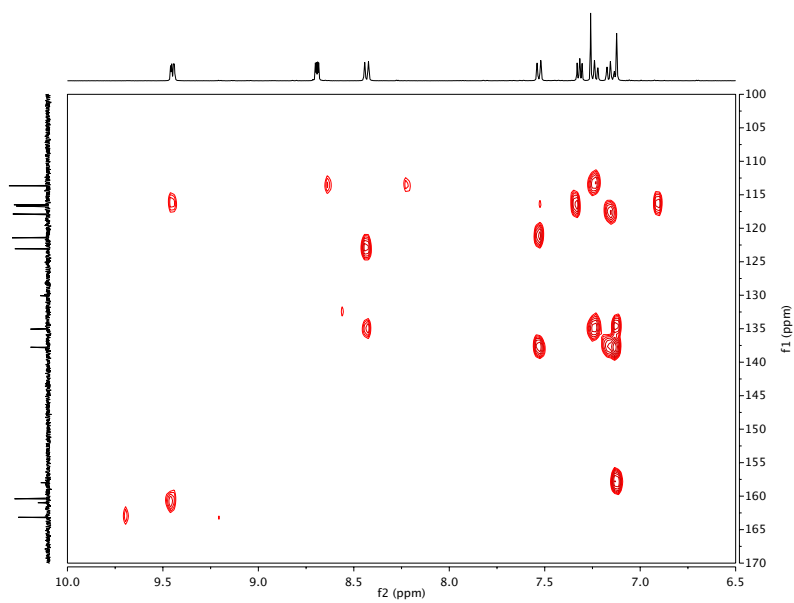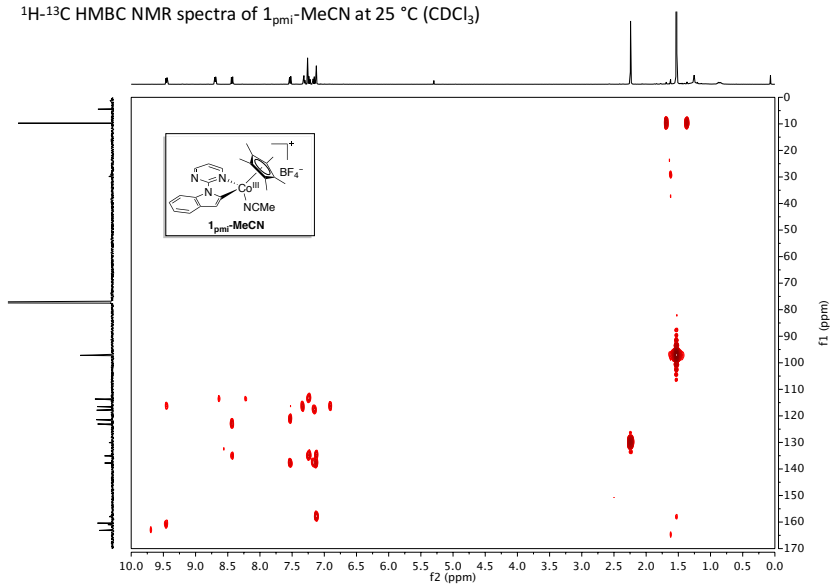
¹⁹F NMR spectra of 1_{pmi}-MeCN at 25 °C (CDCl₃)
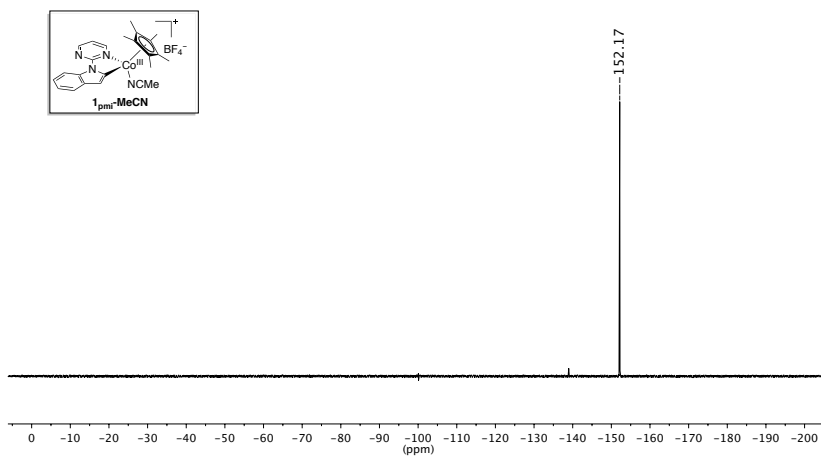
4.5.7.3 Complex 2$_{pmi}$-MeCN

^{1}H NMR spectra of 2$_{pmi}$-MeCN at −20 °C (CD$_2$Cl$_2$)
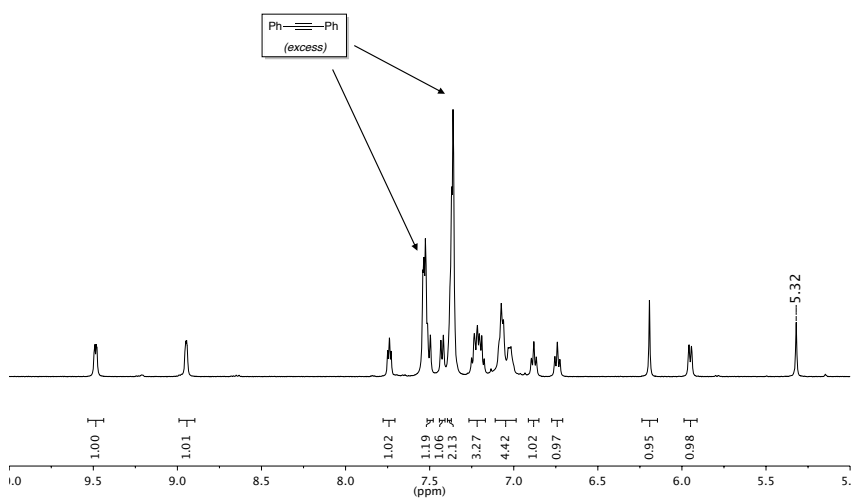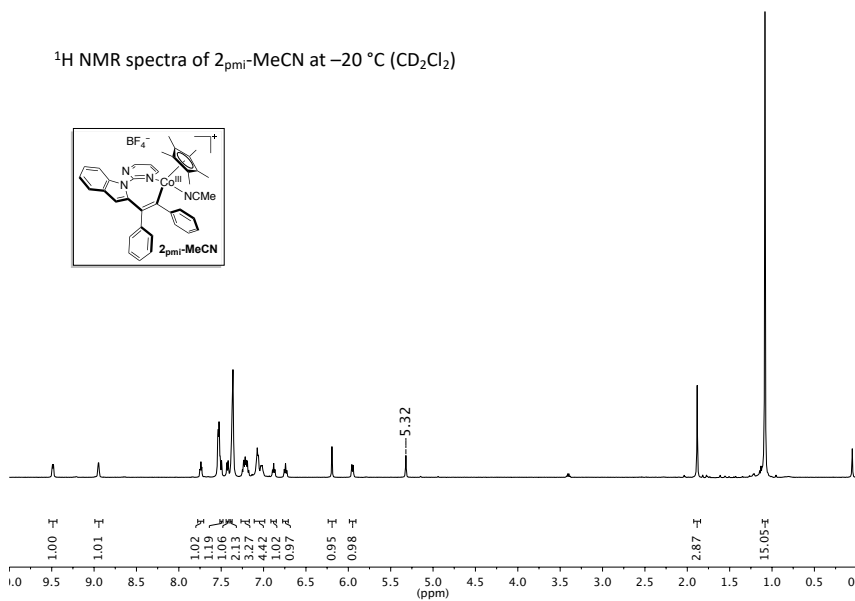
^{13}C NMR spectra of 2$_{pmi}$-MeCN$_4$ at −20 °C (CD$_2$Cl$_2$)
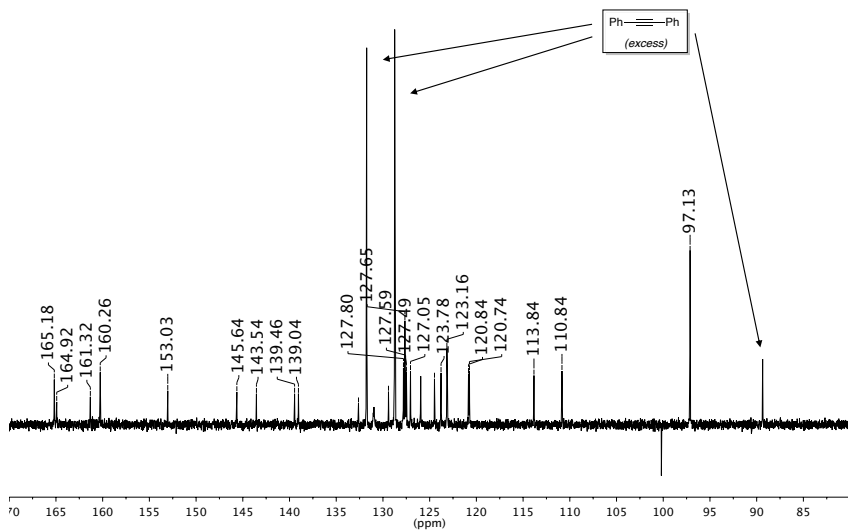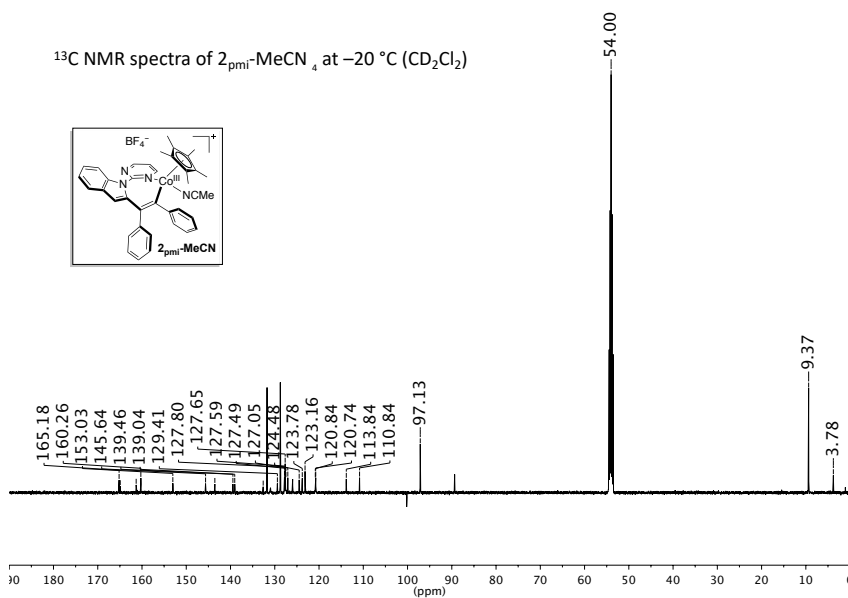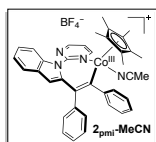
165.18
160.26
153.03
145.64
139.46
139.04
129.41
127.80
127.65
127.59
127.49
127.05
124.48
123.78
123.16
120.84
120.74
113.84
110.84
97.13
54.00
9.37
3.78

Ph———Ph
(excess)

165.18
164.92
161.32
160.26
153.03
145.64
143.54
139.46
139.04
127.80
127.65
127.59
127.49
127.05
123.78
123.16
120.84
120.74
113.84
110.84
97.13
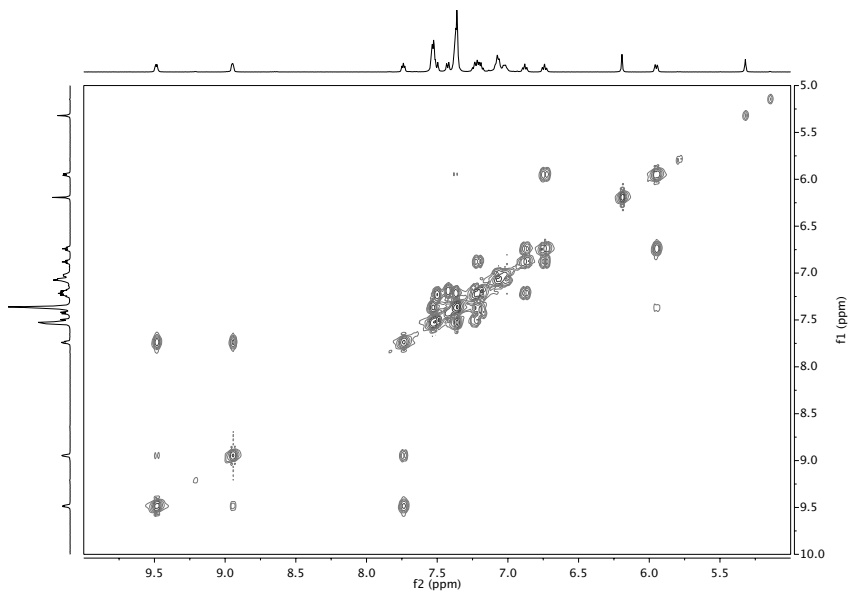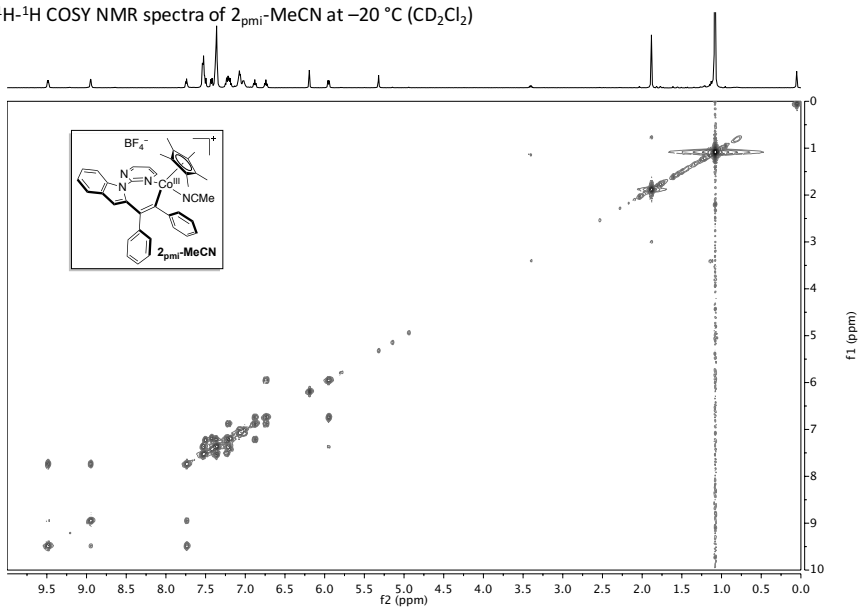
1H-1H COSY NMR spectra of 2$_{pmi}$-MeCN at −20 °C (CD$_2$Cl$_2$)
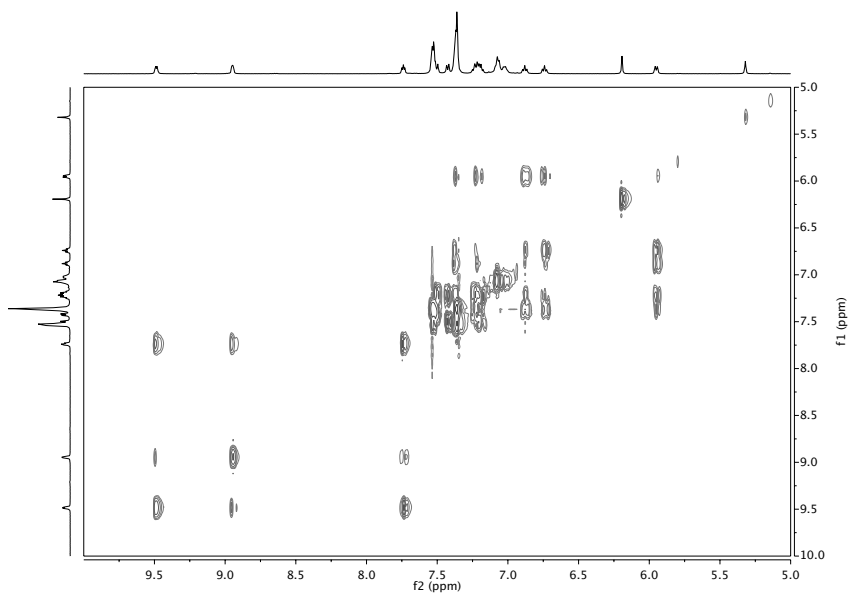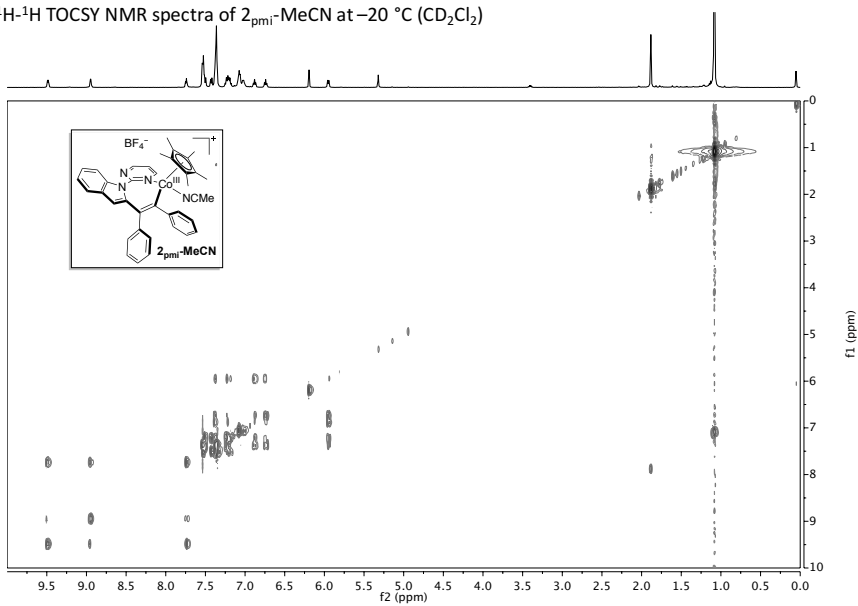
^{1}H-^{1}H TOCSY NMR spectra of 2_{pmi}-MeCN at −20 °C (CD$_2$Cl$_2$)

^{1}H-^{13}C HSQC NMR spectra of 2$_{pmi}$-MeCN at −20 °C (CD$_2$Cl$_2$)
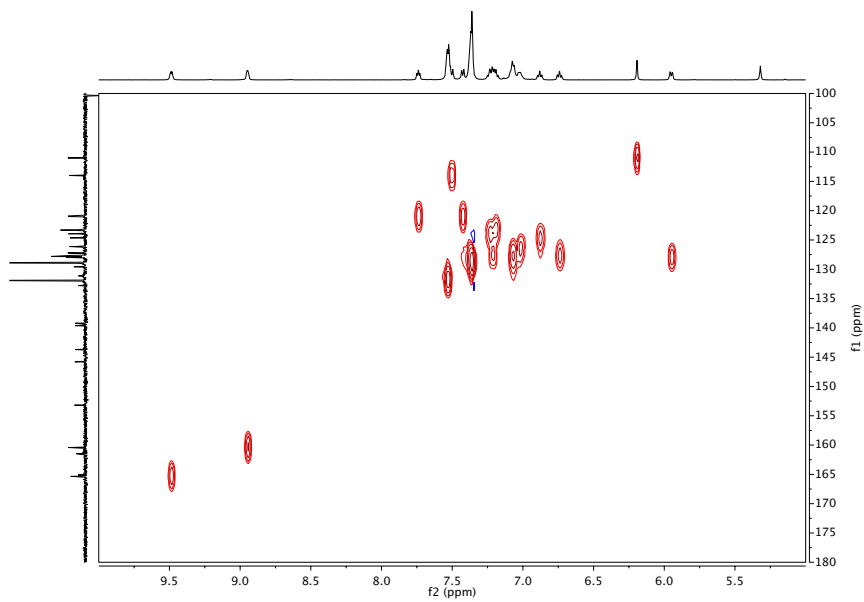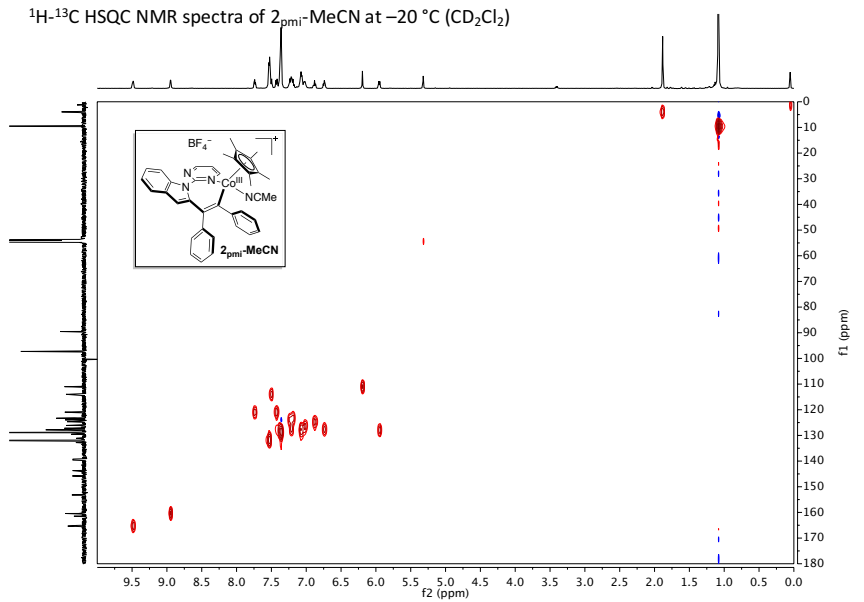
^{1}H-^{13}C HMBC NMR spectra of 2$_{pmi}$-MeCN at −20 °C (CD$_2$Cl$_2$)

¹⁹F NMR spectra of **2**_{pmi}-MeCN at −20 °C (CD$_2$Cl$_2$)
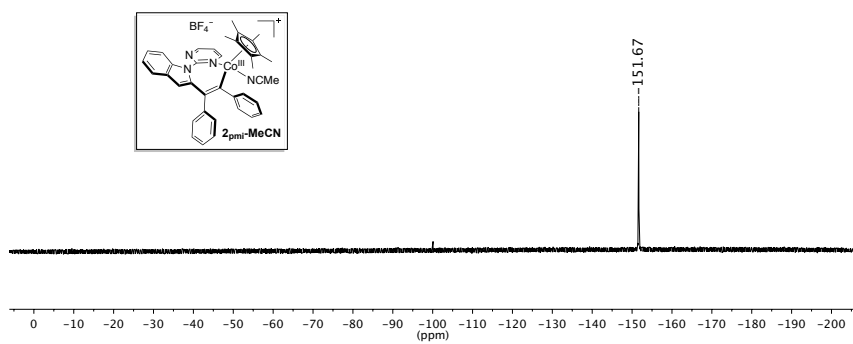
Chapter 5

General Conclusions

From this doctoral dissertation the following conclusions can be extracted:

1. A new and unprecedented synthetic route for the isolation of key Cp*Co^{III} metallacycles was discovered in **Article 1**. The oxidative addition of a C(sp^2)−I bond to a Cp*Co^I metal center afforded the desired metallacycle in excellent yields. For the first time, a direct analogue of a widely invoked cationic cobaltacycle, [Cp*Co^{III}(2ppy)(MeCN)](BF$_4$), was synthesized in an efficient manner, taking advantage of the extraordinary ability of acetonitrile to stabilize otherwise reactive intermediates.

2. Using the recently isolated [Cp*Co^{III}(2ppy)(MeCN)](BF$_4$) compound, a pioneering comprehensive mechanistic picture on the cobalt-catalyzed C−H oxidative alkyne annulation was given. That included the direct observation, under catalytic conditions, of a catalyst resting state and the improvement of the efficiency of the selected transformation. These experimental results support the intermediacy of this type of cyclometalated cobalt complexes in Cp*Co^{III}-catalyzed C−H functionalization processes.

3. The first mechanistic investigation on the migratory insertion of alkynes and alkenes into Cp*Co^{III}−C bonds have been performed in **Article 2**. This work revealed different insertion modes and insertion rates depending on the nature of the corresponding electrophile. The post-migratory insertion complexes were fully characterized by different analytical techniques.

4. Taking advantage of the unique stabilizing capability of MeCN, the reversible nature of the C−H activation step was surmounted in **Article 3**. Thanks to this, access to two of the most widely invoked cationic cobaltacycles (i.e. [Cp*Co^{III}(2ppy)(MeCN)](BF$_4$) and [Cp*Co^{III}(Npmi)(MeCN)](BF$_4$) was described.

5. The accelerating effect of HFIP in the Cp*Co^{III}-mediated C−H cyclometalation was discovered. Further studies showed the crucial influence of HFIP for designing more efficient processes, such as Cp*Co^{III}-catalyzed oxidative annulations and the hydroarylation of alkynes.

Annex *I*

Capturing Thermodynamically Unfavoured Weakly-Coordinated Cp*Co^{III} Cobaltacycles

This annex is dedicated to briefly summarize other collaborative project that has been performed during this doctoral thesis but is not discussed in detail in the main text.

Annex I. Capturing Thermodynamically Unfavored Weakly-coordinated Cp*Co^{III} metallacycles

In **Article 1**, we uncovered the potential of oxidative addition synthetic routes for accessing Cp*Co^{III} metallacycles containing strong σ-donor nitrogen-based directing group. Inspired by these results we applied the same strategy for accessing previously inaccessible metallacyclic Cp*Co^{III} complexes supported by weakly-chelating moieties (e.g. ketones, aldehydes, amides or esters). We used these complexes as platform for capturing direct analogues of putative key cationic transient intermediates formed after the C−H metalation step in Cp*Co^{III}-catalyzed C−H functionalization reactions. Moreover, we unveil that these cobaltacyclic species can be catalytically competent not only in selected Cp*Co^{III}-catalyzed C−H functionalization reactions, but also in a benchmark coupling reaction between an amide-functionalized aryl halide and diphenylacetylene. This manuscript overcomes the intrinsic thermodynamic difficulties associated to the employment of weakly-coordinated substrates and provides unprecedented fundamental knowledge at molecular level in the context of Cp*Co catalysis.
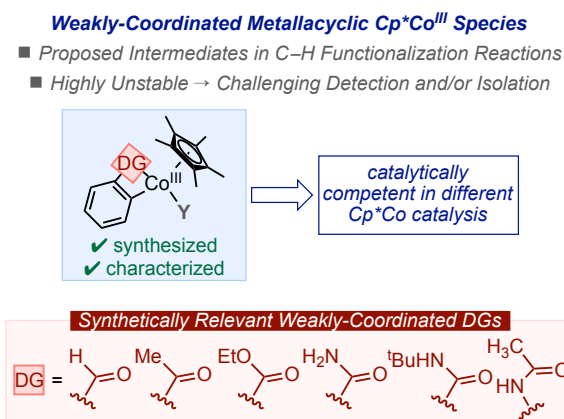
Scheme I.1. Unprecedented access to weakly-coordinated Cp*-based cobaltacycles.

COMMUNICATION

Weakly Coordinated Cobaltacycles: Trapping Catalytically Competent Intermediates in Cp*Co^{III} Catalysis

Sara Martínez de Salinas,[a] Jesús Sanjosé-Orduna,[a] Carlota Odena,[a] Sergio Barranco,[a] Jordi Benet-Buchholz,[a] Mónica H. Pérez-Temprano*[a]

Abstract: *Herein, we disclose the synthesis of metallacyclic Cp*Co^{III} complexes containing weakly-chelating functional groups. We have employed these compounds not only as an exceptional platform for accessing some of the most widely invoked transient intermediates in C–H functionalization processes but also as competent catalysts in different Cp*Co-catalyzed transformations, including a benchmark coupling reaction.*

Over the past several decades, C–H functionalization reactions directed by weakly-coordinated functional groups have emerged as powerful strategies for forming carbon–carbon and carbon–heteroatom bonds.[1] A key advantage of this approach is that the directing substrates contain common moieties found in synthetically relevant organic compounds (e.g., ketones, aldehydes, amides or esters). Therefore, extra synthetic steps for their installation/removal are often not necessary.[2] Usually, the weaker coordination of these directing groups to the metal center affords highly reactive metallacyclic intermediates towards subsequent functionalization. However, this entails a major obstacle, even when employing noble metals:[3] the low thermodynamic stability of the resulting transient species hinders their detection and/or isolation (Figure 1a). The inherent lack of stability has shown to be even more problematic with first-row metals systems, such as cobalt-based platforms.[4] While important synthetic advances have been made in the field of Cp*Co^{III} catalysis,[5] characterizing the putative cobalt intermediates in these transformations remains challenging.[5f] This profound lack of fundamental understanding at the molecular level precludes the rational design and development of novel and more efficient Cp*Co-catalyzed processes. As part of our ongoing interest in uncovering the mechanistic "black box" of Cp*Co^{III}-catalyzed C–H functionalization reactions,[6] we have recently reported the synthesis of well-defined cobaltacycles stabilized by strong σ-donor moieties such as pyridine or pyrimidine. In the present study (Figure 1b), we describe the synthesis of metallacyclic Cp*Co^{III} complexes (**A**) supported by weakly chelating ligands commonly used in Cp*Co-catalyzed C–H functionalizations, via an alternative oxidative addition route. We have leveraged these compounds to explore the access to direct analogues of long-sought-after cationic transient cobalt species (**A$^+$**) that have been widely proposed as key reactive intermediates. Moreover, we demonstrate the intermediacy of the **A**-type compounds in selected Cp*Co^{III}-catalyzed C–H

functionalizations, as well as their potential participation in the functionalization of aryl halides, using a benchmark reaction.
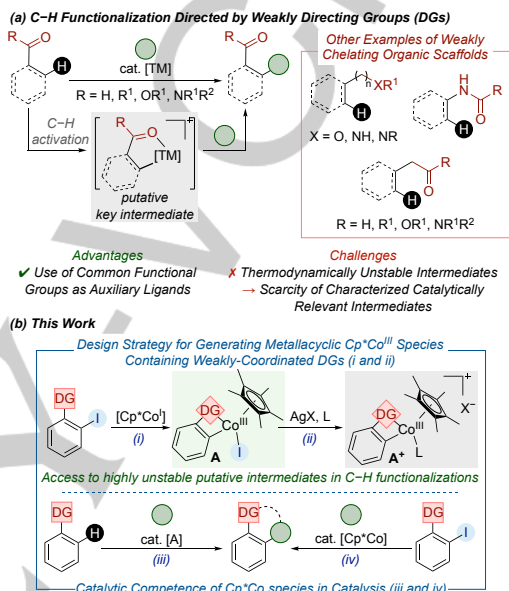
Figure 1. (a) State-of-the-art of C–H functionalization reactions assisted by weakly-coordinated directing groups; (b) the present work.

Initial studies were focused on designing a suitable platform for interrogating the accessibility to isolable Cp*Co^{III} complexes containing weakly-coordinated scaffolds. We explored an oxidative addition route to access complex **A**, which would circumvent the proposed reversibility of the Cp*Co^{III}-mediated C–H metalation.[4,5,6] We selected 2-iodobenzaldehyde (**1$_{ald}$-I**) as the ideal substrate for this oxidative addition given its synthetic relevance, widespread availability, and the opportunity to utilize the aldehydic proton as a spectroscopic handle in ^{1}H NMR analyses. Moreover, reported examples of Cp*Co^I aldehyde complexes support the feasible coordination of this carbonyl group to a cobalt metal center.[7]

The treatment of **1$_{ald}$-I** with [Cp*Co^I(VTMS)$_2$] (**2-VTMS**) in THF at room temperature for 15 minutes afforded the oxidative addition product **3$_{ald}$-I** as a greenish-black solid in 91% isolated yield (Figure 2).[8] The metallacyclic compound was fully characterized by 1D (^{1}H, ^{13}C) and 2D NMR spectroscopy, MS-ESI and single-crystal X-ray diffraction, showing the coordination of the aldehyde group in a σ-fashion.[9] ^{1}H NMR spectroscopy revealed an upfield shift of the aldehydic proton in **3$_{ald}$-I** (δ = 9.04 ppm) compared to **1$_{ald}$-I** (δ = 10.03 ppm) due to its interaction with the cobalt center.

[a]   Sara Martínez de Salinas,[a] Jesús Sanjosé-Orduna,[a] Carlota Odena,[a] Sergio Barranco,[a] Jordi Benet-Buchholz,[a] Mónica H. Pérez-Temprano*[a]
        Institute of Chemical Research of Catalonia (ICIQ)
        Avgda. Països Catalans 16, 43007 Tarragona (Spain)
        E-mail: mperez@iciq.es

COMMUNICATION
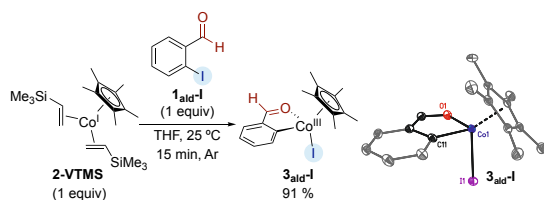
Figure 2. Synthesis and Characterization of **3ald-I** via Oxidative Addition. ORTEP Diagram of **3ald-I** is shown at 50% of probability (H atoms have been omitted for clarity).

We next explored the influence of the (pseudo)halide in the formation of **3ald-X** (X = I, Br, Cl, OMe) (Figure 3). As expected, the nature of X affects the oxidative addition event,[10] as **1ald-Br** reacted more slowly than the iodide derivative (Figure 3).[11] **3ald-Br** was fully characterized by NMR spectroscopy and X-ray diffraction. Under the same reaction conditions, **1ald-Cl** and **1ald-OMe** did not oxidatively add to the metal center, leading to decomposition of **2-VTMS** over time.

Figure 3. (a) Addition of **1ald-X** to [Cp*Co^I(VTMS)$_2$]. ORTEP Diagram of **3ald-Br** is shown at 50% of probability (H atoms have been omitted for clarity). (b) Reaction Profile for the formation of **3ald-X** (X = I, Br) at 25 °C in THF-d$_8$.
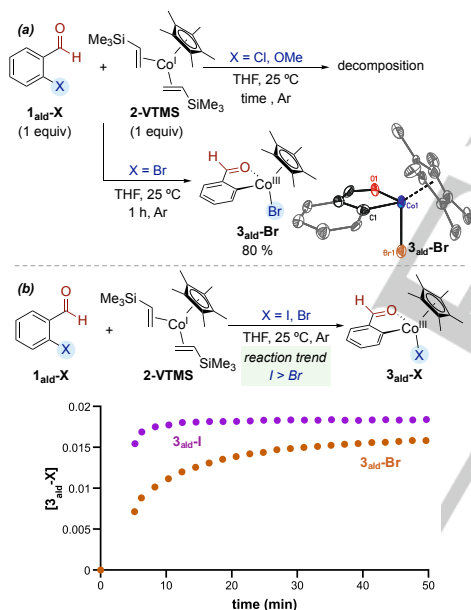
Having confirmed the accessibility and stability of **3ald-I/Br**, we next aimed to expand the scope of chelating groups involved in the formation of these Co^{III} compounds. The oxidative addition approach used to access **3ald-I** proved to be general for a range of substrates, such as ketones, esters and amides, enabling the synthesis of various **3DG-I**-type complexes shown in Table 1.[12] **3DG-I** (DG = ketone, ester, acetanilide) were fully characterized

by NMR spectroscopy at 25 °C, whereas **3CONH2-I** and **3CONHtBu-I** were characterized at –35 °C due to their comparatively lower stability. The nature of the synthesized compounds was confirmed by X-ray diffraction (Figure 4). The solid-state structures of **3DG-I** containing amide groups show its coordination to the cobalt metal center by the oxygen atom, which is the most basic site for neutral amides. The isolation and characterization of **3acetanilide-I** is particularly interesting since access to a six-membered Cp*Co^{III} cobaltacycle had not previously been reported in the literature.

Table 1. Scope of **3DG-I** Containing Different Weakly Chelating Functional Groups[a]
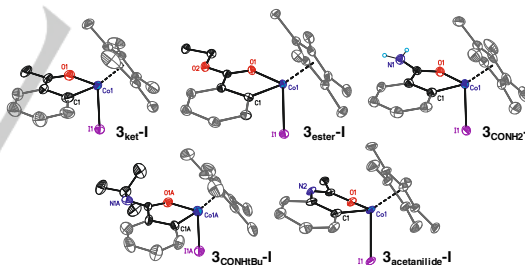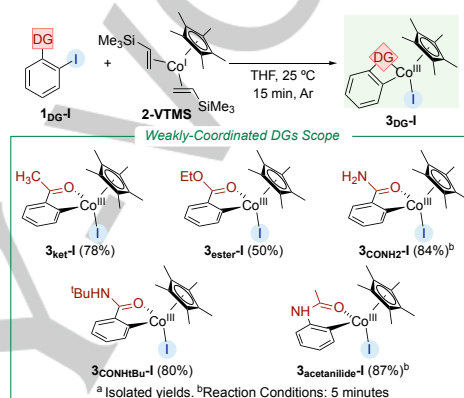
Figure 4. ORTEP Diagrams of **3DG-I**. Thermal ellipsoids drawn at 50% of probability (H atoms have been omitted for clarity).

After demonstrating the accessibility and stability of various Co^{III} complexes supported by catalytically relevant scaffolds, we next pursued detecting the direct analogues of the reactive species formed after the C–H metalation step (Figure 5).[5b, 5d, 5g-h, 13] In this context, we have previously described the employment of coordinating ligands to access otherwise highly reactive cationic metallacyclic Cp*Co^{III} species. Following the same approach[14] and using **3ald-I** as our initial platform, we were able to provide the first experimental evidence of a five-membered cationic cyclometalated Cp*Co^{III} complex bearing weakly coordinated functional groups. The reaction of **3ald-I** with AgBF$_4$ in THF-d$_8$ afforded the *in situ* formation of **3ald-THF** in full conversion by ^{1}H NMR spectroscopy. Although this complex was

COMMUNICATION

too unstable for isolation,[15] its structure could be characterized by multinuclear NMR spectroscopy and X-ray diffraction. After some optimization, the remaining **3_DG-THF** analogues could be detected in the crude ^{1}H NMR spectra by treatment with AgNTf2. **3_keto-THF** and **3_acetanilide-THF** were fully characterized by 1D and 2D NMR spectroscopy, whereas **3_CONH2-THF** and **3_CONHtBu-THF** were only characterized by ^{1}H NMR spectroscopic analyses due to their greater instabilities.
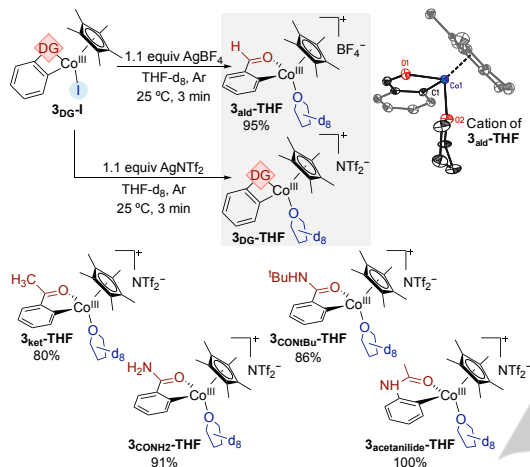
Figure 5. Conversion of **3_DG-I** to **3_DG-THF**. Reported yields were determined by the ^{1}H NMR spectroscopic analysis of the crude reaction mixture. ORTEP plot of **3_ald-THF**. Thermal ellipsoids drawn at 50% of probability, and the hydrogen/deuterium atoms and BF4 anion are omitted for clarity.

Having established the synthesis, isolation and characterization of different **3_DG-I** complexes and the accessibility of their cationic analogues, we next sought to explore the reactivity of **3_DG-I** in Cp*Co[III]-catalyzed C–H functionalization reactions (Figure 6). As mentioned above, these complexes are precursors of the putative intermediates involved in these transformations. However, their inaccessibility had previously hampered investigations of their catalytic competence. We therefore sought to utilize **3_ket-I**, **3_CONHtBu-I** and **3_acetanilide-I** as a platform for determining the intermediacy of these species in representative catalytic reactions. Importantly, these directing groups have been utilized in Cp*Co-catalyzed C–H functionalizations.[5h,13a-b] As shown in Figure 6, these cyclometalated complexes proved to be suitable catalysts for representative C–C coupling reactions, supporting the feasibility of the corresponding cationic intermediates in these transformations.[16]
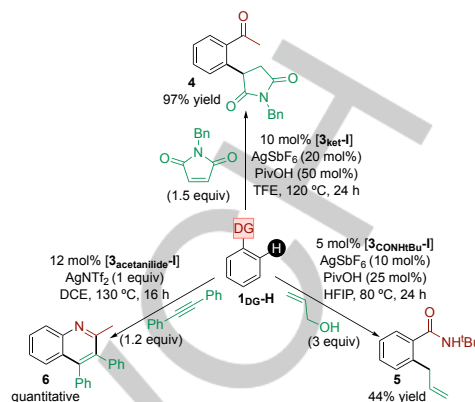

Figure 6. Catalytic competence of **3_DG-I**. Reported yields were determined via ^{1}H NMR spectroscopic analysis of the crude reaction mixture *versus* an internal standard using the substrate as the limiting reagent.

Finally, inspired by the facile formation of **3_DG-I** complexes through oxidative addition, we wondered whether these Cp*Co species could promote cross-coupling reactions of aryl halides containing this type of auxiliary ligands. Different types of cobalt species, normally generated by the combination of cobalt salts and Grignard reagents, have shown to be effective catalysts in aryl halide cross coupling reactions. However, the involvement of Cp*Co intermediates in these types of transformations remains practically unexplored.[17,18] Guided by our previous studies on Cp*Co[III]-catalyzed C–H functionalizations,[6] we selected alkyne annulations as a benchmark reaction. In the context of C–H functionalization reactions, these transformations proceed via Co[I/III] catalytic cycles and involve a re-oxidation step after product formation to regenerate the active Cp*Co[III] species that subsequently participates in C–H bond cleavage. When using aryl halides as starting materials, we envisioned a similar catalytic cycle to the one proposed for the C–H activation but with an oxidative addition/halide abstraction sequence (Figure 7).
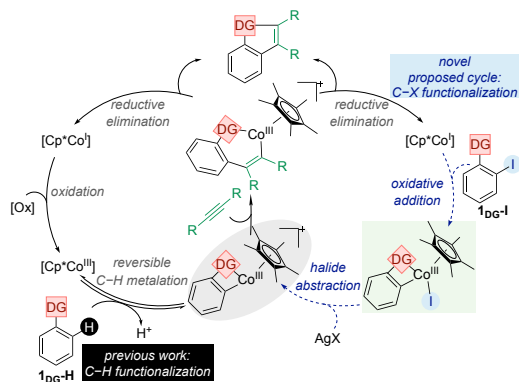
Figure 7. Proposed mechanism for known C–H oxidative alkyne annulation *vs* new pathway involving the activation of aryl halides.

COMMUNICATION

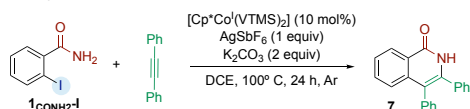To test our working hypothesis, we chose the reaction between 2-iodobenzamide and diphenylacetylene as the representative system (Table 2). It should be noted that the formation of the desired product by Cp*Co-catalyzed C–H functionalization using benzamide as a coupling partner is currently unprecedented in the literature.[19] To our delight, after some experimentation, we found that the desired annulated product (**7**) was obtained in 75% yield in the presence of catalytic quantities of **2-VTMS** in DCE at 100 ºC for 24 hours, using AgSbF₆ and K₂CO₃ as additives. While not anticipated, the choice of silver salt and base had an important effect on the reactivity (entries 4 and 7). **3$_{CONH2}$-I** is a competent catalyst in the annulation reaction, although we observed the desired product in a slightly lower yield (66%) than with **2-VTMS**. These preliminary results provide experimental evidence for the functionalization of **1$_{DG}$**-type substrates by Cp*Co systems. We anticipate this type of cross-coupling reactions can be potentially applied to other Cp*Co-catalyzed transformations involving oxidative addition and reductive elimination steps.

Table 2. Optimization of the Reaction Conditions[a]

Entry	Deviation from standard conditions	7 [%][b]
1	none	75 (66)[c]
2	DCE (0.1 M), AgBF₄, 40 ºC	0
3	DCE (0.1 M), AgBF₄	53
4	DCE (0.1 M), AgBF₄, KOAc	0
5	Dioxane (0.1 M), AgBF₄	38
6	DCE (0.1 M)	70
7	AgBF₄	67

| 8 | **3$_{CONH2}$-I** (10 mol%) | 66 |

[a]Reaction conditions: **1$_{CONH2}$-I** (0.05 mmol), diphenylacetylene (0.15 mmol), **2-VTMS** (10 mol%), AgSbF₆ (0.05 mmol), K₂CO₃ (0.1 mmol) in DCE (0.5 M) at 100 ºC under Ar. [b]NMR yields using an internal standard. [c]Isolated yield.

In summary, we have developed a promising strategy that enables entry to catalytically relevant metallacyclic Cp*Co^{III} complexes supported by synthetically relevant scaffolds. We have demonstrated the competence of these **3$_{DG}$-I**-type complexes, not only in select C–H functionalization reactions but also in a benchmark coupling reaction with aryl halides. This fundamental work is expected to open new avenues for accessing previously elusive reactive intermediates in Cp*Co catalysis and designing novel catalytic systems.

Acknowledgements

Conflict of interest

The authors declare no conflict of interest.

[1] a) K. M. Engle, T.-S. Mei, M. Wasa, J.-Q. Yu, *Acc. Chem. Res.* **2012**, *45*, 788–802; b) S De Sarkar, W. Liu, S. I. Kozhushkov, L. Ackermann, *Adv. Synth. Catal.* **2014**, *356*, 1461–1479; c) Z. Chen, B. Wang, J. Zhang, W. Yu, Z. Liu, Y. Zhang, *Org. Chem. Front.* **2015**, *2*, 1107–1295; d) C. Sambiagio, D. Schönbauer, R. Blieck, T. Dao-Huy, G. Pototschnig, P. Schaaf, T. Wiesinger, M. F. Zia, J. Wencel-Delord, T. Besset, B. U. W. Maes, M. Schnürch, *Chem. Soc. Rev.* **2018**, *47*, 6603–6743.

[2] In some cases, the *in situ* formation of transient imine directing groups is necessary for the C–H functionalization of this type of substrates, for selected examples, see: a) F.-L. Zhang, K. Hong, T.-J. Li, H. Park, J.-Q. Yu, *Science* **2016**, *351*, 252–256; b) K. Yang, Q. Li, Y. Liu, G. Li, H. Ge, *J. Am. Chem. Soc.* **2016**, *138*, 12775–12778; c) X.-H. Liu, H. Park, J.-H. Hu, Y. Hu, Q.-L. Zhang, B.-L. Wang, B. Sun, K.-S. Yeung, F.-L. Zhang, J.-Q. Yu, *J. Am. Chem. Soc.* **2017**, *139*, 888–896; d) P. Gandeepan, L. Ackermann, *Chem.* **2018**, *4*, 199–222; e) B. Li, K. Seth, B. Niu, L. Pan, W. Yang, H. Ge, *Angew. Chem., Int. Ed.* **2018**, *57*, 3401–3405; *Angew. Chem.* **2018**, *130*, 3459–3463; f) G. Liao, H.-M. Chen, Y.-N. Xia, B. Li, Q.-J. Yao, B.-F. Shi, *Angew. Chem., Int. Ed.* **2019**, *58*, 11464–11468; *Angew. Chem.* **2019**, *131*, 11586–11590; g) H. Ge, B. Li, B. Lawrence, G. Li, *Angew. Chem., Int. Ed.* **2019**, DOI: 10.1002/anie.2013126

[3] a) K. Shin, Y. Park, M.-H. Baik, S. Chang, *Nat. Chem.* **2018**, *10*, 218–224; b) A. Tomberg, M. É. Muratore, M. J. Johansson, I. Terstiege, C. Sköld, P.-O. Norrby, *iScience* **2019**, *20*, 373–391; c) J Kim, K. Shin, S. Jin, D. Kim, S. Chang, *J. Am. Chem. Soc.* **2019**, *141*, 4137-4146.

[4] For seminal example on Cp*Co^{III}-catalyzed direct C–H activation, see: a) T. Yoshino, H. Ikemoto, S. Matsunaga, M. Kanai, *Angew. Chem. Int. Ed.* **2013**, *52*, 2207–2211; *Angew. Chem.* **2013**, *125*, 2263–2267. For recent reviews on chelation-assisted Cp*Co^{III}-catalyzed C–H functionalization reactions, see: b) M. Moselage, J. Li, L. Ackermann, *ACS Catal.* **2016**, *6*, 498–525; c) P. G. Chirila, C. J. Whiteoak, *Dalton Trans.* **2017**, *46*, 9721–9739; d) S. Wang, S. Y. Chen, X. Q. Yu, *Chem. Commun.* **2017**, *53*, 3165–3180; e) T. Yoshino, S. Matsunaga, *Adv.*

Synth. Catal. **2017**, *359*, 1245–1262; f) J. Ghorai, P. Anbarasan, *Asian J. Org. Chem.* **2018**, *8*, 430–455; g) P. Gandeepan, T. Müller, D. Zell, G. Cera, S. Warratz, L. Ackermann, *Chem. Rev.* **2019**, *119*, 2192–2452; h) T. Yoshino, S. Matsunaga, *Synlett* **2019**, *30*, 1384–1400.

[5] For selected examples of Cp*Co-catalyzed directed C–H functionalization using weakly directing groups, see: a) H. Ikemoto, T. Yoshino, K. Sakata, S. Matsunaga, M. Kanai, *J. Am. Chem. Soc.* **2014**, *136*, 5424–5431; b) J. Park, S. Chang, *Angew. Chem., Int. Ed.* **2015**, *54*, 14103–14107; *Angew. Chem.* **2015**, *54*, 14103–14107; c) Z.-Z. Zhang, B. Liu, C.-Y. Wang, B.-F. Shi, *Org. Lett.* **2015**, *17*, 4094–4097; d) Q. Lu, S. Vásquez-Céspedes, T. Gensch, F. Glorius, *ACS Catal.* **2016**, *6*, 2352–2356; e) P. W. Tan, A. M. Mak, M. B. Sullivan, D. J. Dixon, J. Seayad, *Angew. Chem., Int. Ed.* **2017**, *56*, 16550–16554; *Angew. Chem.* **2017**, *56*, 16550–16554; f) J. A. Boerth, S. Maity, S. K. Williams, B. Q. Mercado, J. A. Ellman, *Nat. Catal.* **2018**, *1*, 673–679; g) M. R. Sk, S. S. Bera, M. S. Maji, *Org. Lett.* **2018**, *20*, 134–137; h) R. Mandal, B. Emayavaramban, B. Sundararaju, *Org. Lett.* **2018**, *20*, 2835–2838; i) S. Fukagawa, Y. Kato, R. Tanaka, M. Kojima, T. Yoshino, S. Matsunaga, *Angew. Chem., Int. Ed.* **2019**, *58*, 1153–1157; *Angew. Chem.* **2019**, *131*, 1165–1169; j) J. Huang, J. Ding, T.-M. Ding, S. Zhang, Y. Wang, F. Sha, S.-Y. Zhang, X.-Y. Wu, Q. Li, Q. *Org. Lett.* **2019**, *21*, 7342–7345.

[6] a) J. Sanjosé-Orduna, D. Gallego, A. Garcia-Roca, E. Martin, J. Benet-Buchholz, M. H. Pérez-Temprano, *Angew. Chem., Int. Ed.* **2017**, *56*, 12137–12141; *Angew. Chem.* **2017**, *129*, 12305–12309. b) J. Sanjosé-Orduna, J. Sarria Toro, M. H. Pérez-Temprano, *Angew. Chem., Int. Ed.* **2018**, *57*, 11369–11373; *Angew. Chem.* **2018**, *130*, 11539–11543. c) J. Sanjosé-Orduna, J. Benet-Buchholz, M. H. Pérez-Temprano, *Inorg. Chem.* **2019**, *58*, 10569–10577.

[7] a) C. P. Lenges, M. Brookhart, *J. Am. Chem. Soc.* **1997**, *119*, 3165–3166; b) C. P. Lenges, M. Brookhart, P. S. White, *Angew. Chem., Int. Ed.* **1999**, *38*, 552–555; *Angew. Chem.* **1999**, *11*, 535–538.

[8] Brookhart and co-workers have proposed the generation of Cp*Co^{III} acyl hydride complexes via the oxidative addition of an aldehydic C–H bond

COMMUNICATION

to [C5Me5Co(L)] during the hydroacylation of olefins with aromatic aldehydes (ref. 7a). Under our reaction conditions, we only observed the oxidative addition of the Csp^2–I bond.

[9] CCDC 1971411 (**3ald-I**), CCDC 1971412 (**3ald-Br**), CCDC 1971413 (**3ket-I**), CCDC 1971414 (**3ester-I**), CCDC 1971415 (**3CONH2-I**), CCDC 1971416 (**3CONHtBu-I**), CCDC 1971417 (**3acetanilide-I**), CCDC 1971418 (**3ald-THF**), CCDC 1971419 (**7**) contain the supplementary crystallographic data for these structures. These data are provided free of charge by The Cambridge Crystallographic Data Centre.

[10] J. A. Labinger, *Organometallics* **2015**, *34*, 4784−4795.

[11] The participation of radical species in the oxidative addition reaction could not be confirmed or excluded, since the reaction of **2-VTMS** with **1ald-I**, in the presence of TEMPO, afforded the formation of other unknown species. See SI for further details.

[12] Our attempts for synthesizing the corresponding **3DG-I** complexes when using as starting material 2-iodobenzoic acid, 2-iodobenzyl alcohol, 2-iodonitrobenzene 2-iodophenol, 2-iodoaniline and 2-iodomethoxybenzoate led to the decomposition of **2-VTMS**.

[13] a) Y. Bunno, N. Murakami, Y. Suzuki, M. Kanai, T. Yoshino, S. Matsunaga, *Org. Lett.* **2016**, *18*, 2216−2219; b) L. Kong, S. Yu, X. Zhou, X. Li, *Org. Lett.* **2016**, *18*, 588−594; c) W. Yu, W. Zhang, Z. Liu, Y. Zhang, *Chem. Commun.* **2016**, *52*, 6837−6840; d) P. G. Chirila, J. Adams, A. Dirjal, A. Hamilton, C. J. Whiteoak, *Chem. Eur. J.* **2018**, *24*, 3584−3589; e) M. R. Sk, S. S. Bera, M. S. Maji, *Adv. Synth. Catal.* **2019**, *361*, 585-590.

[14] Inspired by our previous works, initial trials targeting **3ald-MeCN** afforded a mixture of the desired cobaltacycle and [Cp*Co(MeCN)3][BF4]2, in 89:11 ratio, respectively. The amount of [Cp*Co(MeCN)3][BF4]2 increases along time in solution. See SI for further details.

[15] When the solvent was removed on a rotary evaporator and the resulting precipitate was re-dissolved in CD2Cl2 we observed decomposition.

[16] Although the employment of **3CONHtBu-I** resulted in moderate yields of **5**, this experimental result is comparable to the one described by Matsunaga and coworkers in the reference 13a when using [Cp*Co(CO)I2] as pre-catalyst.

[17] a) C. Gosmini, J.-M. Bégouin, A. Moncomble, *Chem. Commun.* **2008**, *28*, 3221−3233; (b) G. Cahiez, A. Moyeux, *Chem. Rev.* **2010**, 110, 1435−1462.

[18] Joshi and co-workers have reported the Cp*CoIII-catalyzed coupling between alkenes and aryl halides in the absence of directing groups, see: A. K. Srivastava, N. Satrawala, M. Ali, C. Sharma, R. K. Joshi, *Tetrahedron Lett.* **2019**, *60*, 151283. Our attempts to synthesize different cobaltacycles using Cp*Co(VTMS)2 (**2-VTMS**) and PhI in the presence and abscence of external stabilizing ligands led to a complex mixture of products. See SI for further details.

[19] The formation of **7** by Cp*Co-catalyzed C–H functionalization reactions has been reported using as starting material N-methoxy or N-chloro benzamides, see: a) G. Sivakumar, A. Vijeta, M. Jeganmohan, *Chem. Eur. J.* **2016**, *22*, 5899−5903; b) X. Yu, K. Chen, S. Guo, P. Shi, C. Song, J. Zhu, *Org. Lett.* **2017**, *19*, 5348−5351.

Annex *II*

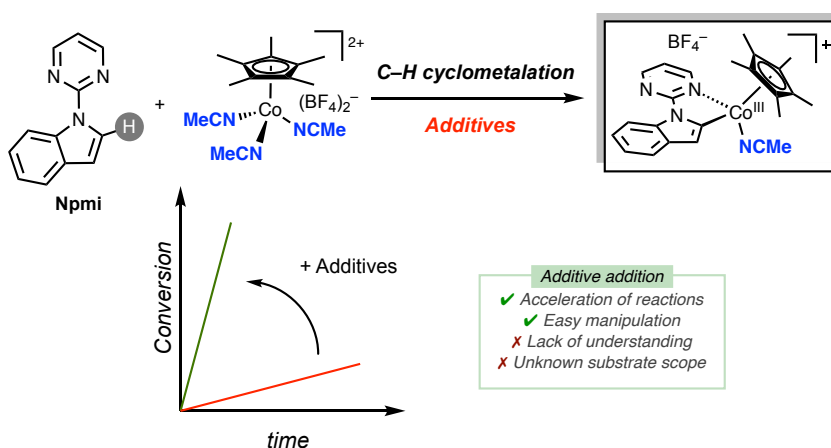## Additives Effect on the Cp*Co^{III} C–H Cyclometalation Reaction

This annex is dedicated to discuss other relevant results that have been obtained during this doctoral thesis, that have not published in any journal so far. These experiments have been designed for uncovering and understanding the effect of certain additives on the Cp*Co^{III}-mediated C−H cyclometalation step. To complement the experimental mechanistic investigations, a short three-month stay was done under the supervision of Prof. Stuart A. Macgregor, to learn and apply Density Functional Theory calculations to these systems.

The following coworkers have contributed to the work presented in this Annex:

Sanjosé-Orduna, **J.;** Sarria, J. M.; Martínez de Salinas, S.; Neale, S. E.; Macgregor, S. A.; Pérez-Temprano, M. H.

## II.1 Cp*Co^{III}-Mediated C−H Metalation of *N*-pyrimidinylindole

During the development of the investigations described in **Article 3**, we discovered that the success of the Cp*Co^{III}-based cyclometalation reactions relied completely on the selection of the additives. For example, the Cp*Co^{III}-mediated cyclometalation of *N*-pyrimidinylindole (**Npmi**) with [Cp*Co(MeCN)$_3$][BF$_4$]$_2$ was extremely slow, and never reached full conversion. However, the same experiment in the presence of two additives: an external base and 1,1,1,3,3,3-hexafluoroisopropanol (**HFIP**), yielded the same product in full conversion in less than 5 minutes. So, encouraged by this dramatic and unexpected result, we aimed to explore, in more detail, the additive effects into this crucial step within the catalytic cycles of Cp*Co^{III}-catalyzed C−H functionalization reactions (Scheme II.1).

Scheme II.1. Acceleration of the Cp*Co^{III} C−H cyclometalation reaction with additives.

For our initial investigation, we monitored by ^{1}H NMR spectroscopy the reaction between [Cp*Co(MeCN)$_3$][BF$_4$]$_2$ and excess of **Npmi**, in the absence of additional additives, in DCM-d$_2$ at 35 ºC. Under these reaction conditions, we observed the slow formation of the corresponding cyclometalated complex, that seems to be in equilibrium with the starting materials (Scheme II.2). This can be attributed to the low basicity of **Npmi** that is acting as surrogate base. This hypothesis is supported by the full conversion into the desired product when 2,6-di-*tert*-butylpyridine is added as external base (**DTBP**). Interestingly, both experiments show similar reaction rates up to 20% of conversion. This is in alignment with a thermodynamic effect of the external base, shifting the equilibrium towards the product.
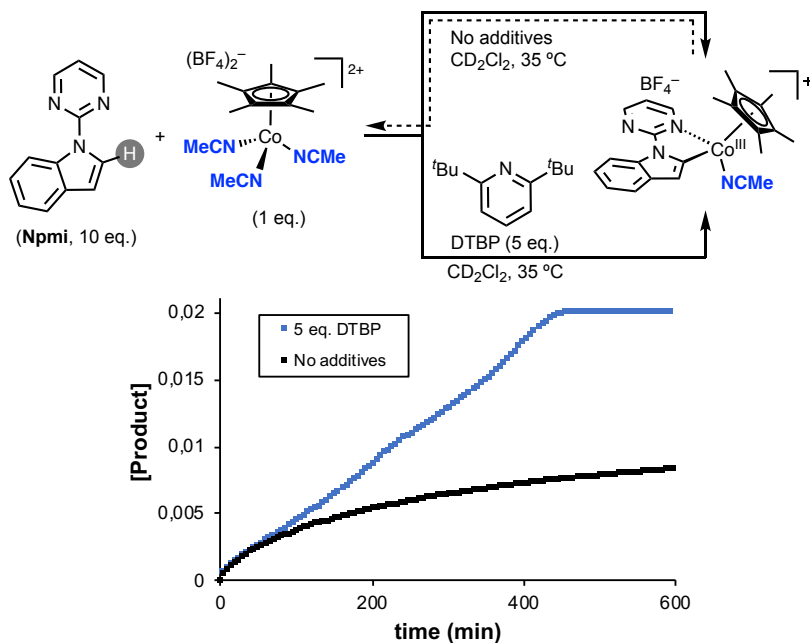
**Scheme II.2.** External base effect in the cyclometalation of **Npmi** with [Cp*Co(MeCN)$_3$][BF$_4$]$_2$.

In order to confirm the existence of this equilibrium, we investigated the reverse reaction: the protodemetalation. The reaction of Cp*Co^{III} metallacycle with PivOH, in the presence of **MeCN** and NaBF$_4$, to keep the stoichiometry of the equilibrium, afforded the formation of [Cp*Co(MeCN)$_3$][BF$_4$]$_2$, also in equilibrium with the corresponding starting materials (Scheme II.3).
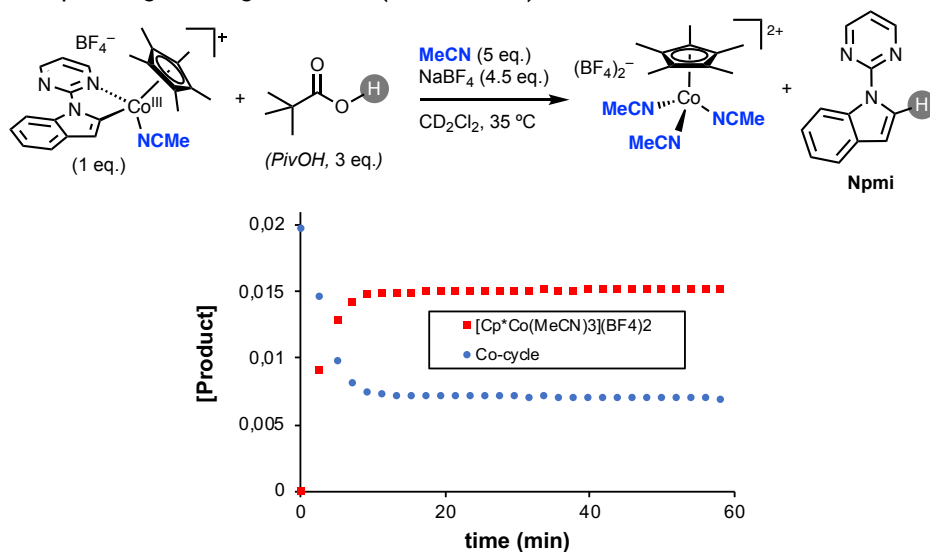
Scheme II.3. Protodemetallation of the Cp*Co^{III} metallacycle monitored by ^{1}H NMR.

To gain further insights into this equilibrium, we carried out computational studies, using the Gaussian 09 program package, for the modelling of the C−H cyclometalation (Figure II.1). The B3PW91 functional was employed for the geometry optimizations along with a mixed basis set (SDDAll for cobalt and 6-31G** for all the other atoms). The solvent effects (dichloromethane) were considered by single-point energy calculations on the gas-phase stationary points, using the B3PW91-D3(zero)(DCM)/def2-TZVP level of theory. Empirical corrections for dispersion interactions were obtained with Grimme's standalone D3 program, with the zero-damping function. The energies given in this work are B3PW91 calculated Gibbs free energies in dichloromethane as solvent.
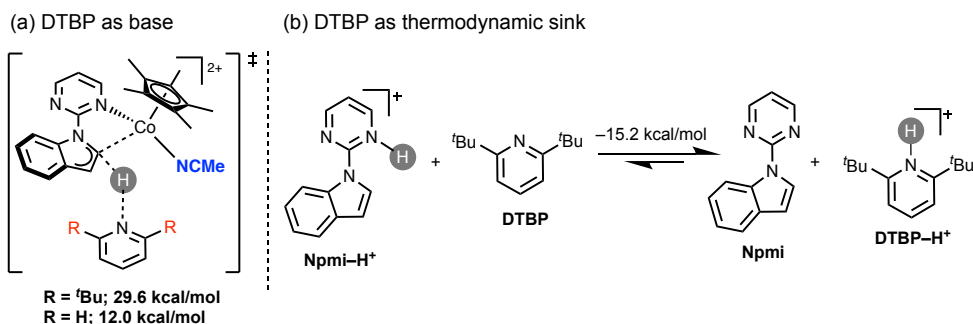
Starting from the initial cobalt complex **I**, we first modeled the coordination of 1 molecule of **Npmi** with the concomitant dissociation of **MeCN**. Then, the consequent dissociation of a second **MeCN** formed the intermediate **IV$_{pmi}$**, a Wheland intermediate, with an interaction between the metal center and the C−H bond of **Npmi**. From this intermediate, we hypothesized that a second molecule of **Npmi** acted as a surrogate base to furnish the final product **V$_{pmi}$**, with re-aromatization of the indole moiety. In the overall reaction, we observed that the final product was slightly exergonic, −2.0 kcal/mol, very close to thermoneutrality. This might explain the reversibility of the reaction experimentally.
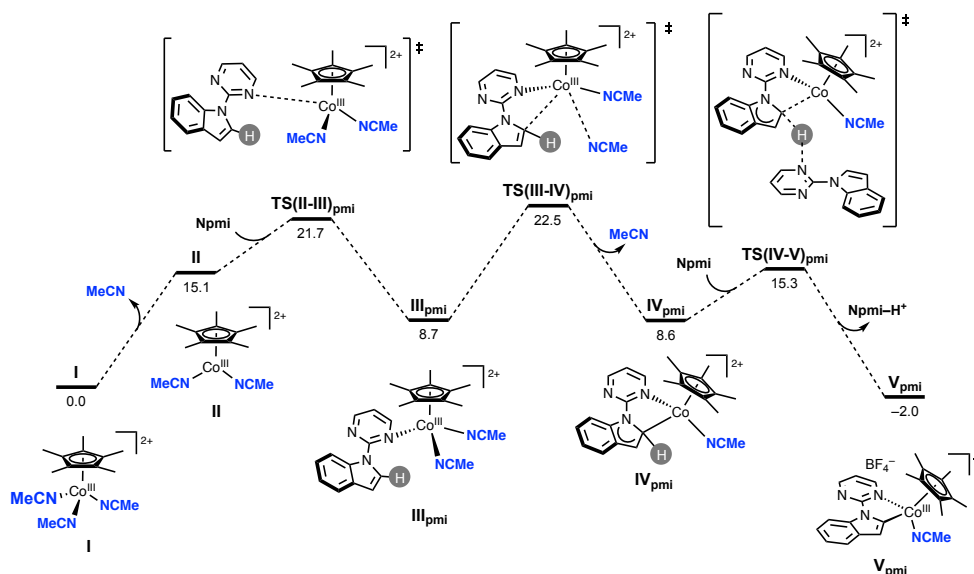
Figure II.1. DFT profile of the cyclometalation of **Npmi** with [Cp*Co(MeCN)$_3$][BF$_4$]$_2$. Energetic values are given as ΔG in kcal/mol.

Next, we investigated the role of 2,6-di-*tert*-butylpyridine (**DTBP**). Initially, we considered this base was responsible of the deprotonation directly from the Wheland intermediate (Scheme II.4a). However, we obtained a high energy barrier (29.6 kcal/mol), presumably due to the steric hindrance of the *tert*-butyl groups.[1] Then, we examined whether **DTBP** could deprotonate **Npmi−H⁺**, generated after the C−H bond-cleavage. The thermodynamic equilibrium of the deprotonation of **Npmi−H⁺** with **DTBP** turned out to be extremely exergonic, being **DTBP** a stronger base, more stable protonated than **Npmi** (Scheme II.4b). If we add this extra step to the overall DFT profile in Figure II.1, we switch the initial equilibrium towards the complete formation of the desired product. This is in full agreement with the experimental evidences shown in Scheme II.2.

(a) DTBP as base
(b) DTBP as thermodynamic sink

R = *t*Bu; 29.6 kcal/mol
R = H; 12.0 kcal/mol

−15.2 kcal/mol

Npmi−H⁺

DTBP

Npmi

DTBP−H⁺

Scheme II.4. Possible roles of **DTBP** in the cyclometalation reaction.

A close examination of the energy profile shows that the barrier of the C−H cyclometalation step is relatively low. Unexpectedly, the coordination of **Npmi** in **TS(I-III)_{pmi}** and dissociation of **MeCN** in **TS(III-IV)_{pmi}** are higher in energy. To further assess the relevancy of the C−H cleavage step in the overall reaction, we synthesized the **Npmi** isotopologue with deuterium in the targeted position, instead of hydrogen, and repeated the initial reaction without any additives. As shown in Scheme II.5, both reactions provide similar kinetic profiles supporting that the C−H bond cleavage is kinetically irrelevant in the overall process, as we anticipated by DFT calculations in Figure II.1.

---

[1] Repeating the same transition state calculation without the bulky substituents (i.e. with pyridine), a lower barrier was obtaied (12.0 kcal/mol). Unfortunately, this additive is incompatible experimentally with the cobalt precursor, due to the formation of a complex mixture of products.
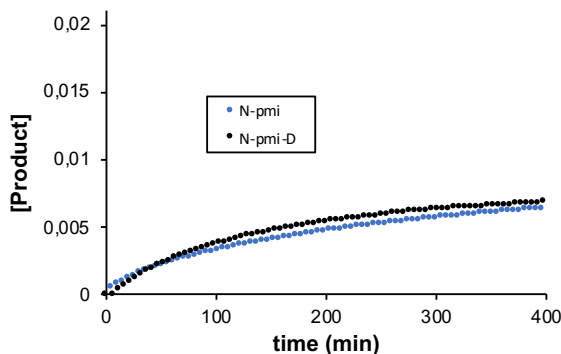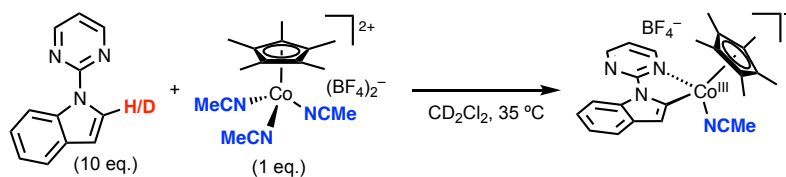
**Scheme II.5.** Effect of the deuteration of **Npmi** in the Cp*Co^{III} cyclometalation reaction.

With these mechanistic insights in hand, we next decided to try to rationalize the boosting effect of **HFIP** in the C−H cyclometalation reaction. As briefly discussed in **Chapter 4**, an increasing amount of research groups are using perfluorinated alcohols to develop new and more efficient chemical transformations. However, the reasons behind their beneficial effect remains elusive so far. As shown in Scheme II.6, when using **HFIP** as the only additive in the cyclometalation reaction we observed an equilibrium, similar to the one detected in the absence of additives, but slightly faster at the early stages of the reactions. In sharp contrast, the reaction is complete in less than 60 minutes combining **HFIP** and **DTBP**.
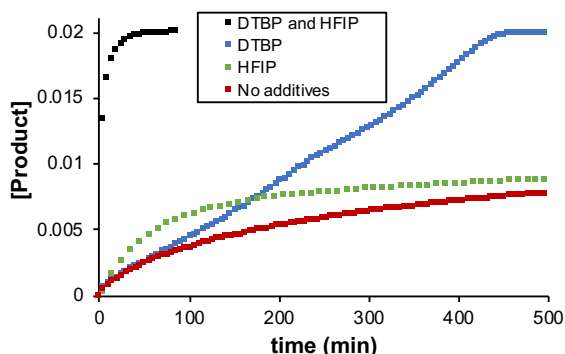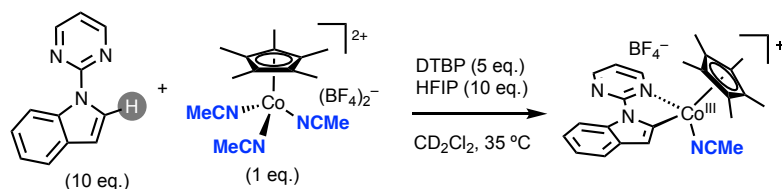
Scheme II.6. Additives combination effect in the Cp*Co^{III} cyclometalation reaction.

As proposed in the literature, one of the unique properties of fluorinated alcohols is their ability to interact via hydrogen-bonding, from the OH group to any Lewis base present in the reaction media. This interaction can lead to a wide variety of changes in the reaction, ranging from stabilization of transient species, to deprotonation of substrates via proton shuttle. In order to test the relevancy of this acidic proton, we compared the effect of **HFIP** to its methylated analogue, **HFIP-OMe,** in the presence of the external base (Figure II.7). Interestingly, the absence of the -OH group eliminates the previously observed beneficial effect, providing a reaction profile analogue to the reaction without **HFIP**. This experimental result indicates that the acidic proton of **HFIP** is involved in the acceleration effect observed during the cyclometalation reaction.
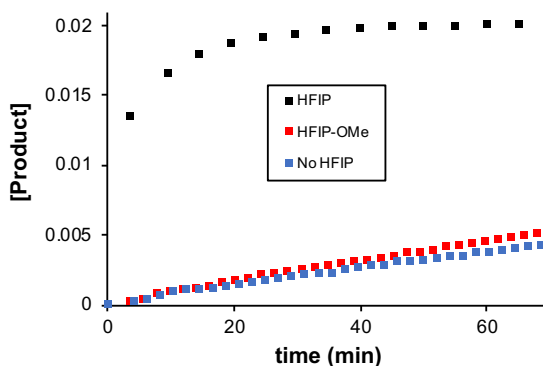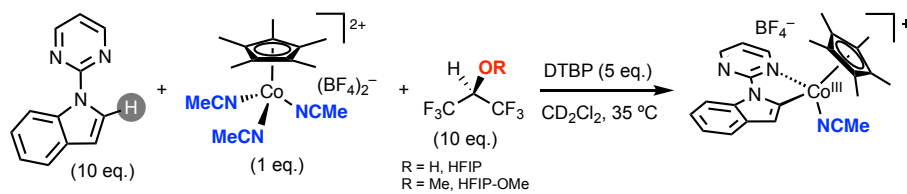
Scheme II.7. Effect of the acidic proton of **HFIP** in the Cp*Co^{III} cyclometalation reaction.

As mentioned before, different literature precedents have proposed that HFIP can act as proton shuttle during C−H activation events. In order to interrogate this potential role in our model system, we performed the cyclometalation reaction using deuterated **HFIP** as additive. As shown in Scheme II.8, similar kinetics are observed when using **HFIP** or **HFIP-d$_2$**, which suggests that the cleavage of the O−H bond is not kinetically relevant in this specific system.
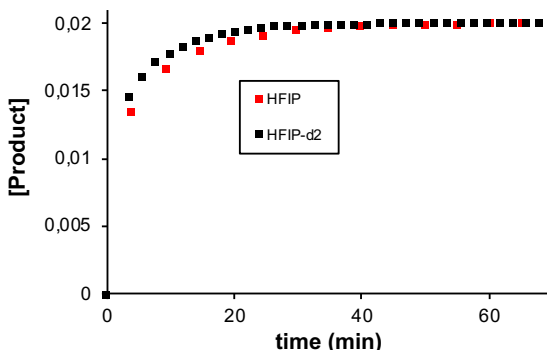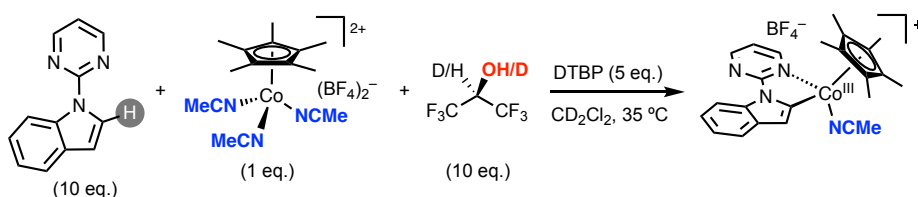
Scheme II.8. Effect of the deuteration of **HFIP** in the Cp*Co^{III} cyclometalation reaction.

These experimental results are supported by the high energy barrier computed for the C−H activation step *via* a **HFIP**-mediated proton shuttle (Figure II.2a). As shown in the reaction energy profile in the absence of additives (see Figure II.1), the C−H bond-cleavage event is not energetically relevant in the overall process. In sharp contrast, the dissociation of 1 or 2 equivalents of **MeCN**, required for accommodating the incoming **Npmi**, are potentially the rate-limiting step of the cyclometalation process. Inspired by this fact, we wondered whether this fluorinated alcohol could facilitate the dissociation of **MeCN**. The computed thermodynamics of the formation of an **HFIP-MeCN** adduct afforded both exergonic and exothermic energies (Figure II.2b).
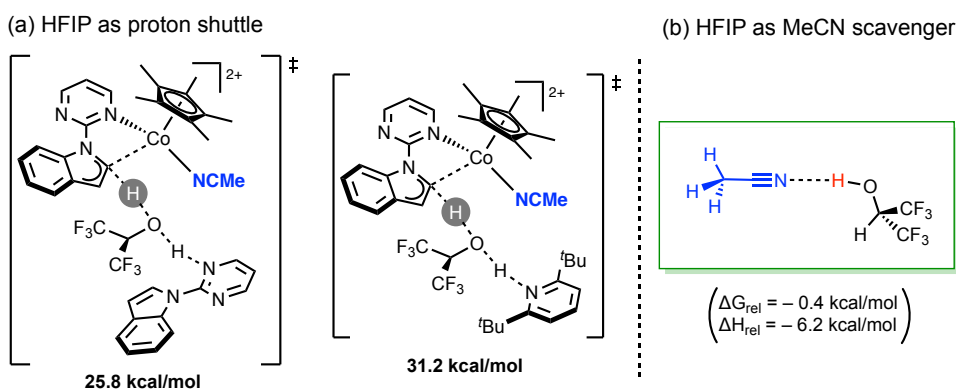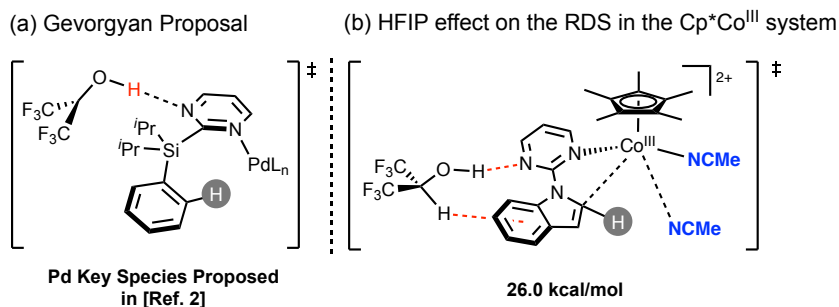

Figure II.2. DFT calculations of **HFIP** possible roles.

Another possible role of **HFIP** has been suggested by Gevorgyan *et al.* in the palladium-catalyzed synthesis of hexafluoroisopropyl benzoate esters.[2] They suggested that a hydrogen-bonding interaction of the perfluorinated alcohol with the second nitrogen of the directing group would be crucial for that particular alkoxycarbonylation reaction (Figure II.3a). The authors detected by ^1H NMR spectroscopy an **HFIP-pyrimidine** adduct. Thus, they hypothesized that the perfluorinated alcohol could have a double effect in the reaction: (1) decreasing the basicity of the directing group, and therefore enhancing its activity in the C−H activation step; (2) increasing the nucleophilicity of the hydrogen-bonded perfluorinated alcohol, facilitating its insertion. Encouraged by these assumptions, we decided to model by DFT an analogous transition state of the rate-determining step in Figure II.1, **TS(III-IV)~pmi~** but in the presence of a molecule of **HFIP** bonded to the second nitrogen of the **Npmi** (Figure II.3b). Unfortunately, a higher energetic barrier was obtained (26.0 kcal/mol). Although kinetically irrelevant, we also

[2] Wang, Y.; Gevorgyan, V. "Synthesis of Active Hexafluoroisopropyl Benzoates through a Hydrogen-Bond-Enabled Palladium(II)-Catalyzed C−H Alkoxycarbonylation Reaction" *Angew. Chem. Int. Ed.* **2017**, *56*, 3191−3195.

decided to model the transition state **TS(IV-V)pmi**, corresponding to the C−H activation, with the **HFIP** in the same position of the DG. A much higher energetic barrier was obtained again (22.9 kcal/mol), discarding computationally these interactions in the Cp*Co^{III} C−H cyclometalation reaction. However, we cannot fully discard this possibility, as more experimental data is needed.

(a) Gevorgyan Proposal   (b) HFIP effect on the RDS in the Cp*Co^{III} system

**Pd Key Species Proposed
in [Ref. 2]**

26.0 kcal/mol

Figure II.3. DFT calculations on the **HFIP** coordination to the second nitrogen of the pyrimidine directing group.

Next, we aimed to investigate the effect of other halogenated alcohols. As shown in Scheme II.9, the addition of trifluoroethanol (**TFE**), trichloroethanol (**TCE**) or tribromoethanol (**TBE**) as additives is also beneficial for the C−H metalation step.
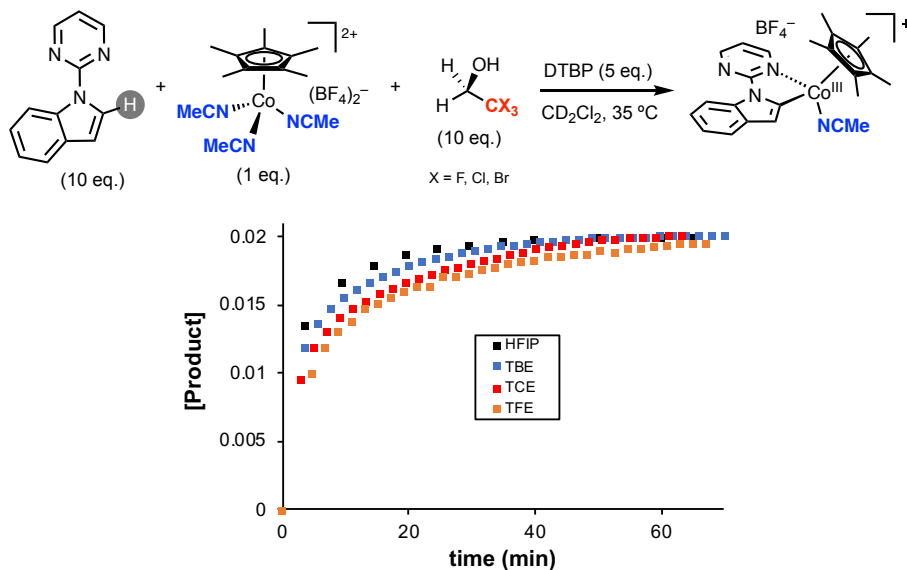
**Scheme II.9.** Effect of other halogenated alcohols as additives, in comparison to **HFIP**.

We also investigated the effect of α-substituted **HFIP** additives. The addition of nonafluoro-*tert*-butanol, where the acidity of the −OH group is enhanced by the presence of the trifluoromethyl group, provides a similar effect than **HFIP**. In sharp contrast, the corresponding phenyl-substituted HFIP derivative did not influence the C−H metalation. (Scheme II.10) This is presumably due to an increase of the steric hindrance compared to **HFIP**.
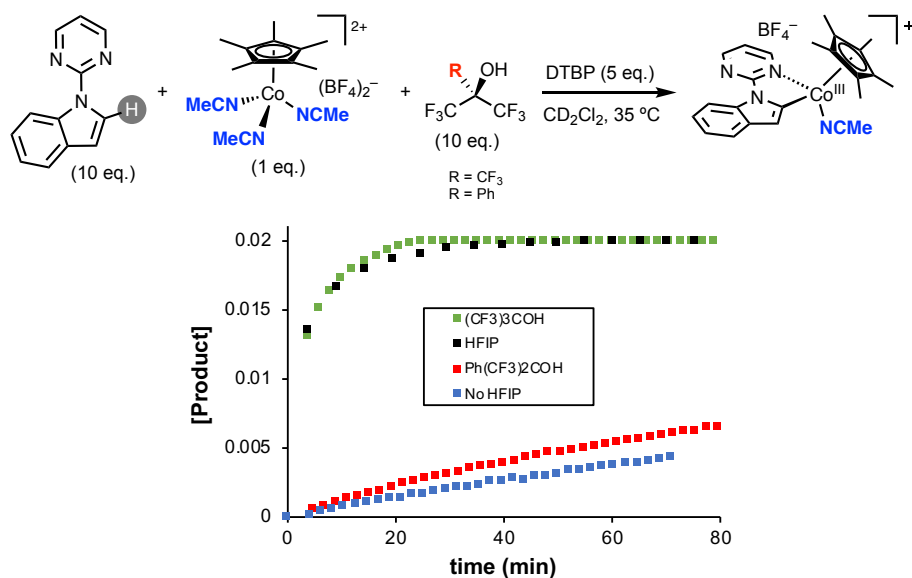
Scheme II.10. Effect of the substitution in the α position of **HFIP**.

II.2 Cp*Co^{III}-Mediated C−H Metalation of 2-phenylpyridine

We were also interested in examining whether the HFIP boosting effect observed in the C−H activation of **Npmi** could be translated to other related substrates. Based on our previous experience, we have investigated the effect of this additive in the Cp*Co^{III}-mediated C−H cyclometalation of 2-phenylpyridine (**2ppy**). First, we monitored by ^{1}H NMR spectroscopy the formation of the corresponding cobaltacycle in the presence of different amounts of **HFIP** (from 0 to 20 eq.).[3] Surprisingly, the addition of **HFIP** did not have any influence on the reaction rate (Scheme II.11).
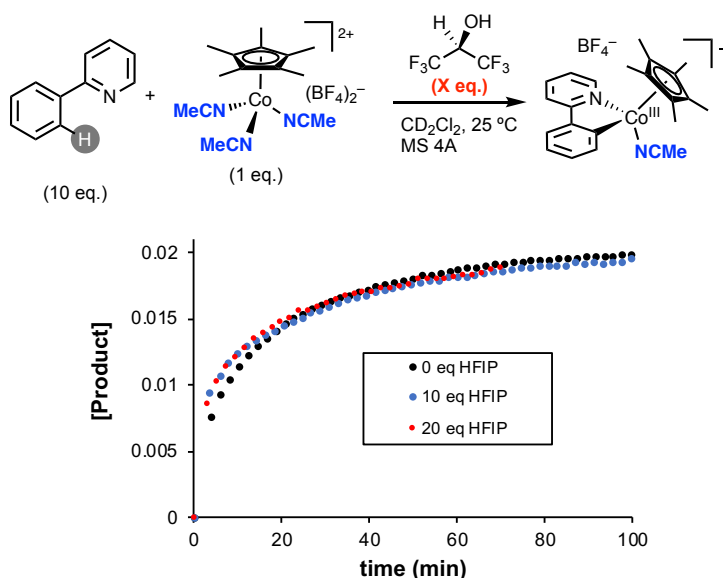
**Scheme II.11.** Effect of HFIP addition to the C−H cyclometalation of **2ppy**.

To further check the interaction between **HFIP** and the substrate, we attempted to see the coordination of **HFIP** to the nitrogen of **2ppy-d₅**.[4] Whereas no adduct was observed in the case of **Npmi**, we were able to detect by ^{1}H NMR spectroscopy a very dramatic shift of the **2ppy-d₅** when excess of **HFIP** was added (Scheme II.12). When we performed a 2D NMR experiment, [1]H-^{1}H NOESY, we observed a diagnostic cross-peak between the alcoholic proton of **HFIP** and the proton at the ortho position of the pyridine moiety. This experimental result suggests the formation of the expected **HFIP-2ppy-d₅** adduct (See SI). Interestingly, the formation of an adduct between the substrate and the fluorinated alcohol does not seem to modify

---

[3] Due to reproducibility issues, these reactions were carried out in the presence of molecular sieves.
[4] We used deuterated 2-phenylpyridine in order to facilitate the analysis of the reaction mixture by ^{1}H NMR.

the Cp*Co^III C−H cyclometalation reaction rate, as observed by the lack of effect of HFIP addition in Figure II.11.
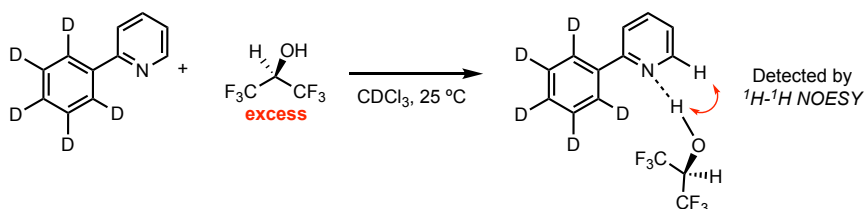
**Scheme II.12.** Adduct formation of HFIP with **2ppy**.

After these results, we were curious about the effect of other halogenated alcohols as additives. Unexpectedly, when using trifluoroethanol (TFE) or trichloroethanol (TCE), a small acceleration in the formation of the final cobaltacycle was observed, in comparison with the lack of additive or HFIP (Scheme II.13).
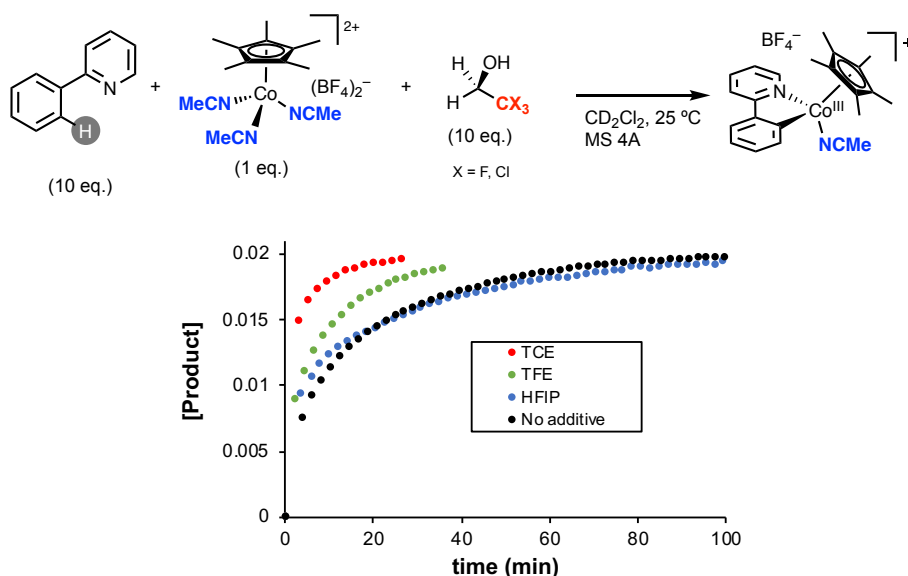
Scheme II.13. Effect of other fluorinated alcohols in the cyclometalation of **2ppy**.

Then, we decided to perform DFT calculations in order to shed light into this complex scenario. Starting from the initial cobalt complex **I** again, we modeled the coordination of 1 molecule of **2ppy** together with the dissociation of **MeCN**. Then, the consequent dissociation of a second **MeCN** formed the analogous intermediate to the **Npmi** system, presenting also a Wheland intermediate. From this intermediate, a second molecule of **2ppy** acted as a surrogate base to furnish the

final cobaltacycle with re-aromatization of the phenyl moiety. In stark contrast to the energy profile computed for **Npmi**, the cyclometalation reaction with **2ppy** is a very exergonic process (−13.9 kcal/mol). This explains why the reaction works even without the addition of any external base. The pyridine-based directing group is basic enough to perform the C−H bond cleavage, and it is stable enough to present the protonated form **2ppy−H⁺**. The elementary step with the highest energy is now the coordination of the substrate to the cobalt metal center. The subsequent steps, i.e. **TS(III-IV)₂ₚₚy** and the C−H activation, are much lower in energy, and therefore kinetically irrelevant for this system (Figure II.4).
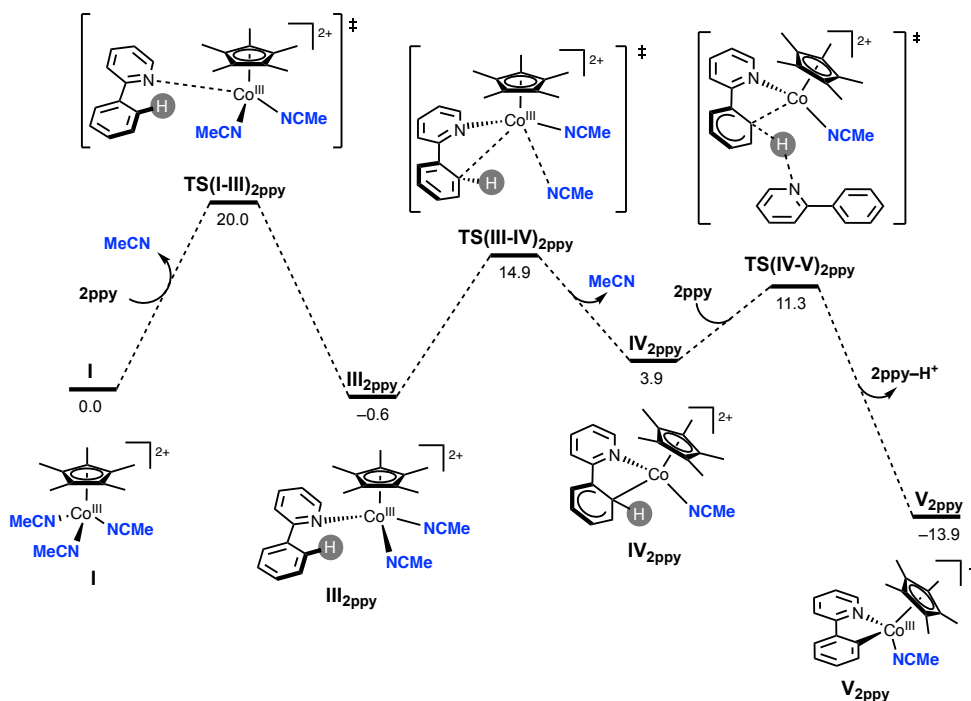
Figure II.4. DFT profile of the cyclometalation of **2ppy** with [Cp*Co(MeCN)₃][BF₄]₂. Energetic values are given as ΔG in kcal/mol.

As we hypothesized before, one of the potential roles of **HFIP** in the **Npmi** system is the formation of the **HFIP-NCMe** adduct. This has an impact in the metalation because the dissociation of **MeCN** from the metal center is involved in the step with the highest energy. In stark contrast, in the cyclometalation of **2ppy**, there is no effect in the addition of **HFIP**. This result is in alignment with the computational results shown in Figure II.4, where the rate-determining step is the approximation of the substrate to the metal center.

II.3 Supporting Information for Annex II

II.3.1 General Procedures

All experiments were conducted under an argon-filled glove box (mBraun Unilab 4420) with concentrations of O_2 and H_2O < 0.1 ppm or using Schlenk techniques under argon atmosphere. All the glassware was oven-dried at 100 ºC overnight and cooled under vacuum prior use. NMR spectra were obtained on a Bruker 400 MHz or a 500 MHz cryoprobe spectrometers. ^{1}H, ^{13}C and ^{19}F NMR chemical shifts are reported in parts per million (ppm), relative to tetramethylsilane (TMS) for ^{1}H and ^{13}C with the residual solvent peak used as an internal reference, and relative to CCl_3F (Freon) for ^{19}F. The data regarding the DFT calculations will be omitted here, and will be provided additionally by other means.

II.3.2 Materials and Methods

Commercially available reagents 2-phenylpyridine, indole, 2-chloropyrimidine, 2,6-di-*tert*-butylpyridine, 1,2,3,4,5-pentamethylcyclopentadiene, 1,3-cyclohexadiene, ^{n}BuLi, $Co_2(CO)_8$, $AgBF_4$, pivalic acid, ethyl acetate, ^{n}hexane, and acetone were used without further purification directly as received from the commercial supplier, and stored under inert gas and/or low temperature when required. 1,1,1,3,3,3-hexafluoroisopropanol (HFIP), 1,1,1,3,3,3-hexafluoro-2-methoxypropane (HFIP-OMe), 1,1,1,3,3,3-hexafluoropropanol-d_2 (HFIP-d_2), 1,1,1,3,3,3-hexafluoro-2-phenylpropan-2-ol ($Ph(CF_3)_2COH$), 1,1,1,3,3,3-hexafluoro-2-(trifluoromethyl)propan-2-ol (($(CF_3)_3COH$), tribromoethanol (TBE), trichloroethanol (TCE), trifluoroethanol (TFE), were stored under argon with activated 4 Å molecular sieves.

CD_2Cl_2 was stored under argon with activated 4 Å molecular sieves. [Cp*Co(MeCN)$_3$][BF$_4$]$_2$,[5] **Npmi**,[6] **Npmi-d**,[7] and **2ppy-d_5**[8] were synthesized according to previous literature procedures.

[5] Yu, D.-G.; Gensch, T.; de Azambuja, F.; Vásquez-Céspedes, S.; Glorius, F. "Co(III)-Catalyzed C−H Activation/Formal S$_N$-Type Reactions: Selective and Efficient Cyanation, Halogenation, and Allylation" *J. Am. Chem. Soc*. **2014**, *136*, 17722−17725.

[6] Ackermann, L.; Lygin, A. V. "Ruthenium-Catalyzed Direct C−H Bond Arylations of Heteroarenes" *Org. Lett*. **2011**, *13*, 3332−3335.

[7] Maresh, J. J.; Giddings, L.-A.; Friedrich, A.; Loris, E. A.; Panjikar, S.; Trout, B. L.; Stöckigt, J.; Peters, B.; O'Connor. S. E. "Strictosidine Synthase: Mechanism of a Pictet−Spengler Catalyzing Enzyme" J. *Am. Chem. Soc*. **2008**, *130*, 710−723.

[8] Luo, C.-Z.; Gandeepan, P.; Jayakumar, J.; Parthasarathy, K.; Chang, Y.-W.; Cheng, C.-H. "Rh^{III}-Catalyzed C−H Activation: A Versatile Route towards Various Polycyclic Pyridinium Salts" *Chem. Eur. J*. **2013**, *19*, 14181−14186.

II.3.3 Npmi C−H Cyclometalation Reactions

II.3.3.1 General Cyclometalation Reaction
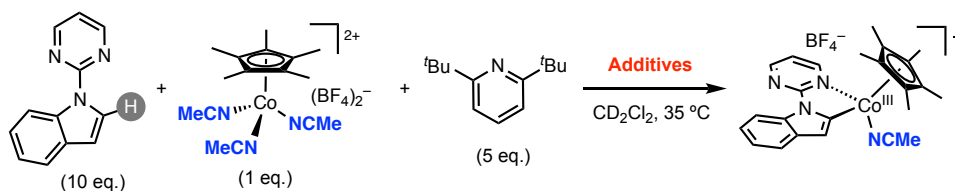
Inside the glovebox an NMR tube was loaded with [Cp*Co(MeCN)₃](BF₄)₂ (4.9 mg, 0.01 mmol), 1,3,5-trimethoxybenzene (1.7 mg, 0.01 mmol) and *N*-pyrimidinylindole (19.4 mg, 0.099 mmol). The tube was then taken out and connected to the Schlenk like *via* an adaptor and cooled down to −35 ºC. The solid was then dissolved in 0.5 mL of CD₂Cl₂ and DTBP was added (10 µL, 0.05 mmol), if necessary, followed by the corresponding additive. The reaction was kept at this temperature until transferred to the NMR instrument for measurement at 35 ºC. The formation of cobaltacycle from [Cp*Co(MeCN)₃](BF₄)₂ was monitored by ¹H NMR spectroscopy.

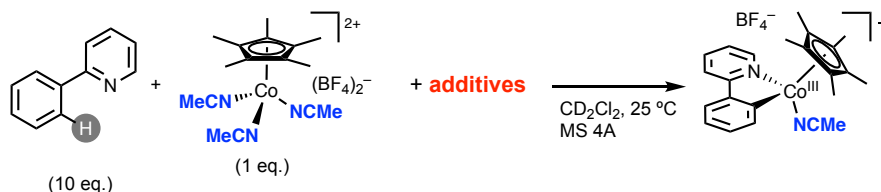### II.3.3.2 Protodemetalation Reaction
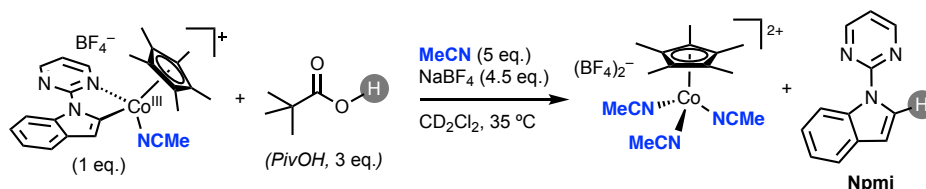
Inside the glovebox an NMR tube was loaded with the corresponding cobaltacycle (5.12 mg, 0.01 mmol), 1,3,5-trimethoxybenzene (1.7 mg, 0.01 mmol), pivalic acid (2 mg, 0.02 mmol) and NaBF₄ (5 mg, 0.04 mmol). The tube was then taken out and connected to the Schlenk like *via* an adaptor and cooled down to −35 ºC. The solid was then dissolved in 0.5 mL of CD₂Cl₂ and MeCN was added (2.6 µL, 0.05 mmol). The reaction was kept at this temperature until transferred to the NMR instrument for measurement at 35 ºC. The formation of Npmi and [Cp*Co(MeCN)₃](BF₄)₂ from the initial cobaltacycle were monitored by ¹H NMR spectroscopy.

II.3.4 2ppy C−H cyclometalation reactions

II.3.4.1 General Cyclometalation Reaction

(10 eq.)   (1 eq.)

Inside the glovebox an NMR tube was loaded with [Cp*Co(MeCN)$_3$](BF$_4$)$_2$ (4.9 mg, 0.01 mmol) and 1,3,5-trimethoxybenzene (1.7 mg, 0.01 mmol). The tube was then taken out and connected to the Schlenk like *via* an adaptor and cooled down to −35 ºC. The solid was then dissolved in 0.5 mL of CD$_2$Cl$_2$ and **2ppy** was added (14.3 μL, 0.10 mmol), followed by the corresponding additive. The reaction was kept at this temperature until transferred to the NMR instrument for measurement at 35 ºC. The formation of cobaltacycle from [Cp*Co(MeCN)$_3$](BF$_4$)$_2$ was monitored by ^{1}H NMR spectroscopy.

II.3.4.2 2ppy-HFIP Adduct Formation
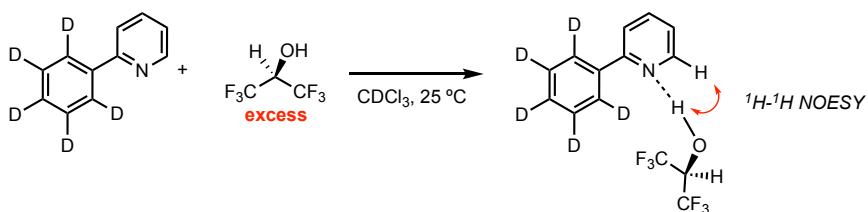
An NMR tube was loaded with **2ppy-d_5** (10 mg, 0.06 mmol) and dissolved in 0.5 mL of CDCl$_3$. Then, an excess of HFIP was added (50 μL, 0.48 mmol). The corresponding mixture was analyzed by ^{1}H NMR at room temperature (Figure II.5, II.6 and II.7).
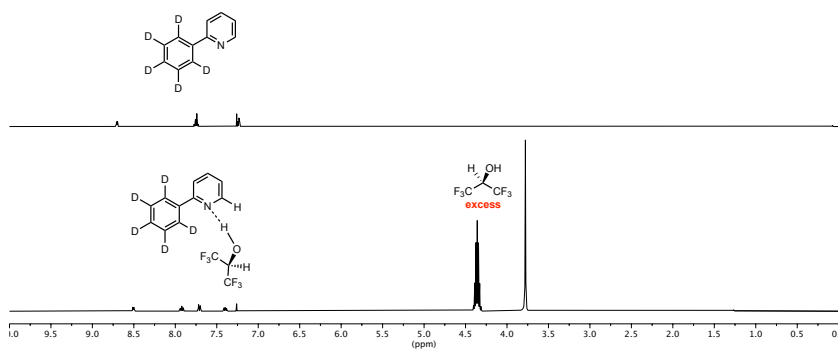
Figure II.5. 2ppy-HFIP adduct formation ^{1}H NMR spectrum.
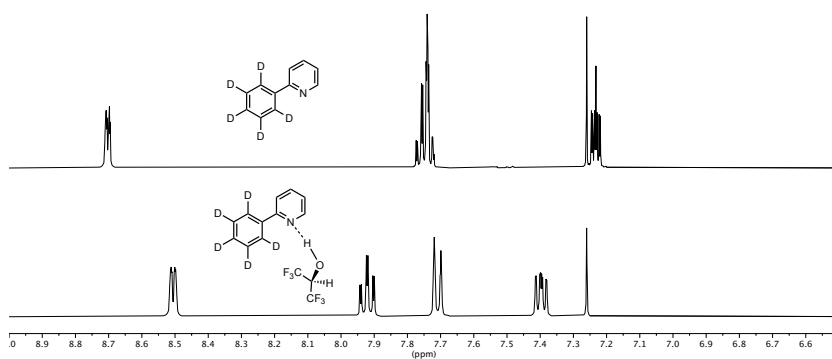

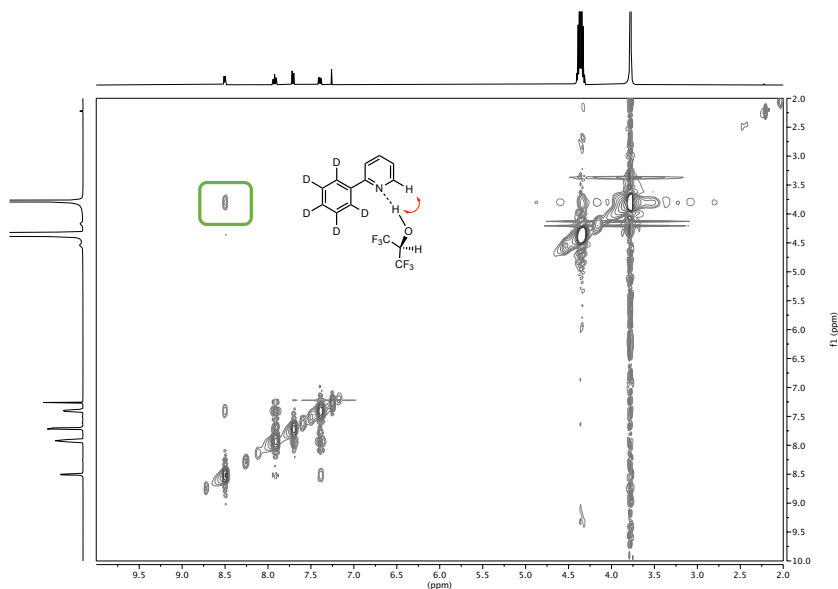**Figure II.6.** Aromatic region of the ^{1}H NMR spectrum in Figure II.5.

Figure II.7. ^{1}H-^{1}H NOESY NMR spectrum.

Annex **III**

Tinker, toiler, solderer, chemist

Last Retort – Chemistry World

Jesús San José Orduna
is a PhD student at ICIQ,
Tarragona, Spain

@jSanjor

Tinkerer, toiler, solderer, chemist

Scientist, builder, mechanic, engineer, nurse, firefighter…

For any research group, someone always has to be its first PhD student. It may sound frightening, but I consider myself extremely lucky to be that person. As part of a three-person team along with my adviser, Mónica Pérez-Temprano, and a postdoc I had to be part of everything. And while the pressure was high (as the sole student I was constantly under the spotlight), I was able to learn countless new things. Everyone expects you to read a million papers, learn how to develop a scientific project and publish your results – but no one tells you about the other roles you must fill too.

We started as builders, literally creating the laboratory from scratch. Before we arrived, it looked like a classic western, with tumbleweeds rolling all around. I spent my first weeks surrounded by wrenches and screwdrivers rather than flasks and beakers. Trying to save as much money as possible, we decided to buy some equipment in pieces and then assemble everything ourselves. This was extremely helpful later whenever we had to fix different malfunctions as they started to appear.

Even so, we still needed help. The group is focused on understanding organometallic mechanisms, and I found myself trying to detect reaction intermediates or, as we called it, catching unicorns. To do so, we refurbished an old glovebox. A friendly technician taught us the tips and tricks of maintenance, including how to use puncture repair patches to fix problems! It was a stark contrast to my previous life in a total synthesis group, doing countless column chromatography purifications – showing that even the 'chemist' part of a job can be radically different from one moment to the next. I even took part in all sorts of security courses, like first aid, CPR and firefighting techniques. Putting fires out for a day was quite cool, but I hope I never need to use that knowledge in real life.

Eventually, things started to work out and more people joined our group. Soon, I even became a mentor to some undergraduates – a new role that was equally rewarding and exhausting. This experience inspired me to start doing some outreach activities. Witnessing the curiosity of children blossom in front of a mundane chemical experiment is one of the most gratifying activities I have ever experienced.

After years of sweat and tears, we were able to publish our first results. That opened the gates for one of the best perks of being in academia: giving presentations at different conferences all around Europe. Thanks to that, I had the chance to meet a lot of people. I also learned the importance of social media. When the Royal Society of Chemistry organised a poster competition on Twitter, I tweeted a gif of my poster and won first prize in my area. I would have never thought during my undergrad that I would be adding a Twitter award to my CV.

My latest adventure featured rainstorms, litres of tea and several hours in front of a computer in Scotland. Under the invaluable tutelage of Stuart Macgregor at Heriot-Watt University in Edinburgh, I explored the distant world of computational chemistry. Although it was overwhelming at first, leaving the flasks behind and starting to see the molecular models break apart and form new bonds gave me a new insight into my own work – and yet another string to my bow.

To date, I've been a chemist, a builder, a mechanic, an engineer, a nurse, a unicorn hunter, a firefighter, a science communicator, a social media influencer and a computer programmer. Now I'm a writer. But it's part of what's great about being a scientist – there's plenty of opportunities when you stick your neck out of the fume hood every now and then.
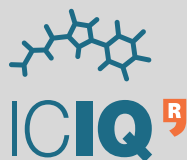
UNIVERSITAT
ROVIRA i VIRGILI

ICIQ[R]

**Institute
of Chemical
Research
of Catalonia**